Effects of CO2 on the biomass pyro-gasification in High Heating Rate and Low Heating Rate conditions

Chamseddine Guizani

THÈSE

En vue de l'obtention du

DOCTORAT DE L'UNIVERSITÉ DE TOULOUSE

Délivré par :

L'École Nationale Supérieure des Mines d'Albi-Carmaux conjointement avec l'INP Toulouse

---

Présentée et soutenue le *(23/09/2014)* **par :**

Chamseddine Guizani

Effects of CO_2 on the biomass pyro-gasification in High Heating Rate and Low Heating Rate Conditions

---

JURY

Roger Gadiou	Professeur, Université de Haute Alsace	Président du Jury
Alberto Gomez Barea	Professeur, Université de Séville	Rapporteur
Lionel Limousy	Maître de conférence, Université de Haute Alsace	Rapporteur
Sylvie Valin	Chargée de Recherche, CEA Grenoble	Examinateur
F. Javier Escudero Sanz	Maître assistant, École des Mines d'Albi-Carmaux	Co-directeur
Sylvain Salvador	Professeur, École des Mines d'Albi-Carmaux	Directeur
Laurent Van De Steene	Chargé de Recherche, CIRAD Montpellier	Invité

École doctorale et spécialité :

MEGEP : Génie des procédés et de l'Environnement

Unité de Recherche :

Centre RAPSODEE, CNRS - UMR 5302, École des Mines d'Albi-Carmaux

Directeur(s) de Thèse :

Sylvain Salvador et *F. Javier Escudero Sanz*

Rapporteurs :

Alberto Gómez Barea et *Lionel Limousy*

To my dear mother.

Remerciements

Tout d'abord je veux adresser mes plus profonds et sincères remerciements à, Khadija, ma chère maman, pour tout ce qu'elle a fait pour moi. Tu es tout simplement une maman magnifique!

Je remercie tous les membres de ma famille pour leur soutien permanent, Zakkouta, Mnigi, Elyes, Mohammed, Amira, Sana, Nadia, Nana, Sami, Kamel.

Mes remerciements s'adressent également à mes encadrants Javier et Sylvain. Javier, merci de m'avoir fait confiance pendant ces trois ans et désolé pour les fois où je partais un peu seul! C'est l'enthousiasme des débutants dira t-on! Un grand merci à "Magic-Salvador", toujours occupé mais toujours disponible! Tes qualités scientifiques et humaines font de toi un encadrant d'exception! J'ai pu apercevoir en toi le savoir des humbles et l'humilité des savants. Dumas disait qu'il est bon d'être bon; tu as donc tout intérêt à le rester, aussi scientifiquement qu'humainement.

Je remercie Docteur Lionel Limousy et Professeur Alberto Gómez Barea d'avoir accepté de rapporter ce travail. La discussion avec vous était très riche et vos corrections tout aussi valeureuses. Merci à Sylvie Valin et à Laurent Van De Steene d'avoir examiné ce travail. Un grand merci au Professeur Roger Gadiou pour avoir examiné ce travail, pour son accueil à l'Institut des sciences des matériaux de Mulhouse où j'ai effectué un séjour durant cette thèse, ainsi que pour son aide et ces éclaircissements.

Un grand merci à Elyes et Wafa Lamine pour votre amitié et votre grande générosité. Un jour, j'assisterais avec grand plaisir aux soutenances de thèses de Yassmine et Isra.

Mes sentiments d'amitié pour Farid. Merci pour tes conseils. Je te souhaite plein de bonnes choses, pour toi, Ammar, et toute ta famille.

Un grand merci à mon ami Mejdi Jeguirim. Tu étais de bons conseils et d'un grand soutien depuis que je t'ai connu.

Merci à Yassine, Karim, Moustafa, Ebsa, Marwein, Omar, Fares, Manel, Anouar et Haithem pour tous les bons moments passés ensemble.

Une pensée pour mes amis d'enfance avec lesquels j'ai grandi, Said, Mohammed Amin, Anis, Nidhal, Spara, Faicel, Ahmed et tant d'autres que je ne peux malheureusement tous citer. Il est clair que je ne vous oublierai jamais.

Je remercie également mes collègues, Baptiste, Santiago, Hélène, Pierre, Bruna et Andrea (do Brasil), Marwa, Marion, Marta (le gâteau à la pomme), Augustina pour tous les moments agréables et les échanges qu'on a eu durant ces années.

Merci à Jean-Louis Dirion et à Olivier Louisnard pour leur aide en modélisation numérique.

Merci à Bernard, Mickael, Denis, Céline et Seppi (IS2M) pour votre aide technique.

Eternal words on knowledge....

"Read !"

Quran 96:1

Knowledge is superior to wealth. Knowledge guards you, whereas you guard wealth. Wealth decreases with expenditure, whereas knowledge multiplies with dissemination. A good material deed vanishes as the material resources behind it vanish, whereas to knowledge we are indebted forever. Thanks to knowledge, you command people's respect during your lifetime, and kind memory after your death. Knowledge rules over wealth. Those who treasure wealth perish while they are still alive, whereas scholars live forever; they only disappear in physical image, but in hearts, their memories are enshrined.

Ali Ibn Abi Taleb

L'esprit scientifique nous interdit d'avoir une opinion sur des questions que nous ne comprenons pas, sur des questions que nous ne savons pas formuler clairement. Avant tout, il faut savoir poser des problèmes.

Gaston Bachelard

Le savoir acquis dans un pays étranger peut être une patrie et l'ignorance peut être un exil vécu dans son propre pays.

Ibn Rochd (Averroes)

Je vis pour connaître, je connais pour vivre, je vis pour aimer, j'aime pour vivre.

Edgar Morin

Pascal a dit : "le Cœur a ses raisons que la Raison ne connaît pas"; ce mot profond n'est pourtant pas d'une exactictude absolue. Car si le coeur a ses raisons, la Raison les connaît et s'y reconnaît. Toute l'œuvre de la Raison consiste à subordonner l'intelligence au Cœur.

Alain

Publications related to this work

Papers already published:

1. C. Guizani, F.J. Escudero Sanz, S. Salvador, Effects of CO_2 on biomass fast pyrolysis: Reaction rate, gas yields and char reactive properties, Fuel, Volume 116, 15 January 2014, Pages 310-320, ISSN 0016-2361, http://dx.doi.org/10.1016/j.fuel.2013.07.101.

2. C. Guizani, F.J. Escudero Sanz, S. Salvador, The gasification reactivity of high-heating-rate chars in single and mixed atmospheres of H_2O and CO_2, Fuel, Volume 108, June 2013, Pages 812-823, ISSN 0016-2361, http://dx.doi.org/10.1016/j.fuel.2013.02.027.

Papers in the intent of publication:

1. C. Guizani, F.J. Escudero Sanz, S. Salvador, High-temperature pyro-gasification of woody biomass in pure CO_2 : experiments and modelling.

2. C. Guizani, F.J. Escudero Sanz, S. Salvador, Influence of temperature and particle size on the single and mixed atmospheres gasification of biomass char with H_2O and CO_2.

3. C. Guizani, F.J. Escudero Sanz, M. Jeguirim, R. Gadiou, S. Salvador, Why is the char reactivity only conversion-dependent during cyclic gasification experiments with H_2O and CO_2?

4. C. Guizani, F.J. Escudero Sanz, M. Jeguirim, R. Gadiou, S. Salvador, Evolution of chemical, textural and structural properties of biomass chars during gasification under H_2O, CO_2 and their mixture.

Contents

List of Figures

List of Tables

General introduction and thesis focus

Energy is the capacity to do work and the lifeblood of civilizations. Sources of energy are various including, fossil fuels, nuclear energy and renewable sources such as solar energy, wind energy and biomass energy among others. Fossil fuels (oil, gas, coal and peat) represent the major part of the world energy supply while the renewable energy part, including hydroelectricity is still minor. The energy demand is increasing due to population growth and economical development. It was clearly the industrial revolution with its emerging fossil fuel consuming technologies that induced the tremendous increasing of fossil fuel consumption. Before 1800, fossil energy production was negligible. From there on, it raised to an annual output of nearly 10,000 million tons of oil equivalents [1].

In less than 200 years, human activities has increased the atmospheric concentration of green house gases by near to 50% relative to pre-industrial levels. Today's concentration of CO_2 (near to 380 ppm) is higher than at any time, at least in the 420,000 past years [2]. This huge increase on CO_2 levels is attributed to the burning of fossil fuels for energy use as well as to provide fuels for transport. Hansen et al suggested that actual CO_2 concentrations exceeds the 300 to 350 ppm level beyond which dangerous anthropogenic interference in the climate system can trigger degradation of land and ocean ecosystems, sea level rise, and disruption of the socio-economic and food-producing infrastructure, making the issue of CO_2 concentration mitigation serious, urgent and worthy of all humans efforts and attention [3]. An analysis of the existing climate data shows that the land-air temperature in both hemispheres increased during the last fifty years by near to 0.6 °C [4]. Best agreements between climate model simulations and observations are obtained when natural and anthropogenic factors are combined [3]. The CO_2 is considered to be the main cause of Global Warming [5]. To trap carbon chemically in earth takes millions of years and modern Man is consuming it at a tremendous rate estimated to be a million time faster than that of carbon trapping. Environmentally speaking, this harms the planet Earth at various levels : air pollution, temperature increase, ecological disequilibrium, species migration and extinction. The twenty-first century is clearly the century in which mankind must cope with fossil fuels depletion, which is unavoidable, and shift towards alternative energies, clean and renewable ones.

Renewable energy sources, comprising solar, wind, geothermal and biomass energy, present two advantages of being alternative routes to fossil ones and to be less harmful to the Planet Earth. Biomass-energy is a promising route for CO_2 mitigation and clean energy production. Indeed, Biomass is considered to be the only natural and renewable carbon resource that can effectively be a substitute to fossil fuels.

Biomass resource includes living water and land based organisms, vegetation, trees as well as dead and waste biomass like municipal organic wastes, sewage sludge, animal wastes (manures), forest and agricultural residues and finally some of the industrial organic wastes. The global energy potential of biomass is huge. It is estimated that the world's terrestrial biomass carbon is approximately 50 times that of total fossil fuel related carbon emission, with forests representing near to 80-90% of the carbon stock [6]. All is about rational and effective use of this energy source. Indeed, biomass constitutes the main energy source for many developing countries, mainly in Africa where it provides 70% of the primary energy used for heating and cooking. Agricultural modernisation as well as good

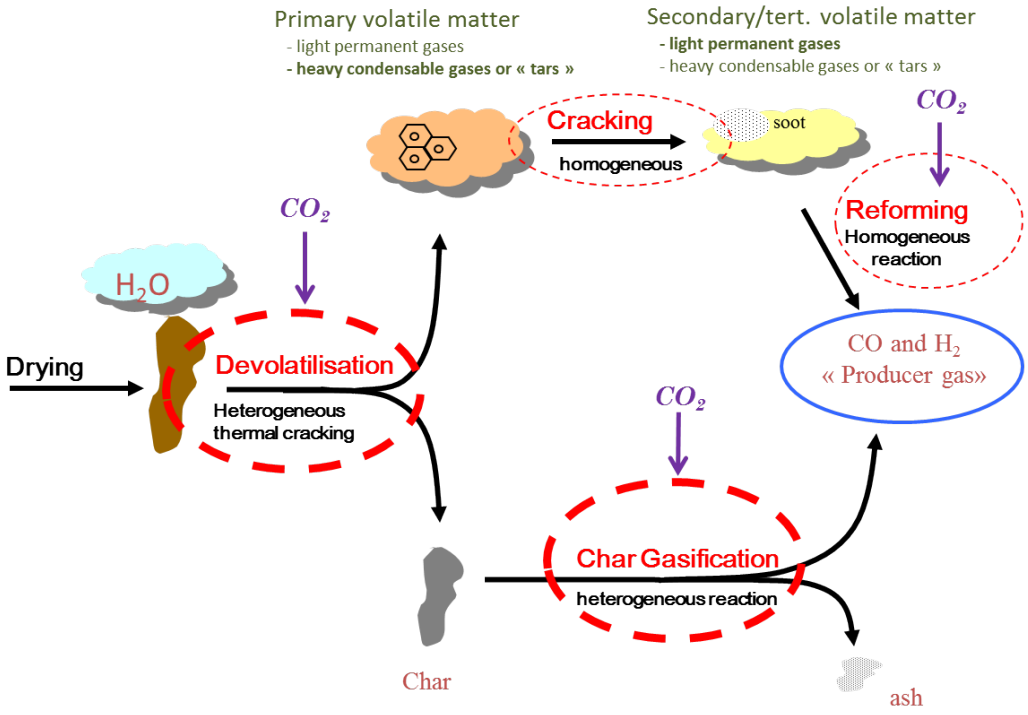

Figure 1: The different steps and reactions occurring during the biomass gasification process and potential actions of added "$\rightarrow CO_2$" (from: S. Salvador. Course on thermochemical conversion of biomass)

land use management have to be developed in parallel with biomass rational and effective usage [6]. Unlike gas or liquid, biomass cannot be handled, stored, or transported easily, especially in its use for transportation. Prior to its use as a fuel, it must be converted to gas or liquid which are more handily and storable products. Biomass conversion can be processed through two major paths : Biochemical path and thermochemical path. The biochemical conversion of biomass including digestion and fermentation is likely the most ancient way of biomass gasification [7]. Biomass thermochemical conversion routes include pyrolysis, combustion, gasification and liquefaction for thermal energy generation, Syngas and biofuels production.

We focus in this work on biomass gasification. As illustrated in figure 1, the biomass gasification process encompasses two main distinct stages: biomass pyrolysis (devolatilisation) and char gasification. Biomass pyrolysis corresponds to the thermal decomposition of the fresh biomass into gas, tars and char. The pyrolysis product distribution depends on the biomass characteristics (biomass type, chemical composition, particle size...) and process conditions (temperature, heating rate...) [7]. Biomass gasification is conventionally operated with steam as the gasifying agent with the aim to obtain Syngas (a mixture of CO and H_2). The global gasification reaction is endothermic. Heat is either externally supplied (allothermal process) or generated by injecting oxygen in the process (autothermal process). A new concept of CO_2 injection in biomass gasifier was proposed recently [8]. External CO_2 supply will provide a more rich CO_2 gasification atmosphere which could impact the product yields and distribution as well as the operation conditions. Injection of this active molecule inside gasifiers therefore provides a potential route for its valorisation as a gasifying medium in biomass gasification processes. The injected CO_2 can potentially participate actively in the heterogeneous biomass pyrolysis and char gasification reactions as well as in gas phase reactions (see figure 1).

The potential use of CO_2 as a gasifying medium has been tackled in the literature for biomass and coal gasification (see section 1.7). It has been observed that the main effects of its use, alone or as a co-reactant with steam, is to increase the carbon conversion and the CO yield while decreasing that of H_2. Encouraging and promising results come out of the literature, but not exhaustive ones, sometimes even contradictory. These observations show that there are several points to clarify and a lot to learn on the potential use of CO_2 in biomass gasifiers. Several advantages of using CO_2 as a gasifying agent have been presented in the literature [8]. For instance, that the CO_2 is in the gaseous state at ambient temperatures unlike steam whose production from water is energy consuming. Moreover, using CO_2 is less harmful for the gasifier, unlike steam which is corrosive. These arguments are quite attractive. However, one must be critical towards certain aspects. Indeed, the CO_2 capture, recycling, transportation and injection inside a gasifier are also energy consuming. Moreover, CO_2 injection modifies the Syngas composition by decreasing the H_2 yield which may not be suitable to certain application like Fisher-Tropsh synthesis for bio-fuel production. There may be thus a need to regulate the Syngas composition by an external H_2 supply, which is also energy consuming. This shows the complexity of the potential CO_2 valorisation in biomass gasifiers and sets the requirement of an exhaustive study, tackling all the issues involved in such a process.

The French National Research Agency (ANR) funded the **RECO2** project, aiming at studying the potential of CO_2 recycling in Circulating Fluidized Bed Gasifiers. The present thesis is in the frame of this project. Different partners are involved in the **RECO2** project due to the various issues dealing about CO_2 valorisation in biomass gasifiers. The partners are Electricité De France (EDF), Commissariat de l'Energie Atomique (CEA) of Grenoble, Système Durable, Technical University of Vienna (TUW) and the RAPSODEE laboratory at the Mine school of Albi. EDF task was to study the CO_2 valorisation in biomass gasifiers using ASPEN+ software. The aim is to model the whole gasification process including biomass gasification, gas cleaning, CO_2 capture and recycling into the gasifier as well as its external injection. They were also partly responsible of the technical and economical feasibility of the process with the help of the CEA of Grenoble. The influence of CO_2 on the producer gas composition was assessed via experiments on a pilot unit fluidized bed reactor in the CEA. The CEA team also developed a gasifier model for the Biomass pyro-gasification including CO_2 injection. Système Durable was responsible of the Life Cycle Assessment as well as of the Carbon foot print calculation of the CO_2 operating gasifier. We were responsible for providing kinetic data for the pyrolysis as well as for the char gasification reaction in the presence of added CO_2. Our study was more fundamental, at the particle level.

The biomass pyrolysis and the char gasification are two key reactions in the whole gasification process. The former is kinetically fast and highly governs the gas, tar and char yields inside the gasifier, while the second is kinetically low and influences greatly the sizing of the gasifier. It is therefore of high interest to understand the impact of added CO_2 on these two complex reactions. The CO_2 can also interact with the gas and tarry species in the gas phase; however, we delimited our study to the heterogeneous reactions because of the affected tasks in the **RECO2** project, and also because of the complexity of these heterogeneous reactions which requires a thesis work to understand them, at least partially.

There exist two main classes of gasification processes wherein the char is whether produced by a fast pyrolysis: High Heating Rate processes (HHR), such as Circulating Fluidized Bed Gasifiers (CFBG) or by a slow pyrolysis: Low Heating Rate processes (LHR), such as Fixed Bed Gasifiers (FBG) or Staged Gasifiers (SG). We judged worth of interest to evaluate the CO_2 injection effects in conditions encountered in these two types of gasifiers.

The **first chapter** of this thesis will be dedicated to the literature review. At first, we will presents some basics of biomass gasification and main technologies. We will then focus on the char gasification reaction and gather different information related to the char chemical, structural and

textural features, those on the gasification reaction phenomenology, on the factors influencing the char reactivity as well as on the different approach of reactivity modelling. Afterwards, we will present a literature review on the effects of CO_2 injection on the gasification process. This review is divided in three parts : the first one is dedicated to the effects of CO_2 on the gas composition, the second one concerns the effects of CO_2 on the char properties while the third and last one will deal about mixed atmosphere char gasification in CO_2 + H_2O atmospheres.

The experimental devices, used in the present thesis will be exposed in **chapter 2**.

The results of the present work are given starting from **chapter 3**. Each chapter is in the form of a scientific paper, already published, submitted or in an intent of submission. The methods related to each part will be presented in the material and methods section of the paper. As the reader would have already read about the experimental devices, we suggest him/her to refer only to the methods.

The first part of the present work will be therefore dedicated to HHR conditions, typical of fluidized bed gasifiers. We will be firstly interested in the effects of CO_2 on the high temperature fast pyrolysis reaction. We will evaluate its effects on the pyrolysis rate, on the gas yield as well as on the char properties including chemical composition, texture and reactivity. The results are given in **chapter 3**.

Afterwards, we will focus on the effects of CO_2 on the HHR-char gasification reaction. We will first determine the gasification rate in single atmospheres of CO_2 and H_2O, then study the mixed atmosphere gasification reaction in CO_2 and H_2O for different atmosphere composition with a total reactants concentration of 40%.vol. We will propose then, regarding the obtained results, a possible mechanism for char gasification in mixed atmosphere. This part is presented in **chapter 4**.

Finally, we imagined a hypothetical case of a pure CO_2 operating gasifier (steam injection would be replaced by CO_2 injection in the CFBG). The case of a pure CO_2 pyro-gasification process will be tackled experimentally and theoretically by numerical modelling with aim to understand the unfolding of the global CO_2 pyro-gasification reaction. The results are presented in **chapter 5**.

In the second part, we will tackle the issue of LHR-char gasification. On one hand, we will provide reactivity data for practical gasification operations. On the other hand, we will try to understand the gasification reaction mechanisms (in CO_2, H_2O and their mixtures) at the molecular level. Understanding the fundamentals of gasification reactions is performed on the LHR-chars as they are more homogeneous from the chemical, structural and textural viewpoints than HHR-chars particles, which chemical composition, structure and texture can vary throughout the particle.

To do so, we will tackle the issue of particle size influence on the single atmosphere gasification in CO_2 and H_2O using the Thiele modulus approach. We will then study the effects of temperature on the char gasification in mixed atmosphere of CO_2 and steam for relatively small particle. Afterwards, we will be interested in larger particle size up to 13 mm to approach practical situation such as in FBG or SG, and have a focus on the mixed atmosphere gasification in the presence of mass transfer limitations. We will also tackle the issue of cyclic atmosphere gasification and study the effects of a prior CO_2 gasification on the char reactivity towards H_2O and vice versa. The results are reported in **chapter 6**.

To further understand the char gasification mechanisms in single and mixed atmospheres of CO_2 and H_2O, we approached the gasification reactions at the char structural units level. As the char reactivity is conditioned by its chemical, structural and textural properties, we opted to monitor the evolution of these properties along the gasification in CO_2, H_2O and their mixtures. Deep char characterization were performed in the "Institut des Sciences des Materiaux de Mulhouse" in the frame of a collaboration between the two laboratories. Small LHR-char particles were partially gasified at 20%, 50% and 70% of conversion in CO_2, H_2O and their mixtures, on which we performed deep textural, structural and chemical analysis. These characterisations are of high interest as they shed light on the unfolding of the gasification reaction in CO_2, H_2O and their mixtures. This part

will be presented in **chapter 7**.

Finally, we will present the main conclusions on CO_2 valorisation in biomass gasifiers as well as the effects of CO_2 on the heterogeneous reactions of biomass pyrolysis and char gasification.

Introduction et objectifs de la thèse

L'énergie traduit la capacité d'un système à effectuer un travail et constitue l'un des piliers de développement des nations. Les sources d'énergie sont diverses, incluant les ressources fossiles, l'énergie nucléaire ainsi que les ressources renouvelables. Les ressources fossiles (pétrole, charbon...) représentent la majeure partie des ressources d'énergie tandis que les ressources renouvelables (solaire, éolien, biomasse) ne représentent qu'une petite partie. La demande en énergie s'accroit constamment suite à l'accroissement démographique et au développement économique. Avant 1800, la production d'énergie fossile était négligeable, mais depuis la révolution industrielle, elle n'a cessé d'augmenter annuellement de 10 millions de tonnes équivalent pétrole [1].

En moins de 200 ans, les activités humaines ont causé une augmentation de la concentration atmosphérique de gaz à effet de serre de 50% relativement à celle de l'ère préindustrielle. La concentration atmosphérique actuelle en CO_2 avoisine les 380 ppm et est la plus haute depuis près de 420,000 ans [2]. Cette forte augmentation est attribuée en majeure partie à la combustion des ressources fossiles. Hansen et al. Suggèrent que les concentrations actuelles en CO_2 peuvent entrainer de graves interférences dans le système climatique et causer la dégradation des terres et des écosystèmes marins, l'augmentation du niveau de la mer ainsi que la perturbation de l'infrastructure socio-économique et agro-alimentaire, rendant ainsi la diminution du CO_2 atmosphérique une question d'actualité valant tous les efforts et l'attention nécessaires [3].

Une analyse des données climatiques existantes montre que la température sol-air dans les deux hémisphères a augmenté pendant les cinquante dernières années de près de 0.6°C [4]. Les meilleurs accords entre les modèles climatiques et les observations sont obtenus quand des facteurs naturels et anthropogéniques sont combinés [3]. Le CO_2 est considéré comme étant la cause principale du réchauffement climatique [5]. L'Homme moderne est entrain de consommer les ressources fossiles à une vitesse un million de fois plus élevée que celle nécéssaire à la formation de cette ressource au tréfonds de la terre. Ceci nuit à la planète Terre à diverses niveaux : pollution atmosphérique, augmentation de la température, déséquilibre écologique, migration d'espèces et extinction. De nos jours, l'humanité doit faire face à l'inévitable épuisement des combustibles fossiles et opter pour le changement vers des énergies alternatives, propres et renouvelables.

Les sources d'énergie renouvelable, comprenant le solaire, l'éolien, la géothermie et l'énergie de biomasse, ont deux avantages principaux : à savoir qu'elles présentent des alternatives aux ressources fossiles et sont moins nuisibles pour la planète. La biomasse a un potentiel prometteur pour la réduction du CO_2 atmosphérique et la production d'énergie propre. On considère que la biomasse est la seule ressource naturelle et renouvelable qui peut efficacement être un substitut aux combustibles fossiles.

Les ressources en biomasse incluent entre autres la biomasse marine (algues), la végétation, les arbres aussi bien que les déchets organiques municipaux, des boues d'épuration, des déchets animaliers (fumiers), des résidus forestiers et agricoles et finalement certains des déchets organiques industriels. Le potentiel énergétique global de la biomasse est énorme. On estime que le carbone que renferme la biomasse terrestre du monde est environ 50 fois celui du combustible fossile brulé. Les forêts représentent à elles seules près de 80-90 % du stock en carbone [6]. La biomasse doit être utilisée

d'une manière raisonnable et effective. En effet, la biomasse constitue la source d'énergie principale pour beaucoup de pays en voie de développement, principalement en Afrique où elle fournit près de 70 % de l'énergie primaire utilisée pour chauffer et cuisiner.

La modernisation agricole aussi bien que le bon usage des terres doivent être développés en parallèle avec la filière biomasse-énergie [6]. Contrairement aux combustibles liquides et gazeux, la biomasse ne peut pas être manipulée, stockée, ou transportée facilement, particulièrement dans le cadre de son utilisation pour le transport. Avant son utilisation comme un carburant, elle doit être converti en gaz ou en liquide qui sont plus facilement stockables. La conversion de biomasse peut être réalisée via deux voies principales : la voie biochimique et la voie thermochimique. La conversion biochimique de la biomasse incluant la digestion et la fermentation est la plus ancienne [7]. La voie thermochimique inclut la pyrolyse, la combustion, la gazéification et la liquéfaction pour la génération d'énergie thermique, de Gaz de synthèse et la production de biocarburants.

Nous nous concentrons dans ce travail sur la gazéification de biomasse. La gazéification de biomasse comprend deux étapes principales de pyrolyse et de gazéification du char comme illustré dans la figure 1. Elle est conventionnellement opérée avec la vapeur d'eau comme agent de gazéification dans le but de produire du gaz de synthèse (un mélange de CO et de H_2). La réaction de gazéification globale est endothermique (incluant le séchage, la pyrolyse et la gazéification du char). La chaleur nécessaire est ou extérieurement fournie ou produite en injectant l'oxygène dans le réacteur.

Récemment, un nouveau concept qui consiste à utiliser le CO_2 comme agent gazéifiant dans les gazéifieurs a été proposé [8]. L'injection externe de CO_2 fournira une atmosphère de gazéification plus riche en CO_2 ce qui pourrait avoir un impact sur les rendements des différents produits. L'injection de cette molécule active dans des procédés de gazéification fournit donc un moyen potentiel pour sa valorisation comme un agent de gazéification dans des réacteurs de gazéification de biomasse. L'utilisation potentielle de CO_2 comme agent gazéifiant pour la gazéification de la biomasse et du charbon a été abordée dans la littérature (voir chapitre 1). Il a été observé que les effets principaux de son utilisation, seul ou comme un co-réactif avec la vapeur d'eau, sont d'augmenter la conversion du carbone et le rendement en CO tout en diminuant celui de H_2.

Des résultats encourageants ressortent de la littérature, mais qui ne sont cependant pas exhaustifs et sont parfois même contradictoires. Ces observations montrent qu'il y a plusieurs points à clarifier et beaucoup à apprendre sur l'utilisation potentielle du CO_2 dans des procédés de gazéification de biomasse. Plusieurs avantages sur l'utilisation du CO_2 comme un agent de gazéification ont été présentés dans la littérature [8]. Par exemple, que le CO_2 soit à l'état gazeux à température et pression ambiantes contrairement à la vapeur d'eau, ou encore qu'il soit moins nuisible pour le réacteur, contrairement à la vapeur d'eau qui est corrosive.

Ces arguments sont tout à fait attractifs. Cependant, il faut être critique envers certains aspects. En effet, la capture, le recyclage, le transport et l'injection du CO_2 dans un gazéifieur sont aussi consommateurs d'énergie. De plus, l'injection de CO_2 modifie la composition du gaz de synthèse en diminuant la concentration de H_2 ce qui peut conduire que le syngaz ne soit plus approprié pour certaines applications comme la synthèse Fisher-Tropsh pour la production de biocarburants. Il devient ainsi nécessaire de régler la composition du gaz de synthèse par une injection externe de H_2 qui est aussi consommatrice d'énergie. Ceci montre la complexité de la valorisation potentielle du CO_2 dans les procédés de gazéification de la biomasse et impose ainsi une étude exhaustive, abordant toutes les aspects impliquées dans un tel processus.

L'Agence de Recherche Nationale française (ANR) a financé le projet **RE**CO_2, visant à l'étude de l'usage potentiel du CO_2 comme agent gazéifiant dans des réacteurs à lit fluidisé pour la gazéification de biomasse. La présente thèse rentre dans le cadre de ce projet. Des partenaires différents y sont également impliqués : Electricité de France (EDF), le Commissariat de l'Energie Atomique (CEA) de Grenoble, Système durable, l'Université Technique de Vienne (TUW) et le laboratoire RAPSODEE à

l'école des Mines d'Albi. EDF était responsable d'analyser le procédé de gazéification de la biomasse en présence de CO_2 via une modélisation de l'ensemble du processus en utilisant ASPEN+. EDF était aussi en partie responsable de l'étude technico-économique avec l'équipe du CEA de Grenoble. L'impact du CO_2 sur le rendement en gaz a été étudié expérimentalement par le CEA via des expériences de gazéification dans un lit fluidisé à l'échelle pilote. Le CEA a aussi développé en parallèle un modèle de gazéifieur opérant au CO_2. La société Système durable était responsable de l'analyse du cycle de vie ainsi que du calcul de l'empreinte carbone d'un tel procédé. De notre cÃ‡té, on avait la tâche de fournir des données cinétiques de pyrolyse et de gazéification du char. Notre étude était plus fondamentale, à l'échelle de la particule.

La pyrolyse de la biomasse et de la gazéification du char sont deux réactions clés dans l'ensemble du processus de gazéification. La première est cinétiquement rapide et détermine les rendements en gaz, goudrons et char à l'intérieur du gazéifieur, tandis que la seconde est cinétiquement lente mais influence fortement le dimensionnement de l'unité de gazéification. Il est donc d'un grand intérêt de comprendre l'impact du CO_2 sur ces deux réactions complexes. Le CO_2 peut également réagir avec les gaz et goudrons dans la phase gazeuse, cependant, nous avons délimité notre étude aux réactions hétérogènes en raison des tâches affectées dans le projet **RE**CO_2, ainsi que du fait de la complexité de ces réactions hétérogènes qui nécessitent un travail de thèse pour les comprendre, au moins partiellement.

Il existe deux grandes catégories de procédés de gazéification, dans lequel le char est soit produit par une pyrolyse rapide comme dans les lits fluidisés ou par une pyrolyse lente comme dans les gazogènes à lit fixe ou les procédés étagés. Nous avons jugé très utile d'évaluer l'effet du CO_2 dans des conditions rencontrées dans ces deux types de gazogènes.

Le premier chapitre de cette étude portera sur l'état de l'art. On abordera en premier lieu les bases et les principales technologies de gazéification de la biomasse. Puis, on mettra particulièrement l'accent sur la réaction de gazéification du char. Afin de comprendre la phénoménologie de la réaction de gazéification, on présentera les différentes données relatives à la composition chimique du char, ses caractéristiques structurales et texturales, ainsi que les facteurs qui influent sur sa réactivité. On abordera aussi les différentes approches de modélisation de la réactivité d'un char. Ensuite, on présentera un état de l'art sur les effets d'injection du CO_2 sur le processus de gazéification. Cet état de l'art sera divisé en trois parties : la première est consacrée aux effets du CO_2 sur la composition du gaz produit, la deuxième concerne les effets du CO_2 sur les propriétés du char obtenu, tandis que la troisième et dernière portera sur la gazéification du char en atmosphère mixte contenant de la vapeur d'eau et du CO_2.

Les dispositifs expérimentaux, utilisés dans la présente thèse sont exposés dans le chapitre 2.

Les résultats de ce travail sont donnés à partir du chapitre 3. Chaque chapitre est sous la forme d'un article scientifique, déjà publié, soumis ou dans une intention de publication. Les méthodes associées à chaque chapitre seront présentés dans la section matériel et méthode qui lui est associÃ‰e. Comme le lecteur aura déjà lu sur les dispositifs expérimentaux, nous lui suggérons de se référer uniquement aux méthodes.

La première partie des résultats sera donc dédiée à des conditions de chauffe rapide, typiques des gazogènes à lit fluidisé. Nous aborderons d'abord les effets de CO_2 sur la réaction de pyrolyse rapide à haute température. Nous allons évaluer ses effets sur la vitesse de pyrolyse, sur le rendement en gaz, ainsi que sur les propriétés du char, notamment sa composition chimique, la texture et sa réactivité. Les résultats sont donnés dans le chapitre 3.

Ensuite, nous allons nous concentrer sur les effets de CO_2 sur la réaction de gazéification du char obtenus en chauffe rapide. Nous allons d'abord déterminer la vitesse de gazéification dans des atmosphères simples de CO_2 et H_2O. Nous étudierons ensuite la réaction de gazéification sous atmosphère mixtes pour différentes compositions en CO_2 + H_2O. Nous proposerons ensuite, au

regard des résultats obtenus, un mécanisme possible pour la réaction de gazéification en atmosphères mixtes. Cette partie est présentée dans le chapitre 4.

Enfin, nous avons imaginé un cas hypothétique d'un gazogène opérant sous CO_2 pur (l'injection de vapeur serait remplacée par le CO_2). Le cas d'un processus de pyro-gazéification sous CO_2 sera abordée expérimentalement et théoriquement par la modélisation numérique avec l'objectif de fournir des informations sur les temps caractéristiques de pyrolyse et de gazéification, et de comprendre le déroulement de la pyro-gazéification sous CO_2. Les résultats sont présentés dans le chapitre 5.

Dans la deuxième partie, nous aborderons la question de la gazéification des chars obtenus par pyrolyse lente avec deux objectifs principaux : d'une part, de fournir des données de réactivités de chars dans des conditions typiques de procédés de gazéification et d'autre part, de comprendre les mécanismes des réactions de gazéification sous CO_2, H_2O et leurs mélanges. Comprendre les principes fondamentaux des réactions de gazéification est entrepris sur des chars obtenus par pyrolyse lente car ils sont plus homogènes du point de vue structural et textural.

Nous allons en premier lieu aborder la question de l'influence de la taille des particules sur la gazéification sous CO_2 et H_2O par une approche de module de Thiele. Nous allons ensuite étudier les effets de la température et de la taille des particules de char sur la gazéification sous des atmosphères mixtes de CO_2 et de vapeur. Nous allons également aborder la question de la gazéification sous des atmosphères alternées et étudier les effets d'une gazéification au CO_2 sur la réactivité du char à H_2O et vice versa. Les résultats sont présentés dans le chapitre 6.

Pour mieux comprendre les mécanismes de gazéification dans des atmosphères simples et mixtes de CO_2 et H_2O, nous avons approché les réactions de gazéification à l'échelle des unités structurales du char. Comme la réactivité char est conditionnée par les propriétés structurales, texturales et chimiques, nous avons opté pour suivre l'évolution de ces dernières le long de la gazéification sous CO_2, H_2O et leurs mélanges. Les caractérisations du char ont été effectuées à l'"Institut des Sciences des Matériaux de Mulhouse" dans le cadre d'une collaboration entre nos deux laboratoires. De petites particules de char ont été partiellement gazéifiés à 20 %, 50 % et 70 % de conversion sous CO_2, H_2O et leurs mélanges, sur lesquels nous avons par la suite effectué les différentes analyses. Ces caractérisations sont d'un grand intérêt car elles mettent en lumière la phénoménologie de la réaction de gazéification sous CO_2, H_2O et leurs mélanges. Cette partie sera présentée dans le chapitre 7.

On présentera enfin les principales conclusions et perspectives de la présente étude.

Chapter 1

State of the art

Abstract

The first chapter of this thesis is dedicated to the literature review. At first, we will presents some basics of biomass gasification and main technologies. We will then focus on the char gasification reaction and gather different information related to the char chemical, structural and textural features, those on the gasification reaction phenomenology, on the factors influencing the char reactivity as well as on the different approach of reactivity modelling. Afterwards, we will present a literature review on the effects of CO_2 injection on the gasification process. This review is divided in three parts : the first one is dedicated to the effects of CO_2 on the gas composition, the second one concerns the effects of CO_2 on the char properties while the third and last one will deal about mixed atmosphere char gasification in CO_2 + H_2O atmospheres.

Résumé

Ce chapitre constitue une revue concise se voulant être les plus exhaustive possible sur la pyro-gazéification de la biomasse en présence de CO_2. Dans ce chapitre, après un aperçu sur la structure et la composition de la biomasse ainsi que les techniques de gazéification, les propriétés structurales, texturales et chimiques des chars sont présentées de façon synthétique. Les facteurs affectant la réactivité des chars sont exposés (fonctions de surface,surface active, composés minéraux, taille des particules de chars, texture des chars, vitesse de chauffe lors de la phase de pyrolyse et température finale). Par la suite, les équations permettant de modéliser la gazéification des chars en régime chimique et en présence de limitations à la diffusion sont présentées. La dernière partie du chapitre bibliographique, se focalise sur les résultats majeurs portant sur l'utilisation du CO_2 lors de la pyrolyse de biomasses et de la gazéification. Une étude exhaustive de la littérature est réalisée afin de permettre d'identifier les points critiques liés à la gazéification en présence de CO_2, les paramètres clés ainsi que les phénomènes complexes à étudier. Il est également mis en évidence que de nombreux auteurs se contredisent concernant l'effet du CO_2 en présence de vapeur d'eau sur la réaction de gazéification du char.

1.1 Biomass gasification: Resources, basics and technologies

1.1.1 Biomass resources

Biomass can be defined as the organic material derived from biological systems. Biological solar energy conversion via the process of photosynthesis produces energy in the form of plant biomass which is about ten times the world's annual use of energy. Biomass does not include fossil fuels, although they also originate from biomass-based sources. Based on their moisture content, biomasses can be classified into two main categories: dry biomasses and wet biomasses [9].

Table 1.1: Classification of biomasses according to [9]

Dry biomasses	Wet biomasses
Forests	Farming waste effluents
(trees, wood-chips)	(liquid manure)
Wood transformation manufactures	Liquid effluents of food-industries
(sawdust, bark)	(vinasses, spent coffee grounds)
Agriculture and food industries	Green wastes
(straw, leaves, trunks, husk)	(grass clippings, branches, leaves)
Energetic crops	Household waste
(Miscanthus, Arundo donax)	(kitchen waste, garden waste, paper)
Herbaceous biomasses	
(papyrus, alfa-alfa, water hyacinth)	

Ligno-Cellulosic biomasses

Ligno-cellulosic material is the non-starch, fibrous part of plant materials. A ligno-cellulosic biomass is composed mainly of cellulose, hemicellulose, and lignin. Wood is a typical example of a ligno-cellulosic biomass. Unlike carbohydrate or starch, ligno-cellulose is not easily digestible by humans. For example, we can eat the rice, which is a carbohydrate, but we cannot digest the husk or the straw, which are ligno-cellulose. As ligno-cellulosic biomass is not part of the human food chain, its use for biogas or bio-oil production does not threaten the world's food supply. Woody biomasses are of great interest for thermochemical conversion into energy and marketable fuels. In the present work, beech wood will be used as the parent biomass. It is therefore interesting to have a look on the wood structure and composition.

Wood structure and composition

description of a tree trunk A living, growing tree has two main domains, the shoot and the roots. Roots are the subterranean structures responsible for water and mineral nutrient uptake, mechanical anchoring of the shoot, and storage of biochemicals. The shoot is made up of the trunk, branches, and leaves. We will be concerned with the trunk as the main ligno-cellulosic part of a tree.

When cutting down a tree and looking at the stump, one can make several gross observations. The trunk is composed of various materials present in concentric bands. From the outside of the tree to the inside are: outer bark, inner bark, vascular cambium, sapwood, heartwood, and the pith (see figure 1.1). Outer bark have a protective function as it provides a mechanical protection to the softer inner bark and also helps to limit evaporative water loss. Inner bark is the tissue through which

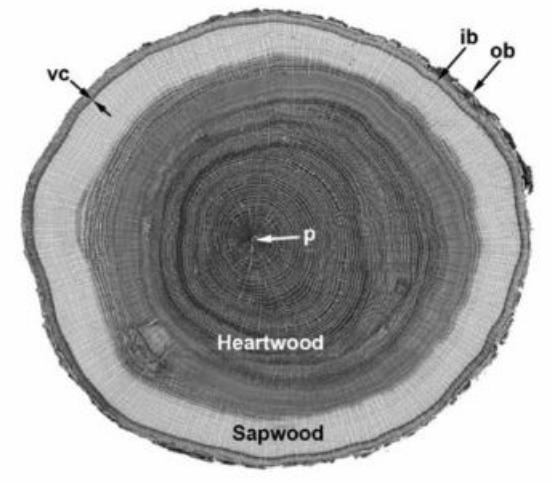

Figure 1.1: Macroscopic view of a transverse section of a Quercus alba trunk. Beginning at the outside of the tree is the outer bark (ob). Next is the inner bark (ib) and then the vascular cambium (vc), which is too narrow to see at this magnification. Interior toward the vascular cambium is the sapwood, which is easily differentiated from the heartwood that lies toward the interior. At the center of the trunk is the pith (p), which is barely discernible in the center of the heartwood. [10]

sugars (food) produced by photosynthesis are transported from the leaves to the roots or growing portions of the tree. The vascular cambium is the layer between the bark and the wood that produces both these tissues each year. The sapwood is the active, 'living' wood that conducts the water (or sap) from the roots to the leaves. It has not yet accumulated the often-coloured chemicals that set apart the non-conductive heart-wood found as a core of darker-coloured wood in the middle of most trees. The pith at the very center of the trunk is the remnant of the early growth of the trunk, before wood was formed [10].

Softwoods and hardwoods There exist two types of woods: softwoods and hardwoods. To define them botanically, softwoods are those woods that come from gymnosperms (mostly conifers) such as pine (Pinus) and spruce (Picea), and hardwoods are woods that come from angiosperms (flowering plants) such as beech, maple (Acer), birch (Betula), and oak (Quercus). Softwoods and hardwoods not only differ in terms of the types of trees from which they are derived, but they also differ in terms of their component cells. Softwoods have a simpler basic structure than do hardwoods because they have only two cell types and relatively little variation in structure within these cell types. Hardwoods have greater structural complexity because they have both a greater number of basic cell types and a far greater degree of variability within the cell types (see figure 1.2).

Elementary composition Wood is mostly composed of *C, H, O* and *N*. It also contains a minor part of mineral matter found in the form of ash. The proportions between these compounds are different from a type of wood to another, but the general trends are conserved. Ash composition varies from a wood to another but the main components are *K, Ca, Na* and *Mg* [12].

Moisture content At cutting, raw wood can contain up to 50 w% of water. After a natural drying, moisture can be decreased to about 10 w% to 20 w%, depending on the storage conditions. Because of its hygroscopic properties, wood is very sensitive to the temperature and ambient hygrometry. In

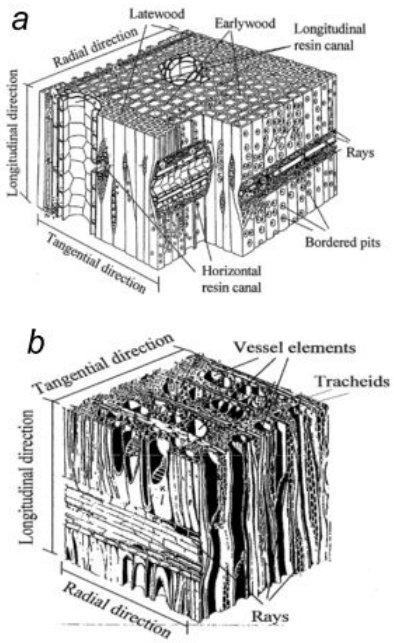

Figure 1.2: Gross structure of softwood (a) and hardwood (b)[11]

raw harvested wood, moisture can exist in three forms: water vapour in the pores, capillary or free water (liquid) in the pores and hygroscopic or bound water in the solid structure [13].

Constituents of wood Cells About 95 % of the wood cells are composed of three molecular components: cellulose, hemicellulose and lignin. Additionally, wood contains some low-molecular weight organic compounds know as extractives, which gather a thousand of species extractable by solvents, like ketones, organic acids, esters, phenolic compounds, resins and terpenes among others.

The repartition of cellulose, hemicellulose and lignin is slightly variable among the wood species. However, a general trend is always respected: cellulose is the major component, 40 to 45 w% daf, followed by hemicellulose and lignin in comparable amounts, 20 to 30 w% daf.

- Cellulose

  Cellulose is the most common organic compound on Earth and the primary structural component of cell walls in biomass. It is represented by the generic formula $(C_6H_{10}O_5)_n$, cellulose is a long chain polymer with a high degree of polymerization. The value of n, the degree of polymerization, reaches even more than 10000 units in an unaltered wood. Cellulose has a crystalline structure of thousands of units, which are made up of many glucose molecules. This structure gives it high strength, permitting it to provide the skeletal and fibrous structure of most terrestrial biomass. Cellulose is primarily composed of d-glucose, which is made of six carbons or hexose sugars . Cellulose is highly insoluble and, though a carbohydrate, is not digestible by humans.

- Hemicellulose

  Hemicellulose is a mixture of polysaccharides of 50 to 200 units, entirely composed of sugars such as glucose, mannose, arabinose, methylglucuronic acid, galacturonic acid and mostly xylose. While cellulose is of a crystalline, strong structure that is resistant to hydrolysis, hemicellulose has a random, amorphous structure with little strength. It is a group of carbohydrates with

a branched chain structure and a lower degree of polymerization (100 to 200), and may be represented by the generic formula $(C_5H_8O_4)_n$. Hemicellulose tends to yield more gases and less tar than cellulose. It is soluble in weak alkaline solutions and is easily hydrolyzed by dilute acid or base [7]

- Lignin

  Lignin is a three-dimensional polymer, mostly constituted of phenolic units of nature highly dependent on the type of wood. As a lignin polymer is severely impacted by the extraction mode, its complex structure is very difficult to define and thus it is not still well known in the scientific community. Lignin is the cementing agent for cellulose fibres holding adjacent cells together. The dominant monomeric units in the polymers are benzene rings. It is similar to the glue in a cardboard box, which is made by gluing together papers in special fashion.

1.1.2 Basics of biomass gasification

The term "biomass gasification" is a gross appellation gathering several steps of drying, pyrolysis, gas phase reactions and char gasification, occurring inside the gasifier. Figure 1 illustrates the different stages of the biomass gasification process. The whole process can be divided in four main steps: drying, pyrolysis, partial oxidation of char an and char gasification.

The first step of drying occurs in a range of temperatures below 200°C. The major part of water (free and bound water) contained in the biomass is evaporated and passes into the gaseous phase.

Follows then the pyrolysis step, which is a thermal decomposition of the biomass into light gases, tars and solid char. Pyrolysis takes place between 230°C and 500°C. The solid char is mostly formed of carbon with few amounts of oxygen, hydrogen and ash. The liquid yield known as tar or bio-oil is a black tarry fluid containing up to 20% water. The light gases comprise in majority CO_2, CO, H_2O, C_2H_2, C_2H_4 and C_2H_6. The nature and yields of the pyrolysis product depends on the operating conditions such as pyrolysis final temperature and heating rate. The influence of pyrolysis final temperature and heating rate on the pyrolysis product distribution is shown in figure 1.3. The production of char is maximized at low temperatures and slow heating rate conditions. The more the temperature and heating rate increase the more light gases are produced. Production of liquids is optimized for fast heating rate conditions in a temperature range of 750 to 800 K.

Homogeneous gas phase reactions such as tar reforming in presence of steam and/or CO_2, reactions between pyrolysis gas products and reactants (water gas shift), as well as combustion reactions of some light gases with oxygen occur in the gasifier.

The last step is char gasification that occurs at high temperature (800-1000°C). This step involves reactions between the steam and/or carbon dioxide (resulting from the combustion reactions of volatiles with oxygen, or injected as gasifying media) with the porous char. The steam-char and CO_2-char gasification reactions are endothermic. Energy can be supplied by the combustion of part of the char and volatiles. The char gasification reactions (steam gasification reaction and Boudouard reaction) produce mainly hydrogen and carbon monoxide which proportions depend on the gasification conditions.

The main chemical reactions occurring in a gasifier are summarized as follows:

Biomass pyrolysis:

$$Biomass \longrightarrow char + tar + H_2O + light\,gas(CO + CO_2 + H_2 + CH_4 + C2 + N_2)\,(endothermic) \quad (1.1)$$

Heterogeneous reactions:

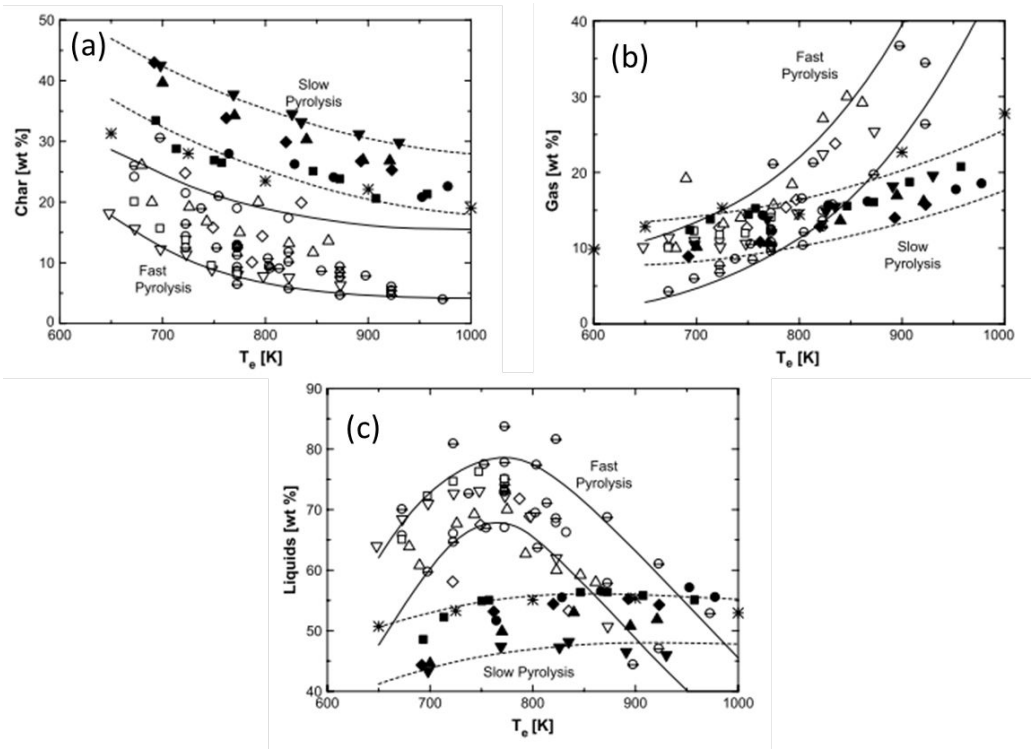

Figure 1.3: Char (a) Gas (b)and Liquid (c) yields as a function of the pyrolysis conditions [14]

Char combustion reactions

$$Partial\,combustion\ : C + 1/2\,O_2 \longrightarrow CO\,(-111kJ/mol) \tag{1.2}$$
$$Complete\,combustion\ : C + O_2 \longrightarrow CO_2\,(-394kJ/mol) \tag{1.3}$$
$$\tag{1.4}$$

Char gasification reactions

$$Boudouard\,reaction\ : C + CO_2 \longrightarrow 2CO\,(+173kJ/mol) \tag{1.5}$$
$$Steam\,gasification\ : C + H_2O \longrightarrow CO + H_2\,(+131kJ/mol) \tag{1.6}$$
$$Hydrogen\,gasification\,(Methanisation)\ : C + 2H_2 \longrightarrow CH_4\,(-75kJ/mol) \tag{1.7}$$

Homogeneous gas phase reactions:

$$Carbon\,monoxide\,oxidation\ : CO + 1/2O_2 \longrightarrow CO_2\,(-283kJ/mol) \tag{1.8}$$
$$Hydrogen\,oxidation\ : H_2 + 1/2O_2 \longrightarrow H_2O\,(-242kJ/mol) \tag{1.9}$$
$$Methane\,oxidation\,CH_4 + 2O_2 \longrightarrow CO_2 + 2H_2O\,(-283kJ/mol) \tag{1.10}$$
$$WaterâĂŞgas\,shift\,reaction\ : CO + H_2O \longrightarrow CO_2\ + H_2(-41kJ/mol) \tag{1.11}$$

1.1.3 Biomass gasification technologies

Investigation on reactor designs in order to optimize the biomass gasification have began since more than a century and leaded to a wide range of gasifiers which can be classified in different ways according to:

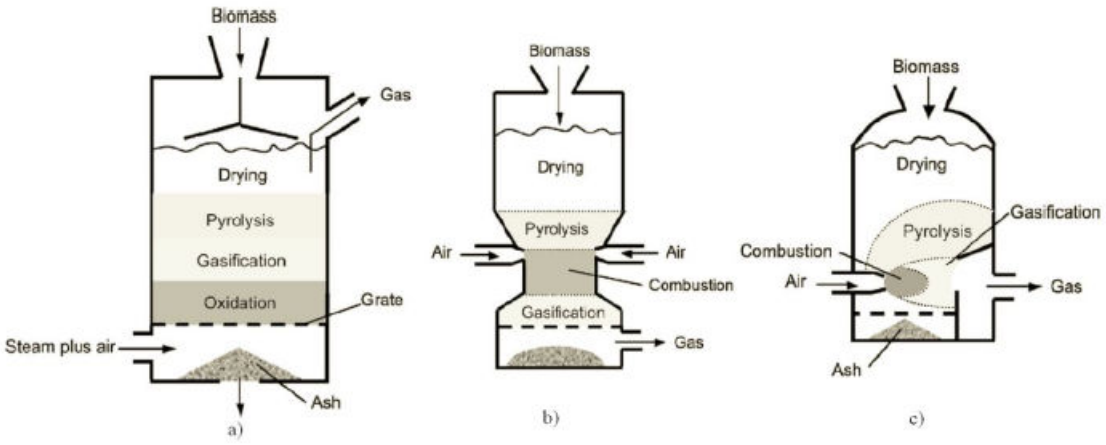

Figure 1.4: The three types of Fixed Bed Gasifiers: (a) Updraft (b) downdraft (c) Cross flow

- The gasification agent: Air-blown gasifiers Oxygen gasifiers Steam gasifiers
- Heat for gasification: Autothermal or direct gasifiers: heat is provided by partial combustion of the biomass and Allothermal or indirect gasifiers: heat is supplied from an external source through heat exchanger or indirect process. (i.e. separation of gasification and combustion zone).
- Pressure in the gasifier: Atmospheric or pressurized
- The reactor design: Fixed bed, Fluidized bed, Entrained flow, Twin-bed.

The choice of a gasification process depends on many parameters such as the installation scale, the fuel type and the future use of the produced gas. In the next paragraph, we will describe briefly some gasification technologies currently available in the market, on the basis of reactor design .

Fixed bed gasifiers

Fixed bed gasifiers can be classified into three categories: Updraft gasifiers, Downdraft gasifiers and Crossdraft gasifiers (see figure 1.4) .

In Updraft gasifiers, biomass is fed at the top of the reactor, moves downwards and is converted as it goes along. As a result of a complete conversion, the biomass reaches the bottom of the reactor in the form of ashes which are continuously removed. A continuous biomass feed allow to balance biomass conversion and keeping the biomass bed in a constant level and thus maintaining a stationary state into the gasifier. The air-intake is located at the bottom of the reactor and the produced gas leaves at the top. The biomass is then moving counter-currently to the gas flow and passes first through the drying zone, then through the pyrolysis zone, afterwards through the reduction zone and finally through the oxidation zone as it is depicted in the opposite figure.

In Downdraft gasifiers, biomass is still fed at the top of the reactor yet the air-intake is located at the top or at sides. The gas is moving in the same direction as the fuel and leaves the reactor at its bottom. The different zones through which the biomass passes are the same but their order is different. The injection of air in the char zone allows achieving low tar gas (less than 100 mg tar/Nm3).

Finally, in Crossdraft gasifiers, the air intake and the gas extraction orifice are located in the same horizontal level while the biomass is fed from the top of the reactor. Unlike the downdraft and

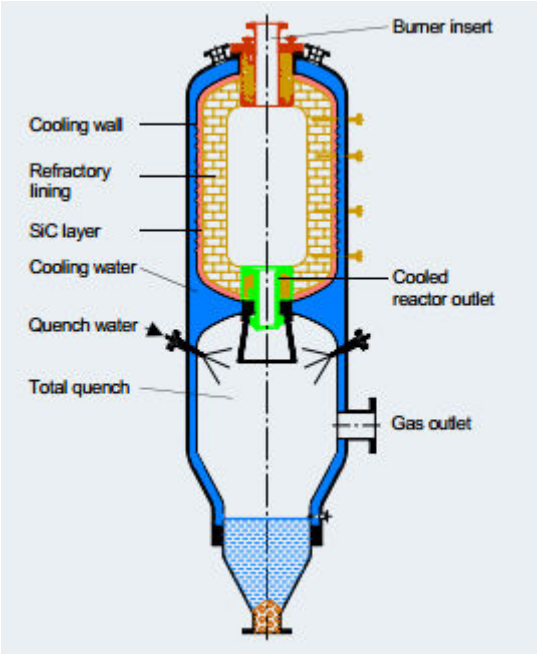

Figure 1.5: Refractory Wall Design of EFR for feed-stocks of less than 4% of ash content (SIEMENS technology)

updraft types, it releases the product from its side wall opposite to the entry point of the air for gasification. Because of this configuration, the design is also referred to as sidedraft.

Entrained Flow gasifiers

In entrained flow gasifiers, very finely pulverized feedstock is gasified in an oxygen/air and steam mixture. Entrained beds are available in large scale (> 100 MW) and often use fossil fuels as the particle size is limited. Temperature is very high (up to 2000°C), and process is often pressurized (up to 35 bar) [7]. Due to the high temperature, the ash melts and flows down on the reactor walls and is removed from the bottom as liquid slag. There are also non-slagging entrained beds gasifiers, but they are not as popular because slagging beds are more fuel flexible and it is impossible to avoid the slagging completely.

Some problems are encountered when considering entrained-flow gasification for biomass. Owing to a short residence time (a few seconds) in entrained-flow reactors, the fuel needs to be very fine, and grinding fibrous biomass into such fine particles is very difficult. However, torrefaction shows one way to unify the inhomogeneous feedstock, improve grindability and process efficiency as basis for use of biomass within a complex industrial plant [15] [16]. For biomass with CaO but no alkali, the ash-melting point is high, and therefore it has a higher oxygen requirement. The melting point of biomass ash with a high alkali content is much lower than that of coal. This reduces the oxygen required to raise the temperature of the ash above its melting point. However, molten biomass ash is highly aggressive, which greatly shortens the life of the gasifier's refractory lining [7].

Entrained Flow Gasification pave the way for large throughput biofuel projects requiring very clean syngas. The SIEMENS group intend to implement a First-time application of Entrained Flow Gasification and Torrefaction in a large-scale Commercial Demonstration Project - the WOOD-SPIRIT Biomethanol Project.

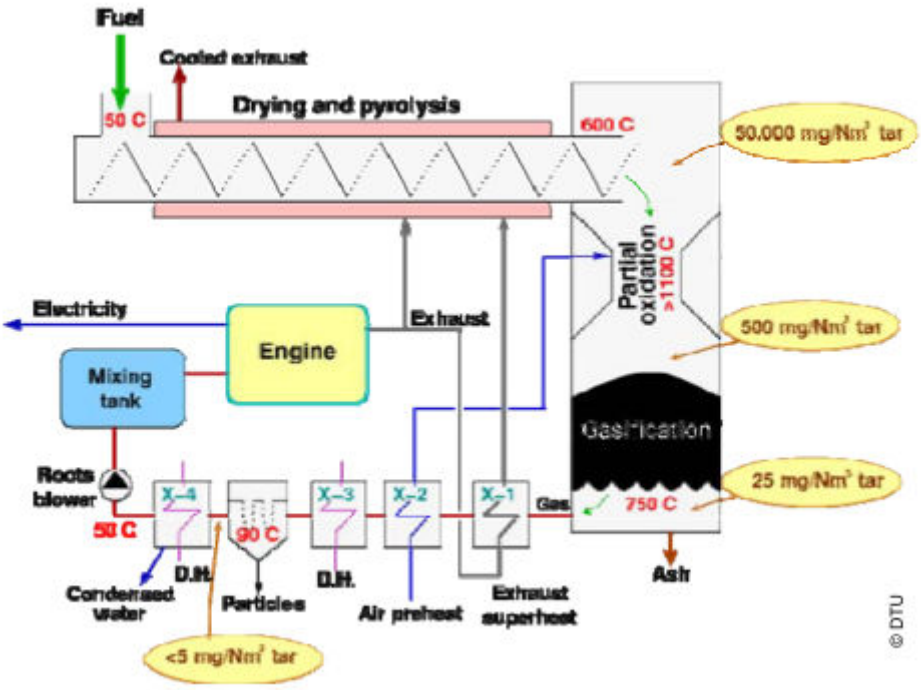

Figure 1.6: Staged gasifier pilot plant in DTU

Staged gasifiers

In conventional fixed bed gasifiers different zones can be identified. Their sequence order varies with the gasifier type. These zones are not physically fixed but moving up and downwards depending on gasification conditions. In a multi-stage gasifier, the two main steps of pyrolysis and char gasification are performed in separate reactors. In the first one, biomass is dried and pyrolysed, the volatiles and char produced are fed in the second reactor. In this latter, the pyrolysis gases are directed into an oxidation zone where they are combusted with a continuous air supply. The hot combustion gases (steam and carbon dioxide) react with the char bed which lead to the H_2 and CO production. An example of a staged gasifier is the Viking Gasifier in Denmark. The installation is at a pilot scale level. It was developed in 2002 by the "Biomass Gasification Group" from the Technical University of Denmark (DTU) in the frame of the "LIFTOFF" project for staged gasification. The pyrolysis is performed at 600°C while the char gasification is done in a second reactor at 1100°C (see figure 1.6).

Staged gasification, as demonstrated by the Viking plant and more recently by the "multi-stage"-type NOTAR reactor designed by Xylowatt (see figure 1.7), has confirmed its potential for low and medium energy production (up to 5 MWth). The "multi-stage"-type NOTAR reactor physically separates the 3 phases of the gasification process, namely pyrolysis, combustion and reduction. Tar content of the syngas upon exiting the reactor is less than 100 mg/Nm^3, the wood-to-gas conversion output is over 98% with no production of clinker (solid residue). Optimism with respect to staged gasifiers is justified as they produce much less tar than other processes.

In such a process the CO_2 and H_2O produced in the combustion zone are reduced by the activated char to produces a syngas principally composed of H_2 and CO. Some researches continue to provide valuable information on the characteristics of the gasification zone for the mastering and efficient design of such gasifiers [17]. The mixed atmosphere gasification of LHR chars with CO_2 and H_2O studied in the scope of the present thesis will concern such kind of process.

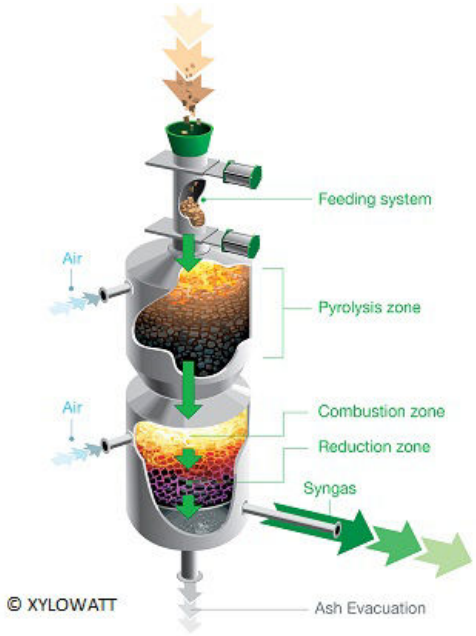

Figure 1.7: The "multi-stage"-type NOTAR reactor from Xylowatt

Fluidised bed gasifiers

The fluidised beds are composed of inert material (sand, dolomite...) and fuel particles. A gasifying agent (air, steam, carbon dioxide or mixture) is injected through the porous bottom of the reactor with a sufficient pressure that allow holding the whole particles in suspension. The more we increase the gasifying agent velocity the more the particles are moving vigorously and giving a shape of a boiling liquid. The inert material is heated first by a fossil fuel combustion. Once it is hot enough, no more fossil fuel is needed. The biomass is then fed via a dosing screw and mixed with the hot sand. The fluidization allows a closely contact between the biomass and the hot sand and leads to a fast pyrolysis and decomposition into a combustible gas. There are mainly two types of fluidised bed gasifiers: bubbling fluidised bed (BFB) and circulating fluidised bed (CFB) (see figure 1.8).

Fluidized bed gasifiers have a number of advantages over fixed beds, especially with regard to mixing, reaction rates, and the possibility of being built in sizes far above those of fixed-bed gasifiers. FB gasifiers are also more tolerant with the fuel particle size and quality. The technology is suitable for biomass, municipal waste or blends of several biomass, coal or lignite[18] [19] [20] [21] [22].

Granular bed works as a heat exchanger so the heat and mass transfer from the fuel is improved and throughput and heating value of the product gas are higher [23] [7] . The main difference between Bubbling and circulating FBG is that the latter type is always built with recirculation of particles. Recycling of fines leads to a greater efficiency and higher carbon conversion by increasing the residence time of particles. The char particles can be gasified alternatively with H_2O, CO_2 (in the gasifier) and O_2 (in the combustor) in the recycling process. CFBG is taller and provided with a continuous solids recycling system for re-injection of particles into the bed (particle separator, return leg and seal). CFBG operates with higher superficial velocities, typically in the range of 2 to 5 m/s,where as the velocity in the BFBG is only 0.5 to 2 m/s which allows particles mixing without carrying them out of the fluidized reaction zone. For the same ratio of fuel-to-fluidization gas and for the same cross-section, the gasifier is fed with higher fuel flow rate in a CFBG than in a BFBG. The entrainment of material from the bottom bed and the recycling in CFBG increase the solids flow as well as the gas-solid contact time in the freeboard.

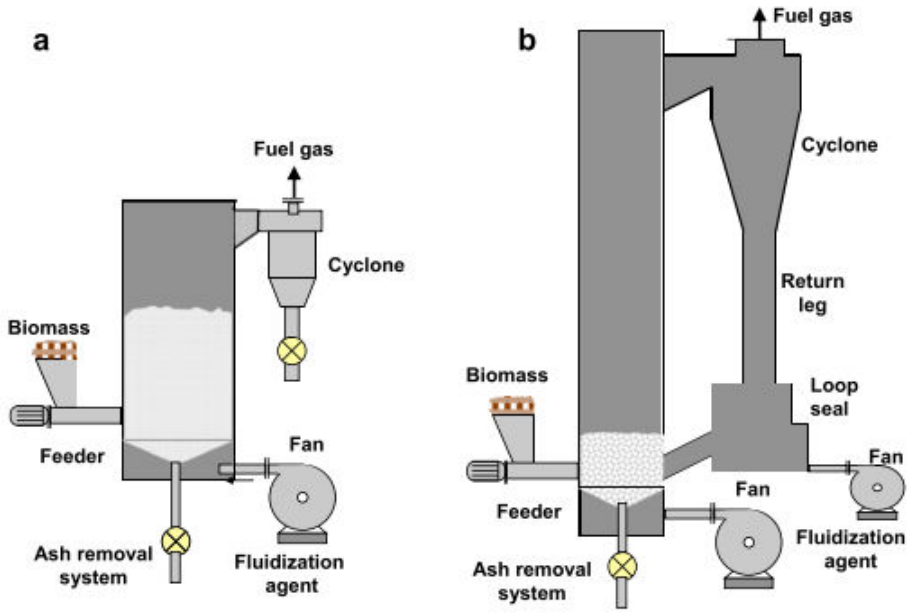

Figure 1.8: The two types of FBG: (a) Bubbling FBG; (b) Circulating FBG

1.2 A focus on the char properties

1.2.1 What is the char?

The char is a carbonaceous and porous solid resulting from the biomass pyrolysis reaction among other products which are gases and tars. The char yield is highly by the pyrolysis operating conditions. The char yield decreases when increasing temperature for both LHR and HHR pyrolysis conditions. However, slow pyrolysis is used to maximize the char yield. For instance, at a temperature of 800 K, the wood char yield for LHR conditions varies between 25% and 35%, while it is in the range of 10-20% in the case of HHR conditions [14]. Intrinsic biomass properties such as the lignin and mineral content influence the char yield. Agricultural residues, which contain higher mineral matter content and a higher lignin proportion than woody biomasses produce higher char yields. The mineral matter, principally alkali compounds, favours charring reactions [14]. The biomass char formed in typical gasification conditions encountered in CFBG or SG, is a quite complex, non-organised material containing a tremendous number of chemical functions. It is highly porous and contains beside carbon, which is its major constituent, oxygen, nitrogen, hydrogen and various mineral species depending on the parent biomass composition. The char properties can be classified into three main groups [24]:

- Textural properties
- Structural properties
- Chemical properties

1.2.2 The char textural properties

The biomass char results from the thermal decomposition of the parent biomass material. Depending on the pyrolysis conditions, it keeps more or less the features of the initial material. The thermal

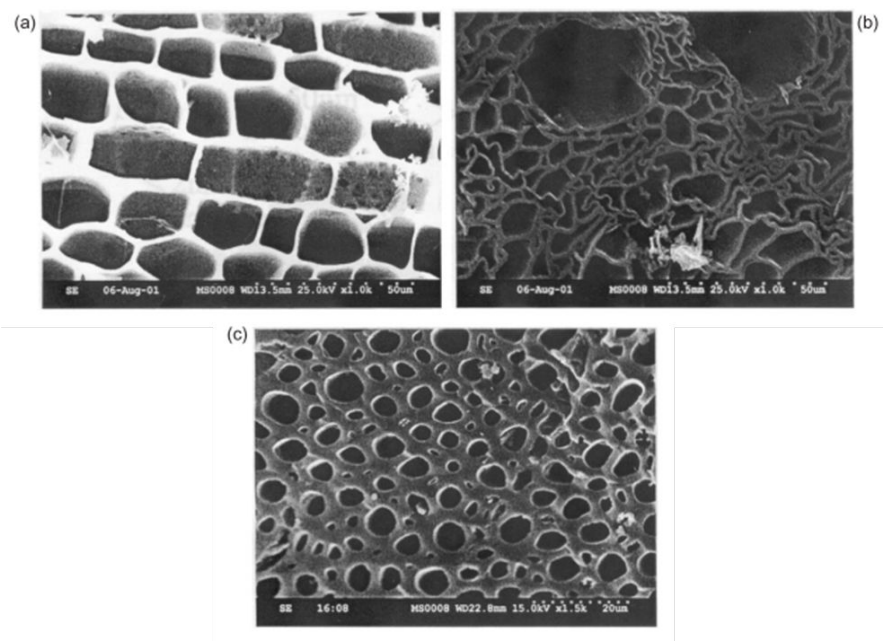

Figure 1.9: SEM micrographs of porous chars: (a) castor oil plantwood, (b) bagasse, and (c) babool wood.

decomposition results in a mass loss of the parent biomass solid material. A part of the solid constituents decompose into tars and gases resulting in less solid and more void [25].

The biomass char is a very porous material. The internal char porosity is most often non uniform. Inside a biomass char, there can a wide distribution of pore size resulting from the anisotropic structure of the parent biomass and the creation, widening of existing pores after the pyrolysis reaction. The pores can also be of different shapes, open or closed, connected or not. Figure 1.9 shows the difference of pore shapes of chars obtained from castor oil plantwood, bagasse, and babool wood [26].

According to their size, the pores are classified usually into three groups: (i) macropores having average diameter higher than 50 nm, (ii) mesopores with an average diameter comprised between 2 and 50 nm, and (iii) micropores having an average diameter less than 2 nm. SEM images of biomass chars are quite insightful for apprehending the porosity distribution as well as the pore shapes and sizes. Nevertheless, micropores are not distinguished with this technique, which limits its use to the analysis of large mesoporosity and macroporosity. An illustration of the char porosity is given shown in figure 1.10.

Other techniques such as Hg porosimetry or gas (N_2, CO_2, Ar, He) adsorption on the porous char are used to determine the char porosity, the Total Surface Area (TSA) and the pore size distribution (PSD) of a porous char. Theoretical model were established to determine these parameters. For instance, the BET model or the Density Functional Theory (DFT) model are widely used to determine respectively the TSA and the PSD of porous carbon materials. They are thought to be quite reliable and have a good degree of precision [27] [28] [29] [30] [31] . An example of N_2 adsorption isotherms and PSD of hemp (Cannabis sativa L.) steam activated chars is shown in figure 1.11.

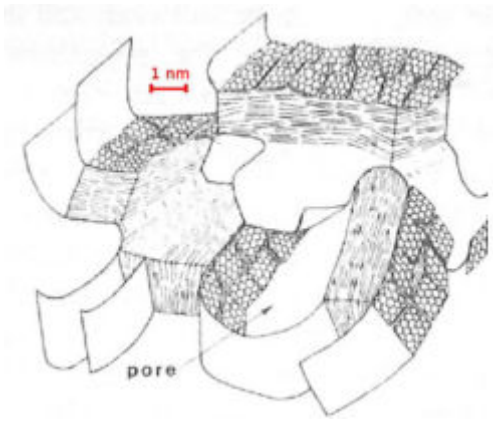

Figure 1.10: Illustration of carbonaceous char structure and porosity [24]

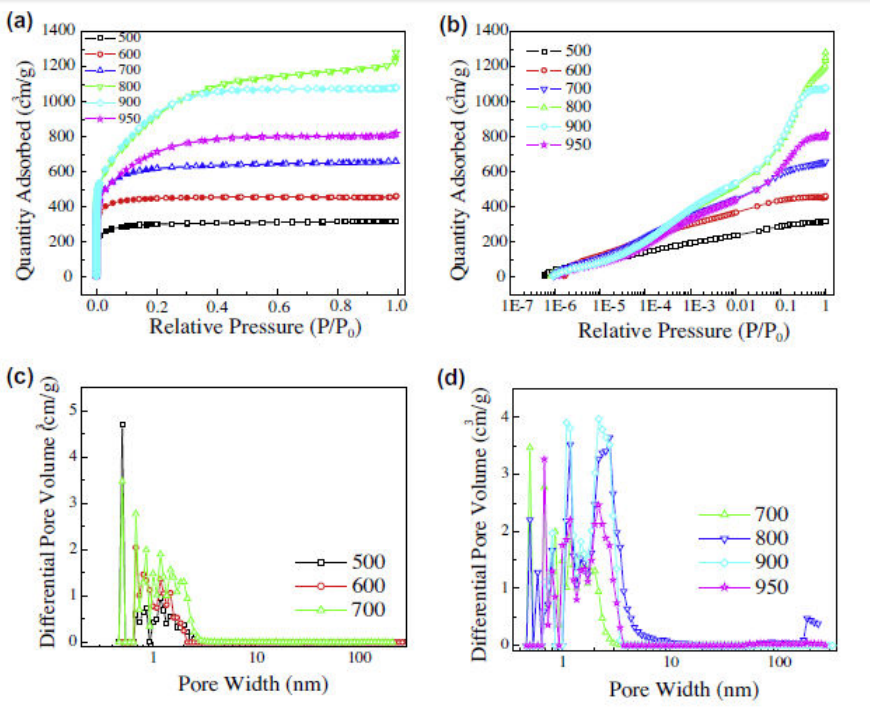

Figure 1.11: Nitrogen adsorption desorption isotherms at 196°C on synthetic activated carbons prepared at different temperatures (a), semilogarithmic scale adsorption isotherms (b) and DFT pore size distributions (c) and (d) full symbols, adsorption; open symbols, desorption [27]

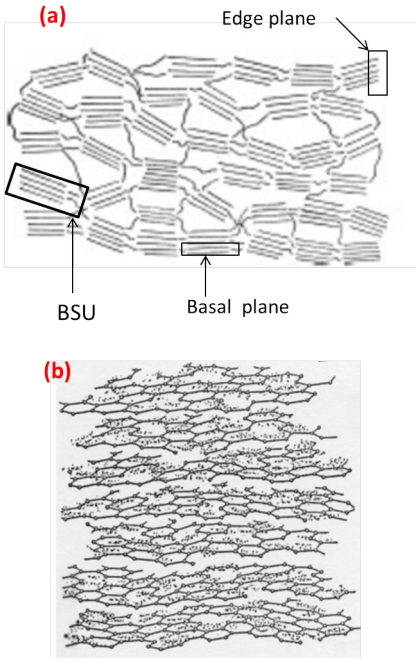

Figure 1.12: Illustration of a biomass char structure (a) and a magnification of a BSU (b)

1.2.3 The char structural properties

The biomass char can be viewed as a disordered assembling of carbonaceous structural units called Basic Structural Units (BSU). BSU are composed of aromatic rings more or less condensed. A biomass char contains different BSU of different sizes. These BSU contain different type of carbons:

- Basal plane carbon sites which contain de-localized sp2 carbons having a low reactivity.
- Prismatic edge carbon sites which contain the functional groups and are thought to be the reactive sites.

A schematic representation of the char structure is shown in figure 1.12 with the illustration of BSU as well as basal plane and prismatic edge carbons.

High Resolution Transmission Electron Microscopy images are very insightful for understanding the structural features of a carbonaceous material [32] [33] [34]. An example of Saccharose coke and Tobacco char HRTEM images are shown in figure 1.13.

According to the literature, the biomass char structural features can be analysed through X-Ray Diffraction (XRD) analysis or Raman Microscopy analysis. Nevertheless, according to several carbon specialists, Raman spectroscopy would be more suitable [35]. These latter emitted severe critics the validity of the Graphitic Microcrystallite Theory linked to the XRD analysis of disordered carbons.

The structure of a biomass char changes with temperature. It becomes more ordered as the temperature increases. The heat treatment induces the carbon enrichment of the char and the desorption of inherent oxygen, hydrogen or other hetero-atoms. The char structure evolves towards that of a graphite material at very high temperature. Figure1.14 illustrates the graphitization process of a disordered carboneaceous material with increasing temperature.

Raman spectra of disordered carbons contain two bands of major interest, namely the D-band (1350 cm^{-1}) and the G-band (1580 cm^{-1}). The D-band is identified with Defective or Disorganized carbon, and the G-band with Graphitic carbon. The origins of the D-band, in terms of possible

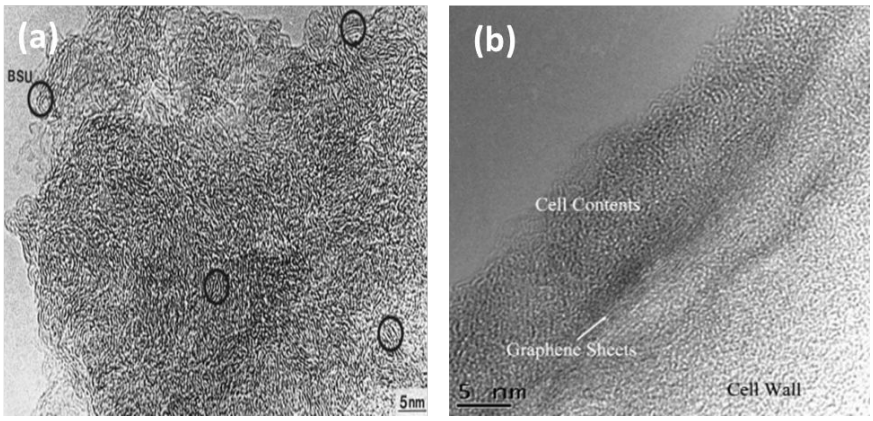

Figure 1.13: Saccharose-based coke heat-treated at 1000°C (a) and Tobacco char heated to 550°C (b)

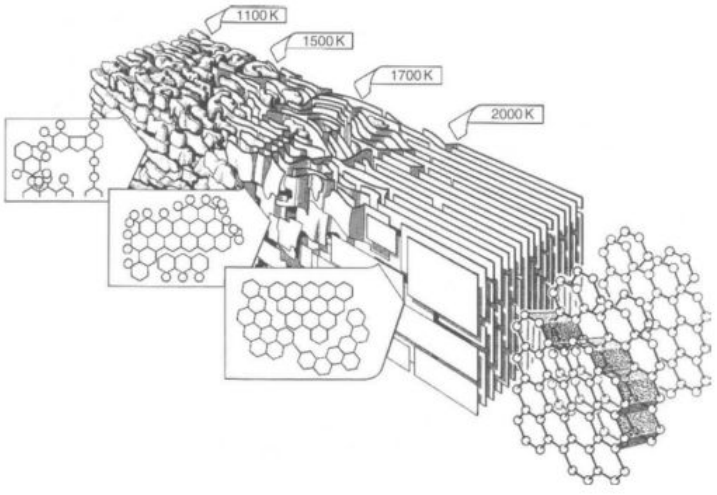

Figure 1.14: Structural changes occurring during the heat treatment of a graphitizable carbon

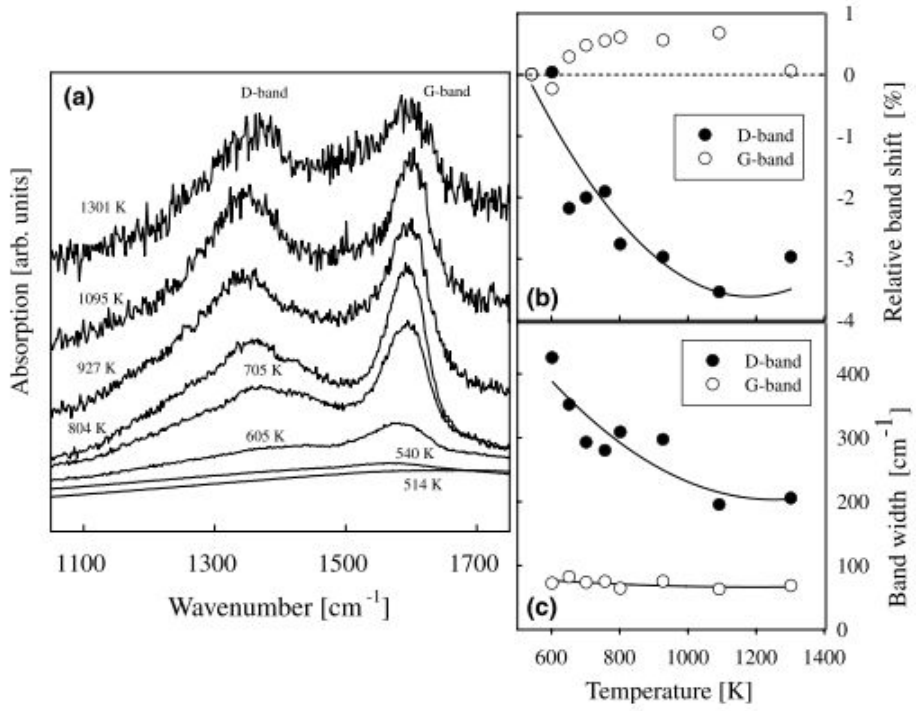

Figure 1.15: (a) Raman spectra from normal wood specimens for selected pyrolysis temperatures. (b) Relative peak shift and (c) peak-width of the D-band and the G-band as function of temperature. Solid lines are drawn as a guide for the eye [36].

defective structures in carbons, remain quite obscure. The D-band origin is associated with arrangements of carbon atoms in hexagonal format ranging from a benzenoid molecular type to defective graphene layers, the defects being lack of continuity in the layer, point defects, multiple vacancy defects, nitrogen or oxygen in the layer or at edges of layers, etc. Similarly, the origins of the G-band cannot be identified with graphitic carbon but is rather linked to an in plane vibration in all sp^2 carbon materials (graphene layer for instance) [35]. RMS technique has been used to study structure in carbons and the changes induced by heat treatment or gasification [37] [38] [39] [40] [41] [42]. Figure 1.15 and 1.16 show the evolution of biomass char structures with temperature and upon contact with steam.

In the first order region (800-1000 cm^{-1}) of disorganized chars Raman spectra, the so-called D and G bands are overlapping. This overlapping is due to the fact that the spectrum is the combinations of several bands corresponding to different carbonaceous structures. The Raman spectrum can be deconvoluted into several bands according to the nature of the carbonaceous structure present in the material. For instance, Jawhari [38] characterized the structure of several commercially carbon black material and found that the Raman spectra of Printex and Vulcan carbons are quite well represented by a 3 bands. Sadezky [43] has successfully reproduced the Raman spectra of Printex and diesel soot considering the presence of 5 carbonaceous structure in these materials. In another register, Sheng [39] evidenced the structural evolution of a coal char during combustion and considered a five band deconvolution of the coal char Raman spectra. He demonstrated the ordering of the coal char while reacting with oxygen. Other authors considered a 10 bands deconvolution of biomass and coal chars while characterizing their structural evolution during pyrolysis and gasification [40] [44] [45] [46] [47]. An example of a curve-fitted Raman spectrum of a coal char is shown in figure 1.17.

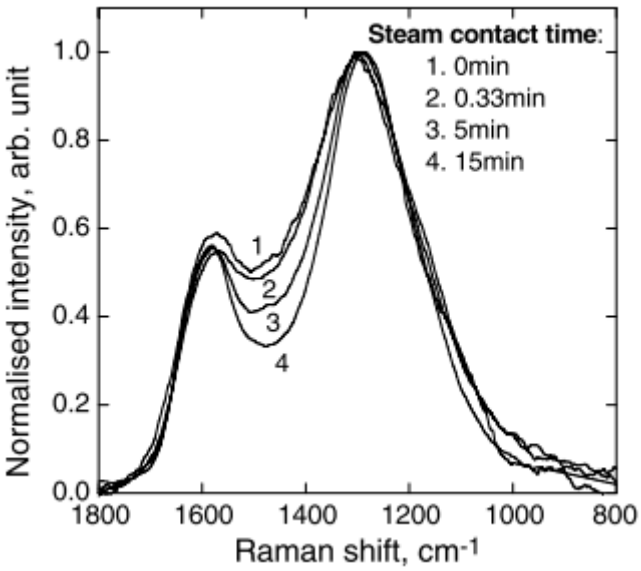

Figure 1.16: Changes in normalised Raman spectra during the gasification of cane trash char in 20% steam and argon at 900°C. Times of char contact with steam are shown [42]

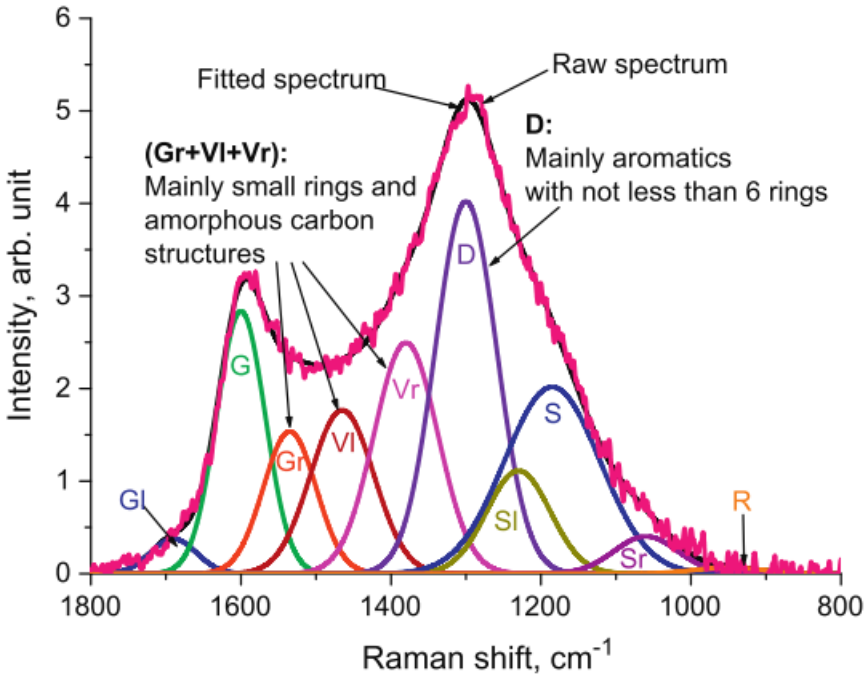

Figure 1.17: A curve-fitted Raman spectrum of the char prepared from the gasification of Collie sub-bituminous coal in pure CO_2 at 800°C [46]

The char texture and structure are highly linked. The disposition of the char BSU forms the porosity inside the char. For instance, the space between two BSU can be affected to a micro-porosity while the arrangement of BSU blocks is linked to the meso-porosity and macro-porosity (see figure 1.10).

1.2.4 The char chemical properties

The char chemical properties can be viewed at two levels: the elemental composition and the surface functional groups.

The char elemental composition

As stated above, the char is mainly composed of carbon. Its elemental composition depends on the initial biomass composition as well as on the pyrolysis conditions[48]. The elemental composition changes with the final pyrolysis temperature as well as along the gasification [30] [31]. The chemical composition comprises an organic part, related to the presence of *C, H, O, N* and *S* atoms, and a mineral part related to the presence of mineral species such as *K, Ca, Na, Mg*, heavy metals etc... The *C, H, O, N* and *S* contents are determined by elemental analysers, while the mineral fraction composition is determined by Inductive Coupled Plasma (ICP) analysis, Atomic Absorption/Emission Spectroscopy (AAS/AES) or X-Ray Fluorescence among others. The char elemental composition is of high interest as it is linked to its High Heating Value (HHV), to the potential pollutant emissions when combusted or gasified (*NOx, SOx, HCN*, Heavy metals etc...)[49]. The mineral species affects highly the char gasification rates and can be classified in tow main groups of catalysts (*K, Ca, Na, Ni..*) and inhibitors (*Si, P, Pb*) [50].

The char surface functional groups

Inside the porous char, the different atoms have a defined disposition forming the BSU which arrangement affects directly the char texture as stated above. More closely, zooming at a BSU level, we can distinguish the organic functionalities on the zigzag and armchair sites. We often refer to them as "Surface Functional Groups" (SFG). Figure 1.18 shows an example of functional groups that can potentially exist on the char surface. Carboxyl, carbonyl, phenol, quinone, and lactone groups, have been identified on carbon surfaces [51]. These sites containing oxygen atoms are highly reactive.

The SFG can be analysed qualitatively and quantitatively by several techniques such as Fourier Transformed Infra-Red (FTIR) spectroscopy [30] [28], X-ray Photo-electron Spectroscopy (XPS) [52] and Temperature Programmed Desorption and gas analysis by Mass spectrometry (TPD-MS) [51] [53] [54] [55] [28]. The TPD-MS technique allows a quantitative determination of the SFG. it consists of heating the char sample in vacuum at a low heating rate. The decomposition of the SFG leads to the emission of CO_2, CO, H_2O and H_2 in major part. According to the temperature and to the nature of the emitted gas, the nature of the surface functional groups can be determined. For instance, Figueiredo et al [51] as well as Zhuang et al [54] used this technique to follow the evolution of coal char functional groups during oxidation with O_2, while Klose et Wolki [55] measured the evolution of the CO surface complex for CO_2 and H_2O gasification reaction. This technique can be coupled to the results given by the XPS technique for a more precise determination of the nature of SFG [52].

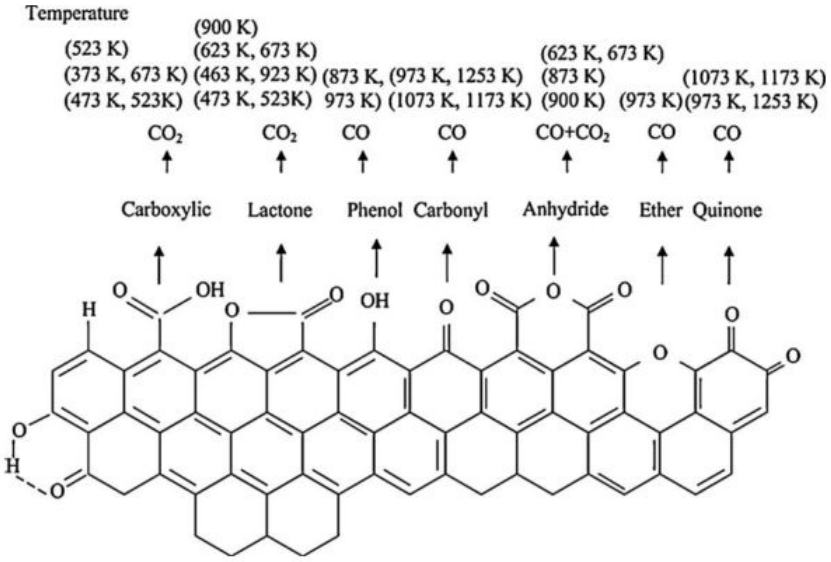

Figure 1.18: Example of functional groups that can potentially exist on the char surface [51]

1.3 Phenomenology of the char gasification reaction

The char gasification reaction is a heterogeneous solid-gas reaction between the carbonaceous char and gasifying medium (steam or carbon dioxide for instance). The char gasification reaction may be described by the following steps: (1) film diffusion of the gasifying agent, (2) diffusion into the particle, (3) adsorption onto the reaction surface, (4) chemical reaction, (5) desorption of the reaction gas product from the char surface, (6) diffusion of the product gas through the particle and ash layer,(7) film diffusion back to the ambient gas. A gross illustration of the gasification reaction is given in figure 1.19.

The reality is in fact much more complicated. There can be diffusional limitations as the char pores are of various sizes and shapes. Some of them are inaccessible to the reactant gas if they are narrower than the reactant gas kinetic diameter. There exist also closed porosity inside the char, which is also inaccessible. Even if the reactant gas enters a pore, it must reach the reactive sites as not all the pore surface is reactive. There are only some reactive sites where the reactant gas can adsorb and react.

1.3.1 Char gasification in the chemical regime

The heterogeneous gasification reaction implies a diffusion-reaction competition. The gas diffuses first in the porous matrix and react in when meeting an active site. If the diffusion characteristic time is greater than the reaction characteristic time, the reactant gas will diffuse in the whole char particle, adsorb on the active sites and reacts afterwards. In this case, the whole char active sites participate to the gasification reaction (assuming that active sites in closed porosity and very narrow pores are negligible). The reaction is, in this case, performed in the chemical regime. Experimental conditions that are required to perform the gasification reaction in the chemical regime are low temperature and very small particle size. Several authors insist on this crucial point and require more attention from experimentalists when determining intrinsic gasification reaction kinetic constants because of quite disparate kinetic data in the literature, and which are likely due to diffusional limitations [14] [57].

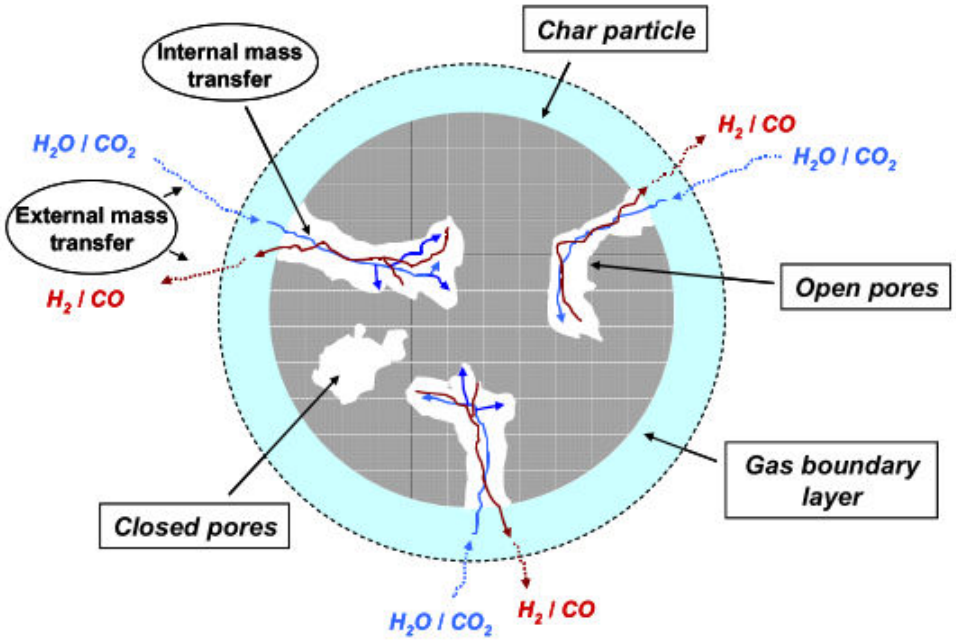

Figure 1.19: Phenomenology of the gasification reaction [56]

1.3.2 Diffusional limitations

Diffusional limitations began to appear when increasing the temperature, the chemical reaction rate becomes higher than the rate of gas diffusion in the particle. The reacting gas is consumed before reaching all the internal available reactive surface. The gasification reaction occurs in only a part of the reactive surface. In this case, internal diffusion limitations exist and the reaction rate is not the intrinsic rate. Internal diffusion limitations are accentuated by increasing the particle size. At a quite high temperature, the chemical reaction rate is so high compared to external gas transfer rate that the consumed quantity of the reacting gas can not be replaced rapidly. A product gas layer with a low concentration of the reacting gas is consequently formed around the char particle which limits the reaction. In this case the gasification reaction is controlled by external mass transfer.

It should be also pointed out that there are two levels of diffusional limitations which must be distinguished:

- diffusional limitations at the particle level
- diffusional limitations at the pore level

For instance, if we consider a spherical char particle, the diffusional limitations at the particle level are related to the reactant gas concentration uniformity along the particle radius (from the surface to the particle core). In the chemical controlled regime, the reactant gas concentration is uniform along the particle radius in the accessible porosity. However, if there exist inside the char particle pores of sizes inferior to the molecular size of the reactant gas, these latter would be not accessible. This situation shows clearly despite of good experimental conditions of small particle and low temperature, ensuring no diffusional limitations at the particle level, there can be diffusional limitations at the pore level which are dependent on the char texture. Figure 1.20 shows a schematic representation of diffusional limitations at the pore level. CO_2 molecules are diffusing inside a micropore, larger than that of their molecular size (>0.3 nm), while they can not access to very narrow micropores (<0.3 nm).

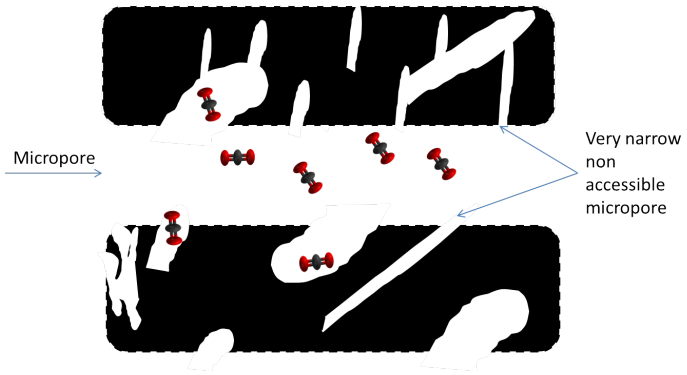

Figure 1.20: Schematic representation of diffusional limitations at the pore level

1.3.3 Heat transfer limitations

Char gasification reaction is an endothermic reaction consuming energy. When the particle is small enough, the characteristic time of heat conduction through the particle is quite low relatively to that of the reaction characteristic time. The particle temperature is uniform. Increasing the particle size increases the heat conduction characteristic time. A temperature gradient may appear inside the char particle.

1.4 Factors affecting the char reactivity

1.4.1 The char reactivity

The char reactivity, towards a gas or a mixture of gases, represents the rate of char consumption divided by an extensive property, namely the char mass, Active Surface Area (ASA) or Total Surface Area (TSA). For instance, when it is divided by the mass, the char reactivity reads:

$$R_{(t)} = \frac{1}{1 - X_{(t)}} \times \frac{dX_{(t)}}{dt} \tag{1.12}$$

Where X is the conversion level given by:

$$X_{(t)} = \frac{m_0 - m_{(t)}}{m_0 - m_{ash}} \tag{1.13}$$

Where m_0, m_t and m_{ash} are respectively the initial mass of char, the mass at a time t and the mass of the residual ash.

Because of the much lower rates of char gasification compared to the biomass pyrolysis, the char yield and reactivity are the main factors affecting the feed rate and size of combustors and gasifiers [7] [14]. The solid char gasification can be performed with steam, carbon dioxide or a mixture of these gases. In practical situations, inside a gasifier, these gaseous species are present and can simultaneously interact with the char. The char yield and reactivity are highly affected by the pyrolysis and gasification operating conditions (temperature and gasifying medium pressure) as well as by the intrinsic properties of the parent biomass and those of the resulting char. A brief literature review is presented in the next paragraphs to state on the complexity and the multitude of factors affecting the char reactivity. The char gasification reaction is governed by a high number of coupled factors inherent to the solid or relative to the gasifier operating conditions. These factors can be

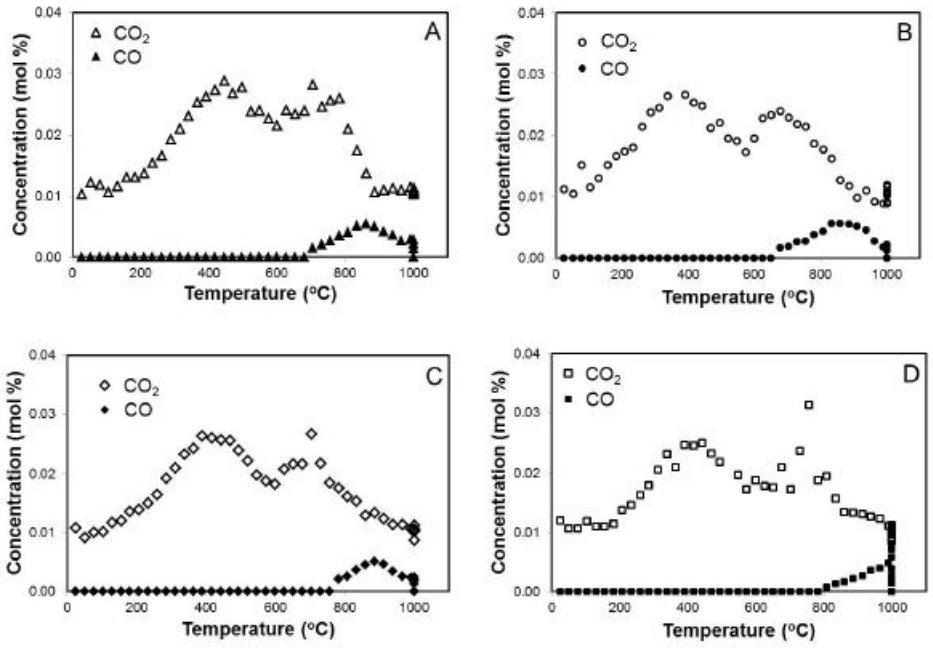

Figure 1.21: TPD profiles of partially gasified chars. A.H_2O-750°C-30% B.CO_2-750°C-30% C.H_2O-750°C-60% D.CO_2-920°C-30%

divided into factors: those influencing physical processes such as gas diffusion and heat transfer, and those affecting the gasification reaction such as the SFG, mineral species and char texture.

1.4.2 Factors affecting the intrinsic gasification reaction rate

Surface Functional Groups

The chemical reactivity of a char finds its origin in the presence of the SFG on the char surface. These latter constitute the active sites were the gasifying agent adsorbs and reacts. Some authors argue that the intrinsic char gasification reactivity is in fact a resultant of a reactivity distribution of the functional groups located at the char surface, which is very reasonable as the chemical functionalities at the char surface do not have the same reactivity toward a gas [24]. For practical reasons, it is more suitable, but not very realistic, to consider a single rate constant for char without accounting for the individual contributions of the SFG to the char reactivity. As discussed in the previous paragraphs, it is possible to quantify the SFG on a char through TPD and mass spectroscopy quantification of the desorbed species [51] [53] [54] [55] [29]. For instance Klinghoffer [29] analysed the nature of SFG on partially gasified chars with CO_2 and H_2O through the CO_2 and CO TPD emission profiles. The results are shown in figure 1.21. Zhuang et al. as well as Figueiredo et al. [51] used the TPD-MS technique to follow the evolution of the SFG during char oxidation with O_2. XPS technique can be coupled to TPD-MS results for a more precise identification of the SFG of a carbonaceous material [52].

Increasing number of studies deal about the mechanism of gasification using a computational chemistry and molecular modelling approach [58] [59] [60] [61]. An example of Biomass- and Coal-Derived Chars optimized molecular geometries is shown in figure 1.22. Through thermodynamic calculations and Density Functional Theory study, researchers evidenced the most plausible mechanisms of gas molecule adsorption and reaction on such molecular model of biomass and coal chars.

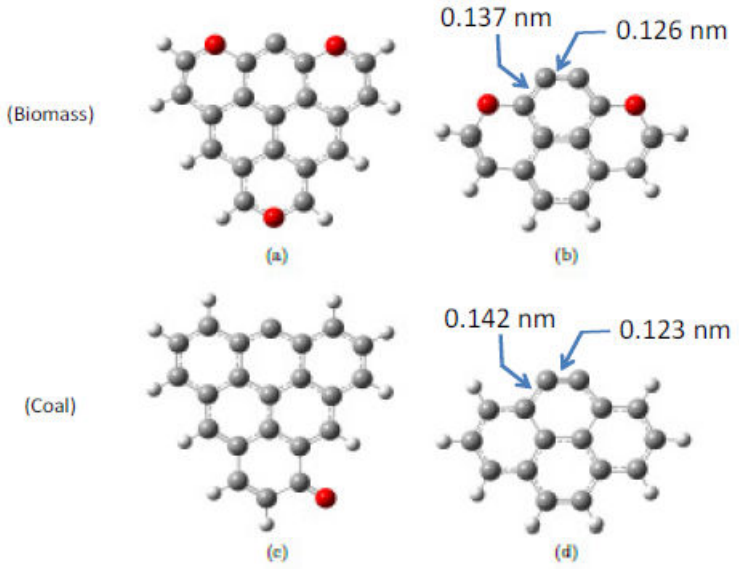

Figure 1.22: Biomass- and Coal-Derived Chars: Optimized molecular geometries

Some authors studied also the effects of the presence of surface functionalities on the gas adsorption process [59].

Reactive Surface Area (RSA) and Active Surface Area (ASA)

Several researchers succeeded to reconcile gasification kinetic models with experimental data by introducing the effective area participating to the gasification reaction [62] [63] [64] [55].

For instance, Lizzio et al [62] measured a "Reactive Surface Area" (RSA) corresponding to the amount of desorbed reactive CO complex from the char surface during CO_2 char gasification reaction by means of Temperature Programmed Desorption. The authors found similar evolution shapes of the RSA and reactivity of bituminous coal char, Saran char, lignite char with the conversion extent.

More recently, Klose et al [55] made the same findings concerning the dependence of the char reactivity on the RSA. As shown in figure 1.23, the reactivity of oil palm shell char and beech wood char increases linearly with the RSA for both H_2O and CO_2 gasification reactions.

Another concept to approach the intrinsic reactivity of a carbon material is the Active Surface Area measurement, which consists roughly in cleaning the char surface by a thermal treatment and adsorbing on O_2 at a low temperature in the range of 200-300°C [64] [65]. The quantity of adsorbed Oxygen on the char surface is an index of the carbon reactivity as it can be related directly to the number of active sites on the char surface. The ASA was found to represent a small part of the TSA. Not all the surface participates to the gasification reaction. Laine et al measured the evolution of the TSA and ASA of chars during combustion with oxygen and showed the high difference that exists between TSA and ASA [64]. The ASA was successfully introduced to measure the reactivity of coal chars to oxygen and would be therefore specific to this molecule. To have a representative char reactivity index to CO_2 or H_2O, it would be more reasonable to replace the O_2 molecule by these latter during the chemisorption step. The obtained ASA would be specific to each gas.

Structural features

As explained above, the char structure highly affects the char reactivity. Many authors evidenced, thanks to Raman spectroscopy, the link between char structure and reactivity. More ordered chars

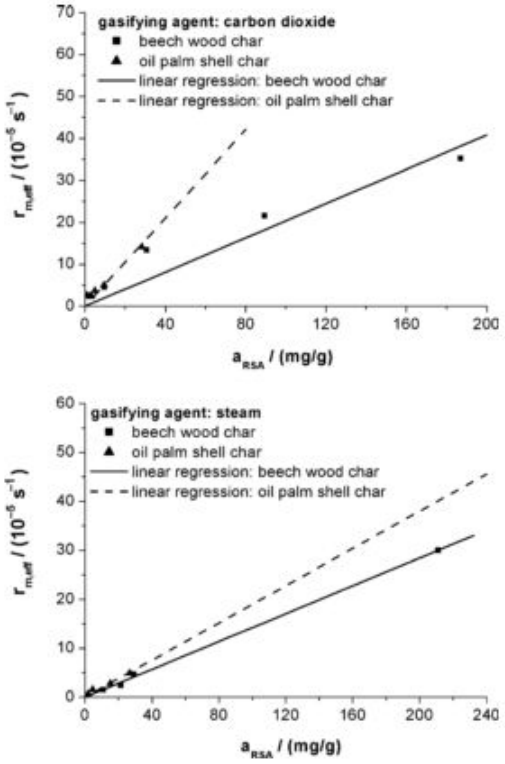

Figure 1.23: Specific reaction rate as a function of the specific reactive surface area

are found to be less reactive. Char structural ordering is promoted at high temperatures and long soaking time. The char structural ordering is accompanied by a loss of oxygen functional groups which are thought to be the major and most reactive sites on the char surface [40]. This shows the intimate relation ship between the different char properties. A brief discussion on this subject given at the end of the present section.

Asadullah at al. [40] found that the reactivity to oxygen of chars obtained from a mallee wood decreases with increasing the temperature from 700°C to 900°C. The increase of temperature was also accompanied by a loss of oxygen functional groups and ordering of the char which are likely behind the decrease in reactivity.

Tay et al. [66] studied the structural features of partially gasified char, in different atmospheres containing reducing (H_2O) and oxidising (CO_2 and O_2) gasifying agents, using FT-Raman spectroscopy followed by spectral deconvolution. The authors found that the presence of H_2O during gasification at 800°C plays a decisive role in the evolution of char structure, in particular by decreasing the relative ratio of small and large aromatic ring structures in char. Keown et al. made similar observations as the structure of cane trash chars changes drastically after contact with steam [42].

Li et al. [46] also studied the evolution of the char structure during gasification with CO_2, H_2O and their mixtures using FT-Raman spectroscopy followed by spectral deconvolution. Drastic changes in char structure were perceived during the reactions. The structural changes were different respectively in CO_2 and H_2O atmospheres. The char char obtained in mixed atmosphere showed a very close structure to that obtained in single H_2O atmosphere (see figure 1.24). The authors came to the main conclusion that CO_2 and H_2O gasification reactions follow different pathways. For a defined gasification reaction, the char structural features did not vary in the temperature range of 800-900°C.

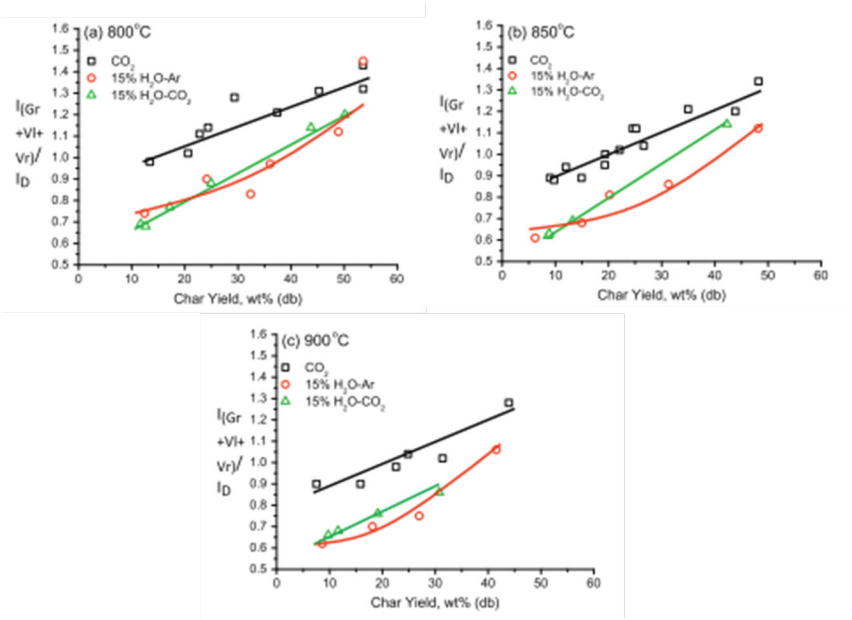

Figure 1.24: Raman band ratios $\frac{Gr + Vl + Vr}{D}$ as a function of char yield for the chars produced in the gasification of Collie sub-bituminous coal in pure CO_2, 15% H_2O balanced with Ar and 15% H_2O balanced with CO_2 at (a) 800°C; (b) 850°C; (c) 900°C

Mineral species

The catalytic effect of minerals in thermochemical reactions of pyrolysis, combustion or gasification has been demonstrated in several studies either by loading minerals in the raw biomass or by removing them by leaching with water or acid solution [67] [68]. The gasification rate increases with loading minerals to a certain saturation limit beyond which carbon pores are blocked. A wide range of minerals are known to enhance the gasification rate when they are present in the biomass. Zhang et al. tested 14 different biomass samples including sawdust, bark and some agricultural wastes by gasifying with 50 kPa steamat 850°C chars which had been formed at 900°C. Char reactivity measurements indicate that the inherent alkali metals are more effective than inherent calcium to catalyse the gasification reaction. For chars containing very high silica contents (rice husks and bagasse), alkali silicates were formed at low temperatures and their catalytic action was curtailed. A random pore model was successfully applied to describe burnout, with the two parameters related to potassium content [69].

Keiichirou Mitsuoka et al [70] studied the gasification of cypress char with carbon dioxide after loading it with alkali catalysts (potassium and calcium). The Ca-loaded char had the highest gasification rate in contrast with the acid washed-char which had the lowest calcium amount and the lowest reactivity. The authors concluded that the C-CO_2 gasification reaction was accelerated on CaO surface. However, they pointed out that at lower temperature (1123 K) and higher carbon dioxide concentration (80%) the rate of gasification decreased which was probably due to the well-known CO inhibiting effect.

Huang et al [71] also reported the effect of 5 catalyst metals on the CO_2 gasification of fir char. They found that loading the biomass samples with catalysts metal improves the char reactivity in the increasing order of Mg, Fe, Ca, Na and K (see figure 1.25).

More recently Dupont et al [72] found that the char reactivity towards steam for various samples can be expressed as the product of kinetic term accounting for temperature and steam partial pressure

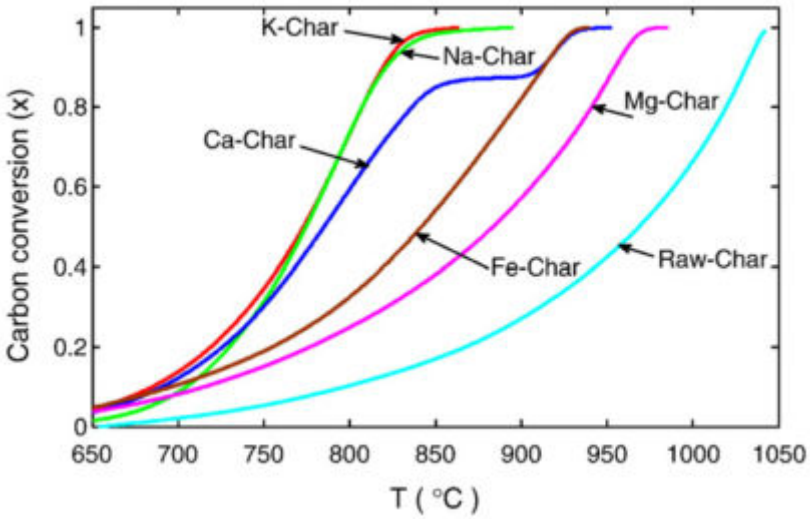

Figure 1.25: Carbon conversion of different metal loaded char samples [71]

dependence, and an empirical correlation bearing the concentration of potassium and silicon which respectively catalyse and inhibit the gasification reaction.

Hognon et al found that the effects of mineral species is preponderant at higher conversion levels beyond 70%[73]. The authors reported two typical behaviour of biomass char, those which reactivity decrease along the conversion having a K/Si ratio below one, and those having a K/Si ratio above one exhibiting a constant reactivity or slight decrease followed by reactivity increase beyond 70% of conversion. It is also reported in a quite exhaustive review on the action of minerals on char gasification, that the catalytic effect of potassium is much more pronounced with ordered graphitic-type structures [50]. The mineral content of the char changes with the extent of conversion. Depending on the nature of the reactant gas, some minerals are retained in the char while others leave it to the gas phase [31].

1.4.3 Factors affecting physical processes of heat and mass transfer

The char particle size

The size of a char particle is a determining factor in whether the gasification rate is controlled by the rate of chemical reactions, heat and mass transfer or both of them. It is acknowledged that the smaller is the particle the more uniform is the gas concentration and temperature inside it. In the case of concentration and temperature uniformity inside the char particle, gasification would be chemically-controlled and heat and mass transfer limitations would not influence the reaction rate. Increasing the char particle size introduces heat and mass transfer limitations, until reaching a critical size above which heat and mass transfer limitations predominate. In several studies [57], [74], authors pointed out that biomass reactivity decreases when increasing the particle size, which is due to an increasing diffusional resistance. Figure 1.26 shows the increase of the char total conversion time with particle size for steam gasification.

Many authors propose a minimal particle size below which the gasification rate is constant and is consequently performed in the chemical regime, however the values are quite disparate from a study to another. For instance, Mermoud et al proposed 1 mm and as a critical size below which char steam gasification is chemically-controlled [75]. Kirubakaran et al proposed that for a practice size less than 2 mm, chemical reactions controls, between 2 and 6 mm, chemical reaction and heat transfer control

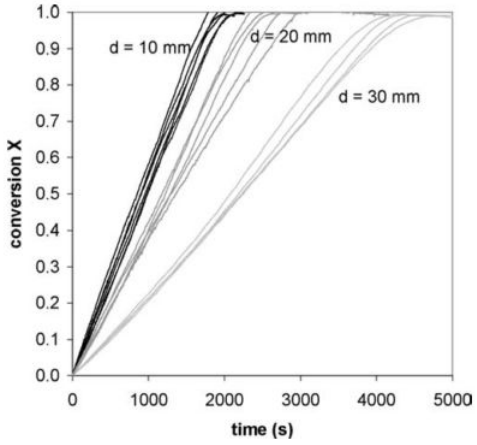

Figure 1.26: Gasification of charcoal particles of different initial diameters: 10, 20, and 30 mm (T = 930°C, P_{H_2O} = 0.2 atm) [74]

and above 6 mm, heat transfer controls the gasification [76]. Van De Steene et al. [77] found that the particle thickness was the characteristic dimension for parallelepiped shape pine char. They also found that for particle thickness below 2.5 mm, the char steam gasification is chemically controlled at 900°C (see figure 1.27).

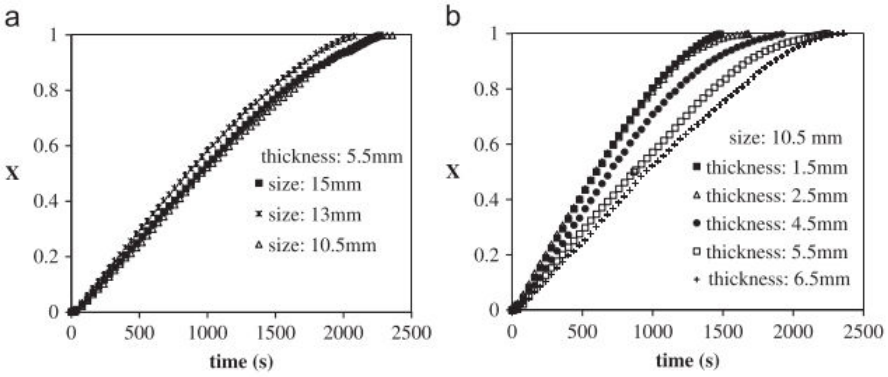

Figure 1.27: Influence of particle size (a) and particle thickness (b) on the steam gasification conversion rate (bulk gas temperature: 900°C, 0.2 atm H_2O (in N_2)) [77]

Gomez Barea et al [57] found that the CO_2 gasification reaction of char from pressed-oil stone is chemically controlled for powder char particles of 0.06 mm which is quite different from the value given above. An increase of particle size increases the time required for total conversion as depicted in figure 1.28. Klose et al. proposed that H_2O-char and CO_2-char gasification reactions are performed in the intrinsic regime for particle size below 0.125 mm and 10 mg of sample mass. Isothermal gasification experiments are done in a thermogravimetric apparatus [55]. This variety of statement about intrinsic conditions show well that it is a quite difficult to state with insurance on the nature of the gasification regime. It depends highly on the experimental conditions as well as on the texture of char. This issue will be discussed in the frame of the present work.

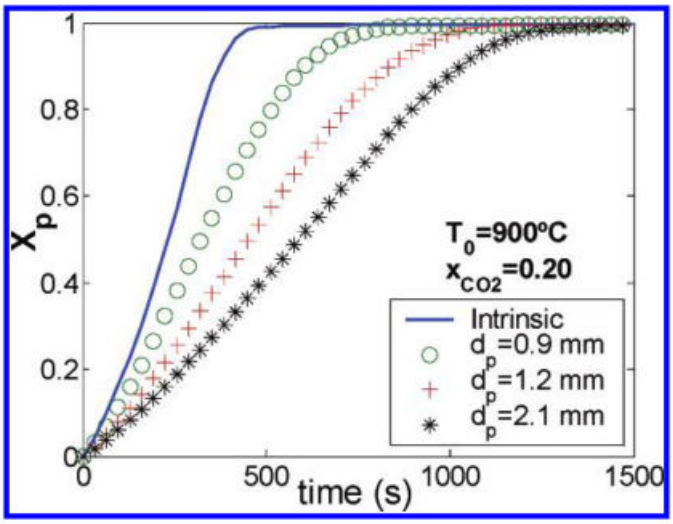

Figure 1.28: Conversion-time graph for various pressed oil char particle sizes at 900°C and x_{CO_2}=0.2. [57]

Char texture

As discussed above, the char texture, namely the TSA, PSD and pore shape, highly affects the gas diffusion inside the porous char. The larger is the pore, the easiest is the gas diffusion inside it. For very narrow pores, the gas diffusivity becomes very low. If the pore diameter is lower than the molecular diameter of a gas, the gas can simply not diffuse inside it. For instance a CO_2 and H_2O molecules can not diffuse in pores having an average size respectively below 0.34 nm and 0.27 nm. The effective diffusivity D_{eff} of a gas inside a porous char is given as a function of its molecular diffusivity (kinetic theory of gas) Di_{mol} and the Knudsen diffusivity (dependence on the pore diameter) $D_{Knudsen}$.

$$Di_{eff} = \frac{1}{\frac{1}{D_{Knudsen}} + \frac{1}{Di_{mol}}} \tag{1.14}$$

$$Di_{mol} = a_i \, 10^{-5} \left(\frac{T}{298}\right)^{1.75} \tag{1.15}$$

$$Di_{Knudsen} = 0.97 \frac{d_{pore}}{2} \left(\frac{T}{M_i}\right)^{0.5} \tag{1.16}$$

Figure 1.29 illustrates the CO_2 and H_2O effective diffusivities at 900°C as a function of the pore diameter.

Heat and fluid transport phenomena depend on the morphological features of the biomass particles such as tortuosity, porosity and pore size distribution. Porous char are more reactive than the non-porous ones, as they present a larger reactive surface and allow gas diffusion inside the particles. Henrisken et al [78] highlighted the influence of the texture on gas transport phenomena and concluded that they were enhanced in the longitudinal direction of fibres whereas they were lowered in the radial one.

C. Avila et al. [79] also established links between reactivity and morphology of 10 biomass chars. They observed by mean of SEM images that biomasses giving the thickest walled char had the lowest reactivities, while those giving the thinnest walled char had the highest ones because of a lower

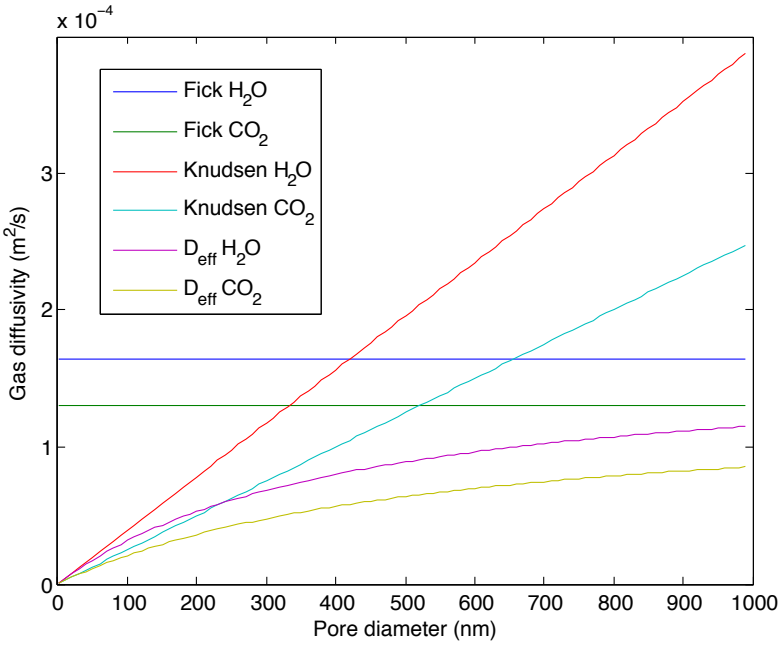

Figure 1.29: CO_2 and H_2O effective diffusivities as a function of the pore diameter at 900°C

resistance to mass and heat transfer. The developed surface area depends on the pyrolysis conditions. HHR chars exhibiting a higher reactivity exhibit a surface area consisting mainly of mesopores and macropores, while LHR chars exhibit a surface area mainly consisting of micropores [80]. Some authors think that the mesopores and macropores are better indicators of the char reactivity owing to the differences observed on LHR and HHR chars. Contribution of micropores to the active surface area is thought to be negligible [80]. The TSA of a char depends on the pyrolysis conditions in terms of temperature, heating rate and pressure [81] [82]. Attempts to correlate the initial reactivity (at X=5%) of the different char with their respective TSA were unsuccessful. Reactivity of biomass char can increase by near to 10 folds at the end of the reaction compared to the initial stages [72]. Several authors explain this reactivity increase by the increase in the reactive surface during the gasification, however, most of studies show that the reactivity increase is not proportional to the increase in the TSA [81] [31]. For instance, Fu et al. [31] investigated the evolution of char textural and chemical features during steam gasification. The char was produced from fast pyrolysis of rice husk. The authors found that the highest TSA was obtained at X=49%. TSA decreased beyond this conversion level, probably because of pore coalescence and collapse (see figure 1.30). Similarly, Laine et al [64] observed that coal chars with nearly the same TSA, have quite different reactivity.

From these observations, it comes out that the textural properties are more related to a porous volume and gas diffusivity inside the char, than to its chemical reactivity. Only a small portion of the TSA is effectively reactive. The use of an appropriate surface area should result in a surface related reaction rate, which is independent from the degree of conversion. Besides, the reaction rate should be proportional to the relevant surface area. Reactive Surface Area (RSA) or Active Surface Area (ASA) were found to be quite representative of the char reactivity [64] [55].

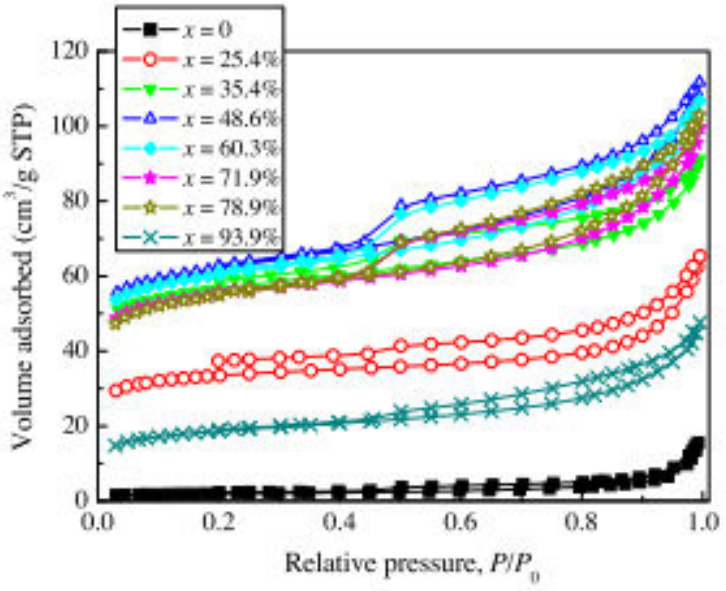

Figure 1.30: Nitrogen adsorption/desorption isotherms of the rice husk chars at different conversion levels of gasification with steam

1.4.4 Some relevant observations coming from the literature on the char reactivity

The influence of pyrolysis heating rate and final temperature on the char reactivity It has been well established that pyrolysis heating rate quite influence biomass char reactivity. Low heating rates produce char with a low reactivity, meanwhile high heating rates generate chars with higher reactivities [80] (see figure1.31).

The parameter HR has no physical meaning when focusing on the char gasification reaction. Saying that LHR conditions produce less reactive chars than HHR conditions does not clarify more the situation. It is more suitable to say that the HR influences directly the char chemical and textural properties that impact on its reactivity. Indeed, HHR produce a more porous char and more cracks and voids, as more volatiles are emitted in a shorter time than the case of LHR. The carbonaceous texture and structure are therefore different from a LHR char. Pore size distribution is also different and the HHR chars have a less ordered structure than the LHR ones. LHR also tend to keep a similar texture as that of the parent wood [82]. Particle shrinkage is more pronounced in the case of LHR conditions. Some authors think that the higher internal pressure developed in HHR conditions tends to resist to the particle shrinkage (see figure 1.32 [83]). This impacts directly the particle porosity.

The pyrolysis final temperature as well as residence time impact the char reactivity. The decrease in the char reactivity with increasing temperature is known as structural ordering of thermal annealing. Here again, the pyrolysis temperature or residence time do not illustrate the physical or chemical cause behind the char reactivity modifications. Pyrolysis final temperature as well as residence time impact the char reactivity through modifying the char properties. The thermal annealing phenomenon is the result of structural ordering of the char into a less reactive one. It involves several inner modifications of the char related to the elemental composition, minerals and porous network among others. Char deactivation during pyrolysis depends on two main parameters: Pyrolysis final temperature and residence time. It has been demonstrated that the char reactivity decreases when increasing the pyrolysis final temperature [84] [85] [86]. The elemental composition of the biomass char changes with temperature. Oxygen and hydrogen continue to be released out of the char porous

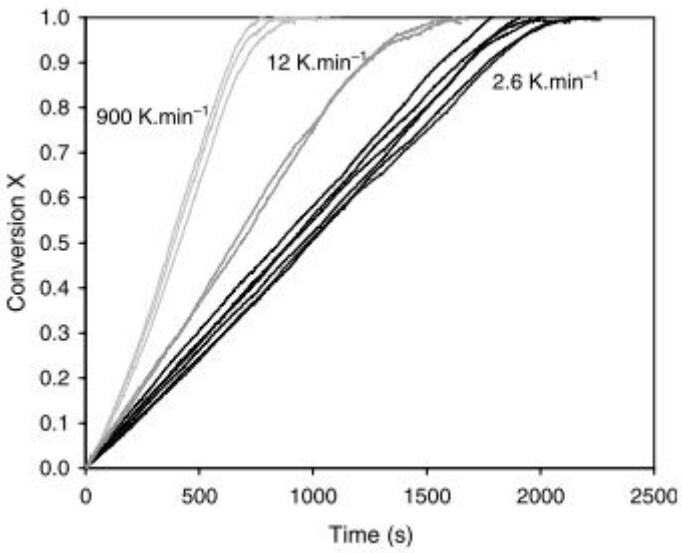

Figure 1.31: Gasification progress under 20% H_2O at 1200 K of char particles pyrolysed at 2.6, 12 and 900 K /min [80]

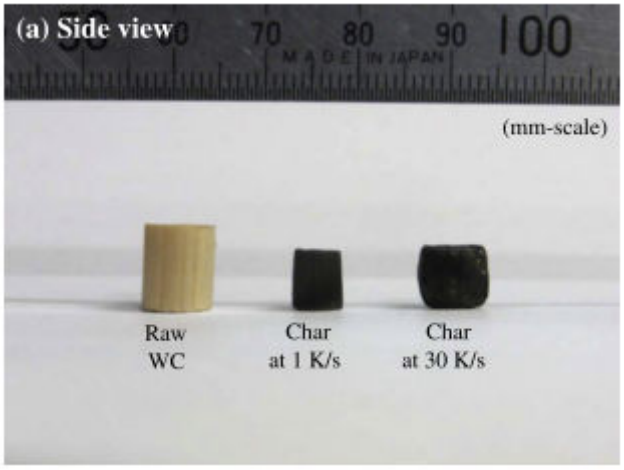

Figure 1.32: Photographs of raw material of wood cylinder and wood cylinder chars prepared at heating rates of 1 and 30 K/s (left to right) captured from (a) side view and (b) top view[83]

matrix as the pyrolysis temperature increases. The high levels of oxygen content in biomass fuels foster cross-linking of the carbon chains and inhibits ordering of the char matrix [87]. The loss of oxygen and hydrogen by elimination of functional groups are clear indicators of subsequent coalescence, ordering and rearrangement of aromatic rings. Increasing the pyrolysis final temperature is also accompanied by and textural structural modifications occurring simultaneously with the release of volatiles. Indeed, studies on the pyrolysis of Maize stlak, rice straw, cotton straw, rice husk [88], Brazil Nut shells [89] and eucalyptus [90], showed that the porous network developed inside the char particle depends markedly on the pyrolysis final temperature. Increasing the pyrolysis temperature from 600°C to 900°C is accompanied by an increase of the micropores volumes, mesopores volumes, surface areas and a decrease in the average pore diameter. Beyond 900°C, the tendencies were reversed for all the parameters.

Physical and chemical influencing factors are highly coupled The factors influencing the char reactivity are in reality highly coupled. For instance, the particle size affect the carbonaceous structure as well as the chemical composition of the char. Indeed, Asadullah et al [91] showed that biomass particle size influence char yield and carbonaceous structure during the pyrolysis process. For biomass particles of 5 mm, the authors evidenced the formation of a secondary char, corresponding to coke deposition originating from re-adsorption and condensation of volatiles formed inside the pyrolysing biomass/char matrix. The authors used Raman spectroscopy to evidence such phenomena. These observations are confirmed by Pattonatai et al [92] who evidenced intra-particle tar cracking during the pyrolysis of thermally thick wood cylinders. Pyrolysis was performed at a low heating rate (HR) and led to a homogeneous char sample. The authors evidenced the uniformity of the elemental composition along the radial direction regardless of the final pyrolysis temperature. The particle size can also impact the mineral retention in the char particle. Mohammed Asadullah et al [91] established also a good correlation between biomass particle size and alkaline earth metallic species retention in the remaining char after the pyrolysis step. The authors noticed an improved retention of the alkaline earth metallic species (*Na, K, Mg* and *Ca*) when increasing the size of biomass particles. As seen above, the loss of H and O atoms is accompanied by a structural modifications which also impact the char texture and consequently the gas diffusivity [88].

Synthesis All these chemical and physical modifications are responsible of the modifications of the char reactivity at two levels: The chemistry of the gasification which is impacted by the nature of the carbon structure forming the char as well as by the presence of catalytic active species and active sites concentration. The mass transport inside the pores which is directly related to the char textural properties. The factors affecting the char reactivity are numerous and highly coupled. To illustrate this complexity, a simplified scheme in which are presented the different factors as well as their inter-dependence is proposed in figure 1.33.

1.5 Char gasification in the chemical regime

Literature on biomass char gasification in the chemical regime is huge. Di Blasi summarized in her review the main findings related to the H_2O and CO_2 gasification of biomass chars as well as their combustion [14]. Most of the studies on small char particles are performed in classical TG devices, fluidized bed reactor or fixed bed reactors and aim at the kinetic modelling, gas composition determination or char structural modification monitoring during CO_2 and/or H_2O gasification. Char gasification reactions were studied for a high number of biomass chars including woods [72] [93] [94], energy crops [95], agricultural residues [96], sewage sludge [97] or algal biomasses [98] [73].

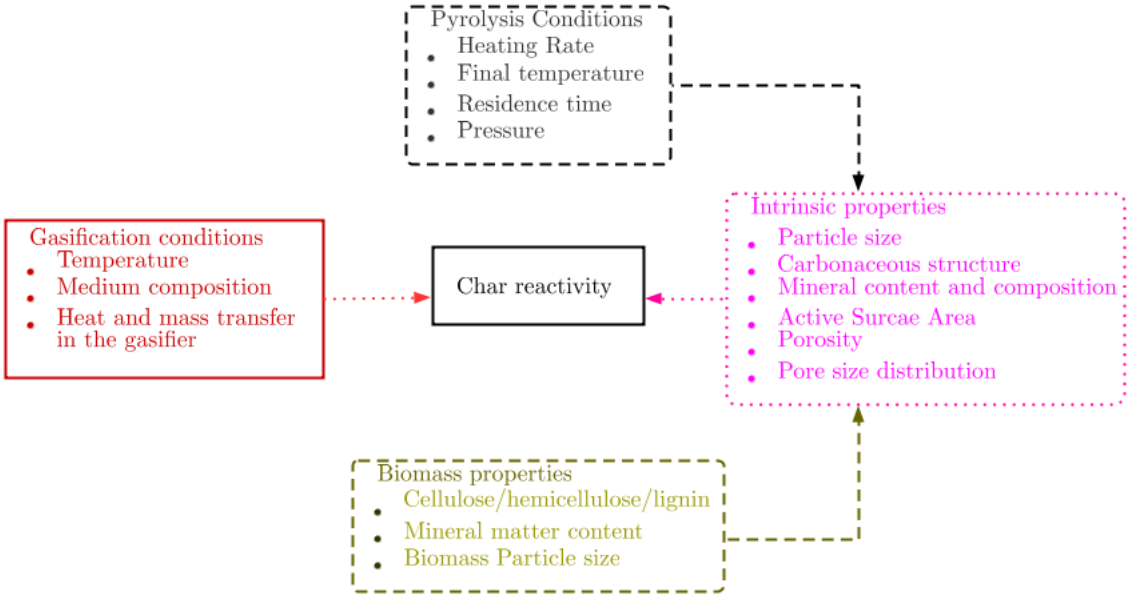

Figure 1.33: A schematic representation of the influencing factors on the char reactivity and their inter-dependence

The previous sections demonstrate well the complexity of the char reactivity modelling due to the numerous factors influencing it. Authors agree about considering three main chief sample characteristics for char gasification modelling: chemical structure, inorganic constituents and porosity. However, most of the kinetic models do not use these fundamental features for char gasification description due to their measurement difficulty and their high variability along the conversion [14]. The common approach is therefore to consider a global reactivity description.

As stated above, the char reactivity depends on the operating conditions (temperature and reactant gas pressure), and char properties (texture, mineral content, structure). It is thus commonly expressed as the product of a reference reactivity $R(Xref)_{(T,P_i)}$(depending on the temperature and reactant gas pressure) and a structural term $f(X)$ accounting for the char properties evolution along the conversion. Owing to the difficulties in the monitoring of the intrinsic char properties along the conversion, the structural term is usually an empirical correlation where the conversion level appears as the sole variable. Changes in the char intrinsic properties are implicitly described by this empirical term. The reference reactivity corresponds to a specific conversion level. Reference reactivity at 10% or 50% of conversion have been used in the literature [99] [100]. The reactivity at 50% conversion level R(50) is the most frequently used as a reference value. The reactivity at any gasification stage can be thus expressed as:

$$R(X)_{(T,P_i)} = R(Xref)_{(T,P_i)} f(X) \tag{1.17}$$

1.5.1 Kinetic constants

As the reference reactivity depends on the temperature and on the gasifying agent partial pressure, the most simple approach is to consider a nth order model. The reference reactivity is expressed as a product of a reaction rate constant $k_{i(T)}$ which depends on the temperature and the reactant gas partial pressure following a power law.

The reference reactivity expression reads:

$$R(Xref) = k_{i(T)} P_{(i)}^{n} \tag{1.18}$$

$k_{i(T)}$ is the reaction rate constant $[s^{-1}.atm^{-n}]$, $P_{(i)}$ [atm] is the reactant gas partial pressure and n is the reaction order.

The rate constant accounting for the reactivity temperature dependence, follows an Arrhenius law:

$$k_{i(T)} = A_i exp \frac{-E_i}{RT} \tag{1.19}$$

Where $A_i[s^{-1}.atm^{-n}]$ is the pre-exponential factor[J/mol], E_i [J/mol] is the activation energy and R [J/(mol.K)] is the universal gas constant.

A more realistic model based on Langmuir-Hinshelwood reaction mechanisms can be used to express the reference reactivity. In this model, the gasification reaction unfolds in two steps. In the first step, called oxygen exchange step, the oxygen atom of the CO_2 molecule (taking the Boudouard reaction as an example), is adsorbed on the active site C() on the char surface. Then in the second step, the oxygen atom, reacts on the carbon active site to produce a C(O) molecule that will be afterwards desorbed. The desorbed carbon monoxide has an inhibiting effect as it can react with the C(O) function and forms again a CO_2 molecule. The Boudourad gasification reaction is decomposed into two elementary steps:

$$C + CO_2 \longrightarrow 2CO \tag{1.20}$$

$$C() + CO_2 \longrightarrow C(O) + CO \tag{1.21}$$
$$C(O) \longrightarrow CO \tag{1.22}$$
$$\tag{1.23}$$

According to Langmuir-Hinshelwood reaction mechanisms, the reference reactivity in the case of CO_2 gasification reads:

$$R_{(Xref)} = \frac{k_{1(T)} P_{(CO_2)}}{1 + (k_{2(T)}/k_{3(T)}) P_{(CO)} + (k_{1(T)}/k_{3(T)}) P_{(CO_2)}} \tag{1.24}$$

The same mechanism is held for steam gasification but with the only difference of an extended set of equations accounting for hydrogen inhibition.

$$C + H_2O \longrightarrow CO + H_2 \tag{1.25}$$

.

$$C() + H_2O \longrightarrow C(O) + H_2 \tag{1.26}$$
$$C(O) + H_2 \longrightarrow C() + H_2O \tag{1.27}$$
$$C(O) \longrightarrow CO \tag{1.28}$$
$$C() + H_2 \longrightarrow C(H)2 \tag{1.29}$$
$$C(H_2) \longrightarrow C() + H_2 \tag{1.30}$$
$$C() + 1/2H_2 \longrightarrow C(H) \tag{1.31}$$
$$C(H) + \longrightarrow C() + 1/2H_2 \tag{1.32}$$

For steam gasification, the reference reactivity has the following expression:

$$R_{(Xref)} = \frac{k_{1(T)} P_{(H_2O)}}{1 + (k_{1(T)}/k_{3(T)}) P_{(H_2O)} + f(P_{(H_2)})} \tag{1.33}$$

1.5.2 The structural function expression

The structural function expression can be developed from structural models that describe the evolution of the char properties during the gasification. These models have a theoretical expression that may contain one or many parameters which are adjusted experimentally to fit the char structural evolution trend [101] [102] [93] [94]. Structural functions can also have a purely empirical expression having a polynomial form [99] [100] [34]. Three basic models can be applied to study the evolution of the reactive surface during heterogeneous reaction: the volume reaction model (VRM), the shrinking core model (SCM) and the random pore model (RPM).

- The VRM, also named homogeneous model, assimilates the heterogeneous reaction of gasification to a homogeneous reaction. The reaction takes place at the totality of the active sites and the structure of the particle is assumed not to change. The structural function corresponding to this model, which decreases as gasification proceeds, is expressed as:

$$f_{(X)} = (1 - X) \tag{1.34}$$

- The SCM assumes that the reaction initially occurs at the external surface of the particle and gradually moves inside it. As the particle size is reduced during the transformation, the reactive surface also decreases, but the particle density remains unchanged. At the intermediate conversion of solid, the char represents a shrinking core of non-reacted solid.

$$f_{(X)} = (1 - X)^{2/3} \tag{1.35}$$

- The RPM considers that gasification takes place on the inside surface of the micropores, which occupy most of the surface area of the particle. As a function of the reaction progress, the reactive surface initially increases due to the pores growth, and then it decreases by the coalescence of adjacent pores.

$$f_{(X)} = (1 - X)(1 - \Psi ln(1 - X))^{1/2} \tag{1.36}$$

  The Ψ parameter, related to the char structure, is most often determined by fitting procedure due to its experimental determination difficulty. Its theoretical expression is the following one:

$$\Psi = \frac{4\pi L_0 (1 - \epsilon_0)}{S_0^2} \tag{1.37}$$

  L_0 is the pore length [m], ϵ_0 is the char initial porosity and S_0 is char total surface per unit volume [m].

Despite that RPM is widely used for coal char gasification modelling, it does not fit to many case of biomass char gasification modelling. There exist besides varieties of modified SCM and RPM with additional semi-empirical parameters introduced for better fitting with the experiments. These parameters are for instance related to the presence of minerals in the char [72] [69] [101].

Many authors use power law models and polynomial functions to account for the char properties evolution along the conversion as the none of the above described models captures the reactivity evolution adequately [23] [14].

The power law model has the following expression:

$$f_{(X)} = (1 - X)^n \tag{1.38}$$

For the polynomial function, the structural function reads:

$$f_{(X)} = \sum_{i}^{n} a_i X^i \tag{1.39}$$

An extensive collection of additional structural functions is available in the literature [23] [14] [103]. These functions are in most of the cases "black box" ones, bearing no physical meaning.

The structural function hides necessarily physical and chemical changes occurring in the char. Very few authors succeeded to reconcile the gasification models with the experiments by introducing the RSA as discussed above [62] [55]. The RSA bears no empirical parameters. It corresponds to the amount of reactive C(O) complex on the char surface. These latter can be determined by the TPD-MS technique.

The structural function is in this case determined experimentally:

$$f_{(X)} = RSA \tag{1.40}$$

The RSA is the most realistic structural function. However, its determination is not at all trivial.

1.6 Char gasification in the presence of heat and mass transfer limitations

1.6.1 Literature review on char gasification in the presence of heat and mass transfer limitations

The literature on char gasification is huge. Most of the char gasification studies are performed using thermogravimetric apparatus and fine char powders to get kinetic data in the chemical regime [14]. However, studies on gasification of large char particle are scarcer.

For instance, Groeneveld and van Swaaij [104] investigated the gasification of wood char particles with dimensions of 40 mm x 20 mm x 20 mm. The gasification reaction was performed in a mixture of H_2O and CO_2. A local volumetric model enabled them to explain conversion profiles found experimentally. The authors adopted an overall reaction of 0.7.

Standish and Tanjung [105] analyzed the effects of temperature, CO_2 gas composition, and particle size in 10-34-mm-sized wood charcoal gasification. They correlated their observations with an apparent nth-order kinetic expression that has a reaction order of 0.71. The initial particle size effect was also included in the expression raised to a power of -0.81.

For instance, Dasappa et al. [106] modelled the gasification of an isolated single charcoal sphere initially in a CO_2/N_2 mixture. The model was afterwards extended to the steam char gasification reaction. The model describes the physical phenomena of diffusion convection and reaction processes of the gas and solid char species as well as energy transport in the pores by mass and energy conservation equations. Immediate outflow of the gas phases is described by convective transport. Modified Langmuir Hinshelwood kinetic model is used for the gasification reaction term. The numerical results fit well the experimental data for the CO_2 char reaction up to 60% of conversion, however, the modelling results are less accurate for the steam gasification reaction.

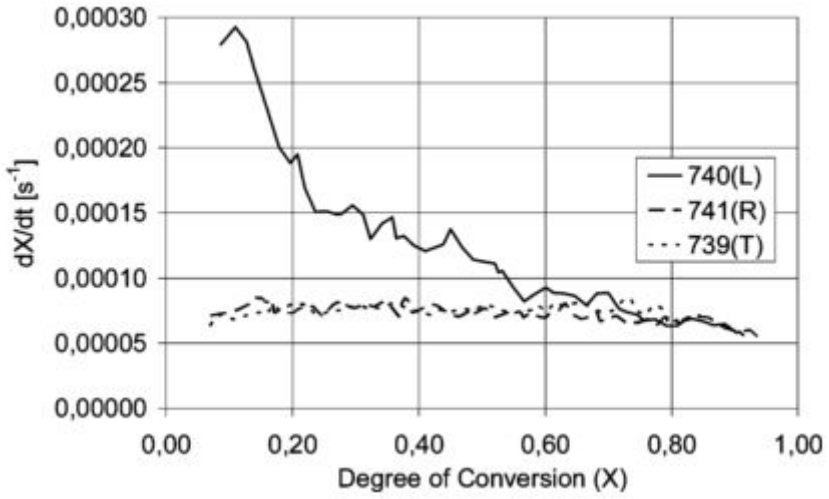

Figure 1.34: Rate of conversion as a function of the degree of conversion (X) for L, R and T series [78]

Gomez Barea et al. [57] evidenced diffusional limitations during CO_2 gasification of pressed-oil stone char. The authors varied the particle size from 0.06 mm to 2.1 mm and calculated experimental effectiveness factors at different temperatures. In an accompanying paper [107], the authors developed an original char gasification model that takes into account the diffusion-reaction processes within a finite-size char particle as well as intra-particle heat effects and heat and mass transfer phenomena that occurs in the external gas layer. Intra-particle mass transfer limitations were identified as the main factor responsible for the strong resistance found at large particle size and high temperature. External heat and mass transfer were also determined to have a relevant role in the CO_2 char gasification reaction.

More recently, Mani et al [108] evidenced diffusional limitations in wheat straw char gasification with CO_2 in a temperature range of 750 to 900°C and particle size range of 0.06 to 0.925 mm. Although the char particle are not large ones, diffusional limitations were observed for particle size higher than 0.06 mm.

Gasification of large char particles where mass transport is the limiting factor was studied by Henriksen et al. [78]. The authors evidenced the preferential transport along the grain direction by coating the char pores with alumina silicate which sinter with heating and form a gas proof. In a steam gasification run, the coating was performed on two of the three possible gas entries (longitudinal (L), tangential (T) and radial (R)). The authors observed that the gasification rate was most influenced when preventing steam to enter along the fibre direction (L). They also noticed that at advanced level of conversion the gasification rate was the same independently from where the coating was initially performed (see figure 1.34). The authors also pointed out that low heating rate (LHR) pyrolysis allows to obtain homogeneous and similar chars.

Mermoud et al [80] studied the influence of the pyrolysis heating rate on the char physical properties and reactivity to steam. The char particle were prepared from spherical wood particles of 10 mm diameter. They showed that increasing heating rate leads to a more porous char containing higher mineral amount and exhibiting a higher reactivity to steam. They also studied showed the macroscopic evolution of a large char particle under steam gasification and performed porosity and surface area measurements on the raw chars. The authors concluded that most probably, the char steam gasification occurred in mesopores. The micropores contribution to the active surface area would be small compared to that of the mesoporosity.

The same authors carried a numerical study on the steam gasification of a single large char particle and evidenced mass and heat transfer limitations for large char particles gasification [74]. The numerical model based on balance equations for gas species and enthalpy, and including heterogeneous reaction kinetics, was able to describe, both qualitatively and quantitatively with an accuracy of 7% until 60% of conversion, the effect of the parameters that can be controlled in an industrial process of gasification of large particles by H_2O: the diameter of the particle (10 to 30 mm), the temperature (830 to 1030°C), and the H_2O partial pressure (0.1 to 0.4 atm) of the surrounding gas phase.

The model allows to characterize the thermochemical situation of the char particle at any date "t". Fields of gas concentrations and temperatures show the existence of gradients inside the particles. The modelling results confirm that the gasification of large particle can not be accurately described using simplified models such as a homogeneous or shrinking-core models. Mass transfer is limiting the process for large particles both outside and inside; the assumption of mass equilibrium between the particle and the surrounding gas is not valid. On the other hand, the assumption of thermal equilibrium between the particle and the surrounding gas can be adopted with minor impact.

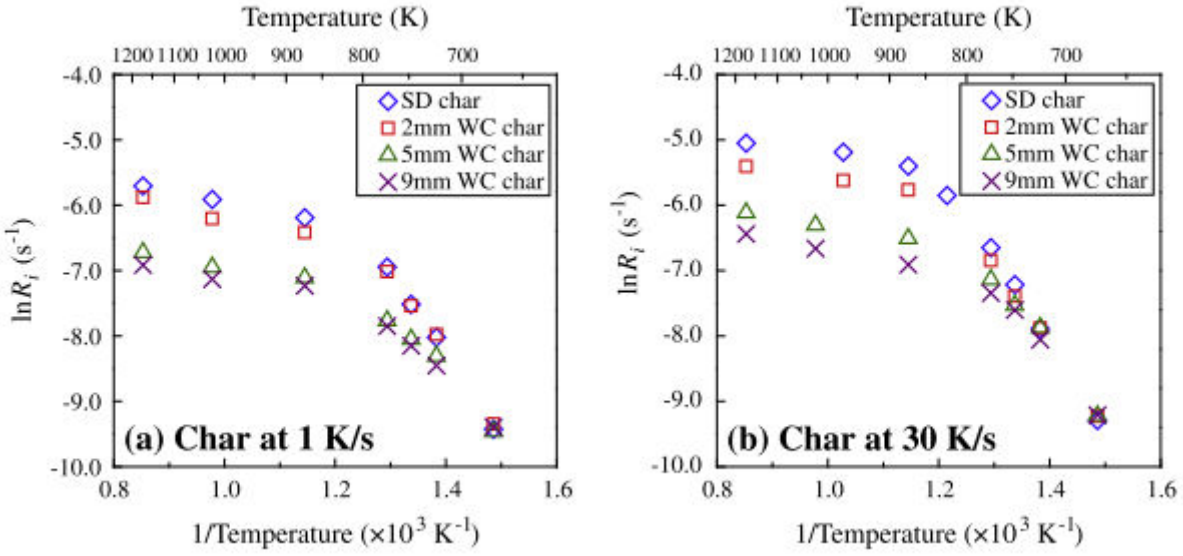

Figure 1.35: Arrhenius plot of reactivity for chars prepared at heating rates of (a) 1 K/s and (b) 30 K/s [83]

To understand better the observed discrepancies beyond 60% of conversion for large particles (having a diameter > 7 mm), in another paper, Golfier et al [109] studied the effect of peripheral fragmentation on the large char steam gasification rate. The authors introduced fragmentation criteria (critical porosity value and gradient) to account for the char matrix dislocation at high conversion levels. The authors observed that When reaction kinetics is the predominant mechanism (for the 7 mm diameter particle), the agreement obtained with the experimental curve remains excellent with or without fragmentation. On the other hand, when the particle is larger and the diffusional effects increase, the model including fragmentation is much more accurate.

Umeki et al [110] also developed a semi-empirical model for steam gasification of large char particles based on the effectiveness factor. The authors set a simple expression for the apparent reaction rate of large wood char (14.3 and 21.2 mm) gasification which was expressed as the product of the intrinsic rate and an effective factor. The authors took into account the change in char diameter and intrinsic reaction rate during the reaction. This model does involve solving mass and energy equations and does not takes into account the physics of gasification.

Tagutchu et al [111] also studied the gasification of pine char particles with a thickness range of 1.5 to 5.5 mm. The gasification of wood char particles during gasification in three atmospheres, i.e., H_2O, CO_2, and H_2O/CO_2, was experimentally investigated in a macro TG device. An important result of this article is that the addition of CO_2 in a H_2O atmosphere led to an acceleration of gasification kinetic. In a mixture of 20% H_2O and 40% CO_2, the gasification rate was 20% higher than the sum of the gasification rates in the two single atmospheres.

Van de Steene et al. studied the wood-chip chars gasification with H_2O, CO_2 and O_2 both experimentally and numerically.The char particles had a parallelepiped shape. The authors showed that the characteristic dimension is the particle thickness. The authors varied the particle thickness and found that there was no rate modification below a particle thickness of 2.5 mm . Experimental results from a macro-Thermogravimetric reactor were compared to those from a char particle model, previously established by Mermoud et al, in which were performed modifications concerning the particle shape and the introduction of surface functions to account for reactive surface evolution through the gasification reactions [77].

More recently, Pattonatai et al [92] evidenced intra-particle tar cracking during the pyrolysis of thermally thick wood cylinders. Pyrolysis was performed at a low heating rate (HR) and led to a homogeneous char sample. The authors evidenced the uniformity of the elemental composition along the radial direction regardless of the final pyrolysis temperature.

The same authors [83] studied afterwards the oxygen gasification characteristics of large wood chars. The authors evidenced the effects of the pyrolysis HR on the char properties and tar yield. They also show that at a temperature of 673 K, the char reactivity towards oxygen was constant regardless of the char particle size and pyrolysis HR which corresponds to the chemical regime (see figure 1.35). The authors pointed out the shrinkage during LHR pyrolysis and that the char would keep its initial size during gasification if it is performed in a chemically controlled regime. However, when increasing the temperature, significant morphological changes occur depicted by the decrease in the particle dimension mainly in the grain direction (see figure 1.36).

This brief review shows that large char particle gasification is not extensively studied in the literature , despite the large particle size in gasifiers and the presence of mass transfer limitations in practical conditions.

1.6.2 Modelling char gasification with heat and mass transfer limitations

As seen before, when the char particle is small enough and the temperature is low, the gasification reaction is performed in the chemical controlled regime. This situation is an ideal one for kinetic parameter determination. In biomass gasifiers, the char particle size is rather in the order of several millimetres, even centimetres. The temperature may also reach 1000-1100°C. This situation is typical of mass and heat transfer limitations. The rate of gas diffusion becomes comparable to the chemical reaction rate leading to a limited penetration of the reacting agent into the char matrix. In the presence of heat and mass transfer limitations, there exist gradients of temperature and gas concentrations in the char particle. The chemical reaction rate is not therefore uniform in the solid matrix. The gasification reaction rate is an apparent rate, lower than the intrinsic rate due to mass and heat transfer limitations.

There exist different methods for formulating the apparent gasification reaction rate [110]. The simplest method is using the pseudo-activation energy which changes with temperature. However, this method cannot express the effect of the particle size and is poorly describing the physical phenomena. The evolution of the gasification rate with particle size can be described through a semi-empirical expression, where the apparent reaction rate is expressed as a function of the intrinsic reaction rate and the particle size [105]. The third method consists in using the effectiveness factor

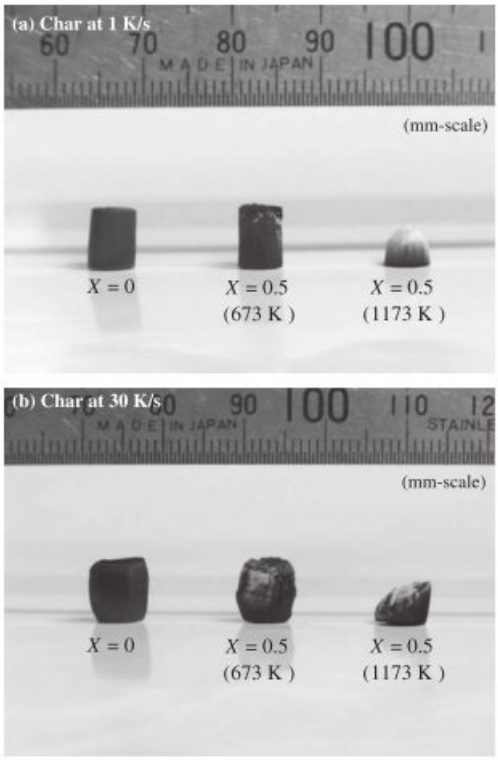

Figure 1.36: Photographs of initial char (X = 0), char at X = 0.5 gasified at 673 K, and char at X = 0.5 gasified at 1173 K (left to right). Char samples are prepared at heating rates of (a) 1 K/s and (b) 30 K/s [83]

from catalyst theory [112] [113] [108]. The fourth method is numerical modelling of partial differential equations (PDEs) formulated from the mass and energy balance equations [74]. This method can express the apparent reaction rate most precisely, but requires much computing time for the gasifier simulation since PDEs for every char particle in the gasifier should be solved. We will briefly develop the last two approach for modelling char gasification in the presence of heat and mass transfer limitations.

The effectiveness factor approach

In the case of mass transfer limitations, the concentration of the reactant gas (CO_2 or H_2O) exhibits a gradient throughout the particle with a maximal value at the surface. In this kind of situation, Thiele [114] defined an effectiveness factor η, that allows to take into account the consumption of the reactant gas while it diffuses inside the porous particle. In such conditions, the apparent reaction rate expression reads:

$$\frac{dm_C}{dt} = \eta \, m_C \, k_{(T)} \, S_r P_g^n \tag{1.41}$$

with m_C: mass of char (kg), $k_{(T)}$: Kinetic rate constant of char gasification ($kg.s^{-1}.m^{-2}.atm^{-n}$) , S_r: Reactive surface area ($m^2.kg^{-1}$), P_g: reacting gas partial pressure at the particle surface(atm) n: reaction order, η: Thiele effectiveness factor.

Reaction order of biomass char gasification differs from a study to another. In Di Blasi's review, CO_2 char gasification reaction order varies between 0.36 and 1.2. That of H_2O char gasification

is comprised between 0.4 and 1 [14]. When using the effectiveness factor approach to model the effect of LHR char gasification, we will consider the gasification reaction as first order reactions. The definition of the effectiveness factor is rigorous only for a first order reaction.

Thiele effectiveness factor, η, comprised between 0 and 1, is the ratio between the apparent reaction rate and the intrinsic one (without diffusion limitations). In the chemical regime, η=1. It tends towards 0 with increasing diffusional limitation. The effectiveness factor expression is obtained by volume integration of the reactant gas balance equation.

$$\eta = \frac{3}{\phi}\left(\frac{1}{tanh\phi} - \frac{1}{\phi}\right) \tag{1.42}$$

The Thiele modulus ϕ has the following expression:

$$\phi = \frac{d_{part}}{2}\sqrt{\frac{\beta\, S_v\, k_{(T)}\, P_g}{M_g\, D_{eff} C_g}} \tag{1.43}$$

Where d_{part} is the particle diameter (m), β is a stoichiometric coefficient equal to ratio between the gas molar mass and that of carbon, S_v is a volumetric surface (m^2/m^3) which is equal to the product of the specific surface by the char density, M_g is the molecular weight of the reactant gas $(kg.mol^{-1})$, C_g the bulk concentration of the reactant gas$(mol.m^{-3})$, D_{eff} is the effective diffusion coefficient (m^2/s).

For a gas "i" (CO_2 or H_2O), Di_{eff} is expressed through the the molecular diffusion coefficient Di_{mol} and the Knudsen diffusion coefficient $Di_{Knudsen}$:

$$Di_{eff} = \frac{1}{\frac{1}{D_{Knudsen}} + \frac{1}{Di_{mol}}} \tag{1.44}$$

$$Di_{mol} = a_i\, 10^{-5}\left(\frac{T}{298}\right)^{1.75} \tag{1.45}$$

$$Di_{Knudsen} = \frac{\epsilon}{\tau} 0.97 \frac{d_{pore}}{2}\left(\frac{T}{M_i}\right)^{0.5} \tag{1.46}$$

Where a_i is a constant taken to 1.67 for CO_2 and 2.1 for H_2O [113], d_{pore} is the pore diameter (m), ϵ is the char porosity and τ is the char tortuosity

Several authors used the effectiveness factor approach to model the char combustion and gasification reactions for different temperature and particle size [115] [57] [110] [108] [116] [97] [113]. The effectiveness approach render the calculation of the char reactivity straightforward. Despite it does not gather all the physics of the gasification reaction, it is a simple method allowing to predict the char apparent reactivity without enormous computational effort.

Numerical modelling approach

Numerical modelling involves setting mass and energy balance equations to model heat and mass transfer inside the char particle. For more details on single large char particle gasification modelling, the reader can refer to [74]. A brief description of external and internal energy and species transport is given in the next paragraphs.

The char particle, identified by the subscript η, can be seen as a porous medium including a fluid and a solid region consisting mainly of carbon, identified as the β-phase and the σ-phase, respectively. For instance, when considering the Boudouard gasification reaction, three species are of concern when establishing the model equations:

- the solid char: approximated as pure carbon
- the reactant gas: CO_2
- the produced gas: CO

The gas transport inside the particle can be modelled by a sum of a convective and a diffusive terms. The convective term includes a superficial velocity which can be determined by the Darcy's law. The diffusive transport is governed by the Fick law.

For a gas specie "j" (CO_2 or CO), the balance equation reads:

$$\frac{\partial(\epsilon_\eta \rho_{\beta\eta} \omega_{j\eta})}{\partial t} + \nabla.(\rho_{\beta\eta} \mathbf{V}_\eta \omega_{j\eta}) = \nabla.(\rho_{\beta\eta} D_{j\eta} \nabla \omega_{j\eta}) + R_{j\eta} \tag{1.47}$$

The first left hand side term corresponds to the accumulation, the second left hand side term corresponds to the convective gas transport while the first right hand side term represents the diffusive transport. Finally, the reaction term (production or consumption) is given by the second right hand side term.

The superficial velocity is given by the Darcy's law:

$$\mathbf{V}_\eta = \frac{K_\eta}{\mu} \nabla P_\eta \tag{1.48}$$

K_η and μ_j are respectively the char permeability and the jth gas specie viscosity.

The gas pressure inside the particle porosity is given by the ideal gas law:

$$P_\eta = \frac{\rho_{\beta\eta} R T_\eta}{M_{\beta\eta}} \tag{1.49}$$

The solid char conservation equation reads:

$$\frac{\partial(\epsilon_\eta \rho_{\sigma\eta})}{\partial t} = R_{j\eta} \tag{1.50}$$

The energy balance equation reads:

$$(\rho Cp)_\eta \frac{\partial T_\eta}{\partial t} + (\rho Cp)_{\beta\eta} \mathbf{V}_\eta . \nabla T_\eta = \nabla.(\lambda_\eta \nabla T_\eta) + Q_\eta \tag{1.51}$$

The first left hand side term corresponds to the accumulation of energy, the second left hand side term corresponds to the convective gas transport of energy while the first right hand side term represents the conductive transport of energy according to Fourier's law. Finally, the energy consumed by the gasification reaction per unit time is given by the second right hand side term.

- External heat transfer

  Considering that the particle environment is at a constant temperature. The heat flux density at the particle surface is given by:

$$\mathbf{q}^{\partial\Omega} . \mathbf{n} = h_{conv}(T^\infty - T^{\partial\Omega}) + \sigma\xi(T^{\infty 4} - T^{\partial\Omega 4}) \tag{1.52}$$

  T^∞ and $T^{\partial\Omega}$ represent respectively the temperature of the surroundings and particle surface. σ is the Stefan-Boltzmann constant $[W.m^{-2}.K^{-4}]$ and ξ is the char emissivity close to the unity (char is assimilated to a black body).

h_{conv} $(W.m^{-2}.K^{-2})$is the convective heat transfer coefficient. It is a function of the dimensionless Nusselt number, the particle diameter,dp [m], and the thermal conductivity of the surrounding gas, λ^{∞} $[W.m^{-1}.K^{-1}]$.

$$h_{conv} = \frac{Nu\lambda^{\infty}}{dp} \tag{1.53}$$

- External mass transfer

  Considering a reacting gas in the particle environment at a constant concentration, the mass flux density of the reacting gas at the particle surface is proportional to the gas concentration differences between the surroundings and the particle surface.

$$\mathbf{N}_i^{\partial\Omega}.\mathbf{n} = k_m(\rho_j^{\partial\Omega} - \rho_j^{\infty}) \tag{1.54}$$

  k_m [m/s] is the convective mass transfer coefficient.It is a function of the dimensionless Sherwood number, the particle diameter (dp) and the diffusivity of the surrounding gas D_j $[m^2.s^{-1}]$.

$$k_m = \frac{ShD_j}{dp} \tag{1.55}$$

  $\rho_j^{\partial\Omega}$ and ρ_j^{∞} represent respectively the reacting gas concentrations in the surroundings and at particle surface.

1.7 The use of CO_2 in biomass pyrolysis and gasification

The present chapter aims to gather the available knowledge on CO_2 utilization in biomass pyrolysis and gasification process. The collected information comprises some reference to coal. The effect of CO_2 on the biomass pyrolysis and gasification was studied at two levels:

- a theoretical level using thermodynamic analysis based on equilibrium calculations,
- an experimental level by studying (i) the effects of CO_2 on the gas composition, (ii), the effects of CO_2 on the char properties and (iii) effects of CO_2 on the char gasification in complex atmospheres containing H_2O

1.7.1 Thermodynamic analysis of biomass gasification with injection CO_2 in the gasifying medium

Thermodynamic simulations (based on equilibrium calculations) of thermochemical conversion of carbonaceous feed-stocks into Syngas at the reactor level using CO_2 in the gasifying medium were performed by Renganathan et al. [117]. The main conclusions to which the authors came to are the following: The CO_2 gasification of biomass under adiabatic condition is not favourable as it results in an incomplete carbon conversion and quite low Cold Gas Efficiency (CGE). The operation has to be done in isothermal conditions with a constant supply of heat. When increasing the temperature, the CGE increases as well as the CO_2 and carbon conversions. The H_2/CO ratio deceases with temperature for a defined CO_2/biomass ratio. Pressure have a negative influence over the carbon and CO_2 conversion and thus the CGE of SynGas. Indeed, when increasing the operating pressure above 4 bars, the reverse Boudouard reaction as well as the reverse Primary Water Gas (PWG) are

favoured as they tend to lower the decrease the pressure. CO concentration decreases with pressure while that of H_2 is almost independent. When increasing the CO_2 flow rate (mol of CO_2/ mol C), CO production increases up to a plateau while that of H_2 monotonically decreases. The CO_2 conversion reaches a maximum at the Carbon Boundary Point (CBP), in which all the solid carbon is transferred to the SynGas. For a higher CO_2 flow-rate, the CO_2 conversion decreases as the CO_2 leaves the reactor without reacting. The authors identified a universal optimal operating temperature of 850°C for minimum energy input. The initial carbon feedstock has an influence on the heat and CO_2 requirements of the process via its elemental composition (H/C and O/C ratios). Among a a variety of carbonaceous feed-stocks, biomass shows the lowest CO_2 and heat requirements while Coal Anthracite showed the maximum ones.

Simulations considering mixed atmosphere gasification showed that for a defined CO_2/C ratio, increasing % of steam or O_2 results in increased carbon conversion and a decreased CO_2 conversion. When introducing steam, the amount of CO decreases while that of H_2 increases which is consistent with experimental data of [8]. Increasing oxygen results in the reverse case: H_2 decreases and CO increases. The heat input required at CBP does not show a minimum with respect to temperature for higher % of H_2O or O_2. Gasification using CO_2/O_2 mixture can be carried out with no heat input over a certain temperature range. Use of H_2O or O_2 as a co-gasifying agent reduces the amount of CO_2 required at CBP and the conversion of CO_2. Finally the use of steam reduces the CGE slightly at low temperature, O_2 has a negative on CGE, more at low temperature than at higher ones.

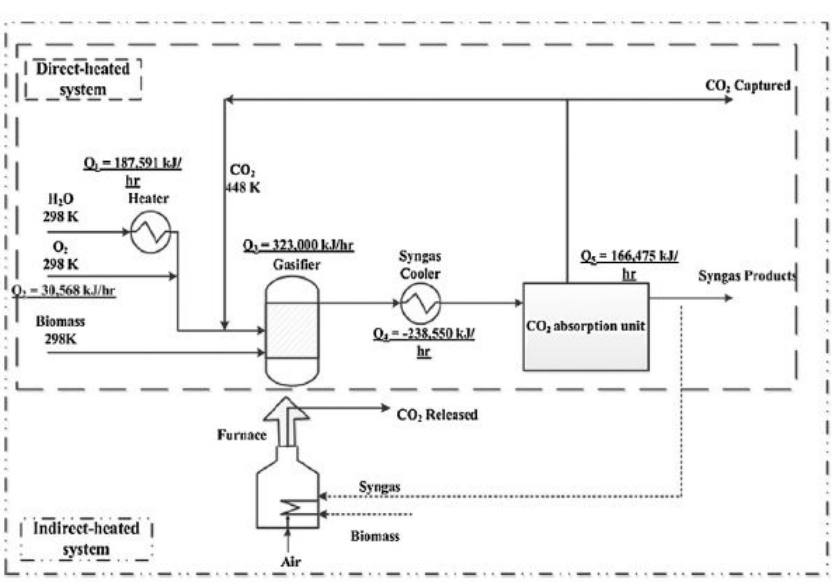

Figure 1.37: Biomass gasification using recycled CO_2 as gasifying agent.[118]

Chaiwatanodom et al [118] also performed thermodynamic analysis of biomass gasification under complex atmospheres of CO_2, H_2O and O_2 using Aspen + software. Thermodynamic analysis are also based on equilibrium calculations. The authors used performance criteria such as the H_2/CO ratio, an efficiency factor based on the entire energy requirement of the process (including energy for O_2 production, CO_2 trapping and recycling, steam production and heat input for the gasifier) as well as a CO_2 emission factor. Direct and indirect heated gasifiers configurations were also studied. The CO_2 recycling concept is shown in figure 1.37. The authors came to the conclusion that CO_2 recycling in the biomass gasification process shows the potential benefit on the Syngas production; however, the study reveals that the additional energy requirement for CO_2 heating may overwhelm this benefit. The indirect gasification, with biomass as fuel for heating is a better gasifier configuration

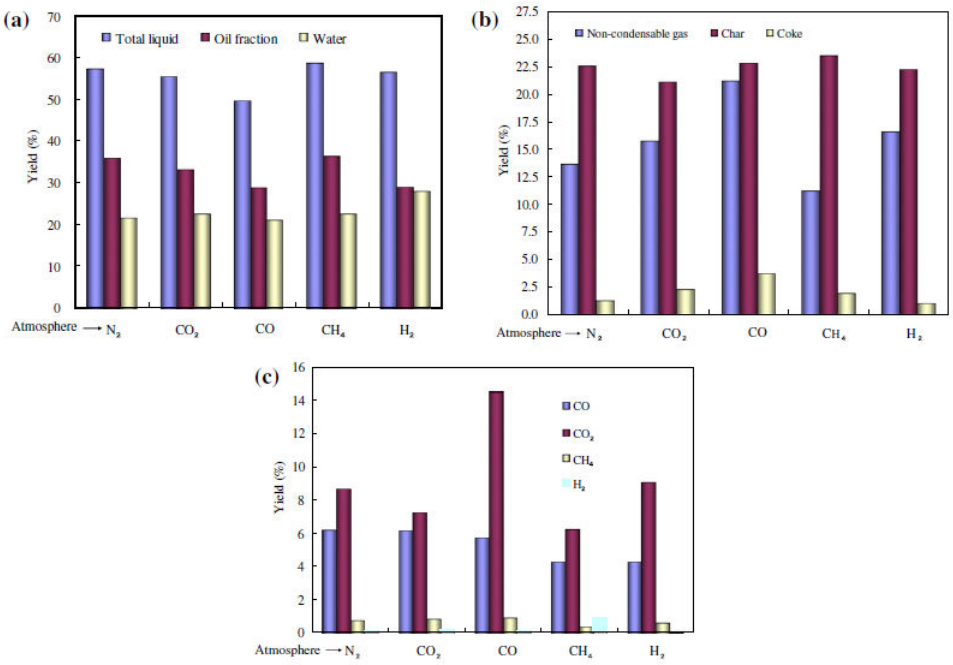

Figure 1.38: Pyrolysis product distribution as a function of the gasification medium composition [119]

when thermodynamic efficiency and CO_2 emissions are considered as performance criteria. CO_2 addition has positive effects on the process efficiency and CO_2 emission factor when operating at a low temperature and high pressure. Optimum CO_2/C ratio of 0.1-0.2 is found for a temperature of 800°C and high pressures. For higher temperatures, CO_2 addition may have a positive impact on the emission factor while the process efficiency factor monotonically decreases. The authors also found that it is worth-noting to consider that CO_2 or O_2 addition also offers more flexibility in adjusting H_2/CO of end product especially at low temperature and high pressure according to the Syngas downstream application.

1.7.2 Effects of CO_2 on the pyrolysis and gasification gas composition

Zhang et al [119] investigated the effect of the pyrolysis medium composition in the biomass fast pyrolysis process in a fluidized bed gasifier at 550° C. The pyrolysis mediums were N_2, CO_2, CO, CH_4 and H_2. The authors found that the liquid yield, composition and higher heating value depend on the pyrolysis bath gas composition. The pyrolysis in a CO_2 atmosphere was seen to produce less char than in the other atmospheres. The CO_2 yield also decreased compared to the yield obtained in an N_2 atmosphere. Moreover, the CO_2 atmosphere led to the highest yield of acetic acid compared to the other atmospheres (see figure 1.38). $GC - MS$ analysis of the liquid products shows that CO and CO_2 atmospheres produced less methoxy-containing compounds and more mono-functional phenols. The authors explained these observation by two possible mechanisms: the CO_2 reacted with the active volatiles or with the biomass char.

Recently, in their study on macro-algae pyrolysis/gasification, Kwon et al [120] found that introducing CO_2 in the pyrolysis process at 550 °C in a tubular reactor minimized the generation of pyrolytic oil (see figure 1.39). They noticed a decrease in the pyrolytic oil by 24.3% and an enhanced pyrolytic gas production. Such observations implies that hydrocarbons emitted in the pyrolysis process can be broken down in the presence of CO_2.

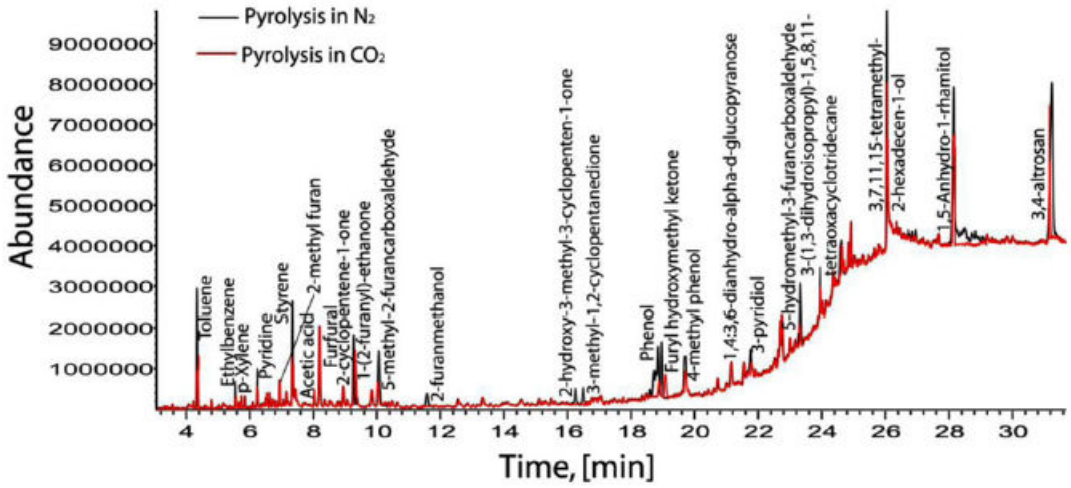

Figure 1.39: Representative chromatogram of pyrolytic oil from red algae (Gelidium amansii) at 550° C in N_2 and CO_2 [120]

The same authors performed another study about the pyrolysis of styrene butadiene rubber [121] and found that the CO_2 enhances C4 hydrocarbons cracking in addition to impeding the gas phase addition reaction by which are formed benzene derivatives. Tyre pyrolysis experiments at 650 °C in a free and in CO_2-containing atmospheres showed that the amount of condensible hydrocarbons decreased by 30 to 50% when introducing CO_2 in addition to a modification of the end products.

The authors also studied the influence of CO_2 on volatile chemical species during the thermal degradation of cellulose and Xylan [122] at low and high heating rates of 10 and 500° C/min. The authors reported substantial increase in H_2 and CO production in the presence of CO_2. The authors performed also Xylan and Cellulose gasification reaction in a tubular reactor. The concentration of H_2, CO and CH_4 in the presence of CO_2 was enhanced by factors of 4, 10 and 7, respectively (see figure 1.40) . As the Boudouard reaction is only thermodynamically favourable at temperatures higher than 700 ° C, this increase of gaseous compounds is related to the fact that CO_2 likely expedites the thermal cracking of volatile compounds evolved from the mixture of cellulose and Xylan, to cite the authors explanations. The condensible hydrocarbons collected during the experimental work were substantially decreased by approximately 67% based on the mass balance. The authors evidenced that the main influence of CO_2 during biomass thermal degradation is perceived in the gas phase were this latter is found to participate to the hydrocarbons cracking leading to more permanent gases. The same results were found using a real biomass: corn stover. The authors did not observe noticeable differences in the thermo-gravimetric analysis of the different biomasses degradation under CO_2 and N_2 respectively.

Kwon et al [120] performed macro-algae gasification tests with steam and variable concentrations of CO_2 in a tubular reactor with temperatures ranging from 600 to 1000 °C. The authors observed that the CO concentration increased by a factor of 2 even at 600 and 700 °C with a CO_2 concentration of 30% compared to a reference state of a CO_2-free atmosphere. The yield of C2 hydrocarbons also increased and the amount of tar was reduced by 51.2% which can be directly correlated with the gas yield augmentation.

In their paper on CO_2 as a Carbon Neutral Fuel Source via Enhanced Biomass Gasification [123], the authors studied the gasification of several woods, grasses, and agricultural residues with steam and CO_2 via thermogravimetric analysis and gas chromatography. The CO_2 concentrations were varied between 0 and 100% with steam as a co-reactant. The authors observed that when only

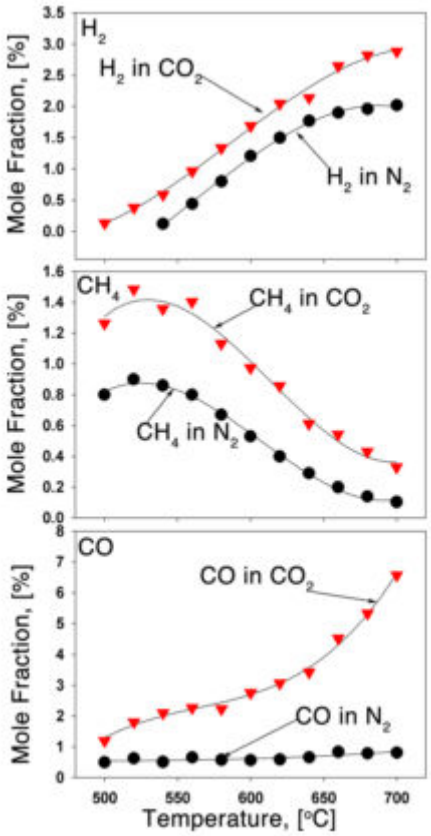

Figure 1.40: Thermal degradation of corn stover: concentration profiles of H_2, CH_4, and CO from the effluent of the tubular reactor in N_2 and CO_2 atmosphere [122]

injecting 5% CO_2 with steam, CO concentration increased by a factor of 10 and H_2 decreased by a factor of 3.3 at 900 ° C. Increasing CO_2 from 5 to 50% resulted in continued CO increases and H_2 decrease by a factor of 3 at 900 ° C. The H_2/CO ratio could be thus adjusted from 5.5 at a 0%CO_2 to 0.25 at a 50% CO_2 concentration depending on the desired application for the Syngas (see figure 1.41) .

CO_2 introduction in biomass gasifier as a reacting gas was also studied by [124] in the case of rice straw gasification. The authors studied the effect of the different gasification atmosphere composition in H_2O, CO_2, O_2 and N_2 on the thermal efficiency of the gasification process and came to the conclusion that CO_2 introduction has a positive effect on the thermal efficiency of a gasifier at temperature of 850°C and above. The gasification experiments were performed on rice straw using a lab scale down-draft gasifier. High CO_2 fraction in gasifying agent generally resulted in low H_2 yield and high CO yield. Indeed, the CO_2 can potentially react in the gas phase with hydrocarbons, such as methane, via a dry reforming reaction:

$$CO_2 + CH_4 \longrightarrow 2H_2 + 2CO \quad \Delta H = +246.9\,kJ/mol \tag{1.56}$$

The CO_2 can also react with hydrogen molecules according to the reverse water gas shift reaction (rWGS):

$$CO_2 + H_2 \longrightarrow H_2O + CO \quad \Delta H = +41.2\,kJ/mol \tag{1.57}$$

In a biomass gasifiers, CO_2 can react with the carbon of the char form after the pyrolysis step, via the heterogeneous Boudouard reaction:

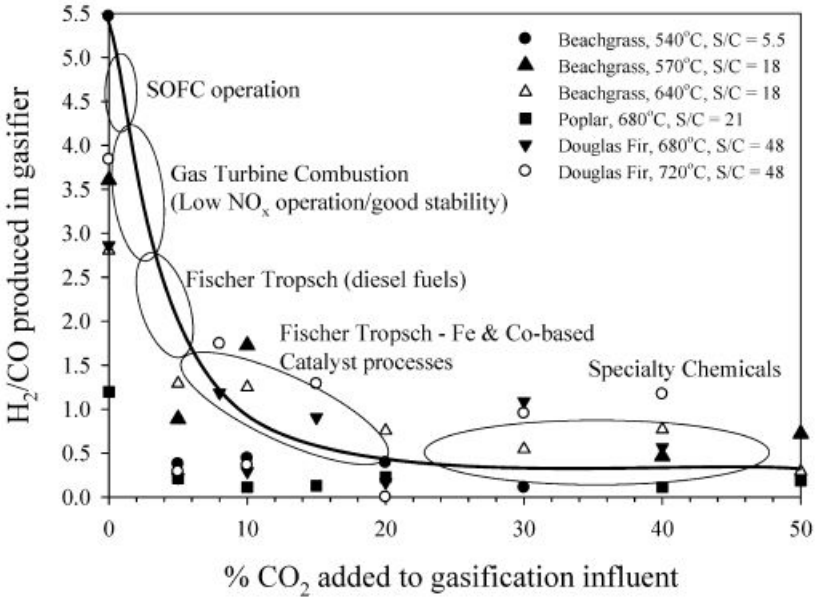

Figure 1.41: Syngas composition adjustment as a function of CO_2 reactant [123]

.

$$C + CO_2 \longrightarrow 2CO \quad \Delta H = -179.5\, kJ/mol \tag{1.58}$$

The main results of these reactions is the enhanced CO production. The authors came to the conclusion that introduction of CO_2 mostly lowers the energy yield of the producer gas, but on the other hand also reduces the preheating energy of gasifying agent resulting in a greater thermal efficiency under defined conditions. Highest thermal efficiency of the process without O_2 was 52% under N_2 (40 vol.%) CO_2 (60 vol.%) atmosphere at the temperature of 850°C. For the process with O_2, where the part of gasifying agent preheating energy supplied by the biomass partial combustion, the highest thermal efficiency was 60% under the CO_2 (60 vol.%) O_2 (8.3 vol.%) and N_2 (31.7 vol.%) atmosphere at the temperature of 950°C. In addition to the good thermal efficiency, the authors argued that such use of CO_2 in biomass gasifiers can provide an N_2-free Syngas which is more suitable for the synthesis of liquid fuels and chemicals.

Other researchers [125] found that the use of CO_2 in biomass gasification, in the process of catalytic biomass gasification, had a significant positive impact on the conversion of biomass fuel into gaseous calorific compounds and on lowering the yield of tarry compounds. The authors performed their study on beech wood-chips in a fluidized bed gasifier. The bed material was dolomitic limestone preheated at 500°C with the gasification medium. The gasification reactions were performed at 850°C, respectively in ($H_2O + O_2$), ($N_2 + O_2$) and $CO_2 + O_2$ atmospheres. The highest cold gas efficiency was achieved when gasifying biomass with a CO_2 containing atmosphere (see figure 1.42).

The gasification of Gulfweed, an aqueous biomass was studied by Toshiaki Hanaoka et al. [126] with a concept of a novel Biomass To Liquid process (BTL) and gas desulfurization using the produced char as a bed material. The authors operated with an atmosphere containing He, CO_2 and O_2 using a down-draft fixed-bed gasifier at ambient pressure and 900°C at equivalence ratios (ER) of 0.1 to 0.3. The Syngas content increased while the conversion to gas on a carbon basis decreased with decreasing ER. At an ER of 0.1 and He/CO_2/O_2 molar ratios of 0/85/15%, the Syngas content was maximized at 67.6% and conversion to gas on a carbon basis reached 94.2%.

Concerning catalytic gasification, Hurley et al. studied the catalytic and non-catalytic gasification

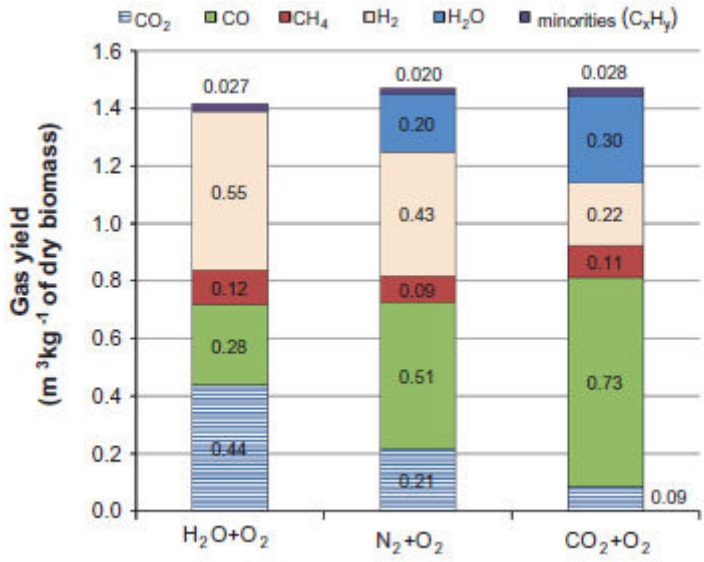

Figure 1.42: Gas yields as a function of gasification atmosphere [125]

of pine sawdust in a fixed-bed tubular reactor at 700 and 800°C with a heating rate of 20°C/min [127]. Typical tests were performed on 1.0 g of dried pine sawdust sample (with or without catalyst) in a gasification atmosphere containing 100% air, or 100% CO_2 or 17 vol.% CO_2 83 vol.% air. The authors found that the yields of char and tar both increased with increasing CO_2 content in the feed gas for the non-catalytic gasification case which is due to the quite lower biomass reactivity to CO_2 compared to oxygen. All the impregnated metal ions, in particular Ni (II), Co (II) and Ru (IV), were very effective for promoting biomass gasification in CO_2. The metal impregnation led to greatly reduced yields of tar and char accompanied by significantly enhanced formation of CO and H_2.

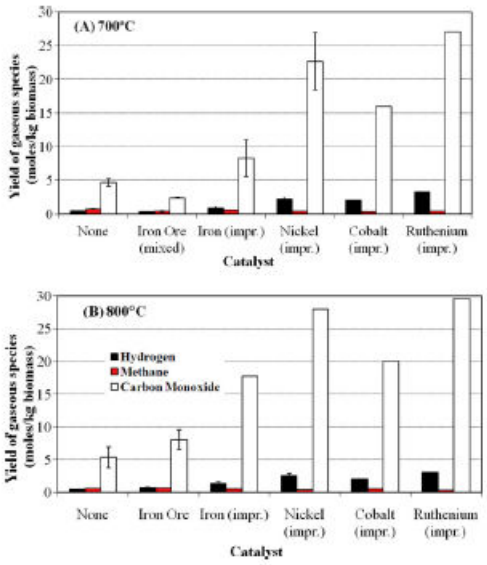

Figure 1.43: Effects of catalysts on yields of major combustible gas species of H_2, CH_4 and CO from CO_2-gasification of pine sawdust at 700°C (A) and 800°C (B). [127]

Synthesis What comes out from the literature concerning the effects of CO_2 on the gas composition is that this latter enhances mainly the production of CO via the homogeneous and heterogeneous reactions. The syngas composition can be adjusted by adjusting the CO_2 concentration in the gasifying medium. According to several authors, CO_2 introduction may be beneficial in well defined conditions of temperature and gasifying medium composition.

1.7.3 Effects of CO_2 on the char properties

Introduction of CO_2 in a biomass pyro-gasification process may affect the char properties. Indeed, Hanaoka et al [128] found that preparing chars in a $N_2/CO_2/O_2$ containing atmosphere leads to a more developed surface area and a higher reactivity towards pure CO_2, especially in a 18% N_2/41% CO_2/41% O_2 atmosphere. The char yield was similar to that obtained under nitrogen but there was an increase in the BET surface area from 275 m^2/g in pure nitrogen to 417 m^2/g and an increase in the char reactivity by a factor of 1.7 to 2.5 depending on the gasification temperature.

Nevertheless, Borrego et al [129] performed pyrolysis experiments of pulverised wood (particle size of 36 to 75 μm) in a drop tube furnace at 950°C under N_2 and CO_2. They performed textural characterisation of the residual chars and found similar specific areas: 277 and 331 m^2/g under N_2 and CO_2. The char reactivity toward air at 550°C in a TG device was also the same. The residence time was estimated at 0.3 s which may be short for the CO_2 to react with the char.

In a recent paper, Watanabe et al investigated the effect of high CO_2 concentrations on the char formation mechanisms [130]. The authors performed cellulose, lignin, and metal-depleted lignin pyrolysis experiments using a thermo-balance in CO_2 and Ar atmospheres. They observed that at a temperature of 1073 K, when proceeding at heating rate of 1 K/s, the char yield of lignin in the presence of CO_2 increased by about 10% compared with that under Ar. However, for cellulose and metal-depleted lignin, no significant difference appeared between pyrolysis under CO_2 and that under Ar. The authors performed FT-IR analysis on the chars along the pyrolysis reaction. At around 1650 to 1770 cm^{-1}, a significant difference appeared in the FTIR spectra of chars formed under CO_2 and those formed under Ar. C=O groups not associated with an aromatic ring were found only in chars formed under CO_2. They concluded that salts such as Na_2CO_3 or K_2CO_3 were formed during the lignin pyrolysis under CO_2. They suggested that these salts affected the char formation reaction, in that the char formed during lignin pyrolysis under CO_2 had unique chemical bands that did not appear in the lignin-derived char prepared under Ar (figure 1.44).

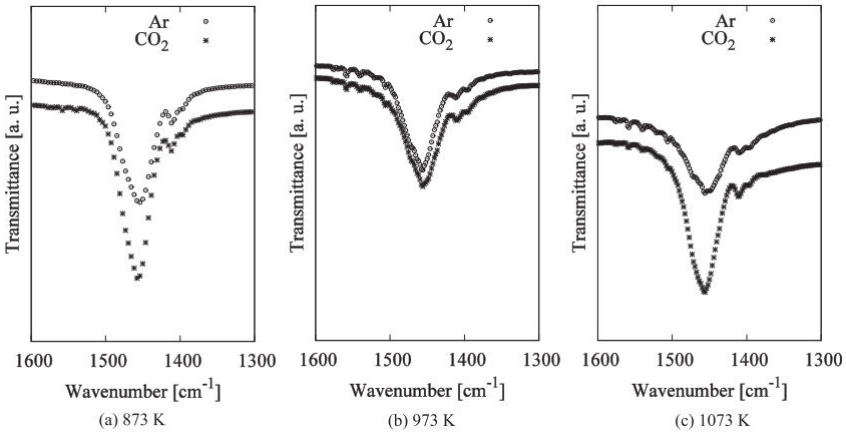

Figure 1.44: FT-IR spectra of the chars derived from lignin focusing on 1450 cm^{-1} groups (C - H, aromatic C - C, carbonate) after heating at 1 K/s [130]

Altogether, the effect of CO_2 on the biomass char properties during pyrolysis was not very widely studied. Few works exist on this subject and were reported above. It is therefore interesting to have a look on the effects of CO_2 on the char properties during pyrolysis of other carbonaceous material such coal or lignite.

Song-ping et al also studied the effects of CO_2 on a lignite pyrolysis. The authors studied the influence of CO_2 through gas yields and distribution, char yield and properties such as elemental composition, surface structure and surface functional groups [131]. The authors found that the CO_2 enhances the gasification of the nascent char, which destroys the hydrogen-containing char structure, and promotes cracking of benzene ring and fracture of hydroxyl, methyl and methylene groups. They also found that CO_2 weakens the interaction between H and char matrix and increases the H fluidity, leading to the increase in the generation of H radicals. These H radicals can combine with other free radical fragments generated from fracture of the coal macromolecules to produce more volatiles. The gas yield was effectively higher in presence of CO_2. The produced char has a higher specific surface and higher pore volume and porosity compared to a free CO_2 pyrolysis. The authors concluded that the introduction of CO_2 promotes the coal pyrolysis and generation of volatile, resulting in decrease in char yield and increase in the evolution amount of H_2, CO, CH_4 and other small molecules hydrocarbons.

Jamil et al made the same findings [132] when studying the fast and slow pyrolysis of a Victorian brown coal under He or CO_2. The authors found that the change of atmosphere from He to CO_2 influenced the char yield. Initial CO_2 gasification of the nascent char occurred at a considerably high rate simultaneously with its thermal cracking above 600°C. The high heating rate pyrolysis generates a radicals on the char surface which are attacked by CO_2. The CO_2 gasification of the nascent char caused an extra weight loss of 2 to 3 wt% of the char under CO_2 atmosphere when compared with that under inert atmosphere (see figure 1.45).

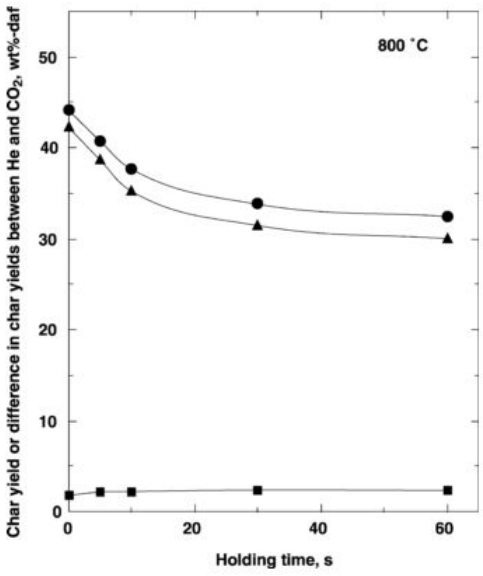

Figure 1.45: Changes in char yields from raw coal with holding time at 800°C. Heating rate; 1000°C/s. rounds: Pyrolysis in He, triangle: pyrolysis in CO_2, square: difference between char yields in He and CO_2 [132].

Bai et al [133] investigated recently The gas release properties and changes in the char structure during lump coal pyrolysis in Ar and CO_2 atmosphere. The authors performed coal pyrolysis experiments in a fixed bed reactor. Coal char was generated at four pressures (0.1 to 1.5 MPa in 0.5 MPa

increments). The chars prepared in CO_2 atmosphere have more cycloalkane and aliphatic structures. The effect of atmosphere on the char structure is particularly evident when the pressure exceeds 0.5 MPa. There are more content of hydroxyl, secondary hydroxyl, olefinic C=C bonds, aromatic C=C structure left in chars prepared under CO_2 atmosphere compared with those prepared under Ar atmosphere. XRD analysis of chars showed that Ar atmosphere is more helpful to the graphitization of char during pressurized coal pyrolysis. The stacking height Lc of char sample prepared in CO_2 is always higher than that prepared in Ar atmosphere within 1.0 MPa indicating that CO_2 atmosphere is beneficial to the growth of crystal layer in vertical position.

Synthesis The literature on the effect of CO_2 on the char properties during pyrolysis is not very developed. From the few studies on biomass, coal and lignite pyrolysis, it comes out that the CO_2 is not inert during the pyrolysis. It can influence the char yield, texture as well as the nature of SFG on the char surface. The data are very scarce.

1.7.4 Char gasification in complex atmospheres containing CO_2

In contrast with the huge work done in the last decades on the char gasification in a single atmospheres of H_2O or CO_2, very few studies deal with the gasification of biomass or coal char in a mixed atmosphere of carbon dioxide and steam. The related conclusions to the effect of a such multi-gas atmosphere differ from a study to another. Several authors assume that adding the carbon dioxide to the steam slows down the gasification reaction, whereas others think that it enhances it. Several models are proposed in accordance with these conclusions where in the two gases are whether reacting on separate active sites (**additivity**) or competing for the same ones (**common active sites**). Others found that there is an active cooperation (**Synergy**) between the two gases. The drawn conclusions are contradictory, somewhat hasty and lack of proofs to definitely state on the action of a mixed atmosphere of H_2O and CO_2 in the global gasification reaction.

The main findings in the literature about mixed atmosphere gasification of biomass chars as well as coal and lignite chars are summarized below.

Biomass char gasification in complex atmospheres containing CO_2

Groeneveld and Van Swaaij studied the wood char gasification reaction in a mixture of H_2O and CO_2. A n^{th} order model has been proposed for wood char gasification in a mixed atmosphere of H_2O and CO_2 [104]:

$$R_{(mix)} = k_{(T)}(P_{(H_2O)} + P_{(CO_2)})^n \tag{1.59}$$

The authors assumed a single reaction order, a single activation energy and frequency factor for the mixed atmosphere gasification reaction. Regarding the literature on the biomass char gasification, the steam and Boudouard gasification reaction do not have the same rate. The steam gasification is 2 to 5 times faster than the Boudouard reaction. Activation energies, pre-exponential factors as well as sensitivity to the gas partial pressure are different. This model is therefore criticable in a sense that it does not takes into account the particularity of each reaction.

Maria Barrio and co-workers [134] performed experiments of wood char gasification in a steam-carbon dioxide mixture to check its effects on the reaction rate. They determine first the reaction constants for CO_2 (k_{1c}, k_{3c}) and steam (k_{1w}, k_{3w}) gasification reaction. The inhibition effects of CO and H_2 were neglected. The two models describing CO_2-carbon and H_2O-carbon gasification reaction fit well the experimental results. They adapted the following gasification reaction scheme and proposed a model for the gasification in a mixed atmosphere of H_2O and CO_2:

$$C() + H_2O \longrightarrow C(O) + H_2 \tag{1.60}$$
$$C(O) \longrightarrow CO \tag{1.61}$$
$$C() + CO_2 \longrightarrow C(O) + CO \tag{1.62}$$
$$C(O) \longrightarrow CO \tag{1.63}$$

$$R(Xref)_{(mix)} = \frac{k_{1w}P_{H_2O} + k_{1c}P_{CO_2}}{1 + \frac{k_{1w}}{k_{3w}P_{H_2O}} + \frac{k_{1c}}{k_{3c}P_{CO_2}}} \tag{1.64}$$

The reaction constants for H_2O and CO_2 gasification reactions were different, which implies that desorption of C(O) complex has different pathways in steam and in carbon dioxide gasification $k_{3w} >> k_{3c}$. In order to predict the reactivity in H_2O/CO_2 mixture based on single atmosphere experimental data, the authors tested three alternatives since the rate constant for adsorption step were nearly equal ($k_{1w} = k_{1c}$):

The first case where $k_3 = k_{3w}$, the second case: $k_3 = k_{3c}$ and Third case: model equation. The authors found that the gasification reaction is best predicted for $k_{3w} = k_{3c}$. In the two other cases, the reactivity of char in a mixture of H_2O and CO_2 was under-predicted. This would imply that the carbon conversion is mainly due to steam gasification meanwhile the carbon dioxide, which is less reactive, has potentially another role when it is injected as a co-reactant with steam but in any case would inhibit the gasification reaction. Barrio and co-workers also determined the different rate constants based on experimental data involving experiments in mixed atmospheres of H_2O and CO_2, but the kinetic model under-predicted the char reactivity in this case.

In 2008, Tagutchu et al [103] observed a synergy between steam and the carbon dioxide when mixed together as a gasifying agent. Indeed, the authors found that the rate of the wood char gasification reaction increases in a mixed atmosphere of $H_2O + CO_2$ and is higher than those obtained in a single reactant atmosphere (H_2O and CO_2 respectively diluted with nitrogen) (see figure 1.46). They found that the char reactivity in mixed atmosphere of CO_2+H_2O was higher than the sum of the single reactivities and concluded to synergy effects between the two gases. They proposed a model based on the work of Robert and Harris in which the H_2O and CO_2 react on separate active sites.

$$R(Xref)_{(mix)} = \frac{1 - \theta_{H_2O}}{1 + \theta_{H_2O}\theta_{CO_2}} R(Xref)_{(CO_2)} + \frac{1 - \theta_{CO_2}}{1 + \theta_{H_2O}\theta_{CO_2}} R(Xref)_{(H_2O)} \tag{1.65}$$

Where θ_{H_2O} and θ_{CO_2} are the covering ratios when the char is gasified respectively in single atmospheres of H_2O and CO_2.

The gasification of large variety of biomass samples was investigated in a TG apparatus with a heating rate of 10°C/min up to 1000°C using steam, carbon dioxide or a mixture of both reactant as a gasification medium [8]. The authors observed that regardless of the biomass type, introducing CO_2 with a minimum amount of 30 % next to steam into the flow stream resulted in a complete char burnout with a light mineral film remaining in the crucible, whereas a black char residue remains when using only steam as a gasification medium.

Similar findings are exhibited elsewhere [135] for the gasification of various biomass samples in a TG apparatus up to a temperature of 750°C with a heating rate of 10°C/min. The CO_2-H_2O gasification environment led to a more enhanced pore structure and surface area development than with only steam as a gasification medium.

Susana Nilsson et al studied the gasification of dried sewage sludge (DSS) chars in a pilot fluidized bed reactor under CO_2, H_2O and their mixtures [136]. The experiments were performed in the

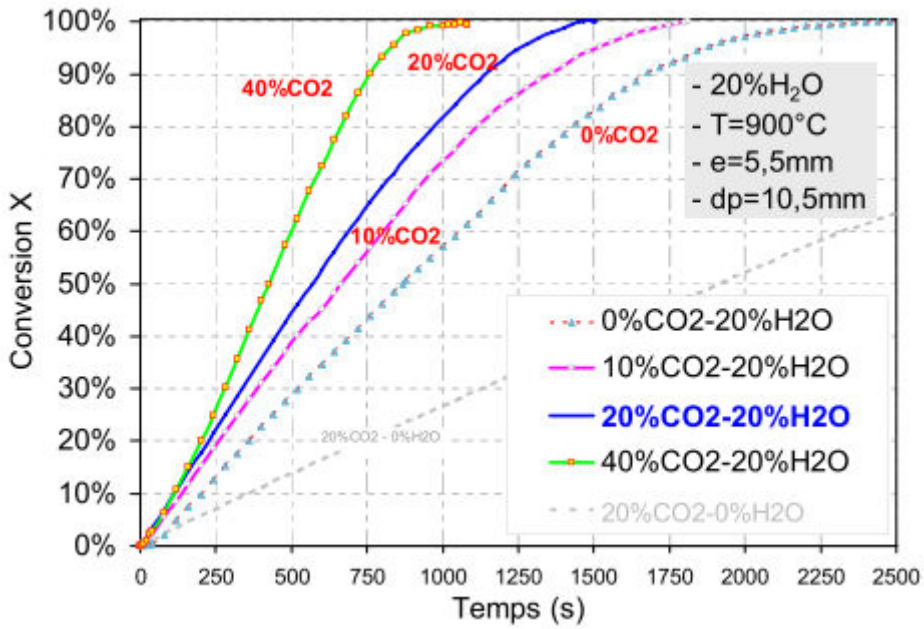

Figure 1.46: Effects of CO_2 addition on the steam-char gasification reaction (e: particle thickness, dp: particle average size) [103].

temperature range of 800-900°C and gas partial pressure of 0.1-0.3 bar. One important fact that must be mentioned is that DSS chars when prepared in the fluidized bed reactor, cooled down and re-introduced for gasification have a lower reactivity than chars prepared and gasified in-situ without being cooled down. The authors demonstrated that the DSS char reactivity in mixed atmospheres of H_2O and CO_2 can be expressed as the sum of the single atmosphere gasification reactivites.

$$R_{(mix)} = R_{(CO_2)} + R_{(H_2O)} \tag{1.66}$$

Susana Nilsson et al. also studied the gasification reactivity of olive tree pruning [137] in the same fluidized bed apparatus. The experiments were done in the temperature range of 760-900°C in mixtures of CO_2, H_2O, H_2, CO and N_2. The authors determined the reaction kinetic constants respectively for the CO_2 and the H_2O gasification reactions. Afterwards, they performed gasification experiments in mixtures of H_2O and CO_2 and found that their experimental results are correctly described by summing the two single rates.

The main results on biomass char gasification in mixed atmospheres of CO_2 and H_2O as discussed before are summarized in table 1.2.

Coal and lignite char gasification in complex atmospheres containing CO_2

Liliedahl and Sjostrom [138] studied the gasification of finely ground lignite char samples of 0.5-1 g in a thermo-balance at atmospheric and elevated pressures, at temperatures between 750 and 850°C, using a number of CO-CO_2-H_2O-Ar mixtures. The authors found that the mixed atmosphere char gasification reactivity can be modelled following:

$$R_{(mix)} = \frac{(k_{H_2O}P_{H_2O} + k_{CO_2}P_{CO_2})}{(1 + K_{CO}P_{CO})} exp(bX^2)(1-X)^{(1/3)} \tag{1.67}$$

Where K_{CO} is an equilibrium constant for carbon monoxide. This expression originates from Langmuir-Hinshelwood kinetics, but the retarding effect of carbon dioxide and steam relative to that

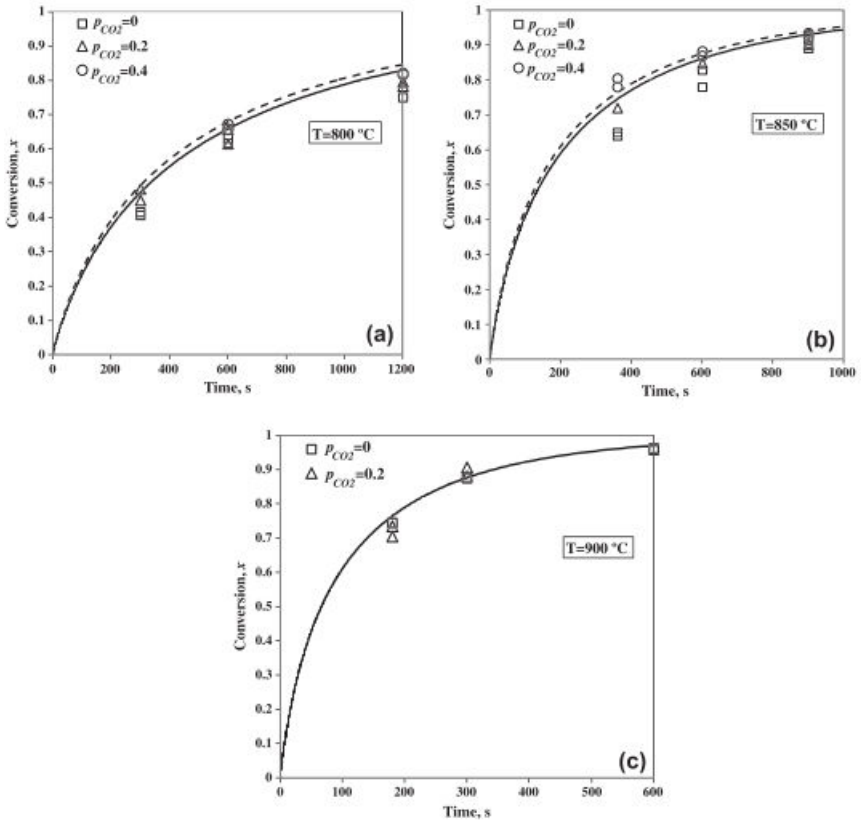

Figure 1.47: Char conversion as a function of time at three different temperatures: (a) 800°C; (b) 850°C; (c) 900°C. The points are the values measured using $CO_2 + H_2O + N_2$ mixtures at fixed PH_2O = 0.20 bar for the indicated values of pCO_2. The x vs t curves are calculated using the additive law for PCO_2 = 0.20 bar (solid lines) and PCO_2 = 0.40 bar (dashed lines)

of carbon monoxide was considered to be minimal at atmospheric pressure and therefore, those terms are omitted in the denominator.

Roberts and Harris [139] performed a comparative study on the gasification of a charcoal in single atmospheres of H_2O and CO_2 and in a mixture of the two gases. The authors compared the different char reactivities in the aforementioned gasification medium. The highest one was observed in pure steam gasification medium, whereas the lowest one was obtained for carbon dioxide gasification. In a mixed atmosphere, the char conversion rate decreased comparatively with that obtained in a pure steam gasification medium which led the authors to conclude on the inhibiting effect of CO_2 on the steam-gasification reaction (see figure 1.48). They proposed a model assuming a competition between steam and carbon dioxide for the same surface reaction sites:

$$R(Xref)_{(mix)} = R(Xref)_{(CO_2)} + R(Xref)_{(H_2O)}(1 - \theta_{(CO_2)}) \tag{1.68}$$

Where $\theta_{(CO_2)}$ is the active sites covering ratio by carbon dioxide.

$$\theta_{(CO_2)} = \frac{\dfrac{k_{1C}}{k_{3C}P_{CO_2}}}{1 + \dfrac{k_{1C}}{k_{3C}P_{CO_2}}} \tag{1.69}$$

The authors made the assumption that the CO_2-carbon gasification reaction rate is so low that

Table 1.2: Literature review on biomass chars gasification in mixed atmospheres of CO_2 and H_2O

Reference	Char	Pyrolysis conditions	Mixed atmosphere mechanism
[104]	Wood char (4 cm)		Same activation energy and dependance on the sum of partial pressure
[134]	Birch wood char (45-63 μm)	Slow pyrolysis 24°C/min	Competition
[103]	Pine wood char (5.5 mm)	Medium rate pyrolysis in a screw reactor at 60°C/min	Synergy
[8]	Various biomasses	Slow pyrolysis 10°C/min	Synergy
[136]	Dried Sewage sludge char (1.2 mm)	Fast pyrolysis in FBR	Additivity
[137]	Olive tree prunning char (1.9 mm)	Fast pyrolysis in FBR	Additivity

the reduction in the available surface area by adsorbed C(O) species from the CO_2 reaction is likely behind the decrease in steam gasification reaction upon addition of CO_2. These conclusions are nonetheless hasty as far as they were drawn for a 0-10% char conversion level. The carbon dioxide seems to inhibit the steam-carbon reaction in the earlier stage of gasification, yet there is a lack of evidences to conclude on a permanent inhibiting effect throughout the gasification reaction.

Everson et al [140] also investigated the effect of a mixture of carbon dioxide and steam on the gasification of char-coals. Firstly, they conduct gasification experiments in binary gas mixtures (H_2O/H_2 and CO_2/ CO) for the determination of the rate constants according to Langmuir-Hinshelwood model respectively for carbon dioxide and for steam gasification. Afterwards, they carried out experiments with multi-component gas mixture containing (H_2O, H_2, CO_2 and CO) and proposed two reaction models based on the Langmuir-Hinshelwood expressions for the prediction of the experimental results. They assumed that the gasification reaction can proceed with two possible surface mechanisms:

- In the first model, the carbon-carbon dioxide and carbon-steam gasification reactions occur at a common active sites, the reactivity would have the following expression:

$$R(Xref)_{(mix)} = \frac{k_{1w}P_{H_2O} + k_{1C}P_{CO_2}}{1 + \frac{k_{1W}}{k_{3W}P_{H_2O}} + \frac{k_{1C}}{k_{3C}P_{CO_2}} + \frac{k_{2W}}{k_{3W}P_{H_2}} + \frac{k_{2C}}{k_{3C}P_{CO_2}}} \tag{1.70}$$

  When neglecting the inhibiting effects of CO and H_2, the reactivity will have the same expression as proposed by Barrio et al [134].

- In the second assumption, the carbon dioxide and steam gasification reactions are assumed to react on separate active sites, resulting in the expression:

$$R(Xref)_{(mix)} = \frac{k_{1w}P_{H_2O}}{1 + \frac{k_{1W}}{k_{3W}P_{H_2O}} + \frac{k_{2W}}{k_{3W}}P_{H_2}} + \frac{k_{1C}P_{CO_2}}{1 + \frac{k_{1C}}{k_{3C}P_{CO_2}} + \frac{k_{2C}}{k_{3C}P_{CO}}} \tag{1.71}$$

The gasification reaction was best described with the assumption that the reactions occurred on separate sites (see figure 1.49). The model fits very well the experimental data while the former

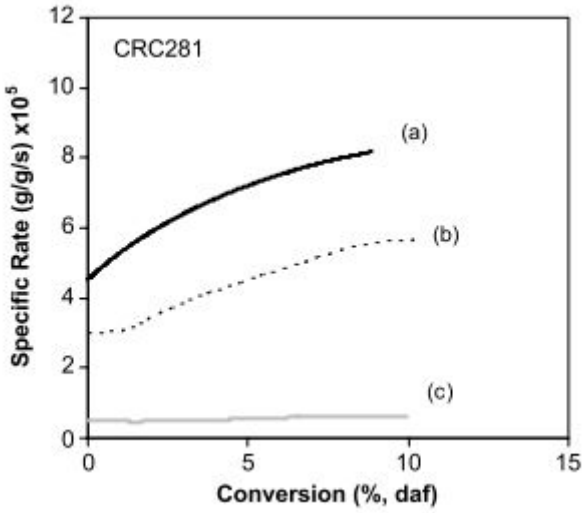

Figure 1.48: Example of a conversion profile for a char sample reacting at 1123 K in (a) 0.5 MPa H_2O, (b) a mixture of 0.5 MPa H_2O + 0.5 MPa CO_2, and (c) 0.5 MPa CO_2 [139].

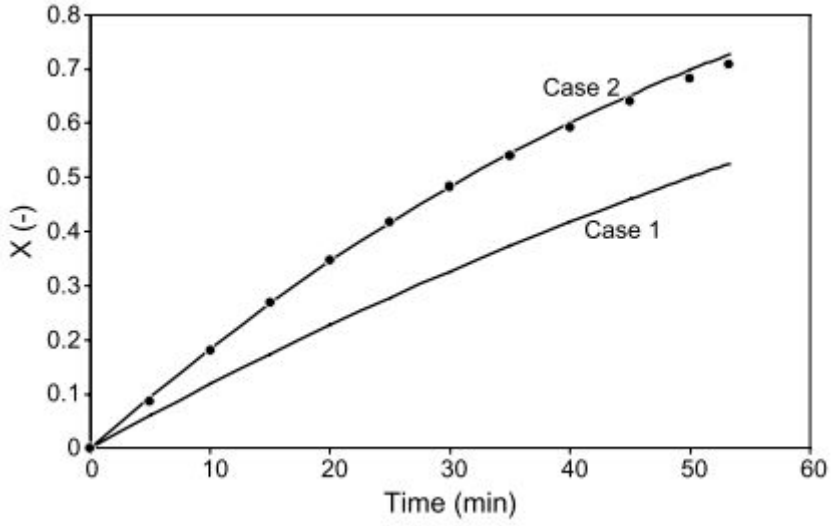

Figure 1.49: Coal-char gasification with multi-component mixture at 1223 K. Case 1 involves Rate 1 (same site) and Case 2 involves Rate 2 (separate sites), full lines represent models and the symbol represents experimental points [140]

assuming reactions on common active sites clearly under-predicted the experimental results. It is also worth noting that the authors evidenced the possibility of using the rate constants determined in binary mixtures of H_2O/H_2 and CO_2/ CO for the modelling of the gasification with a multi-components atmosphere according to scheme involving reactions on separate active sites.

More recently, Huang et al [141] carried the same gasification experiments as Everson et al. They determined the different gasification constants by studying the char gasification with binary gas mixtures H_2O/H_2 and CO_2/CO. Experiments with multi-component gasifying mixtures (H_2O + H_2 + CO_2 + CO) were also carried out showing results which fit well with the "separate reactive sites" reaction model given above. The comparison was based on the char reactivity at the conversion level of 50%. The calculated predictions according to the model were very close to the experimental values. This study also showed that reaction constants obtained with binary gas mixtures can be used to predict gasification with a multi-component gasification medium according to the previous model. The drawn conclusion was in accordance with that given by Everson et al [140].

The assumption of reaction on separate active sites was also held by Tay H.L et al [41] for coal char gasification. The authors performed gasification experiments at 800°C with different gasification atmospheres (15 % H_2O balanced with Ar; 4000 ppm O_2 balanced with CO_2; 4000 ppm O_2, 15 % H_2O balanced with CO_2) and gasification holding times. Char conversion rate calculations show that the degree of char conversion during the gasification in an O_2 + H_2O + CO_2 mixture was approximately equal to the sum of those during the gasification in 15% H_2O (balanced with argon) and in O_2 + CO_2 mixture, except for the 20 min holding time experiments were the gasification mechanisms would have changed due to the low char yield in the case of the $O_2/H_2O/CO_2$ gasification medium (see figure 1.50). They suggest that the additivity in char conversion means that O_2, H_2O and CO_2 do not compete for the same active sites on the coal/char. There would be enough vacant sites for the gasifying agents to react with. The authors measured the intrinsic reactivities of partially reacted chars with air in a thermogravimetric analyser (TGA) at low temperatures (380 or 400°C). Also, they characterised the char structural features evolution using FT-Raman spectroscopy and spectral deconvolution. The authors found that the presence of steam in the gasifying atmosphere has a drastic effect on char structure, in particular by decreasing the relative ratio of small and large aromatic ring structures in char, and on the subsequent reactivity of char with air at low temperatures. Moreover, it was found that the presence of steam during the gasification at 800°C also impacts on the volatilisation of Mg and Ca by altering the char structure and consequently improving their retention. The authors concluded that the $charH_2O$ gasification follows a reaction pathway different from the $charCO_2$ gasification, at least for the gasification of Victorian brown coal under their experimental conditions.

More recently, Chao Chen et al [142] investigated the effect of the pyrolysis conditions on the gasification reactivity of lignite chars in mixtures of H_2O + CO_2. Two kinds of char were prepared from a lignite by fast pyrolysis using a drop tube furnace and by slow pyrolysis using a fixed-bed furnace at the temperature of 1273 K. Char gasification reaction with CO_2, H_2O and their mixtures were performed in a thermogravimetric analyser (TGA) system. The gasification rate equations derived from TGA were afterwards validated by fluidized-bed gasification experiments. The authors found that both fast-char and slow-char are dense char. The gasification reaction of both chars were quite well described by a shrinking core model, which means that the reaction occurs mainly in the external particle surface. The authors found that the char gasification rate in the mixtures of CO_2 and H_2O was lower than the sum of the two single reaction rates, but higher than the rate of each independent reaction, for both fast-char and slow-char gasification. The gasification rate in mixtures of both gases could be written as a linear combination of the two single gasification rates (see figure 1.51).

The regressed coefficient of $R_{(CO_2)}$ is about 0.65 and the coefficient of $R_{(H_2O)}$ is about 1 for both

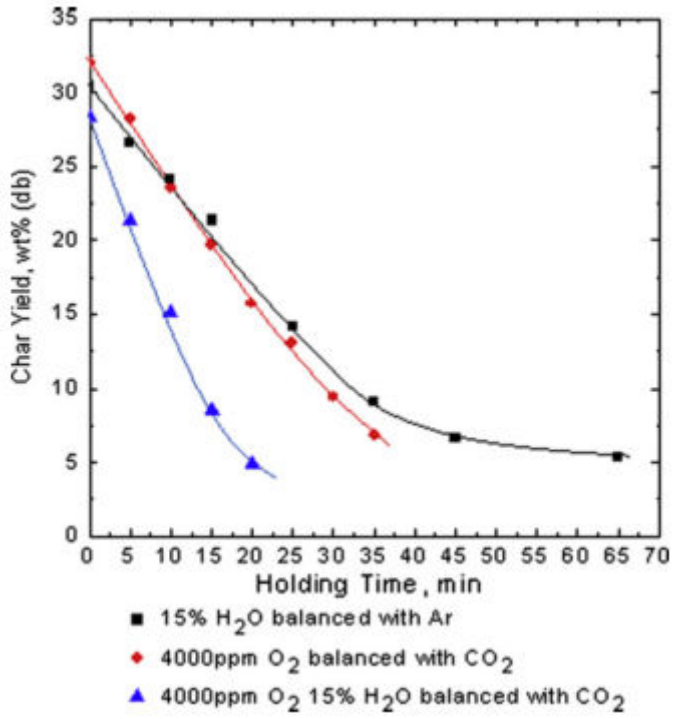

Figure 1.50: Char yields as a function of the holding time at 800°C (Additivity of the reactivities in a multi-component atmosphere) [41].

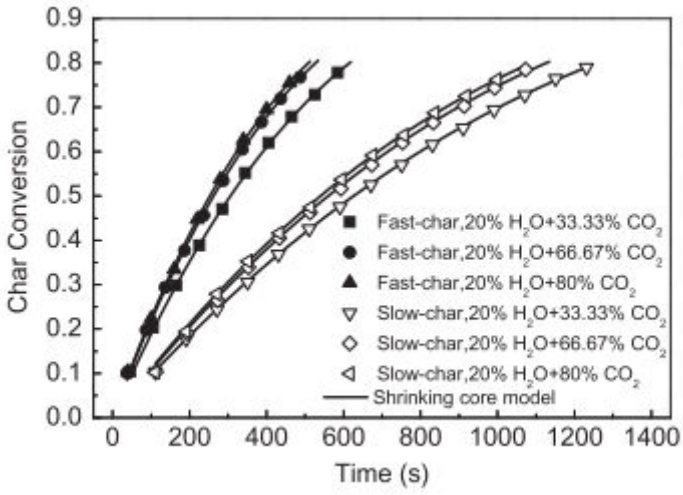

Figure 1.51: Comparison of fast- and slow-chars conversion gasified in mixtures of CO_2 and H_2O with the change of CO_2 concentration. [142].

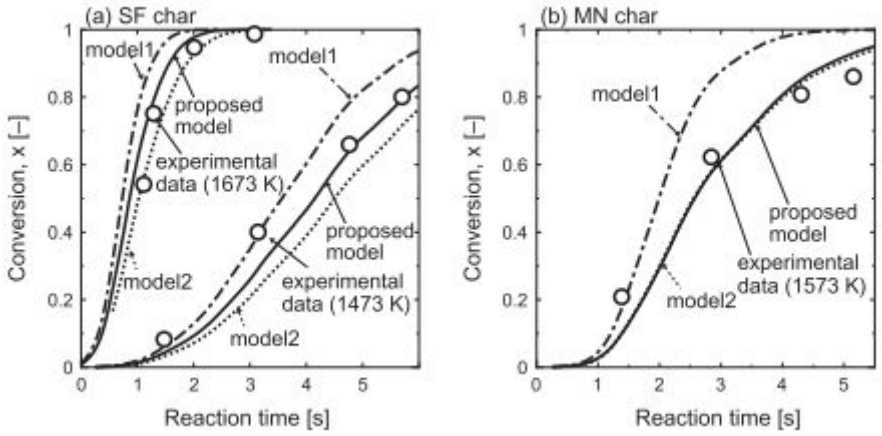

Figure 1.52: Coal char gasification experimental results and modelling [143]

fast-char gasification and slow-char gasification. Both of the results from the TGA and the fluidized-bed reactor showed that char-H_2O reaction was independent on char-CO_2 reaction, while char-CO_2 reaction was inhibited by char-H_2O reaction. It is worth-noting that the chars were dense ones and that the gasification reactions followed a shrinking core model. It is likely that only a small part of the reactive surface is participating to the gasification reaction.

$$R_{(mix)} = 0.65R_{(CO_2)} + R_{(H_2O)} \tag{1.72}$$

Umemoto et al [143] studied the coal gasification reaction in mixed atmospheres of CO_2 and H_2O. The coal chars were prepared in a drop tube furnace at 1673 K. The authors performed gasification reaction in a TG apparatus. They found that the gasification reaction rate in mixed atmospheres was neither well described by a model were the H_2O and CO_2 react on separate active sites (the model over-predicted the experimental data, see figure 1.52), nor by a common active sites model as it under-predicted the gasification rate.

The authors proposed that the two reactants, H_2O and CO_2, share partially their respective active sites. The authors modified the LH expression for the chemical reaction rate term proposed by Everson et al and introduced new parameters to account for the sharing of the active sites.

The mixed atmosphere reaction rate is be expressed as:

$$R(Xref)_{(mix)} = \frac{k_{21}P_{H_2O}}{1 + bck_{21}P_{CO_2} + bck_{13}P_{CO} + k_{22}P_{H_2O} + k_{23}P_{H_2}} \tag{1.73}$$

where

$$a = \frac{n_{share}}{n_{tH}} \tag{1.74}$$

$$b = \frac{n_{share}}{n_{tC}} \tag{1.75}$$

$$c = \frac{a}{b}\frac{1 + (1-b)k_{22}P_{H_2O} + (1-b)k_{23}P_{H_2}}{1 + (1-a)k_{12}P_{CO_2} + (1-a)k_{13}P_{CO}} \tag{1.76}$$

n_{share} is the total number of shared active sites for CO_2 gasification and H_2O gasification. n_{tH} is the total number of active sites for H_2O gasification. n_{tC} is the total number of active sites for

CO_2 gasification. c is the number of vacant active sites for CO_2 gasification to the number of vacant active sites for H_2O gasification.

The authors studied the gasification on three different coal chars. They found two different values for the parameters [a,b] to best fit the experimental results for the three chars: [0.5,0.62], [0.42,1] and [0.47,1]. The results are similar for the two last chars. When parameter b is equal to 1, it means that H_2O can react on any active site. The authors think that this fact is due to the lower molecular size of the H_2O molecule which can penetrate in all the pores. For the first char, the authors argued that the parameter b is not equal to unity due to the higher content of catalytic alkali species compared to the two others which provide more active sites for the CO_2 molecule. The authors used a random pore model to describe the reactivity evolution along the conversion. As an assumption and a perspective for future works, the authors proposed that b is higher than a because the molecular size of CO_2 is larger than that of H_2O allowing H_2O to access to more active sites located in pores where CO_2 can not enter.

Bai et al [144] studied recently the char coal gasification reactivity with CO_2, H_2O and their mixtures. The coal samples were pyrolyzed under an argon atmosphere at temperatures of 800°C, 900°C, 1000°C and 1100°C adopting slow pyrolysis operating conditions. The chars were afterwards gasified isothermally in CO_2 and H_2O environments ranging from pure CO_2 to pure H_2O in 20 vol% increments. The authors found that at temperatures of 900°C, 1000°C and 1100°C, the coal char has a maximum reactivity in a 100% H_2O atmosphere. Its reactivity decreases with CO_2 addition. However, at a temperature of 800°C, the coal char has a higher reactivity in a mixed atmosphere than in pure H_2O or pure CO_2. Even more, the reactivity in mixed atmosphere of CO_2 and H_2O was higher than the individual reactivities in H_2O and CO_2 respectively. The same results were obtained at 750°C, meaning that the mixed atmosphere gasification showed competition beyond 800°C and Synergy at 800°C and below [144].

The authors performed acid washing on the coal sample to remove minerals.After removing minerals, and at the same temperatures of 750°C and 800°C, the synergy effects disappeared and the maximum reactivity was obtained in pure H_2O. Moreover, the authors noted that the reactivity decrease in pure atmospheres of CO_2 and H_2O was not the same. The CO_2 gasification was more affected by the mineral specie removal. The extent of the effect of mineral matter on the CO_2 gasification was that the gasification reaction could not take place when removing minerals at 750°C. The authors concluded that the synergy effect was due to these catalytic species which influenced mainly and selectively the CO_2-char gasification reaction. The Ca was the most abundant alkali active mineral in the raw coal. When adding calcium by loading it into acid washed coal samples, the chars recovered their enhanced reactivity in mixed atmosphere of CO_2 and H_2O which was higher than in pure steam. The authors explained their observation by the fact that Ca cations would react with the carboxyl ions present on the coal surface to form $-(COO)_2Ca$ structures which enhance the gasification reactivity of the char towards CO_2 and H_2O.

$$Ca^{2+} + 2[-(COOH)] \rightarrow -(COO)_2Ca + 2H^+ \tag{1.77}$$

More recently Li et al [46] performed Collie sub-bituminous coal gasification in a fluidised-bed/fixed-bed reactor in three atmospheres of pure CO_2, 15% H_2O in Ar and 15% H_2O in CO_2) in the temperature range of 800 to 900°C. The main purpose of this study is to investigate if the pathways for char-CO_2 and char-H_2O gasification would be the same. The authors found that the conversion of char proceeded fastest during the gasification in the mixture of H_2O and CO_2 (15% H_2O in CO_2). However, the char conversion during the gasification in the mixture was lower than the sum of the char conversion during the gasification in pure CO_2 and 15% H_2O in Ar separately (see figure 1.54).

One has to remember that the structural and chemical properties of coal and biomass chars are

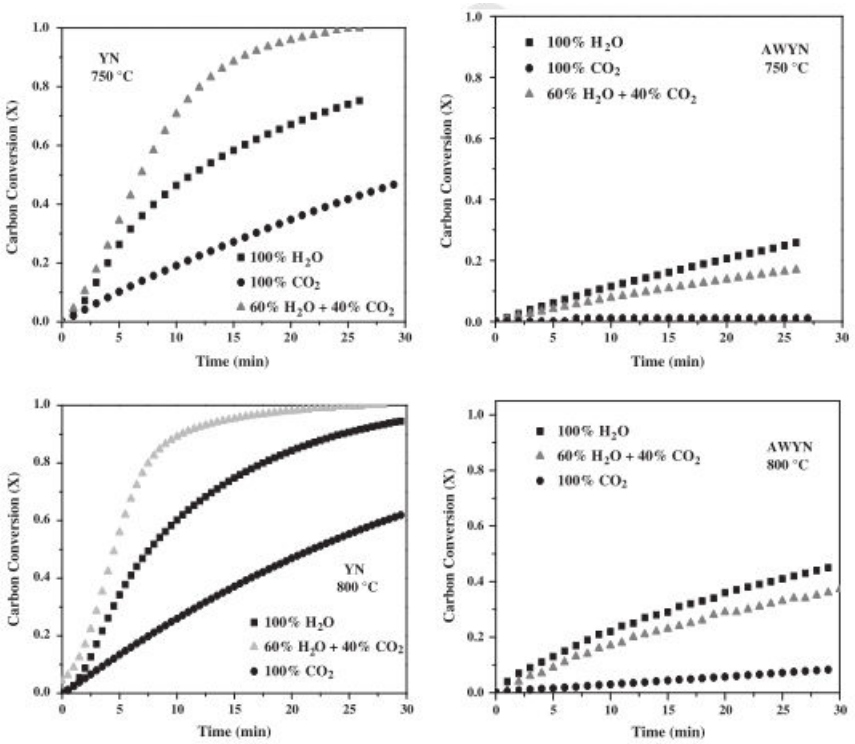

Figure 1.53: Carbon conversion comparison of YN and acid washed YN (AWYN) gasification under different gasifying agents at 750°C and 800°C [143]

quite different. Moreover, coal chars contain a much higher mineral content than woody-biomass chars. The catalytic/inhibiting activity of the mineral species is much more pronounced in coal char gasification. These factors influence the chemistry of gasification in mixed atmosphere gasification, as the interaction of catalytic active species with H_2O and CO_2 may be different as well as the internal gas transport and access to the active sites due to the difference in molecular size of the two molecules. Consequently, observations, results and models validated on coal chars may not be representative of the mixed atmosphere biomass char gasification. Table 1.1 summarizes the main findings on the char gasification in complex atmospheres containing CO_2.

The main results on coal and lignite char gasification in complex atmospheres are summurized in table 1.3.

Synthesis Char gasification in complex atmosphere is far less developed than that in single atmospheres regardless of the type of char (biomass, lignite or coal char). The mixed atmosphere reaction mechanism is poorly understood. The type of mechanism (separate active sites, common active sites or Synergy) is different from a study to another and seems to depends on the nature of the char as well as on the experimental conditions. CO_2 and H_2O gasification reactions seem to have different pathways. Both molecules impact differently the char structure as well as the retention of catalytic active species. It is therefore quite interesting to develop this point in the present work in order to shed light on the unfolding of the char gasification reaction in mixed atmospheres of CO_2 and H_2O.

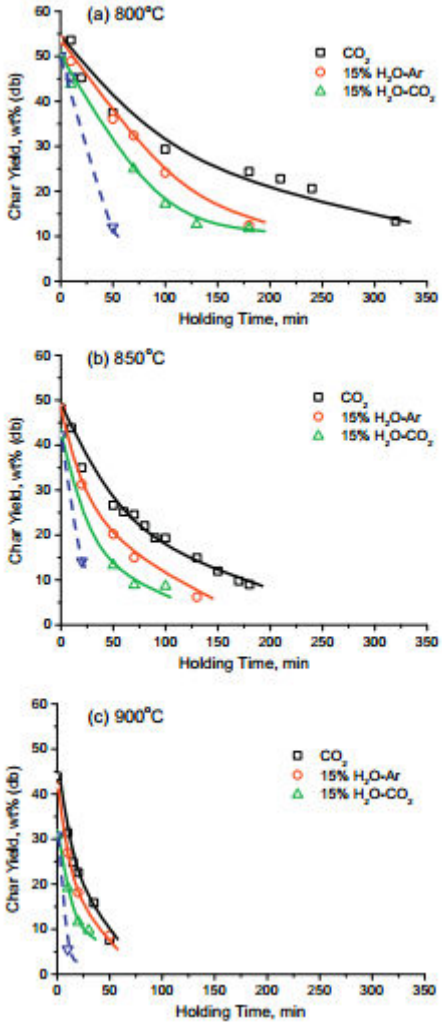

Figure 1.54: Char yields (dry base) from the gasification of Collie sub-bituminous coal in pure CO_2, 15% H_2O balanced with Ar and 15% H_2O balanced with CO_2 as a function of holding time at (a) 800°C; (b) 850°C; (c) 900°C. The dashed lines show the predicted char yields based on those in 15% H_2O balanced with CO_2. [46]

Table 1.3: Literature review lignite and coal chars gasification in complex atmospheres

References	Fuel type	Pyrolysis	Mixed atmosphere mechanism
[138]	lignite char (200-900 μm)	Slow pyrolysis	Competition
[139]	coal char (600 μm)	Slow pyrolysis 10°C/min	Competition
[140]	coal char (20-70 μm)	Slow pyrolysis 20°C/min	Additivity
[141]	coal char (20 μm)	Fast pyrolysis in FBR 1000°C/s at 840°C	Additivity
[41]	Coal char (63-150 μm)	Fast pyrolysis in FBR at 800°C	Additivity
[142]	lignite char (70-106 μm)	Slow pyrolysis 10°C/min Fast pyrolysis in FBR at 800°C	Competition
[143]	Coal char (40 μm)	Fast pyrolysis in DTF at 1400°C	Competition
[144]	Coal char (125 μm)	Slow pyrolysis 10°C/min	Synergy below 800°C and inhibition beyond

Chapter 2

Materials: Biomass samples, experimental reactors and characterisation techniques

Abstract

This chapter deals about materials and methods. First of all, we will describe the biomass as well as the reactors used for pyrolysis and char gasification in LHR and HHR conditions. The experimental procedure for LHR-chars preparation in the SLFI batch reactor), HHR-chars preparation, and gasification experiments in the macro-thermogravimetry reactor will be also presented. In the second part, we will describe the different techniques that were used for char characterisation.

Résumé

Le deuxième chapitre "Matériels et méthodes" décrit en un premier lieu la biomasse utilisée puis les différents dispositifs expérimentaux utilisés lors de la préparation des LHR-chars (pyrolyse lente) à partir du four de pyrolyse batch, et des HHR-chars (pyrolyse rapide) et des tests de réactivité sur le réacteur macro-thermogravimétrique (MTR). Les procédures expérimentales, la correction des blancs de mesures ainsi que l'acquisition des données sont présentées. Un réacteur tubulaire horizontal a également été utilisé pour l'analyse des gaz de pyrolyse. Enfin, les différentes techniques de caractérisation des chars sont listées, des informations précises sur l'apport de ces techniques permettent d'en comprendre l'utilité et l'intérêt pour la compréhension des mécanismes impliqués dans la réaction de gazéification.

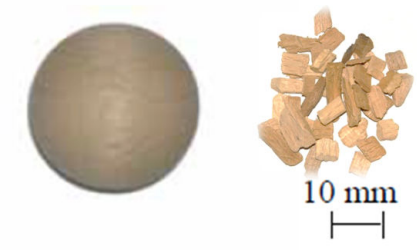

Figure 2.1: Beech wood spheres and chips used for the present study

2.1 Parent wood sample

Beech wood was chosen as the reference biomass. The choice is justified by the availability of this biomass resource in large quantity in France. Two categories of beech sample were used for the pyrolysis and gasification tests:

- 1 mm thick wood-chips having a 5 mm screen size.
- 20 mm diameter wood spheres

The biomass samples are shown in figure 2.1. The proximate and ultimate analysis of the beech samples is given in table 2.1.

Table 2.1: Proximate and ultimate analysis of the beech wood-chips (% dry basis)

Proximate analysis			**Ultimate analysis**			
VM	Ash	FC	C	H	O	N
88.1	0.4	11.5	46.1	5.5	47.9	0.1

Beech wood contains carbon and oxygen in large majority and a quite low ash content. Beech belongs to biomasses having the lowest inorganic content.

2.2 Pyrolysis and gasification reactors

In the present section, we will present the main details of the experimental reactors that were used to perform the biomass pyrolysis as well as the char gasification experiments. The slow pyrolysis was performed in a batch reactor with the only aim to produce LHR-char. The mass loss evolution with time was not monitored. Fast pyrolysis is done in the Macro Thermogravimetry Reactor which allows to monitor the mass loss in HHR conditions as well as in the Horizontal Tubular Reactor that allows to determine the gas composition during a HHR pyrolysis. HHR-chars and LHR-chars gasifications are both performed in the Macro Thermogravimetry Reactor that allows to monitor the char mass evolution during the gasification reaction.

2.2.1 Retorting furnace (RF) for LHR-char preparation

The Retorting Furnace allows to perform LHR pyrolysis of the biomass samples (HR=5°C/min) to obtain LHR-chars. In the RF reactor, the biomass particles are placed in a plateau and are spaced enough to avoid chemical and thermal interactions. The furnace is afterwards sealed and nitrogen

Figure 2.2: Retorting Furnace for LHR-char preparation (RF)

.

gas is injected through its bottom. The furnace is electrically heated. The pyrolysis gas leaves from the top of the reactor. A condenser is placed at the reactor exit to collect condensate composed of high molecular weight species (tars) and water. The reactor is shown in figure 2.2.

2.2.2 Macro Thermogravimetry Reactor for HHR-pyrolysis and char gasification

The Macro-TG experimental device shown in figures 2.3 and 2.4 consists of three major parts:

- The heating system, including a liquid H_2O evaporator, a gas pre-heater and an electrically-heated alumina reactor.
- The gas flow control system consisting of 3 mass-flow meters / controllers.
- The weighing system that comprises an electronic scale, a stand and a platinum basket.

The 2-m long, 75-mm i.d. alumina reactor is electrically heated. The temperatures of the three reactor zones are independently controlled to ensure good temperature homogeneity throughout the furnace. Gas flow rates are controlled by means of mass-flow meters/controllers from Brooks instruments. Before entering the reaction zone, the reactant gases (N_2, CO_2 and H_2O) are preheated up to the reactor temperature. When H_2O is added in the gasification medium, the H_2O + gas mixture passes first through an electrically-heated evaporator maintained at 180°C to vaporize the water. The reacting gas flow inside the reactor is laminar and flowing at an average velocity of 0.2 m/s. The weighing system comprises a set of electronic scales with an accuracy of ± 0.1 mg, a metallic stand placed over the balance, on which are fixed three ceramic hollow tubes with a length of 1 m and a 2.4 mm external diameter. These ceramic tubes hold up a platinum basket with a 50 mm diameter, a solid bottom and a side wall made from a 0.5 mm grid to allow the gas to pass through it. The weighing system can be moved in the vertical direction using a crank handle. The final position of the platinum basket (bearing biomass or chars) is nearly at the reactor mid-length. Example of temperature profiles along the MTG-R measured with a K-type thermocouple are shown

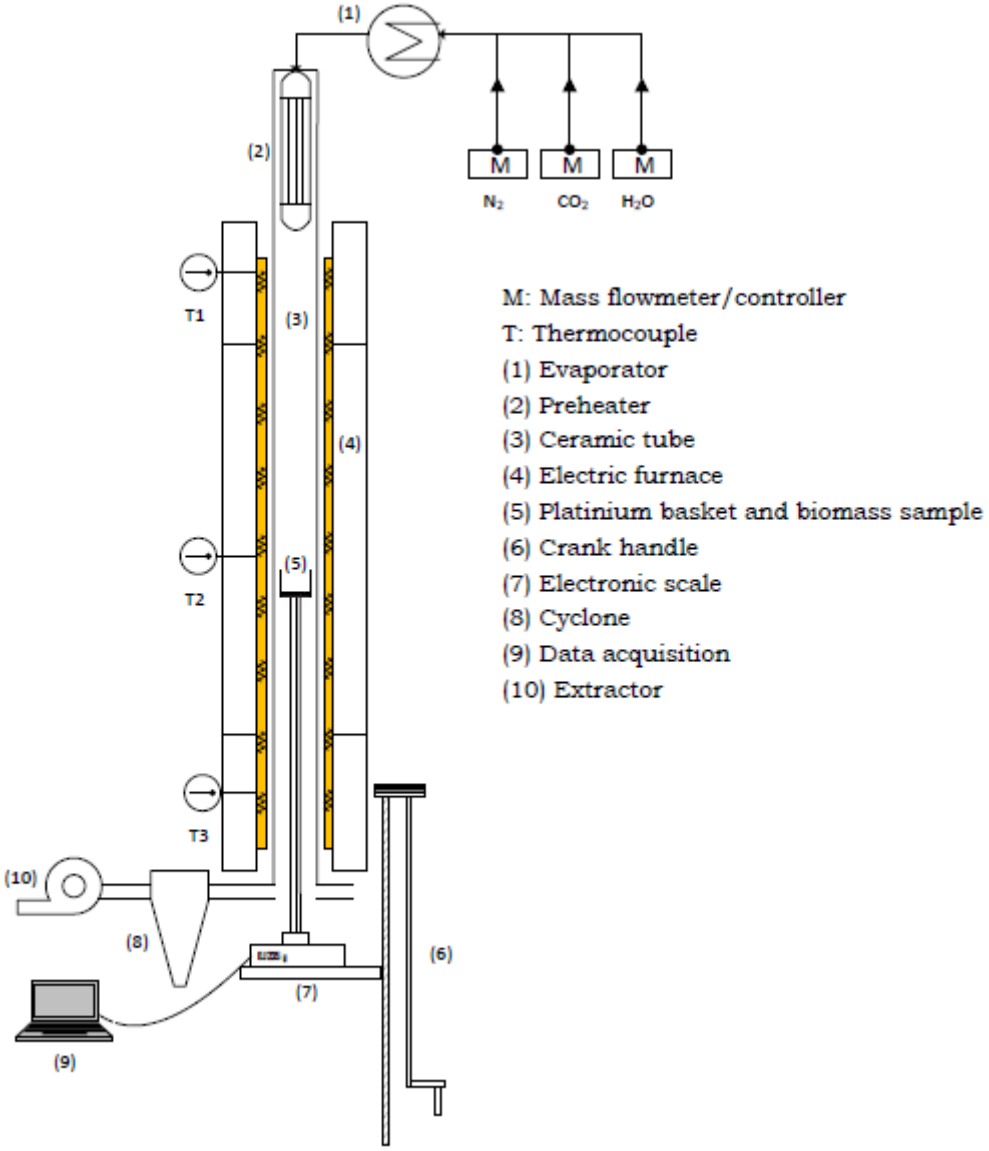

Figure 2.3: Schematic representation of the Macro Thermogravimetry Reactor

.

in figure 2.5. At the final position of the basket, the temperature corresponds to the regulation temperature.

HHR pyrolysis experiments in the MTG-R

The MTG-R was used for rapid pyrolysis of wood particles. The time duration was typically 15 s. The biomass particles are placed into the platinum basket (see figure 2.6) and are spaced enough to avoid chemical and thermal interactions. Moreover, this makes sample representativeness better because of an average result for several wood-chips is obtained for each run.

During the heating of the platinum basket and the ceramic tubes, the flowing gas dynamic pressure (force exerted on the basket) in addition to the drag forces along the ceramic tubes caused the displayed mass value to change. Once a thermal equilibrium was reached inside the reactor, the displayed mass remained constant. For HHR pyrolysis experiments, there was a necessity to correct

Figure 2.4: Photo of MTG-R experimental device

.

the mass change due to these physical phenomena. Blank tests (without biomass) were performed to correct the raw data. We defined for this purpose an experimental procedure, described below, allowing a good reproducibility of the blanks and experiments.

Experimental procedure, data acquisition and blank correction

Once the mass record is launched on the computer, we wait for three seconds before starting the introduction of the basket inside the furnace. After several tests, we choose to turn the crank handle with a speed of 2 rounds/s, corresponding to a 7 cm/s vertical displacement of the basket. Almost 13-14 s are necessary to have the basket in the final position inside the isothermal zone of the reactor. This choice is justified by preserving the High Heating Rate character of the pyrolysis reaction, as well as by the convenience of the introduction operation. For data processing, we subtracted the blank test mass data from that of the pyrolysis experiment. For pyrolysis experiments performed at 850°C, such a procedure allows reaching heating rates near to 100°C/s, which is quite close to conditions encountered in fluidized bed gasifiers.

Gas flow regime inside the MTG-R

For all pyrolysis and gasification experiments, the gas velocity inside the MTG-R was maintained at 0.2 m/s. When changing the reactor temperature, the velocity was maintained at this value by changing the gas flow-rate. For our experimental conditions and based on Reynolds number

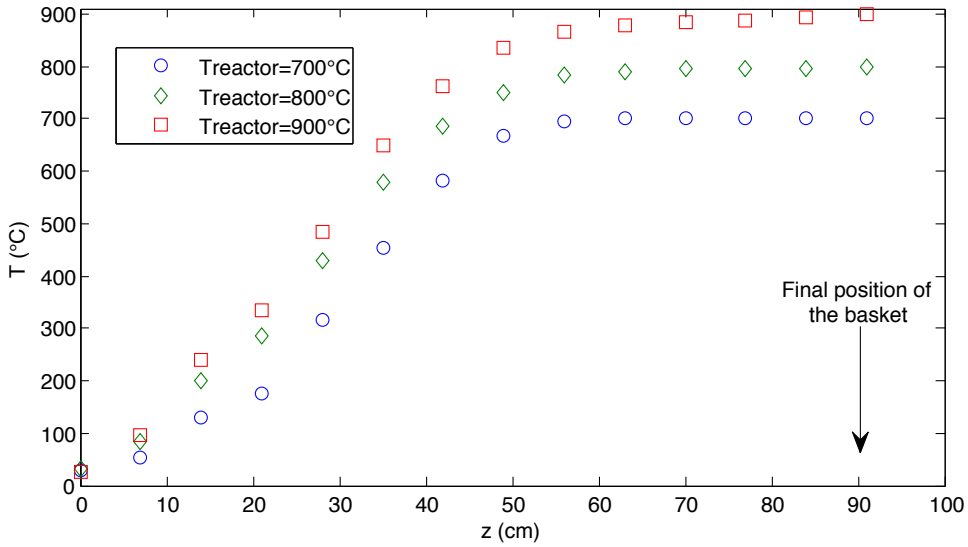

Figure 2.5: Temperature profile along the Macro Thermogravimetry Reactor

.

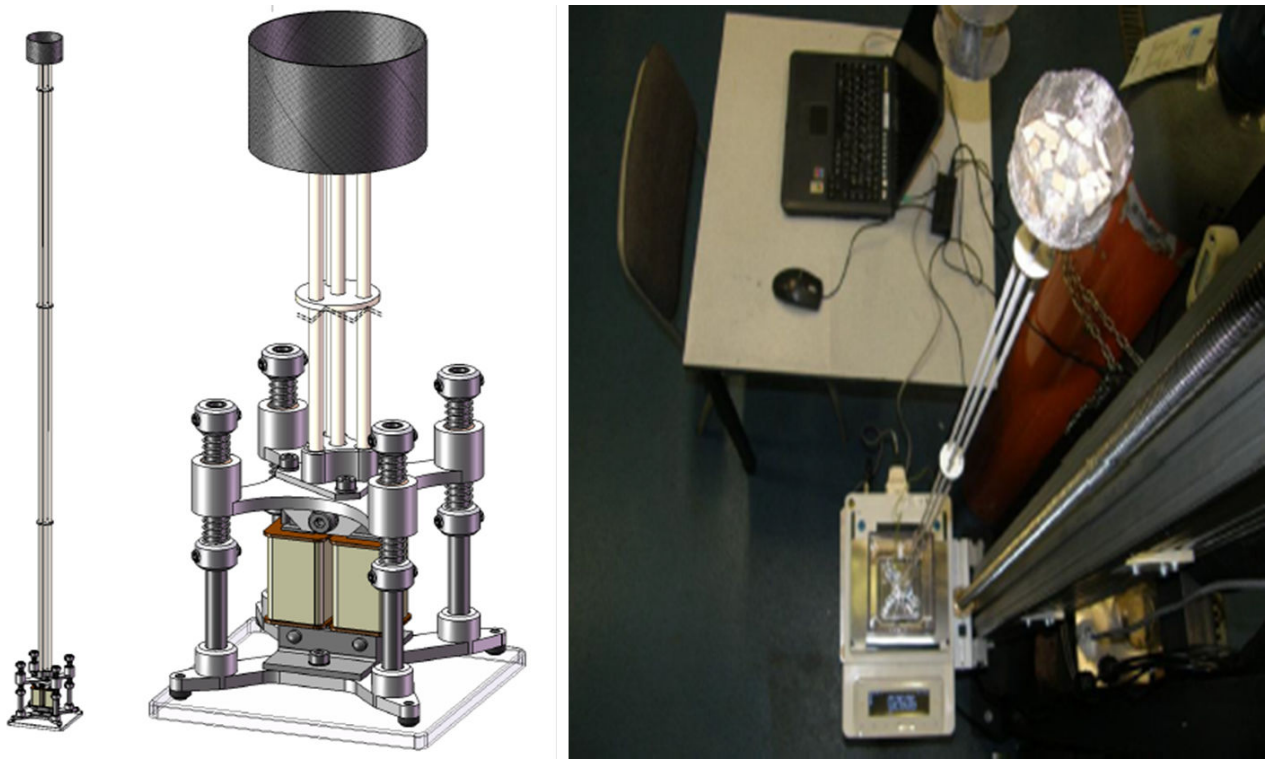

Figure 2.6: Details of the platinum basket holding the particles at the top, and the load cell at the bottom

.

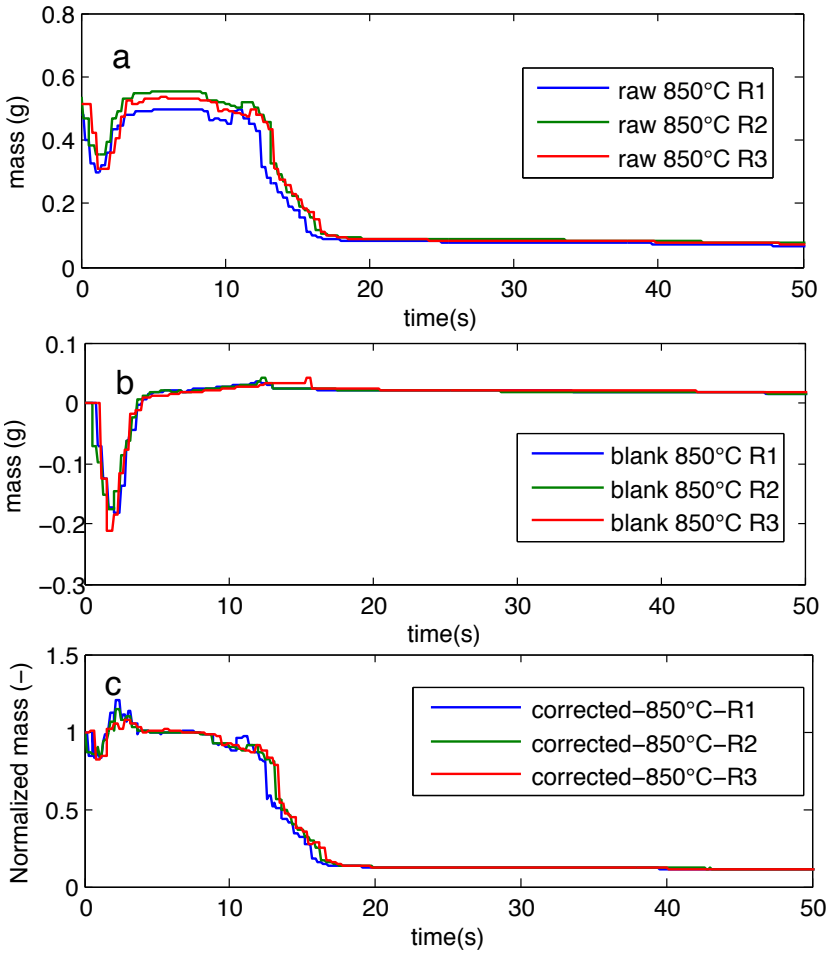

Figure 2.7: Example of wood-chips pyro-gasification experiments in pure CO_2 at 850°C. (a) raw data, (b) blank data, (c) corrected data

.

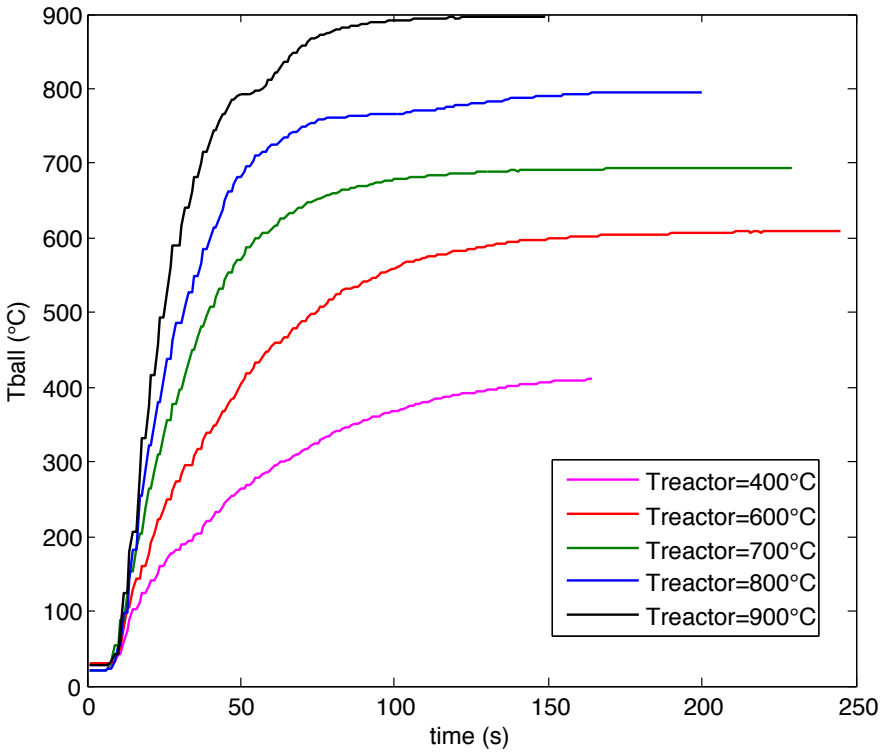

Figure 2.8: Temperature evolution of the steel ball

.

calculations, the gas flow regime is laminar.

External heat transfer in the MTG-R

In order to characterize the heating rate inside the MTG-R, we measured an external heat transfer coefficient. For the determination of the external heat transfer coefficient in the MTG-R, we adopted a lumped heat capacitance method [145]. We drilled a steel ball of 0.5 cm diameter and inserted in its centre a K-type thermocouple. The ball was then placed in the basket that normally bears the biomass sample and introduced in the reactor the same way as in pyrolysis experiments. Temperature evolution of the steel ball is shown in figure 2.8 for various reactor temperatures.

The steel ball is assumed to be isothermal. This can be verified by calculating the Biot number which represents the ratio of the internal thermal resistance to the boundary layer thermal resistance.

$$Bi = \frac{h_{global} \times d_b}{\lambda_b} \tag{2.1}$$

An overall energy balance on the steel ball gives:

$$\rho_b \times V_b \times Cp_b \times \frac{dT}{dt} = h_{global} \times S_b \times (T_b(t) - T_\infty) \tag{2.2}$$

The ball's temperature evolution with time is given by:

$$\frac{T_b(t) - T_\infty}{T_b(0) - T_\infty} = exp(-\frac{h_{global} \times S_b}{\rho_b \times V_b \times Cp_b} \times t) \tag{2.3}$$

The thermal time constant τ or characteristic time, representing the required time for the ball to reach 63% of the environment temperature is defined by:

$$\tau = \frac{\rho_b \times V_b \times Cp_b}{h_{global} \times S_b} \tag{2.4}$$

τ is determined by fitting the model to the experiments. Knowing the physical characteristics of the steel ball, we can calculate the global heat transfer coefficient h_{global} according to the previous formula.

The heat transfer inside the reactor occurs by convection and radiation. The global heat transfer coefficient is here expressed as the sum of a convective and a radiative heat transfer coefficient:

$$h_{global} = h_{conv} + h_{rad} \tag{2.5}$$

To determine the contribution of each mode to the global heat transfer, we estimated the convective heat coefficient and determined the radiative one by difference. The convective heat transfer coefficient is given by:

$$h_{conv} = \frac{Nu \times \lambda_{N_2}}{d_b} \tag{2.6}$$

Where $\lambda_{N_2}[W/(m.K)]$ and $d_b[m]$ are respectively the thermal conductivity of nitrogen at the reactor temperature and the steel ball diameter. The Nusselt number can be determined by the Whitaker correlation for flow over a spherical body:

$$Nu = 2 + 0.4 \times (Re^{0.5} + 0.06 \times Re^{2/3}) \times Pr^{0.4} \tag{2.7}$$

Where Re and Pr are respectively the Reynolds and the Prandlt numbers given by:

$$Re = \frac{\rho_{N_2} \times u_\infty \times d_b}{\mu_{N_2}} \tag{2.8}$$

$$Pr = \frac{\mu_{N_2} \times Cp_{N_2}}{\lambda_{N_2}} \tag{2.9}$$

Where $u_\infty[m/s]$ is the average gas velocity, $\mu_{N_2}[Pa.s]$ the nitrogen dynamic viscosity and $Cp_{N_2}[J/kg.K]$ the nitrogen specific heat capacity.

Figure 2.9 shows the evolution of the global heat transfer coefficient with temperature. We can see that for typical gasifier operating temperature of 800 to 1000°C, the global heat transfer coefficient varies between 120 and 150 $[W/m^2.K]$ which is in the range of values presented in the literature for external heat transfer coefficient in CFBG [146].

Table 2.2 shows the contributions of convection and radiation to the global heat transfer coefficient. It can be seen that above 600°C, external heat transfer in the MTG-R occurs mainly by radiation. The radiative heat transfer coefficient is at least two times higher than the convective heat transfer coefficient. The assumption of the isothermal character of the steel ball is valid as the Biot number is inferior to 0.1 regardless of the temperature.

Estimation of the particle heating rate in the MTG-R For a biomass particle introduced in the reactor hot zone, we can approximate the particle average heating rate at $t = 0$ by [147]:

$$\beta_0 = \frac{\partial T}{\partial t}|_{t=0} = (T_\infty - T_{w,0}) \times \frac{h_{global}}{L_0 \times \rho_w \times Cp_w} \tag{2.10}$$

Where $L_0[m]$ is the characteristic length, $\rho_w = 710\,[kg/m^3]$, $Cp_w = 1500\,[J/kg.K]$ are respectively the wood density and specific heat of beech wood. For biomass particles of 1 mm thickness taken

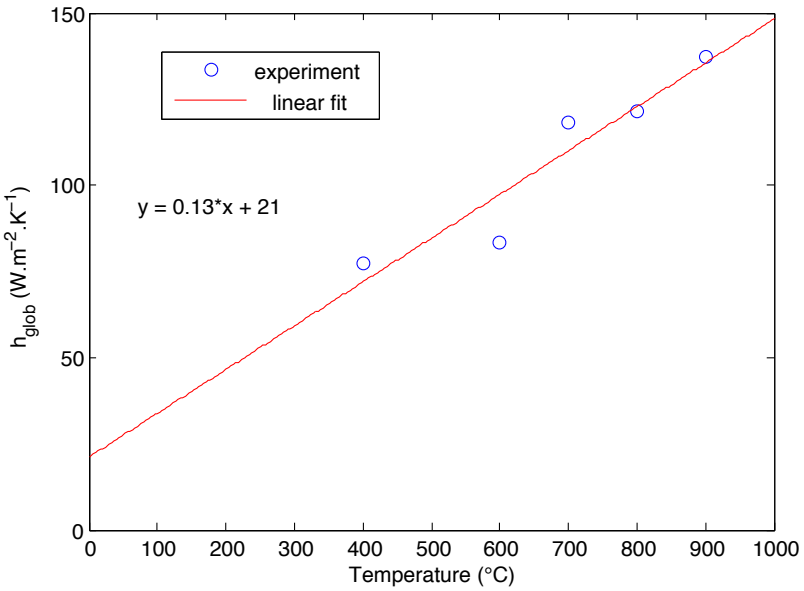

Figure 2.9: Variation of the global heat transfer with temperature

.

Table 2.2: Heat transfer coefficients and Biot Number evolution with temperature in the M-TG

Temperature (°C)	400	600	700	800	900
$h_{glob}\,[W/m^2.K]$	85.9	92.6	131.25	135	152.41
$h_{conv}\,[W/m^2.K]$	31.1	35.5	37.5	39.11	40.32
$h_{rad}\,[W/m^2.K]$	54.8	57.13	93.7	95.8	112.09
$Biot$	0.019	0.020	0.028	0.029	0.033

as the characteristic size, we estimated the initial heating rates for the different temperatures. The values are given in table 2.3.

This straightforward calculation is recommended to determine the initial heating rate of biomass particles as it is proportional to the external heat flux imposed by the reactor properties as well as to the biomass characteristics [147]. The value of β_0 at 800°C and above are typical of HHR conditions.

Char gasification experiments in the MTG-R

For experiments were the pyrolysis stage is not of interest (char gasification experiments), we adopted a 5 min stabilization time -after which the mass displayed by the electronic scale is stable- before starting the gasification experiments. Figure 2.10 shows an example of 0.25 mm LHR-char gasification experiment with 20% CO_2 in N_2 at 900°C. We can distinguish the first stage of mass stabilization (the char is introduced under a flow of N_2) and the char gasification stage which starts with CO_2 injection.

The displayed mass on the electronic scale fluctuates around an average value. The mass fluctuations are quite low and are most likely due to small fluctuations of the gas flow (see figure 2.11). Nevertheless, in the data processing step, we chose to smooth the raw data for a better representation as well as to avoid noisy data when calculating the reaction rate or the char reactivity which involve derivation of the mass-time data. The smoothing operation is done with a MATLAB program. An

Table 2.3: Evolution of the 1 mm thick biomass initial heating rate in the M-TG

Temperature (°C)	400	600	700	800	900
β_0 $(°C/s)$	70.8	76.3	108.1	111.2	125.6

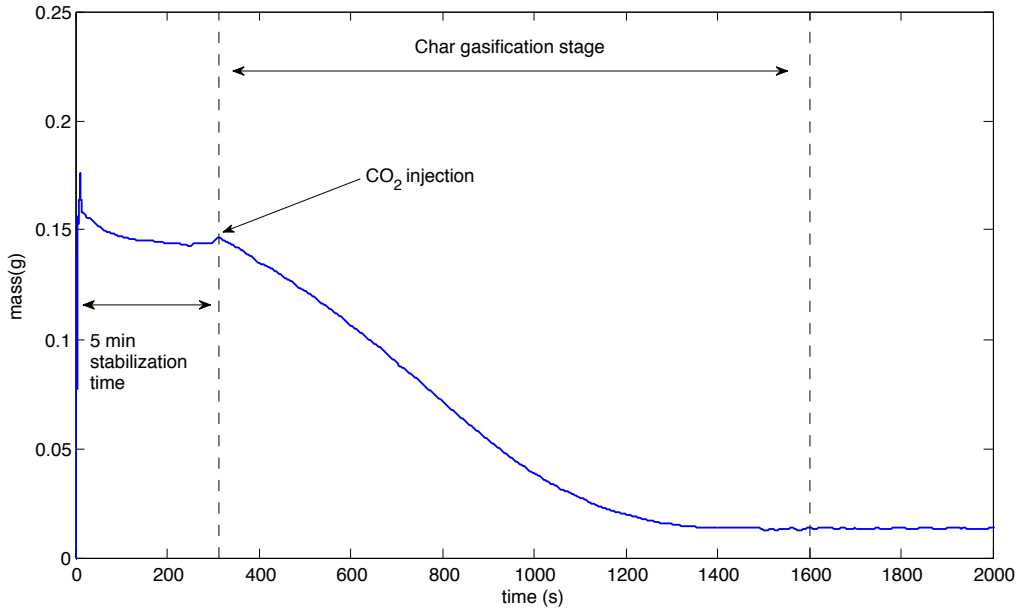

Figure 2.10: Example of 0.25 mm LHR-char gasification experiment with 20% CO_2 in N_2 at 900°C

.

example of the time-conversion level data smoothing is shown in figure 2.12 for 0.25 mm LHR-char gasification experiment with 20% CO_2 in N_2 at 900°C.

Finally, to our best knowledge, it is not possible to perform isothermal gasification experiments in a classic TG device without preheating the char sample to the desired temperature over a considerable time which is not representative of practical conditions.

2.2.3 Horizontal Tubular Reactor (HTR) for HHR-pyrolysis

The Horizontal Tubular Reactor (HTR) was used to study the biomass pyrolysis gas composition. It allows HHR of the biomass by a fast introduction of the biomass samples in the hot reaction zone and capture of the pyrolysis gas in a bag. It consists of a double-walled quartz pipe. The length and inside diameters are respectively 850 mm and 55 mm for the inner tube, and 1290 mm and 70 mm for the outer tube. Nitrogen and CO_2 flow rates are controlled by means of mass flow-meters/controllers. The major part of the incoming gas flow (75%) is introduced on right hand-side of the reactor and passes through the annular space to be heated before reaching the biomass samples. The rest of the gas flow is injected on the left hand-side to cool the injection spoon when pooled out from the hot zone and to prevent a backward flow of the pyrolysis gases. The pyrolysis experimental device is presented in figure 2.13.

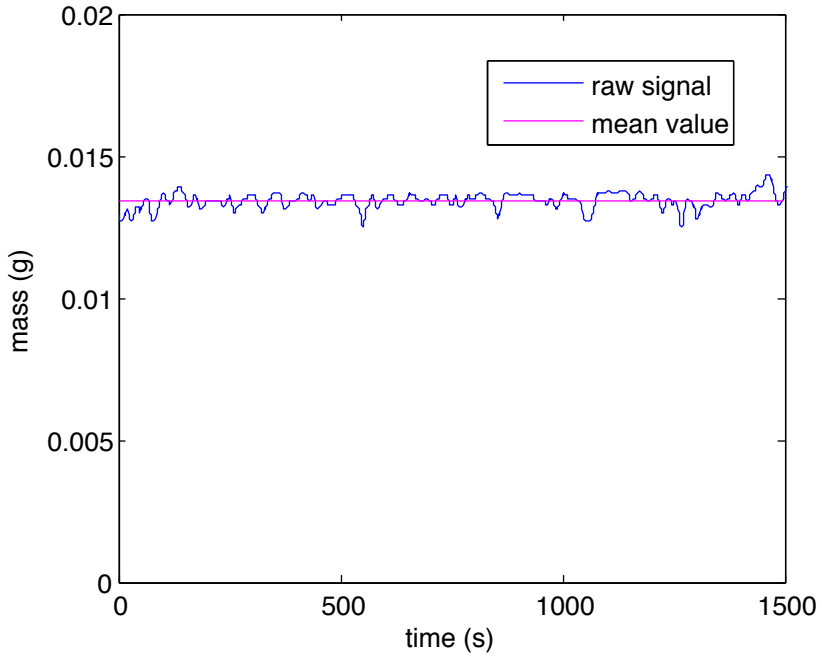

Figure 2.11: Mass VS time data for a flow of 12.3 l(STP)/min of 20% CO_2 in N_2 at 900°C

.

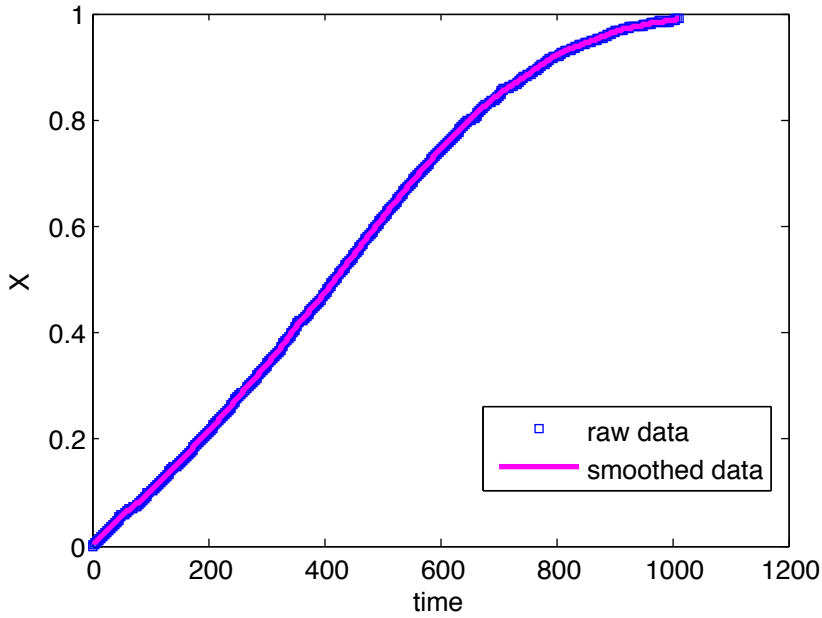

Figure 2.12: Smoothing example of conversion level (X) VS time data (0.2 mm LHR-char gasification experiment with 20% CO_2 in N_2 at 900°C)

.

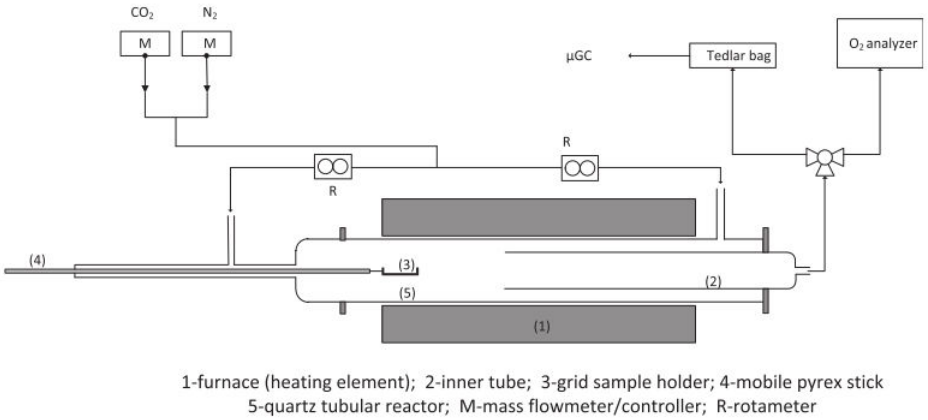

Figure 2.13: Horizontal Tubular Reactor (HTR)

.

2.3 Characterisation of chars

A part of the present thesis will be dedicated to the monitoring of the char properties during gasification with CO_2, H_2O and their mixtures. The aim is to understand the unfolding of these reactions and point out the potential interactions between the CO_2 and H_2O when used as co-reactants in the gasifying medium. As the gasification is a heterogeneous reaction influenced by the char texture, structure, minerals and surface chemistry, we opted to follow these characteristics along the gasification reaction to better understand it.

2.3.1 Chemical composition

Ultimate analysis

The chemical composition of chars in term of *C, H, N* and *S* are determined by an elemental analyser. The general principle is that the chars are combusted at 1500°C in an excess of oxygen for a complete combustion. The emitted quantity of CO_2, NO_2 and H_2O are determined by gas chromatography coupled to a TCD detector. The quantity of *C, H, N* and *S* are consequently known which allows to determine the char content of these species. The ash content is determined by combustion of 100 mg of char sample in a muffle furnace at 550°C. The oxygen content is determined by difference to total percentage of *C, H, N, S* and Ash.

Determination of mineral species concentration

Inductively Coupled Plasma Atomic Emission Spectroscopy (ICP-AES) ICP-AES is a type of emission spectroscopy. The general working principle is that the solution containing the elements to be analysed is firstly nebulized and introduced in a plasma flame created by the ionization of argon gas in an intense electromagnetic field. The sample immediately collides with the electrons and charged ions in the plasma and is itself broken down into charged ions. Excited atoms and ions emit electromagnetic radiation at wavelengths characteristic of a particular element. The intensity of this emission is indicative of the concentration of the element within the sample.

X-Ray Fluorescence (XRF) In X-Ray Fluorescence analysis, the sample to be analysed is exposed to short X-rays wavelength. Ionization of the sample component atoms may take place when

atoms are exposed to an energy greater than their ionization potential. X-rays can be energetic enough to expel tightly held electrons from the inner orbitals of the atom. The removal of inner electrons makes the electronic structure of the atom unstable. This causes electrons of higher orbitals "fall" into the lower orbital to fill the hole left behind. In falling, energy is released in the form of a photon, the energy of which is equal to the energy difference of the two orbitals involved. Thus, the material emits radiation, which has energy characteristic of the atoms present. The XRF technique is suitable, less time consuming and requires only one calibration with a reference char sample containing well defined concentrations of the minerals to be analysed. This calibration is necessary to have accurate results. Without a prior calibration, the concentrations of minerals may be under or over estimated because of matrix effects. The two techniques are therefore coupled. ICP-AES technique is used to determine the mineral composition of a reference char sample. This reference char sample is taken afterwards as a calibration sample in the XRF analysis [148]. Mineral content of the different chars was measured by X-ray fluorescence (XRF) spectrophotometer (PHILIPS PW2540) equipped with a rhodium target X-ray tube and a 4 kW generator. 100 mg of char were priorly ground and mixed with 200 mg of boric acid, and then pressed into a pellet under a 9 tons pressure for 45 minutes.

2.3.2 Structure of chars

Biomass chars are non-organized carbonaceous materials. Their structure is heterogeneous as there exist a variety of carbon bond types and orientations. A qualitative determination of the different structural units forming the char can be achieved by Raman Spectroscopy. Raman microspectroscopy is a powerful characterisation technique for carbonaceous materials. It allows a differentiation of the different carbon allotropes (pyrolytic carbons, graphitic carbon...) in the char sample due to their different carbon bonds type and orientations. Raman spectroscopy have been used to determine the structural features of the chars during gasification with CO_2, H_2O and their mixtures. Raman spectroscopy can provide information about an average structural composition of the chars and thus allows a comparison between the different char sample at the different conversion levels.

Raman spectroscopy

Principle of Raman spectroscopy In a Raman spectroscopy experiment, photons of a single wavelength (in the visible range this would be light of a single color) are focused onto a sample. Most commonly, a laser is used as it is a powerful monochromatic source. The photons interact with the molecules and are either reflected, absorbed or scattered. With Raman spectroscopy, we study the scattered photons.

Photons interacting with molecules most commonly scatter elastically. This is called Rayleigh scattering. Rayleigh scattered photons have the same wavelength as the incident light. However, approximately 1 out of a million photons are inelastically scattered...an effect first described by Sir Chandrasekhar Raman in 1922.

With Raman scattering, the incident photon interacts with matter and its wavelength is either shifted lower: "Stokes shift" or higher: "Anti-Stokes shift". Lower shifted photons are the most common. What has happened is that the photon has interacted with the electron cloud of the functional groups bonds, exciting an electron into a virtual state. The electron then relaxes into an excited vibrational or rotational state (see figure 2.14). This causes the photon to lose some of its energy and is detected as Stokes Raman scattering. This loss of energy is directly related to the functional group, the structure of the molecule to which it is attached, the types of atoms in that molecule and its environment.

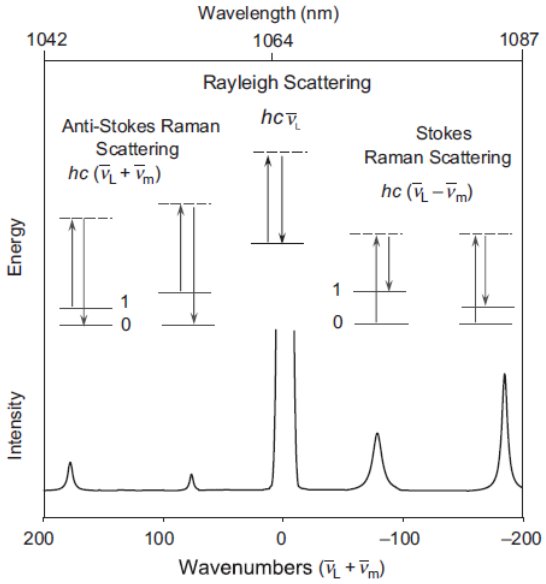

Figure 2.14: Schematic illustration of Rayleigh scattering as well as Stokes and anti-Stokes Raman scattering. The laser excitation frequency is represented by the upward arrows and is much higher in energy than the molecular vibrations. The frequency of the scattered photon (downward arrows) is unchanged in Rayleigh scattering but is of either lower or higher frequency in Raman scattering. The dashed lines indicate the "virtual state"

.

Acquisition and deconvolution of the char samples Raman spectra Raman spectra of the chars were recorded with a BX40 LabRam, Jobin Yvon/Horiba spectrometer at the IS2M laboratory. Several char particles were sampled and deposited on a rectangular glass slide for the Raman analysis. Raman spectra were obtained by a backscattered configuration with an excitation laser at 632.8 nm. The Raman spectra at each position gives an average structural information of a large number of carbon micro-crystallites. The area of analysis is visualized by a video camera coupled to a microscope. The microscope optics were used to focus the excitation laser beam onto the sample and to collect the backscattered light (180°). The Rayleigh scattering component was removed by a filter, and the Raman-scattered light was dispersed by an optical grid and detected by a CCD camera. The Raman spectra were recorded at six locations by mapping the char sample selected area. To avoid the char degradation, the laser power was decreased one hundred folds by an optical filter.

The Raman spectra of heterogeneous carbon materials shows in the first order region (800-2000 cm^{-1}), two main broad and overlapping peaks with maximum intensities at 1350 cm^{-1} and 1590 cm^{-1} [149] [43]. In the literature, we frequently refer to these two peaks as respectively the D and G bands. In the case of highly ordered carbon materials, the Raman spectra can be expressed as the result of these two bands. The G band corresponds to an in-plane bond-stretching motion of pairs of sp^2 carbon atoms in the graphitic structure (aromatic ring breathing mode) while the D band corresponds to the defects in the graphitic structure and is forbidden in pure graphitic ordered materials.

For heterogeneous carbon materials such as biomass or coal chars, we can no longer speak about those two peaks. The Raman spectra is rather the combinations of several bands corresponding to different carbonaceous structures. The Raman spectrum can be deconvolved into five main bands as proposed by Jawhari [38] or more recently by Sadezky [43], Sheng [39] and by Chabalala [150]. The five bands correspond to well defined carbon structures are summarized as follows:

- G band at 1590 cm $^{-1}$: stretching vibration mode with E2g symmetry in the aromatic layers of the graphite crystalline
- D1 band at 1350 cm^{-1}: graphitic lattice vibration mode with A1g symmetry and in-plane imperfections such as defects and hetero-atoms
- D2 band at 1620 cm^{-1}:lattice vibration similar to that of the G band. The D2 band results from graphene layers which are not directly sandwiched between two other graphene layers. Sheng [39] reported that the D2 band is always present when the D1 band is present and that its intensity decreases with the increase of the degree of organization in the char.
- D3 band at 1500 cm^{-1}: Related to amorphous carbon structures and appears as a very broad band. It is suggested to originate from the amorphous sp^2-bonded forms of carbon (organic molecules, fragments or functional groups, in poorly organised materials).
- D4 band at 1200 cm^{-1}: appears only in very poorly organised materials, such as soot and coal chars [39] [43] . It is attributed to sp^2-sp^3 mixed sites at the periphery of crystallites and to C-C and C=C stretching vibrations of polyene-like structures.

The D3 and D4 bands are suggested to be responsible of the reactive sites in the char and thus determine the char reactivity.

The deconvolution procedure was performed with a MATLAB program. Spectrum fitting was performed following a least square minimization procedure between the raw signal and the calculated one, so that the objective function to be minimized is:

$$OF = \sum_{i=1}^{i=n} (I_i^{cal} - I_i^{exp})^2 \tag{2.11}$$

I_i^{cal} and I_i^{exp} are respectively the experimental recorded intensity (photon counts) and the calculated one.

2.3.3 Textural properties of chars

The gasification reaction is highly influenced by the char textural properties as they govern the reactant diffusion inside the porous char. The char textural properties include the Total Porosity (TP), the form of pores, the Total Surface Area (TSA) as well as the Pore Size Distribution (PSD). The macroporosity of chars can be examined by Scanning Electron Microscopy (SEM) technique while a deep textural characterisation is performed by nitrogen adsorption at 77 K.

Scanning Electron Microscopy coupled to Energy-Dispersive X-ray microanalysis (SEM-EDX)

Scanning Electron Microscopy - SEM - is a powerful technique in the examination of materials. It is used in a wide range of scientific fields, including metallurgy, geology, biology and medicine, to name a few. In the present work, it has been used to monitor the char textural evolution at a micro-metric scale, during the gasification reaction. Images from SEM are insightful to understand the unfolding of the gasification reaction and follow the evolution of macroporosity and large mesoporosity.

An SEM apparatus comprises an electron gun housed on the top of the column that generates a beam of electrons that rushes towards the sample housed in the specimen chamber. Electrons are very small and easily deflected by gas molecules in the air. Therefore, to allow the electrons to reach the sample, we operate under a high vacuum. The electron gun comprises a filament made of tungsten

which is heated to generate a fine beam of electrons. The electron beam is accelerated through a high voltage (e.g.: 20 kV) and pass through a system of apertures and electromagnetic lenses to produce a thin beam of electrons. Accelerated electrons in an SEM carry significant amounts of kinetic energy, and this energy is dissipated as a variety of signals produced by electron-sample interactions when the incident electrons are decelerated in the solid sample. These signals include secondary electrons (that produce SEM images), backscattered electrons (BSE), diffracted backscattered electrons (EBSD that are used to determine crystal structures and orientations of minerals), photons (characteristic X-rays that are used for elemental analysis), visible light (cathodo-luminescence), and heat.

When used in conjunction with the closely-related technique of energy-dispersive X-ray microanalysis (EDX), the composition of individual clusters or particles on the char surface can be determined. The chemical information comes from the backscattered electrons "chemical image", while that related to the topography comes from the secondary electrons "topography image". The backscattered electrons is used typically to image a polished section; the brightness of the backscattered electrons image is dependent on the atomic number of the specimen (or, for compounds, the average atomic number). For example, lead will appear brighter than potassium and calcium oxide will appear brighter than calcium carbonate. The backscattered electrons image is, in essence, an atomic number map of the specimen surface. It enables the operator to determine qualitatively the elemental composition of the char sample and to analyse the fate and dispersion of the mineral species on its surface.

N_2 adsorption at 77 K

The textural properties of the materials were investigated with a Micromeritics ASAP 2020 instrument using N_2 adsorbate at 77 K. Prior to the analysis the char samples were out-gassed overnight in vacuum at 300°C. The Total Surface Area (TSA) was calculated for the linear plot in the relative pressure range of 0.05 to 0.15 while the micropore volume (Vmicro) was estimated by using the αs-plot method. This technique was applied to study the porosity distribution and TSA evolution during the gasification of LHR-chars of 0.2 mm in the chemical regime at 900°C under H_2O, CO_2 and their mixtures. The mesopore volume (Vmeso) was obtained by substracting the micropore volume from the total pore volume of N_2 adsorbed at relative pressure of 0.95. The pore size distribution was determined using the Density Functional Theory model on carbon slit pores model.

2.3.4 Char Surface Functional Groups (CSFG) and Active Surface Area (ASA)

The char surface does not entirely participates to the gasification reaction. Only a small part is reactive. The char surface contains "Active sites" which are effectively participating to the gasification reaction. These sites are formed by the functional groups located at the char surface directly exposed to the gasifying agent and which are known to be highly reactive. These latter are directly related to the char reactivity. The more they are abundant, the more the char is reactive.

Surface functional groups determination by Temperature programmed desorption and mass spectrometry TPD-MS

The TPD-MS technique allows a quantification of the surface functional groups located on the char surface. It allows to follow the surface functional groups during gasification. It was applied to study the surface functional groups of chars gasified at 3 conversion levels of 20%, 50% and 70% respectively under H_2O, CO_2 and their mixtures.

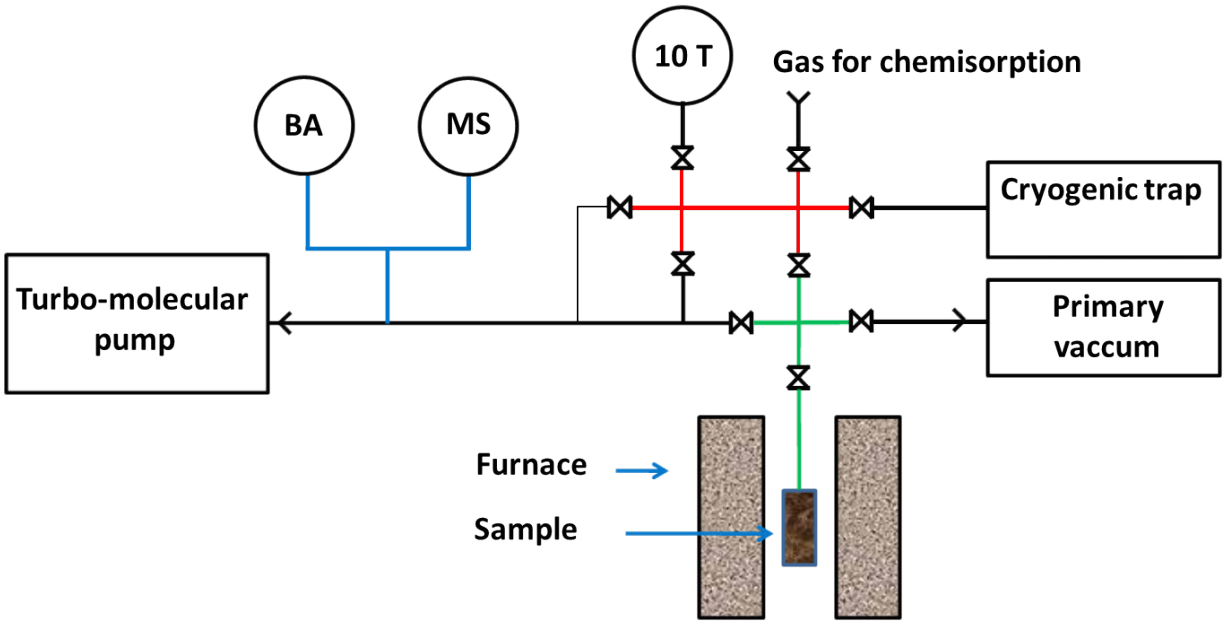

Figure 2.15: Schematic representation of the TPD-MS experimental bench

.

A Schematic representation as well as a photography of the the TPD-MS experimental bench are shown in figure 2.15 and 2.16. It comprises a quartz tubular reactor (3) electrically heated (1-2) on which is introduced a quartz crucible containing the char sample, a pumping system to create vacuum and a mass spectrometer for gas analysis. The reactor is first outgased in a primary vacuum down to 1 mm Hg of pressure (4), and then in a second step to a secondary vacuum down to 10^{-4} mm Hg of pressure by means of a turbo-molecular pump (5-6). The char sample in the crucible is afterwards heated up to 900°C at constant rate of 5°C/min and kept at this final temperature during 1 h. During the analysis, the functional groups are removed from the char surface which results, depending on the nature of the functional groups, in the emission of H_2O, CO_2, CO and H_2. The rate of emission as well as the quantities emitted depends on the temperature. The gases evolved during the heating process were continuously analysed quantitatively by a mass spectrometer (8) which is calibrated using commercial H_2, CO, CO_2, and N_2 prior to the experiments. The total pressure of the gas released during the heat treatment was also measured as a function of the temperature using a Bayard-Alpert gauge (7). The total gas pressure could then be compared to the one calculated from the sum of the partial pressure of the gas species deduced from the quantitative analysis of the gas phase. From the TPD analysis, the desorption rate of each gas as a function of temperature was determined. The total amount of each gas released was computed by time integration of the TPD curves.

Active Surface Area (ASA) determination by O_2 chemisorption

The Active Surface Area (ASA) of the biomass chars was determined following the method of Laine and Co-workers [64] consisting on O_2 chemisorption on the char sample at 200°C. The ASA experiments were done in the same experimental bench as in the TPD-MS experiments. The char sample surface was first cleaned by heating the sample up to 900°C with a constant heating rate of 5°C/min and kept 1 h at this final temperature (classical TPD-MS experiment). Afterwards, the char sample is cooled down to 200°C, keeping the reactor under vacuum. When the temperature stabilizes, Oxygen is introduced (pressure close to 0.5 mm Hg) and chemisorbed on the char surface for a period of

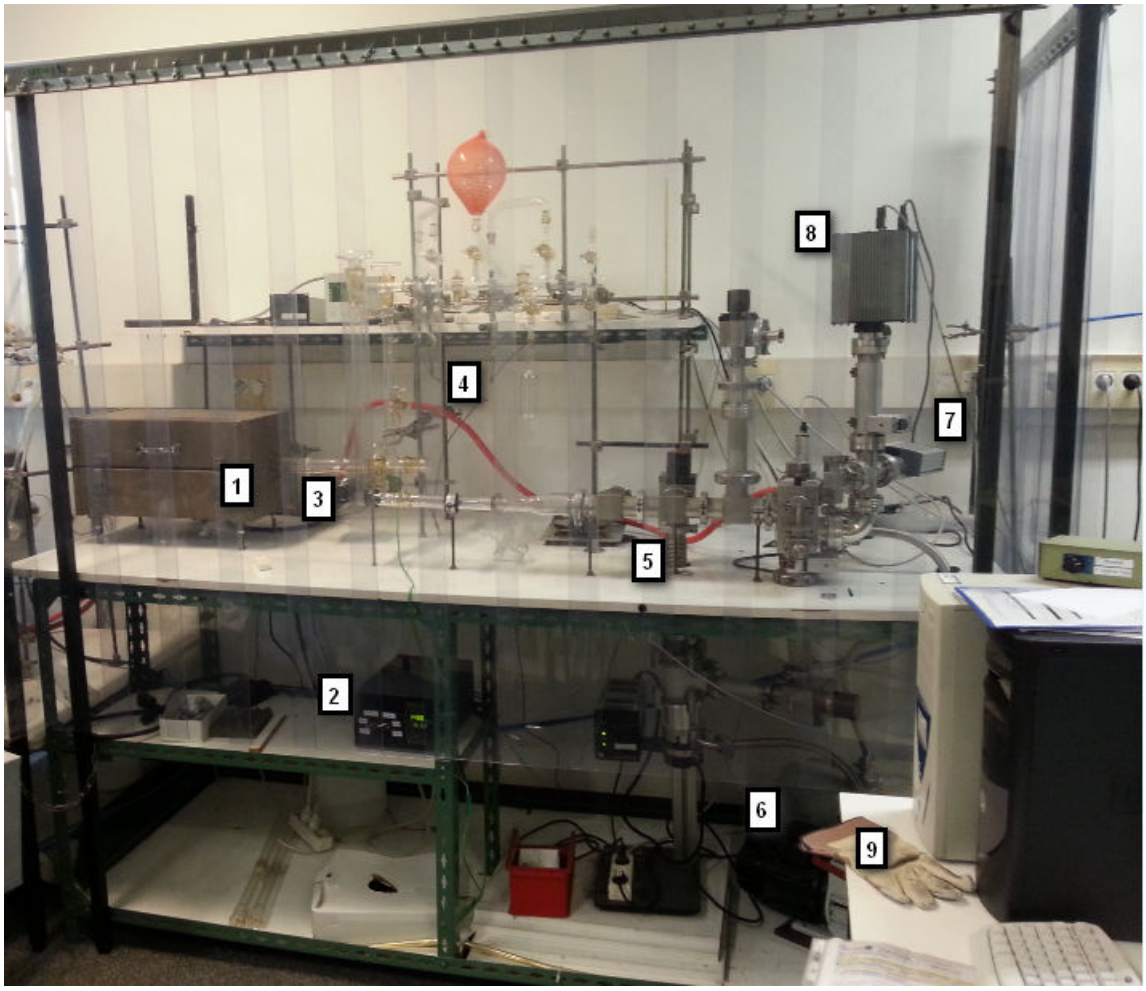

Figure 2.16: Photograph of the TPD-MS experimental bench at the IS2M laboratory

.

15 h leading to the formation of surface oxygen complexes.

After the chemisorption step, a TPD experiment is performed and the oxygenated char sample is heated up to 900°C with a constant heating rate of 10°C/min and kept for 20 min at this final temperature. CO and CO_2 are emitted consequently. The ASA (m^2/g) of a char sample may be calculated using the equation:

$$ASA = \frac{n_O \sigma_O N_{Avo}}{m_{char}} \tag{2.12}$$

n_O is the total number of oxygen moles calculated from the relation:

$$n_O = n_{CO} + 2n_{CO_2} \tag{2.13}$$

n_{CO} and n_{CO_2} are obtained from the time integration of the TPD curves:

$$n_{CO} = \int_{t_0}^{t_{end}} Q_{CO}\, dt \tag{2.14}$$

$$n_{CO_2} = \int_{t_0}^{t_{end}} Q_{CO_2}\, dt \tag{2.15}$$

Q_{CO} and Q_{CO_2} are the molar emission rate of CO and CO_2 (mol/s).
N_{Avo} is Avogadro number and σ_O is the cross sectional area of an oxygen atom (0.083 nm^2).

Chapter 3

Effects of CO_2 on biomass fast pyrolysis: reaction rate, gas yields and char reactive properties

This chapter was published as a research paper in an international journal, reference: Guizani, C., Escudero Sanz, F. J., Salvador, S. (2014). Effects of CO_2 on biomass fast pyrolysis: Reaction rate, gas yields and char reactive properties. Fuel, 116, 310-320. doi:10.1016/j.fuel.2013.07.101

Abstract

The effect of CO_2 introduction in a biomass fast pyrolysis process at 850°C was investigated. It was found that CO_2 impacts the final gas yield and composition, and the char yield and properties. Introducing CO_2 in the pyrolysis medium alongside nitrogen enhanced CO production as a result of homogeneous and heterogeneous reactions of CO_2 with gases, tars and char. The char yield was lower compared to a reference char yield in pure nitrogen. The char obtained in a CO_2-containing atmosphere has its surface area increased nearly sixfold and has a chemical composition different from that of chars obtained in N_2 atmosphere. However, the reactivity of the two chars towards H_2O, CO_2 and O_2 was almost the same. Temperature-programmed oxidation experiments on both chars - those obtained in pure nitrogen and those obtained in a CO_2 - containing atmosphere - revealed quite different oxidation profiles and peak temperatures. Taken together, these results tend to confirm that CO_2 is impacting the biomass fast pyrolysis process. In the light of these results and of the literature findings, we propose a mechanism illustrating the role of CO_2 during fast pyrolysis of biomass.

Keywords : Biomass; pyrolysis; CO_2; Char properties.

Résumé

L'effet du CO_2 sur la pyrolyse rapide de la biomasse a été étudié a 850 °C. On a constaté que le CO_2 impacte le rendement final en gaz et sa composition ainsi que les propriétés réactives du char et son rendement. La présence du CO_2 conduit a une production plus importante de CO suite a des réactions avec les gaz de pyrolyse, les goudrons et le char. Le char obtenu sous une atmosphére contenant du CO_2 a une surface specifique six fois plus grande que celle du char obtenu sous N_2. Sa composition chimique est aussi différente. Cependant, les réactivités des deux chars à H_2O, au CO_2 et à O_2 sont similaires. L'oxidation en température programmée des deux chars a montré deux profils différents. Ces résultats montrent que les CO_2 impacte la pyrolyse rapide de la biomasse. On propose, suite à ces résultats un mécanisme d'action du CO_2 sur le processus de pyrolyse.

Mots clés : Biomasse, pyrolyse, CO_2, propriétés du char.

3.1 Introduction

Biomass pyrolysis is a thermal decomposition of the biomass into gas, liquid, and solid [7]. The yields and distribution of the pyrolysis product depend on various parameters such us the physico-chemical characteristics of the biomass (origin, chemical composition, ash and moisture contents, particle size) and the operating conditions (reactor design, temperature, residence time). The production trends of pyrolysis products as a function of temperature and heating rate are reported in Di Blasi's review [14].

For instance, high temperature and small particle size promote gas production and decrease the char yield [151]. Higher residence times in the reactor are also required to maximize the tar thermal cracking to gas. The particle heating rate - which depends on the particle size and shape, as well as on the operating conditions in the reactor (temperature and gas flow)- is a key parameter which influences the pyrolysis product yields and the char properties [7] [74].

Despite the huge amount of study devoted to biomass pyrolysis and dealing with issues related to the aforementioned parameters, noticeably few papers focus on the gas surrounding the solid and its potential effects on the pyrolysis reaction.

For instance, Zhang et al [119] investigated the effect of the composition of the pyrolysis medium in the biomass fast pyrolysis process in a fluidized bed gasifier at 550° C. The pyrolysis mediums were N_2, CO_2, CO, CH_4 and H_2. The authors found that the liquid yield, composition and higher heating value depend on the composition of the pyrolysis bath gas . The pyrolysis in a CO_2 atmosphere was seen to produce less char than in the other atmospheres. The CO_2 yield also decreased compared to the yield obtained in an N_2 atmosphere. With regard to the liquid product distribution, the CO_2 atmosphere led to the highest yield of acetic acid compared to the other atmospheres. The acid products yield under N_2 was 9% while it increased to 16% under CO_2 . Ketones yield also increased slightly from 15 to 17% while the phenol yield decreased from 33% to 26%. The authors explained these observations by alluding to two possible mechanisms: either the CO_2 reacted with the active volatiles or with the biomass char. The former assumption seems to be more plausible in view of the pyrolysis temperature.

In a recent study, Kwon et al [120], observed that introducing CO_2 in the macro-algae pyrolysis process resulted in a breakdown of a significant amount of chemical species. The gas yield was enhanced while the oil yield decreased. The same authors performed another study of the pyrolysis of styrene butadiene rubber [121] and found that the CO_2 enhances C4 hydrocarbon cracking in addition to impeding the gas phase addition reaction by which benzene derivatives are formed. Tyre pyrolysis experiments at 650 °C in free and in CO_2-containing atmospheres showed that the amount of condensable hydrocarbons decreased by 30 to 50% when introducing CO_2. There was also a modification of the end products.

Other studies focused more on the effect of the pyrolysis atmosphere on the char properties. Hanaoka et al [128] found that preparing chars in a $N_2/CO_2/O_2$ -containing atmosphere leads to a more developed surface area and a higher reactivity towards pure CO_2, especially in a 18% N_2/41% CO_2/41% O_2 atmosphere. The char yield was similar to that obtained under nitrogen. The authors observed an increase in the BET surface area from $275m^2/g$ in pure nitrogen to $417m^2/g$ in a 18% N_2/41% CO_2/41% O_2 atmosphere. The char reactivity towards CO_2 also increased by a factor of 1.7 to 2.5 for chars prepared in a CO_2 -containing atmosphere.

Jamil et al [132] performed coal pyrolysis experiments in a wire-mesh reactor respectively under He and CO_2 with slow and high heating rates. The authors found that the nascent char obtained after a fast heating is very reactive to CO_2. The authors proposed that the char gasification with CO_2 occurs simultaneously with the thermal cracking during fast heating. The CO_2 would mainly react with radicals generated at the char surface, which systematically induces an extra mass loss

compared to the inert atmosphere.

In a quite recent study, Gao at al [131] studied the influence of CO_2 in the lignite pyrolysis process. The authors found that CO_2 impacts the lignite pyrolysis process on different levels. They concluded that the introduced CO_2 promotes the occurrence of coal pyrolysis by enhancing the cracking of the benzene ring and the fracturing of hydroxyl, methyl and methylene groups. Further gasification by CO_2 caused the char to have a higher specific surface area and enhanced the gas yield.

Borrego et al [129] performed pyrolysis experiments on pulverised wood (particle size of 36 to 75 μm) in a drop tube furnace at 950°C under N_2 and CO_2. They performed textural characterisation of the residual chars and found similar specific areas : 277 and 331 m^2/g under N_2 and CO_2. The char reactivity towards air at 550°C in a TG device was also the same. The residence time was estimated at 0.3 s.

Other studies have focused more on coal pyrolysis but it is still interesting to analyse their results as a means of comparison with biomass pyrolysis. For instance, Gil et al [152] performed pyrolysis experiments on pulverised coal chars in a drop tube furnace under N_2 and CO_2 atmospheres at 1000°C. The authors observed an enhanced volatile yield in the CO_2 atmosphere in comparison with the N_2 atmosphere.

Other studies highlighted the role of CO_2 in oxy-fuel conditions. Rathnam et al [153] studied the reactivity of pulverised coals in air (N_2/O_2) and oxy-fuel conditions (CO_2/O_2). Experiments were performed in an entrained flow reactor at 1400°C and the residence time was estimated to be 0.62 s. The authors observed that replacing 79% N_2 by 79%CO_2 alongside O_2 results in a higher volatile yield. The char specific area and reactivity also increased with the introduction of CO_2. The authors imputed these results to the char-CO_2 reaction occurring simultaneously with the pyrolysis and the combustion reactions.

Thus, according to the literature, the surrounding gas impacts the pyrolysis reaction and product yields. However, very little information about the phenomena involved is available in the literature. The aim of the present study is to assess the effect of the presence of CO_2 in the surrounding gas on the pyrolysis reaction and to deepen understanding of its potential impacts. The present study concerns biomass fast pyrolysis at a high temperature of 850° C. These experimental conditions come close to those encountered in fluidized bed gasifiers. The potential effects of CO_2 are assessed through the pyrolysis reaction rate, the pyrolysis product yields and composition and the char properties.

3.2 Material and methods

3.2.1 Parent wood sample

The biomass samples were beech wood-chips provided by the French company SPPS. Raw samples were initially sieved. Biomass particles with a size in the range of 4 to 5 mm and a thickness of about 1 mm were selected to perform the pyrolysis experiments. Proximate and ultimate analysis of the biomass samples are presented in table 1. The results are given on a dry basis. The moisture content of the wood-chips was 10% ± 1%.

Table 3.1: Proximate and ultimate analysis of the beech wood-chips (% dry basis)

Proximate analysis			**Ultimate analysis**			
VM	Ash	FC	C	H	O	N
88.1	0.4	11.5	46.1	5.5	47.9	0.1

3.2.2 Experimental devices and procedures for wood-chips pyrolysis

The macro-thermogravimetry experimental device and procedure

The thermal degradation of the wood-chips in a macro-thermogravimetry device (M-TG) was used to determine the pyrolysis rate and final char yield. Experiments were performed under two atmospheres: N_2 and 20% CO_2 in N_2 at 850° C.

M-TG apparatus

The new M-TG device is described in detail in our previous work on char gasification in mixed atmospheres of CO_2 and H_2O [154]. In general terms, the experimental apparatus consists of a 2-m long, 75-mm i.d. alumina reactor that is electrically heated, and a weighing system comprising an electronic scale having an accuracy of ± 0.1 mg, a metallic stand placed over the scale on which three hollow ceramic tubes are fixed, each having a length of 1 m and a 2.4 mm external diameter. These ceramic tubes hold up a platinum basket in which the biomass particles are placed. The gas flow rates are controlled by means of mass flow-meters/controllers. The gas flow inside the reactor is laminar and flowing at an average velocity of 0.20 m/s. This device allows fast heating of the biomass particles as they are introduced in the hot furnace within less than 15 s.

Experimental procedure

A load of 20 to 25 wood-chips with a total weight of about 0.5 g was placed in the platinum basket and uniformly spaced to avoid thermal and chemical interactions. The biomass particles were submitted to a thermal shock as if they had been placed in a fluidized bed gasifier. For this purpose, a new rapid sample introduction procedure - involving a blank test - had to be developed in order to run short duration experiments. During the heating of the platinum basket and the ceramic tubes, the flowing gas dynamic pressure (force exerted on the basket) in addition to the drag forces along the ceramic tubes caused the displayed mass value to change. Once a thermal equilibrium was reached inside the reactor, and the gas flow around the basket and the ceramic tubes had stabilized, the displayed mass remained constant. Blank tests (without wood-chips in the basket) were performed to correct the mass decay. The reproducibility of the blank tests was verified and an experimental protocol was established so that the pyrolysis tests were always performed in the same way. For data processing, we subtracted the blank test mass record from that of the pyrolysis experiment. Figure 3.1 shows reproducibility pyrolysis test results with 20% CO_2 in N_2 after correcting the mass record. The mass loss is recorded via the electronic scale every 0.1 s.

Pyrolysis experiment results were very reliable after 13.5 s; before this time, results remained acceptable except at 2-3 s when lifting the device and at 11-12 s when stopping the motion of the device. One can note a time delay of approximately 8 s before the particle mass loss began, which was attributed to the heating of the metal basket.

The horizontal tubular reactor experimental device and procedure

To determine the effect on the gas yield and composition of introducing the CO_2, pyrolysis experiments were performed on the wood-chips in a Horizontal Tubular Reactor (HTR) at 850° C under three different atmospheres: N_2, 20% CO_2 in N_2 and 40% CO_2 in N_2.

HTR apparatus

The Horizontal Tubular Reactor (HTR) consists of a double-walled quartz pipe. The length and inside diameters are respectively 850 mm and 55 mm for the inner tube, and 1290 mm and 70 mm

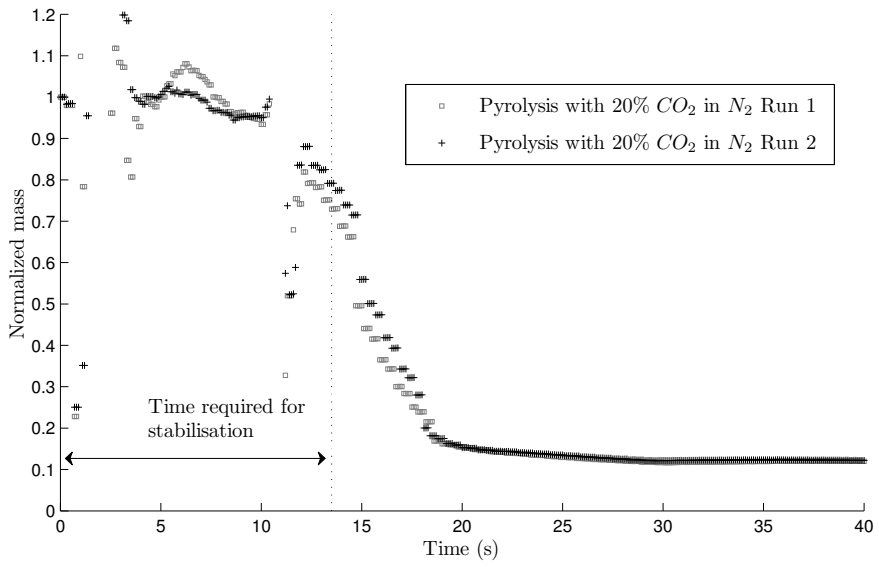

Figure 3.1: Repeatability tests of high-temperature flash pyrolysis experiments

for the outer tube. Nitrogen and carbon dioxide flow rates are controlled by means of mass flow-meters/controllers. The major part of the incoming gas flow (75%) is introduced on right hand-side of the reactor and passes through the annular space to be heated before reaching the biomass samples. The rest of the gas flow is injected on the left hand-side to cool the injection spoon when pooled out from the hot zone and to prevent a backward flow of the pyrolysis gases. The pyrolysis experimental device is presented in figure 3.2.

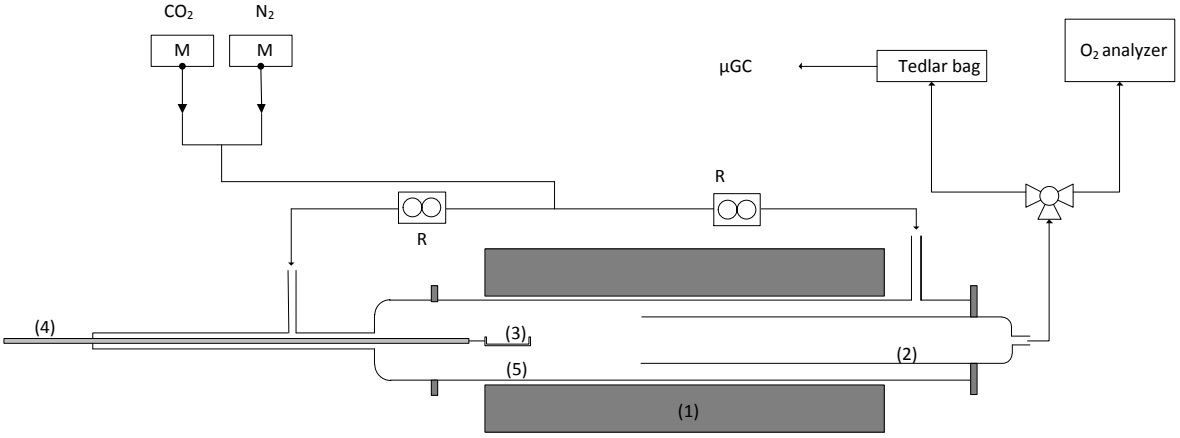

Figure 3.2: Horizontal tubular reactor experimental device

Experimental procedure

A load of 20 to 25 wood-chips with a total weight of about 0.5 g was placed in a basket made with a stainless-steel grid of 0.5 mm thickness and attached to the end of a mobile stick made of

pyrex. The wood-chips were spaced widely enough to avoid chemical and thermal interactions. The mobile stick bearing the basket containing the biomass samples was kept in the non-heated zone until the stabilization of the reactor atmosphere. The flow rate of the pyrolysis gas medium (pure nitrogen or mixtures of carbon dioxide and nitrogen) was set to 2 l/min (STP). Part of the gas flow was initially deviated to a SERVOMEX paramagnetic analyser to quantify the oxygen. Once the O_2 concentration reached zero, the pyrolysis experiment could start. At t=0, the reactor outlet was connected to a Tedlar gas sampling bag. Then, the mobile stick was introduced in the hot reactor until the grid basket reached the entry of the isothermal zone, which had a length of 40 cm and a temperature of 850 ± 10° C. The gas collection time was set to 3 min according to preliminary pyrolysis tests showing that the pyrolysis reaction lasts less than 1 min. When CO_2 was introduced alongside nitrogen, the stainless-steel basket was pulled out in the cooled zone after 1 min to avoid char gasification by CO_2. CO_2, CO, H_2, CH_4, C_2H_4 and C_2H_2, which are the major permanent gases emitted during pyrolysis, were subsequently analysed with a micro-chromatograph analyser (Agilent 3000 μGC). As the pyrolysis emitted a considerable amount of water (0.10-0.17 g/g wood (db)), calculations and precautions were made to ensure that the water partial pressure in the bag was below its saturation pressure to avoid water condensation inside the bag, which could distort the measurements. We also filled the bag periodically with air to force any eventually condensed water to evaporate.

Pyrolysis product yields

N_2 was used as a gas tracer. As the quantity collected in the bag was known, and its molar fraction was given by the μGC, it was possible to determine the total moles of gas in the bag:

$$n_{tot} = \frac{n_{N_2}}{x_{N_2}} = \frac{Q_{N_2(STP)} \times \rho_{N_2(STP)} \times t_{sampling}}{M_{N_2} \times x_{N_2}} \tag{3.1}$$

and to calculate the molar quantity of the aforementioned gaseous species:

$$n_i = x_i \times n_{tot} \tag{3.2}$$

With : n_{tot}: total gas moles [moles], n_{N_2} : nitrogen moles [moles], x_{N_2} : nitrogen molar fraction, $Q_{N_2(STP)}$: nitrogen flow rate [l/min], $rho_{N_2(STP)}$ nitrogen density [kg/m^3] and $t_{sampling}$: sampling duration [min].

The results are given hereafter as mass yields on a dry ash-free basis (kg gas / kg wood (dafb)). The total gas yield represents the mass of permanent gases emitted during the pyrolysis (daf):

$$Y_{gas}\,(\%) = \frac{m_{gas}}{m_{wood\,(dafb)}} \times 100 = \frac{\sum m_i}{m_{wood\,(dafb)}} \times 100 \tag{3.3}$$

The energy content of the gas is assessed through the variable CGE (cold gas efficiency). This variable represents the ratio between the energy content of the permanent gas (HHV_{gas}) and the energy content of the initial biomass feedstock ($HHV_{wood(dafb)}$) without taking into account the heat input in the reactor:

$$CGE = \frac{HHV_{gas}}{HHV_{wood(dafb)}} \tag{3.4}$$

At the and of the experiment the residual chars were weighed and stored in a sealed recipient for further characterisation. The char yield is expressed as the ratio of the residual char to the initial mass of wood (db)

$$Y_{Char}\,(\%) = \frac{m_{Char}}{m_{wood_{db}}} \times 100 \tag{3.5}$$

Similarity of the experimental conditions in both reactors

A fact worth noting is that we characterized the M-TG and HTR reactors in terms of flow properties and heat transfer coefficients at sample surface. The global heat transfer coefficient at sample surface in the two reactors was determined following a lumped capacitance method [145], and the contributions of both convection and of radiations were estimated. Details about the procedure are given in appendix A. The gas flow inside the two reactors was laminar. The Reynolds number was estimated to be 13.4 in the M-TG reactor and 3.7 in the HTR reactor. The results for the global heat transfer coefficients in the M-TG and in the horizontal tubular reactor are given in table 3.2.

Table 3.2: Flow properties, convective and radiative heat transfer coefficients and particle heating rate in the M-TG and HTR experimental devices

Reactor	**M-TG**	**HTR**
$h_{conv}[W/m^2.K]$	26	20.3
$h_{rad}[W/m^2.K]$	104.7	178.7

Given the similarities in the gas flow properties, in the global heat transfer coefficients and heat transfer mode (the same magnitude and radiative for more than 80 %), it can be stated that the operating conditions in both reactors are similar and that it is legitimate to establish comparisons between experiments performed in the two experimental devices.

Based on the above results, we also estimated the initial heating rate of the biomass particle β_0 to be respectively 122 and 101 [K/s] in the M-TG and in the HTR reactor [147]. Details are given in Appendix B.

3.2.3 Characterisation of the remaining char

To determine if pyrolysing wood under a CO_2-containing atmosphere impacts on the char properties, we performed a set of characterisation tests and reactivity measurements with CO_2, H_2O and O_2 of chars obtained respectively after pyrolysis in pure nitrogen and pyrolysis in 20% CO_2 in N_2.

Chemical composition

The remaining char chemical composition was determined by ultimate analysis in terms of C, H O and N contents. The ash content was determined by combustion of 100 mg of char in a muffle furnace at 550°C.

Textural and structural characterisation of the remaining char

Observations of the char structure were made through a Scanning Electron Microscopy (SEM) device. The chars were also characterized for specific surface measurement. The Brunauer-Emmett-Teller (BET) surface area was determined respectively for chars pyrolysed under N_2 and 20% CO_2 in N_2 in a Micrometrics, Gemini instrument using liquid nitrogen at 77 K. Chars were out-gassed under vacuum for 24 h prior to the gas adsorption experiments in order to eliminate moisture or any condensed volatiles which could prevent the adsorbate from gaining access.

Char reactivity measurement

After the pyrolysis step in the M-TG reactor, we performed gasification tests on the residual chars with steam, carbon dioxide and oxygen. The gasification experiments were made respectively with

20% CO_2 in N_2, 20% H_2O in N_2 and 5% O_2 in N_2. The chars were kept in the furnace and the atmosphere composition was switched to that of the gasification conditions.

The char conversion level is given by:

$$X_{(t)} = \frac{m_0 - m_{(t)}}{m_0 - m_{ash}} \tag{3.6}$$

Where m_0, m_t and m_{ash} are respectively the initial mass of char, the mass at a time t and the mass of the residual ash.

The char reactivity was calculated over time following the relation:

$$R_{(t)} = \frac{1}{1 - X_{(t)}} \times \frac{dX_{(t)}}{dt} \tag{3.7}$$

Temperature programmed oxidation

The temperature-programmed oxidation (TPO) technique provides relevant information about the carbonaceous material contained in the chars. Oxidation profiles of the chars in non-isothermal conditions can inform about the type of carbon materials and their peak oxidation temperatures. For instance, it is possible to distinguish between different forms of carbons if the char oxidation profile exhibits more than one peak. Temperature-programmed oxidation (TPO) experiments were performed on the chars obtained in N_2 and in 20% CO_2 in N_2. The char samples were firstly ground gently with a mortar and pillar. A sample mass of 2 to 4 mg was mixed with 100 mg of silicon carbide (SiC) and introduced in an electrically-heated quartz reactor. First, a temperature-programmed desorption with 50 mL/min of helium was performed from room temperature up to 900°C with a slope of 15°C/min in order to clean the char surfaces of any exterior deposit. Then, after cooling and return to baseline, an oxidizing gas mixture of 1% oxygen in helium (total flow of 50 ml/min) was introduced in the reactor. The temperature was increased at a rate of 15°C/min from room temperature to 900°C. The CO_2 emitted during the char oxidation was monitored by a Mass Spectrometer (Quadrupole Pfeifer Omnistar).

3.3 Results and discussion

3.3.1 Pyrolysis rate

High-temperature fast pyrolysis tests show a good repeatability with the established protocol. The data presented hereafter are average values from at least two experiments. The results of pyrolysis experiments in N_2 and 20% CO_2 in N_2 are shown in figure 3.3. In the figure, a mass loss of 10% at the beginning, perhaps attributable to particle drying, has been indicated. Devolatilisation can be divided into two stages : an active phase corresponding to the major mass loss, and a passive phase within which the rate of mass loss decreases abruptly corresponding to lower emissions of gas and tars [155]. It can be seen that the pyrolysis reaction rate is almost the same for pyrolysis under N_2 and for pyrolysis under 20% CO_2 in N_2.

3.3.2 Final char yield

In M-TG pyrolysis experiments, an additional mass decay was observed when the CO_2 was introduced, which resulted in a lower char yield. The char yields after pyrolysis in N_2 and in 20% CO_2 in N_2 at t=60 s were respectively 13.1±0.3 % and 11.32±0.25 %. These results indicate that either less char was formed, or that there was a char consumption when introducing CO_2 along with nitrogen.

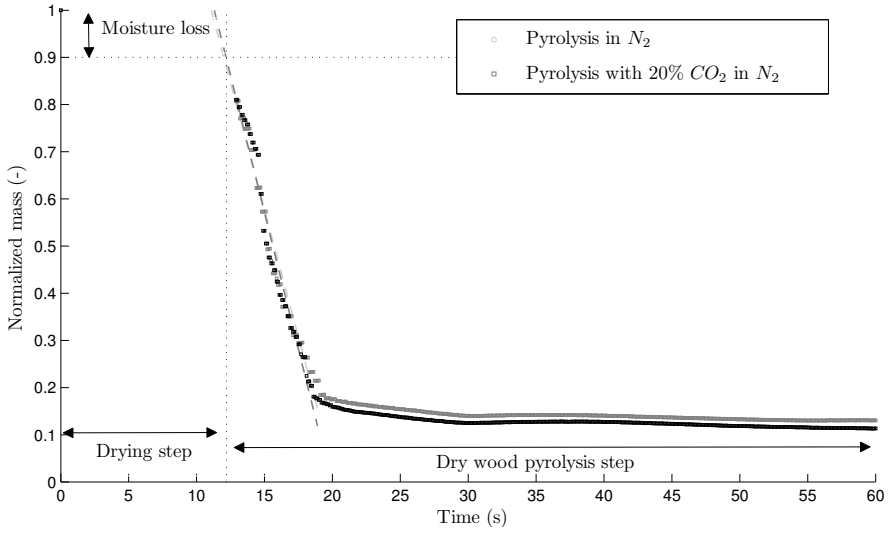

Figure 3.3: High temperature flash pyrolysis of beech wood-chips in N_2 and in 20% CO_2 in N_2 (M-TG)

In HTR experiments, a decrease in the char yield from 11.7 %±0.04 down to 10.5%±0.38 in a 20% CO_2 containing atmosphere was also observed. The char yield remained constant when increasing the CO_2 concentration further to 40%, as shown in figure 3.4.

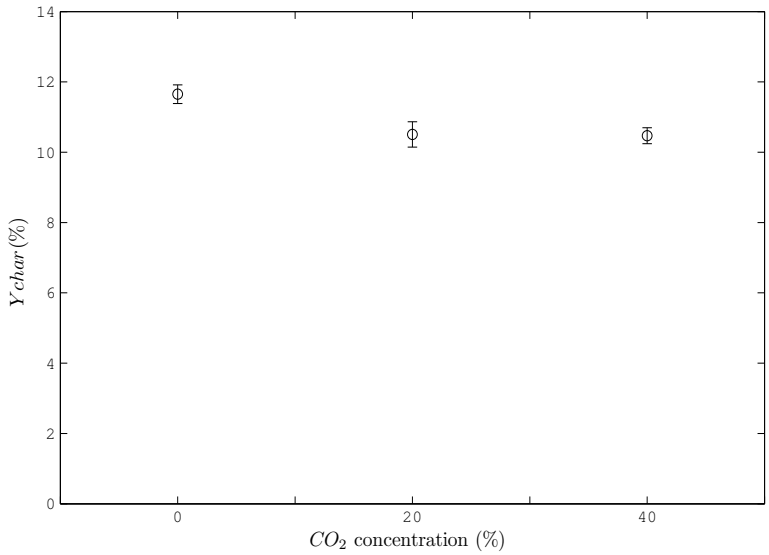

Figure 3.4: Char yield as a function of the CO_2 concentration in the pyrolysis medium (HTR)

These results confirm those obtained in pyrolysis experiments in the M-TG device, although the decrease in the final mass of the char in pyrolysis experiments with CO_2 was slightly smaller. It is also worth noting that the char mass remained constant even after the CO_2 partial pressure was increased to 40%.

The mass of the residual char is known to depend on the temperature and on the pyrolysis heating rate [14] [74] [90]. The final temperature was the same in the two experiments. The additional mass

loss may be due to a thermal effect or to a chemical effect prompted by the CO_2.

As regards thermal effects, the higher specific heat of CO_2 in addition to its radiative properties in comparison to N_2 can modify the heating rate of particles when introduced in the pyrolysis medium. To verify this, we measured the global heat transfer coefficient h_{global} in both atmospheres, keeping the gas velocity constant. We found a slight increase when adding the CO_2, but the order of magnitude was the same: 131 and 148 $[W/m^2.K]$ respectively. The thermal effect is thought to be negligible.

As for the potential chemical effects, there are two possibilities: (i) the CO_2 can inhibit secondary char formation by reacting with tars, and (ii) the CO_2 may react directly with the char according to the Boudouard reaction. At this level, we can not go beyond assumptions with regard to the mechanisms that may be unfolding. These assumptions will be discussed later.

3.3.3 Final gas yields

Figure 3.5 shows the pyrolysis gas yields under 100% N_2, 20% CO_2 and 40% CO_2 in N_2. Note that the CO yields were divided by 10 to fit the figure.

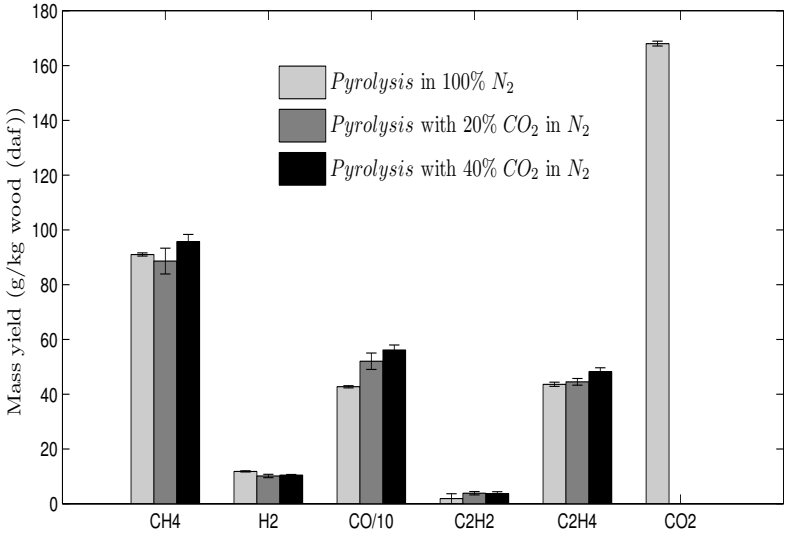

Figure 3.5: Pyrolysis gas yields at 850°C under 100% N_2, 20% CO_2 and 40% CO_2 in N_2 (HTR)

We can see that the major change involved the carbon monoxide. A net increase was observed for CO, whose yield increased from 427 (g/kg wood (daf)) in pure nitrogen to 520 (g/kg wood daf) when introducing 20% CO_2, and further to 561 in a 40% CO_2-containing pyrolysis atmosphere. The CH_4 and C_2 hydrocarbons yield increased slightly in a 40% CO_2 atmosphere compared to a free CO_2 atmosphere. The H_2 yield decreased slightly from 11.8 to 11.4 (g/kg wood daf) when increasing the CO_2 concentration from 0 to 40%. In a nitrogen atmosphere, the CO_2 was produced with a yield of 168 (g/kg wood daf). It was not possible to give a reliable result on the CO_2 yield in pyrolysis experiments with CO_2 introduction due to high uncertainties: the amount of produced CO_2 is much smaller than the amount of CO_2 introduced in the atmosphere gas (ratio of 60 approximately) as the introduced CO_2 to biomass ratio was calculated to be 6.5 and 13 g/g wood (daf) respectively for experiments done with 20% CO_2 and 40% CO_2 in N_2.

The total permanent gas yield (excluding CO_2) increased with the increase in the CO_2 concentration in the pyrolysis medium from 576 (g/kg wood (daf)) in a free CO_2 medium to 667 (g/kg

wood (daf)) with 20% CO_2 and further to 719 (g/kg wood (daf)) with 40% CO_2 in the pyrolysis medium. The energy content represented by the variable CGE increased accordingly by 13% from 0.66 (0% CO_2) to 0.75 (40% CO_2). However the H_2/CO ratio decreased with the increase in the CO_2 concentration in the pyrolysis gas medium.

Interpretation and discussion of results

As mentioned in the introduction section, several studies have dealt with the effects of CO_2 in biomass and coal pyrolysis. For instance, Kwon et al [120] found that introducing CO_2 alongside nitrogen in the pyrolysis process at 550 °C in a tubular reactor decreased the generation of pyrolytic oil and enhanced pyrolytic gas production. The authors propose that hydrocarbons emitted in the pyrolysis process can be broken down in the presence of CO_2, or at least not formed. The authors also carried out steam gasification tests at higher temperatures (600 to 1000 °C) and noticed that the yield of C2 hydrocarbons also increased and the amount of tar was reduced by 51.2%.

In a more recent study the same authors [121] found that the CO_2 enhances cracking of C4 hydrocarbons in addition to impeding the gas phase addition reaction by which benzene derivatives are formed. The authors also made tyre pyrolysis experiments at 650 °C in a CO_2-free and in a CO_2-containing atmosphere. They found that the amount of condensable hydrocarbons decreased by 30 to 50% when introducing CO_2 in addition to there being a modification of the end products. The authors proposed that the CO_2 participates in the cracking reactions as well as impeding other reactions by which tars are formed.

In another study, Zhang et al [119] investigated the effect of the pyrolysis medium composition on the biomass fast pyrolysis process in a fluidized bed gasifier at 550° C. The pyrolysis in a CO_2 atmosphere was seen to produce less char than in the other atmospheres. The CO_2 yield decreased and the CO yield increased compared to N_2 atmosphere. Moreover, the CO_2 atmosphere led to the highest yield of acetic acid compared to the other atmospheres. Ketones yield also increased in a CO_2 atmosphere while the phenol yield decreased. The authors explained these observation by two possible mechanisms: the CO_2 reacted with the active volatiles or with the biomass char. The former assumption seems to be more plausible in view of the pyrolysis temperature.

Ahmed et al [156] also evidenced a CO_2 consumption during the pyrolysis of cardboard and paper.

Based on these literature findings, it is clear that CO_2 influences the pyrolysis process by modifying the product yields. One of the major findings is that the CO_2 hinders condensable hydrocarbon formation and enhances the CO yield.

Primary tars can undergo polymerisation reactions and form secondary char as proposed by Gilbert et al [157] and Zhang et al [158]. According to the literature findings, a plausible explanation for the char mass decay may be that the CO_2 prevents tar polymerisation reactions and secondary char formation. The decrease in the final mass of char and the increase in the gas yield may be due to the enhanced tar cracking by CO_2 according to:

$$C_nH_m + nCO_2 \longrightarrow 2n\,CO + \frac{m}{2}H_2 \tag{3.8}$$

The CO_2 may also participate in homogeneous gas reforming reactions, as reported by Sutton et al for methane and propane reforming [159].

Methane dry reforming reaction (MDR) by CO_2 is promoted at high temperatures (thermodynamically possible above 640 °C) and leads to an enhanced CO production according to:

$$CO_2 + CH_4 \longrightarrow 2H_2 + 2CO \quad \Delta H = +246.9\,kJ/mol \tag{3.9}$$

The CO_2 can also react with hydrogen molecules according to the reverse water gas shift reaction (rWGS), which is the dominant reaction at high temperature (above 700 °C):

$$CO_2 + H_2 \longrightarrow H_2O + CO \quad \Delta H = +41.2\,kJ/mol \tag{3.10}$$

The observations of improved gas yields at low temperature found in the literature are probably related to homogeneous reactions and tar cracking by CO_2. A straightforward thermodynamic approach based on the Gibbs available energy variation shows that at temperatures below 650 °C, the Boudouard reaction does not promote CO formation (1) but on the contrary its disproportionation (2) into CO_2 and carbon deposit.

$$CO_2 + C \rightleftharpoons 2\,CO \tag{3.11}$$

At a high temperature of 850°C, the char gasification reaction must be taken into account, especially when the pyrolysis is performed at a high heating rate. Jamil et al [132] performed coal pyrolysis experiments in a wire-mesh reactor respectively under He and CO_2 with heating rates of 1°C/s and 1000°C/s from ambient to a prescribed peak temperature. They found that, in fast pyrolysis experiments, the char yield in CO_2 is slightly but systematically lower than that in He over the range of the holding time. The difference in the char yield was in the range 1-2 wt%-daf at a peak temperature of 700°C, but was outside the range of experimental error. Fast heating rate pyrolysis up to 800°C showed a difference in the char yields in the range of 2-3 wt%-daf from the very beginning of the holding time period at this peak temperature. These results confirm the observations made in the present study concerning the lower char yield in a CO_2-containing pyrolysis atmosphere. The authors went further in investigating this observation and concluded that fast pyrolysis (high heating rate) improves the thermal cracking of the char and provides high concentrations of radical species at the char surface, compared to a slow pyrolysis. These radicals constitute the active sites and are very reactive towards CO_2 molecules. The authors proposed that the rate of the gasification reaction is closely related to the rate of the thermal cracking that generates the radicals . The reactivity of the nascent char towards CO_2 during fast heating from 600 to 900°C was two or more orders of magnitude higher than reactivity data found in the literature for similar coal chars.

These observations, made by Jamil et al, can explain the additional mass decay observed in our experiments. The nascent char obtained after the fast pyrolysis may contain a high concentration of radicals at its surface, which reacted with the surrounding CO_2 and led to the char consumption.

Di Blasi reported in her review a panoply of kinetic rate constants for the CO_2-char gasification reaction of numerous biomasses [14]. A characteristic time approach shows that the rate of the Boudouard reaction is low at 850 °C. However, the mechanisms of the char gasification seems to be different for a nascent char prepared at a high heating rate [132]. The Boudouard reaction is therefore a potential cause behind CO yield increase and char mass decay:

$$CO_2 + C \longrightarrow 2\,CO \quad \Delta H = +172.5\,kJ/mol \tag{3.12}$$

Taking the results obtained in the present study together with the literature analysis, the improved CO yield and the final char mass decay can be the result of three combined effects of improved tar cracking by CO_2: the gas phase reactions of methane reforming and reverse water gas shift, and char gasification. The next sections will shed more light on the pyrolysis process unfolding in a CO_2-containing atmosphere.

3.3.4 Effect of CO_2 co-feeding on the char properties

Structural and textural properties

- **SEM analysis**

Figure 3.6 shows SEM images of chars pyrolysed at 850°C in N_2 and 20% CO_2 in N_2. Both chars show a similar amorphous, heterogeneous and disordered structure. No clear difference was observed between the two char structures, both of which kept the fibrous aspect of the raw wood with extensive cracks and breakages, probably due to the violent release of volatiles during the pyrolysis stage.

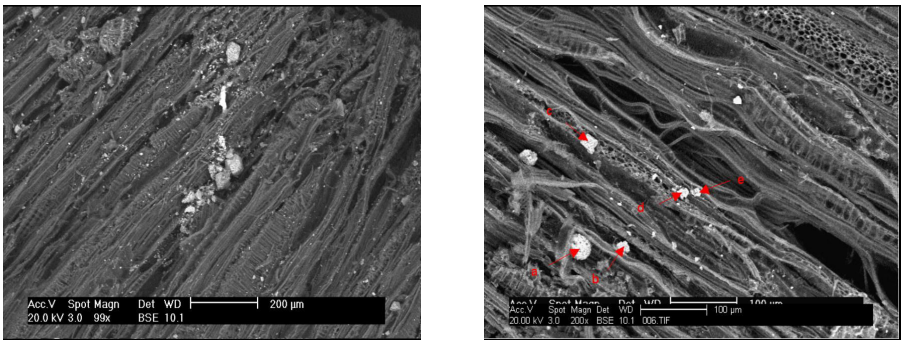

Figure 3.6: SEM images of chars obtained at 850°C respectively under N_2 and 20% CO_2 in N_2 (HTR)

- **Char specific area measurement**

Figure 3.7 shows the N_2 adsorption isotherms of two chars. The reported data are the average of two repeatability experiments.

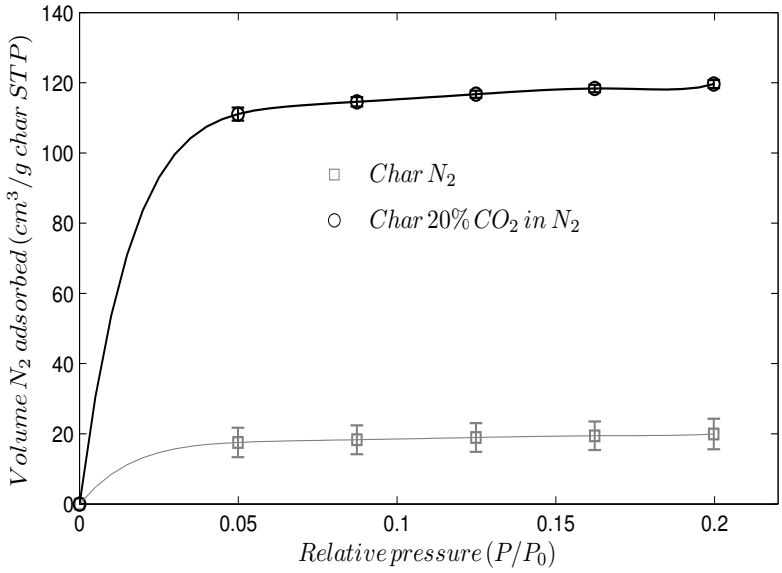

Figure 3.7: N_2 adsorption isotherms of beech wood chars pyrolysed respectively under pure nitrogen and 20% CO_2 balanced with nitrogen (HTR)

The adsorbed volume of N_2 per unit mass of porous carbon (char) is more than 6 times greater for chars prepared with 20 % CO_2 in the heating medium than those obtained with a pure N_2 heating medium. The respective BET specific surfaces are $68.9 \pm 14.33 m^2/g$ and $408.3 \pm 3.1 m^2/g$.

Former studies showed the same order of magnitude for the specific area of chars prepared with a high heating rate under nitrogen: $S_{BET} < 70m^2/g$ [74]. The specific area greatly expanded in the presence of CO_2. In a study on biomass char pyrolysis in a drop tube furnace respectively under N_2 and CO_2 [129], Borrego at al performed textural characterisation on wood-chip chars and found similar specific areas: 277 and 331 m^2/g respectively under N_2 and CO_2. The char reactivity towards air at 550°C in a TG device was also the same. The operating conditions were not the same (particle size of 36 to 75 μm, residence time of 0.3 s and reactor temperature of 550°C), which makes the comparison rather difficult. However, in another study, Klinghoffer et al prepared biomass chars in a fluidized bed reactor with a heating rate of 20°/min under steam and CO_2. They found that the chars were active with respect to hydrocarbon cracking. The chars exhibited similar surface areas in the range of 400-700m^2/g depending on the operating conditions. However the char yield in a CO_2 medium is highly micro-porous. The authors imputed this micro-porosity to the CO_2, which is in accordance with our findings [29].

The physical activation of chars by CO_2 for activated carbon preparation has been extensively studied, and it is well established that the CO_2 develops the microporosity inside the char [35] [160]. However, such char activation procedures for microporosity development are quite different, as they usually involve several steps of pyrolysis, carbonisation at high temperature with holding times exceeding sometimes 1 h, and finally char gasification by CO_2 for extensive microporosity development. In their review on carbon molecular sieve preparation from lignocellulosic biomass, Mohammed et al reported on the experimental conditions and procedures for preparation of highly porous materials by CO_2 activation. The experimental procedures are usually of long duration, involving a chemical activation step, a pyrolysis/carbonisation step that may lasts from 1 to 8 h, and a CO_2 or steam activation step whose duration is in the range of 15 to 1080 min. The char burn-off is also high in the range of 34 to 80% [161]. These procedures are, in most cases, time- and energy-consuming. In the present study, the char specific area increased sixfold within a very short duration and using a quite simple one-step procedure. The high heating rate coupled to CO_2 introduction during pyrolysis are procedures worthy of consideration for the effective production of porous carbon material with a good surface area.

- **Char chemical composition**

The proximate and ultimate analysis of the two chars are presented in table 3.3.

Table 3.3: Proximate and ultimate analysis of chars obtained under N_2 and 20 % CO_2 in N_2 (% dry basis)

	Proximate analysis	**Ultimate analysis**			
	Ash	C	H	O	N
$N_2 - char$	3.00±0.24	87.91±0.81	1.97±0.56	6.16±0.04	0.96±0.28
$CO_2 - char$	3.79±0.15	89.82±0.51	0.78±0.17	5.05±0.23	0.63±0.09

The ultimate analysis showed a difference in the chemical composition of the two chars. Indeed, we observe that the hydrogen, oxygen and nitrogen amounts decreased in the $20\%CO_2 - char$. It seems that the functional groups containing oxygen and hydrogen are removed preferentially under CO_2. The hydrogen amount decreased by 60% and that of oxygen by 18%.

The H/C and O/C ratios of the $CO_2 - char$ decreased in comparison with the $N_2 - char$. Adding carbon dioxide into the pyrolysis atmosphere enhances hydrogen and oxygen loss and carbon enrichment of the residual char. Another fact worth noting is that the ash amount increased for the

$20\%CO_2 - char$, which is synonymous of char conversion and confirms the char yield decrease when CO_2 is added in the pyrolysis atmosphere.

Char reactivity measurements

The reactivity tests on the two chars with alternatively 20% of steam in N_2, 20% CO_2 in N_2 and 5% O_2 in N_2 were performed after the pyrolysis step by switching the reactor atmosphere to the desired composition (CO_2, H_2O and O_2 . The purpose here was to characterise the influence of the pyrolysis atmosphere composition on the char reactivity. Reactivity profiles along the char conversion are shown in figure 3.8. These reactivity results are the average of three repeatability tests. The mean reactivities (X=0.2-0.9), as well as the standard deviations (error bars), are presented in figure 3.9.

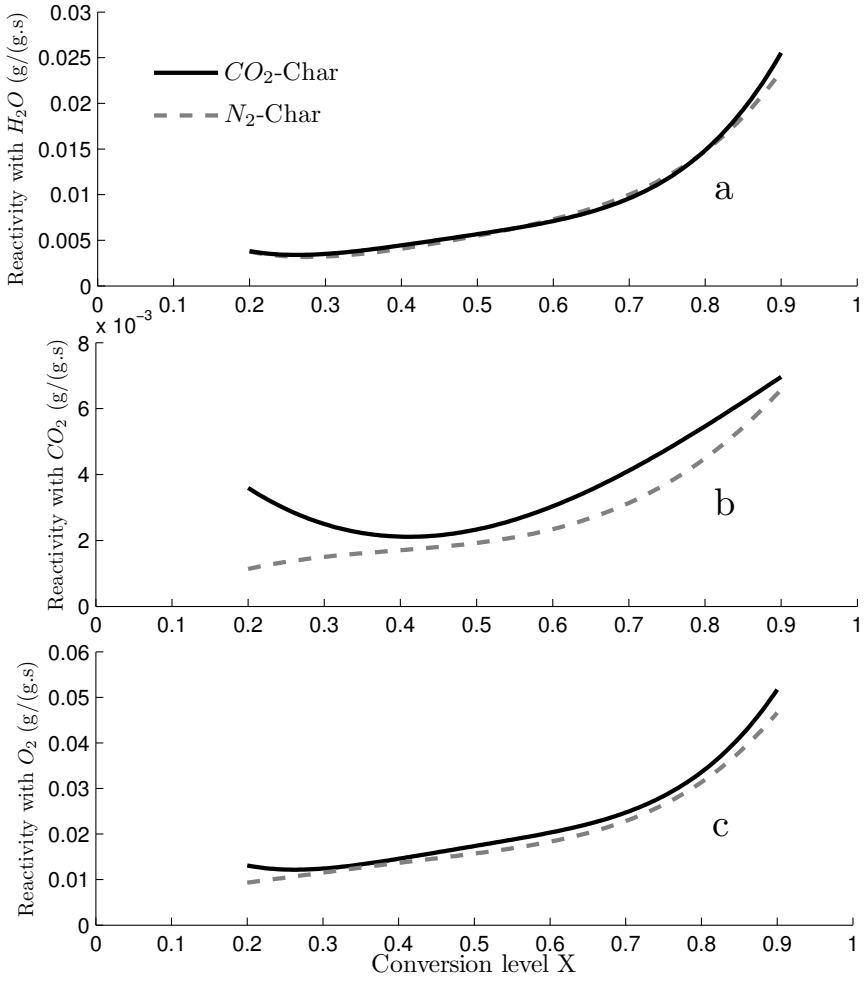

Figure 3.8: Influence of the pyrolysis atmosphere on the char reactivity with (a): H_2O, (b):CO_2 and (c): O_2 at 850°C (M-TG)

In steam gasification experiments (figure 3.8.a), we observed that the char reactivity profiles remained the same regardless of the pyrolysis atmosphere composition, and the average reactivities (between X=0.2 and X=0.9) are respectively 0.0081 and 0.0083(g/g.s) for chars obtained in N_2 and in 20% CO_2 in N_2 pyrolysis atmosphere. In the char gasification experiments with CO_2 (figure 3.8.b), we observed an increase in the char reactivity towards CO_2 for the chars prepared in a CO_2-containing pyrolysis atmosphere, especially in the earlier stages of the gasification reaction (up to

40% of conversion). The average reactivities are respectively 0.0028 and 0.0038 (g/g.s) for chars obtained in N_2 and in 20% CO_2 in N_2 pyrolysis atmosphere, which represents an increase of 26% in the reactivity (the relative standard deviation is below 5%). This tendency may be explained by the higher surface area of chars obtained in a CO_2-containing pyrolysis atmosphere which influences the Boudouard heterogeneous gasification reaction. The CO_2 diffusion to the carbon active sites can be promoted by this developed surface area, which explains the higher reactivity in the initial stages of the gasification.In fact, total pore volume was estimated to be 0.185 cm^3/g for chars prepared with a CO_2-containing atmosphere, while it was only 0.031 cm^3/g for chars obtained under N_2. In a more recent study [128], Hanaoka et al found that preparing chars in an $N_2/CO_2/O_2$ atmosphere leads to a more developed surface area and a higher reactivity towards pure CO_2, especially in a 18% N_2/41% CO_2/41% O_2 atmosphere. The char yield was similar to that obtained under nitrogen but there was an increase in the BET surface area from $275m^2/g$ in pure nitrogen to $417m^2/g$ and an increase in the char reactivity by a factor of 1.7 to 2.5 depending on the gasification temperature.

Despite the micro-porosity that developed in chars prepared in a CO_2-containing atmosphere, their reactivity towards steam was the same as that of chars prepared in N_2. Micro-porosity does not seem to influence the char-steam gasification reaction. This can be explained by the difference in char porosity development with both gases [35]. In fact, it has been demonstrated that submitting a char to activation with steam or CO_2 does not lead to the same porosity development. The CO_2 promotes the development of narrow microporosity up to about 20 % burn-off, followed by a widening up to about 40 % burn-off. On the other hand, steam widens the microporosity from the earlier stages of the gasification [160]. This observation can explain why a developed microporosity enhances the reactivity of the char towards CO_2 while it has no effect on its reactivity towards H_2O. The findings of Rodriguez et al [160] can also explain the reactivity profile obtained for char prepared in a CO_2-containing pyrolysis atmosphere which exhibits a higher reactivity in the first stages of the reaction (developed microporosity) and which decreases up to 40 % of conversion due to burn-off. The increase in the reactivity from 40 to 50% of conversion is due to a developed char porosity and a higher catalytic activity of the minerals. Moreover, we found in our previous study on char gasification in mixed atmospheres of H_2O and CO_2 [154], that gasifying biomass chars with CO_2 up to 30% of conversion does not affect its reactivity towards H_2O, which corroborates the current findings.

In a fluidized bed, a major part of the char will be carried in the riser and combusted with air. With this in mind, we also performed combustion tests on the two chars with an oxygen concentration of 5% to assess the impact of the CO_2 during pyrolysis on the char reactivity with oxygen (figure 3.8.c). The average N_2-char and CO_2-char reactivities were respectively 0.0214 and 0.0234 with relative standard deviations below 5%. Average char reactivity results for the different gasification atmosphere are summarized in figure 3.9 .

On the basis of these results we can conclude that the presence of CO_2 during pyrolysis mainly affects the char reactivity towards CO_2 and, to a lesser extent, with O_2, but does not affect the steam gasification of the char.

Temperature programmed oxidation Temperature programmed oxidation experiments were performed on both chars and brought relevant insights. Figure 3.10 shows the outflow of CO_2 as a function of temperature. The two chars exhibited two different oxidation profiles: both signal shapes and peak temperatures are different. The peak temperatures are respectively 580 and 600°C for the N_2-char and for the CO_2-char.For the CO_2-char TPO curve, a single peak is observed. On the contrary, the N_2-char TPO curve shows a more complex shape during signal increase and a last peak at 635°C. We believe that the CO_2-char contains a single type of carbon material while the N_2-char may contain more.

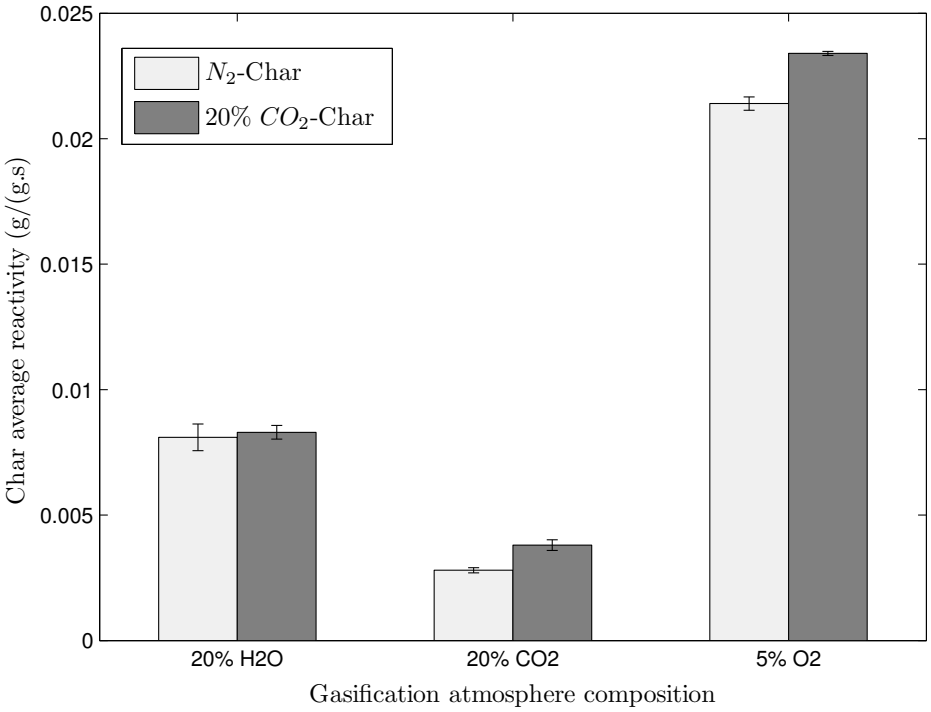

Figure 3.9: Mean reactivities (X=0.2-0.9) of N_2-char and CO_2-char towards H_2O, CO_2 and O_2 at 850°C (M-TG)

The TPO profiles were modelled using one or several parallel reactions converting char into CO_2 and CO following:

$$\frac{dm_{char}}{dt} = -k_{(T)}.m_{char} \tag{3.13}$$

The rate constants $k_{i(T)}$ follow an Arrhenius law that gives:

$$k_{(T)} = A.exp(-\frac{E}{R.T}) \tag{3.14}$$

A and E are the frequency factor $[s^{-1}]$ and the activation energy $[J/mol]$.

Figures 3.11 a and b show temperature programmed oxidation experimental profiles and models for the N_2-char and the CO_2-char. The CO_2-char oxidation is well described by a single reaction: this tends to show that it contains a single type of carbon. It was not possible to model the N_2-char oxidation with a single reaction. However, the oxidation reaction is well described - as reported in table 3.4 - when assuming the presence of three types of carbons. The model reads:

$$\frac{dm_{char-N_2}}{dt} = -k_{1(T)}.m_{carbon-a} - k_{2(T)}.m_{carbon-b} - k_{3(T)}.m_{carbon-c} \tag{3.15}$$

Where $m_{carbon-a}$, $m_{carbon-b}$ and $m_{carbon-c}$ are the amount of carbon materials.

The frequency factors A_i and the activation energies E_i were identified by fitting the model to the experimental results.

The identified carbon masses, frequency factors and activation energies for the two chars are given in Table 3.4. The N_2-char appears to be composed of approximately 40% of a carbon with a small activation energy of 135 $[kJ/mol]$, 51% of a high activation energy carbon 350 $[kJ/mol]$ and 9% of a third carbon having an activation energy lying between these to values 190 $[kJ/mol]$. The activation

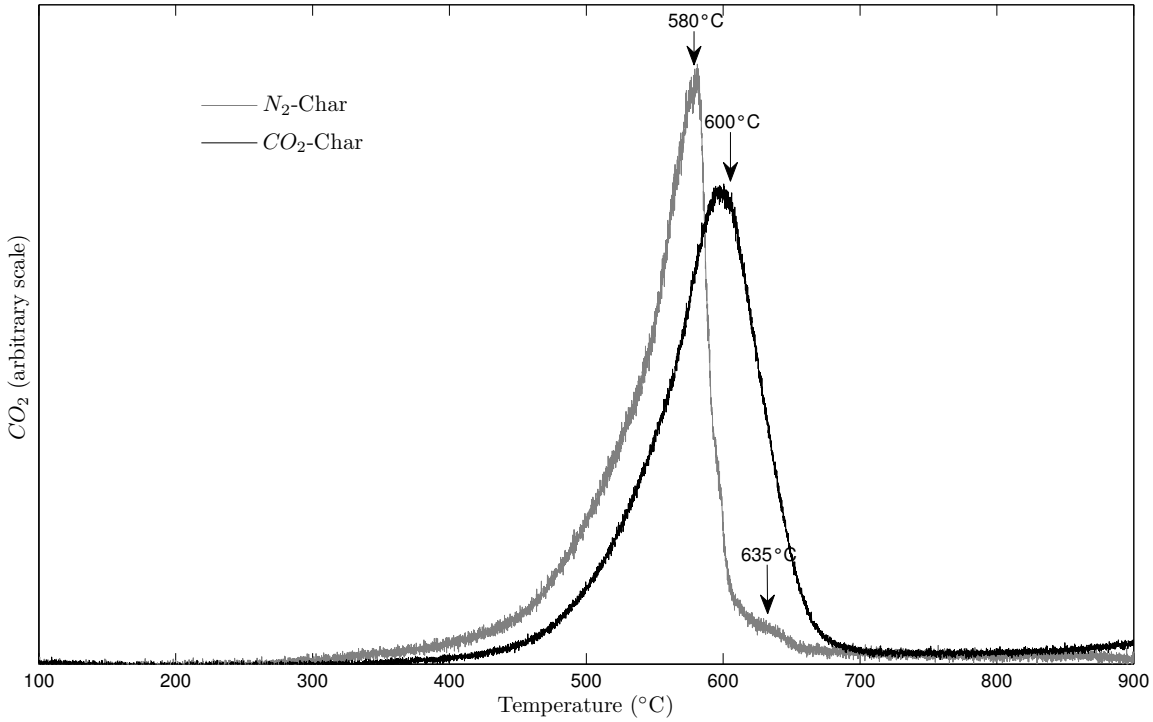

Figure 3.10: TPO profiles of N_2-char and CO_2-char (HTR)

energies of the first and the third carbons lie in the activation energy range for the lignocellulosic char-O_2 reaction (76-229 $[kJ/mol]$) given in Di Blasi's review [14]. However the second carbon has a higher activation energy in addition to a quite high pre-exponential factor. With an activation energy of 170 $[kJ/mol]$, the oxidation reaction of the CO_2-char is typical of lignocellulosic biomass chars.

Table 3.4: Temperature programmed oxidation kinetic parameters

	CO_2**-char**	N_2**-char**		
		Carbon(a)	Carbon(b)	Carbon(c)
mass (g)	1	0.4	0.51	0.09
A_i $[s]^{-1}]$	12.10^7	5.10^6	6.10^{19}	3.10^8
E_i $[kJ/mol]$	170	135	350	190

With regard to these results, the CO_2 may inhibit the last peak char formation by reacting with the tars, and therefore hinder their deposition and secondary char formation. The tars may have also been deposited on the char surface and removed afterwards by gasification. The last peak corresponds to the most stable form of carbon amongst the three identified forms. Logically, it should be the most difficult form to remove by gasification with CO_2, unless it is deposited on the char surface and is thus exposed first to this gasifying agent. A fact worth noting is that the mass of this third form of carbon corresponds to 10% of the total char mass, giving the TPO results. A link may be established with char mass decay observed in the MTG and HTR experiments when introducing CO_2. This char mass decay was in the range of 10 to 13%. Concerning the two other forms of carbon, introducing CO_2 may have changed the mechanisms of char formation and led consequently to an another type of char. It is clear that we cannot go beyond assumptions at this

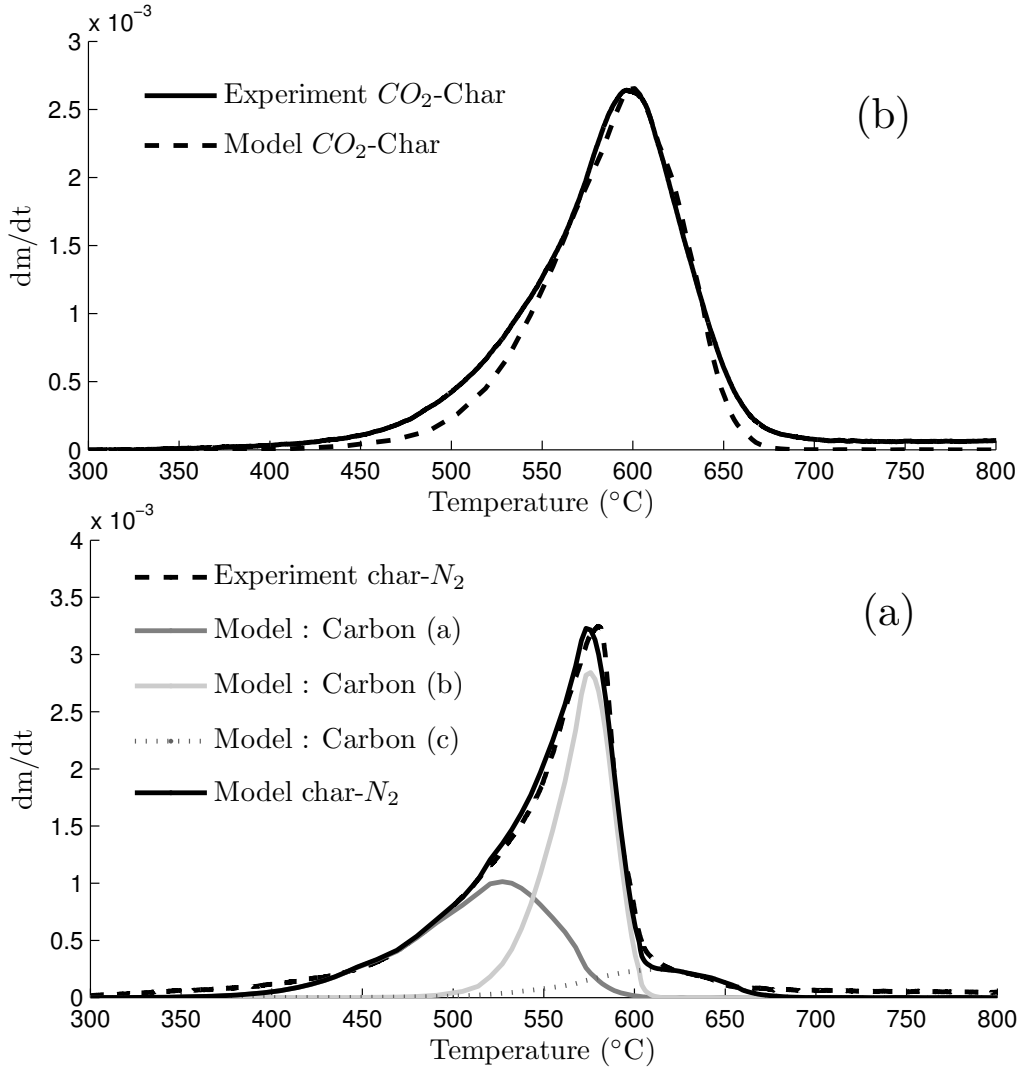

Figure 3.11: TPO profiles modelling of N_2-char and CO_2-char

level. These interpretations constitute a starting point towards highlighting the effect of CO_2 on the char properties and formation mechanisms.

3.4 Synthesis

Introducing CO_2 in the pyrolysis process atmosphere causes additional mass decay of the residual solid by 10 to 13% compared to pyrolysis in pure N_2. This mass decay can be explained either by char gasification by CO_2, which overlapped with the biomass pyrolysis, or by the fact that CO_2 hinders polymerisation reaction and secondary char formation by reacting and breaking some tar compounds that may lead to its formation. The mass decay is associated with an increase in the final permanent gas yield. With regard to the char ultimate analysis, the CO_2 seems to have an affinity to react with hydrogenated and oxygenated groups, leading to a more carbon-rich char, as amounts of these element decreased in the CO_2-char. Finally, we observed an almost sixfold increase in char specific area. These observations are probably well correlated. In figure 3.12, we propose a representation of the potential effect of CO_2 when introduced in the pyrolysis bath gas and its interaction with the pyrolysis products.

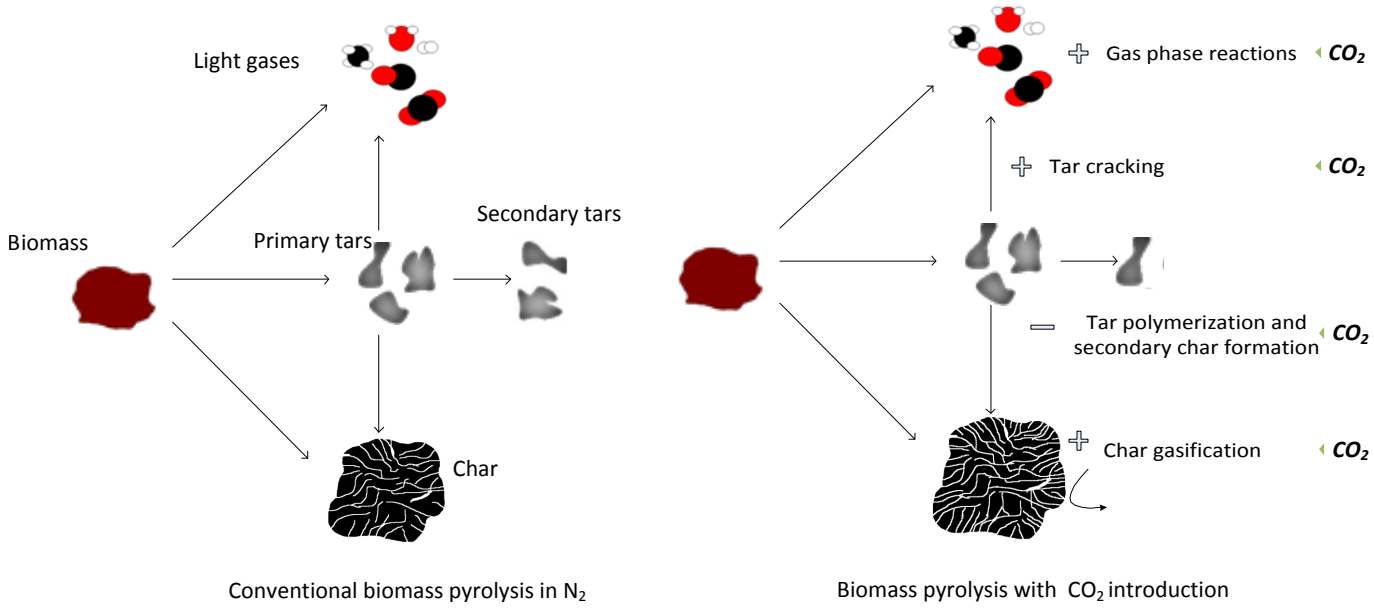

Figure 3.12: The potential mechanisms in biomass pyrolysis with CO_2 introduction in the pyrolysis bath gas

The following scenario could be assumed as an interpretation for the different experimental observations and literature findings:

During the pyrolysis process, the CO_2 reacts with tars and enhances their cracking into light gases. This results in an increase in the gas yield and a reduction in tar polymerization, which is behind the secondary char formation. A more homogeneous carbon-rich char with an enhanced microporosity is obtained. The TPO experiments tend to confirm this assumption: the TPO profile in the case of the CO_2-char is best described by a single reaction pathway, while the N_2-char exhibits several peaks, one of which may be imputable to the secondary char (carbon deposit). This carbon deposit is likely to contain a significant amount of hydrogenated and oxygenated groups and is probably deposited at the entry of the char pores, resulting in a lower surface area of the char.

3.5 Conclusion

CO_2 clearly has an influence during the biomass fast pyrolysis process. Its effects can be seen at two main levels: the pyrolysis gas yield and composition, and the char yield and properties. Introducing CO_2 induces an increase in CO concentration of the pyrolysis gas as a result of homogeneous and heterogeneous reactions of CO_2 with gases, tars and char. The char produced is also different and has high specific surface compared to a char obtained in N_2 atmosphere. TPO experiments show more than a single char oxidation peak in the N_2 char and sustain the assumption of tar polymerisation and secondary char formation. The CO_2 would appear to impede the secondary char formation and hinder tar polymerisation reactions.

Acknowledgements

The authors acknowledge the national research agency ANR-France for its financial support in the RECO2 project. They also wish to express their appreciation to Bernard Auduc for his technical support. Finally, the authors would also like to thank Laurent Bedel, Sylvie Valin and Claire Courson for their assistance and insightful conversations.

Chapter 4

The gasification reactivity of high-heating-rate chars in single and mixed atmospheres of H_2O and CO_2

This chapter was published as a research paper in an international journal, reference: Guizani, C., Escudero Sanz, F. J., Salvador, S. (2013). The gasification reactivity of high-heating-rate chars in single and mixed atmospheres of H_2O and CO_2. Fuel. doi:10.1016/j.fuel.2013.02.027

Abstract

Gasification reactivity of high-heating-rate chars (HHR-chars) in steam, carbon dioxide and their mixtures was investigated in a new macro-TG experimental device. The higher reactivity of the HHR-chars was highlighted by a comparison with reference chars prepared at a low heating rate (LHR-chars). It was found that the char reactivity in a mixed atmosphere of steam and carbon dioxide can be expressed as the sum of the individual reactivities obtained in single-atmosphere gasification experiments. This result was not dependent on the pyrolysis heating rate. In addition, gas-alternation gasification experiments, for both HHR-chars and LHR-chars, showed that gasifying the char with CO_2 up to 30% of conversion does not affect its reactivity to H_2O. Altogether, the results tend to indicate that the two reactant gases H_2O and CO_2 react on separate active sites when mixed atmospheres are used, and that CO_2 does not affect the char structure to favor or inhibit the char-H_2O gasification reaction.

Keywords: Biomass char, Gasification, H_2O and CO_2, mixed atmospheres, Kinetics

Résumé

La réactivité de chars obtenus par pyrolyse rapide est étudiée dans le cas d'une gazéification à H_2O, CO_2 ainsi que leur mélange dans un nouveau dispositif de Macro-thermogravimétrie. La réactivité plus importante des chars en chauffe rapide est mise en exergue par comparaison avec celle des chars obtenus en pyrolyse lente. On a trouvé que la réactivité de ces chars en atmosphère mixte peut être exprimée en additionnant les deux réactivités individuelles. De plus, des experiences spécifiques de changement d'atmosphere lors de la gazéification ont montré que gazéifier le char jusqu'à un taux de conversion de 30% ne modifie pas sa réactivité vis à vis de H_2O. Ces résultats montrent que les deux gaz réagissent séparément et que le CO_2 n'affecte pas la structure du char en inhibant ou en accélérant sa réactivité à l'eau.

Mots clés: Char de biomasse, Gazéification, H_2O and CO_2, Atmosphéres mixtes, Cinétique

4.1 Introduction

Industrialized countries as well as developing ones are more and more working on the development of renewable energies as a response to the unavoidable fossil fuel depletion and to the continuous and alarming environmental problems, especially the global warming which is a direct consequence of the increasing concentration of the greenhouse gases in the atmosphere, namely CO_2, which concentration has risen drastically since the industrial revolution. Biomass to energy is considered to be a pathway toward clean and renewable energy production, regarding the availability of the resource and the carbon-neutral feature of the thermochemical processes. Among the thermochemical processes, biomass gasification is gaining further interest as it allows the production of clean fuel gases (e.g. H_2, CO, CH_4) that can be either used to produce electricity and heat or as an input stream to produce chemicals or transportation biofuels.

Biomass gasification can be processed with various gasifying reagents like air, steam or carbon dioxide. Using carbon dioxide in such a process would provide a long term solution to mitigate its increasing concentration in the atmosphere. The CO_2 will be then incorporated in a valorisation cycle for the production of marketable fuels rather than being only captured and stored. The biomass gasification reaction includes three main steps: pyrolysis, volatile matter reforming and char gasification. The char gasification reaction is considered to be the limiting step of the process because it is kinetically slow compared to the two other steps.A huge amount of studies can be found in the literature as well as very good reviews on char gasification in steam or carbon dioxide containing atmospheres [162] [23] [14]. Still, the majority of these studies do not tackle the issue of char gasification in mixed atmospheres; only few ones do so and are performed mainly on coal char gasification [115] [138] [140] [139] [141] [163] [164] [135] [134] [134] [8] [103]. The drawn conclusions differ from a study to another; some authors assume that adding the carbon dioxide to the steam slows down the gasification reaction: *(i)* **inhibition and competition for the same carbon active sites** ([139] [163] [164]), others think that the two gases operate on separate active sites: *(ii)* **passive cooperation** ([141] [140] [115]), whereas others think that there is a kind of *(iii)* **synergy or active cooperation** between the two gases that leads to an enhanced char reactivity [103] [8]. Several models are proposed in accordance with these conclusions and a brief review and discussion are presented later in this paper. These contradictions prevent a clear conclusion on the unfolding of the gasification reaction in a mixed atmosphere of H_2O and CO_2. The present work was performed with the aim to further understand the biomass gasification reaction mechanisms in mixed atmospheres of steam and carbon dioxide. Gasification processes such as fluidized beds or entrained flow reactor are of interest in this study. Beech wood chips were used to study the gasification reaction with steam, carbon dioxide and their mixtures. Gasification experiments in single and mixed atmospheres of steam and carbon dioxide were initially made on high heating rate chars (HHR-chars) where conditions are of interest for gasification in fluidized beds in which rapid pyrolysis plays an important role as a first stage. The results showed that an additive law is representative of the char reactivity obtained in mixed atmospheres (Passive cooperation). Experiments were made afterwards on a low heating rate char (LHR-chars) to serve as a reference. Gasification experiments with gas alternation were performed to test the gas synergy assumption that was held elsewhere [103] [8].

4.2 Material and methods

4.2.1 Macro-TG experimental device

The new Macro-TG experimental device represented in 4.1 consists of 3 major parts: The heating system including a liquid H_2O evaporator, a gas pre-heater and an electrically heated alumina reactor.

The gas flow control system consisting of 3 mass flow meters/controllers. The weighing system that comprises an electronic scale, a stand and a platinum basket.

The 2-m long, 75-mm i.d. alumina reactor is electrically heated. The temperatures of the three reactor zones (high, medium and low) are independently controlled to ensure good temperature homogeneity throughout the furnace. Gas flow rates are controlled by mean of mass flow meters/controllers. Before entering the reaction zone, the reactant gases (N_2, CO_2 and H_2O) pass through a pre-heater which heat them to the reactor temperature before entering into it. When H_2O is added in the gasification medium, the H_2O + gas mixture passes first through an electrically heated evaporator maintained at 180°C to vaporize the water.

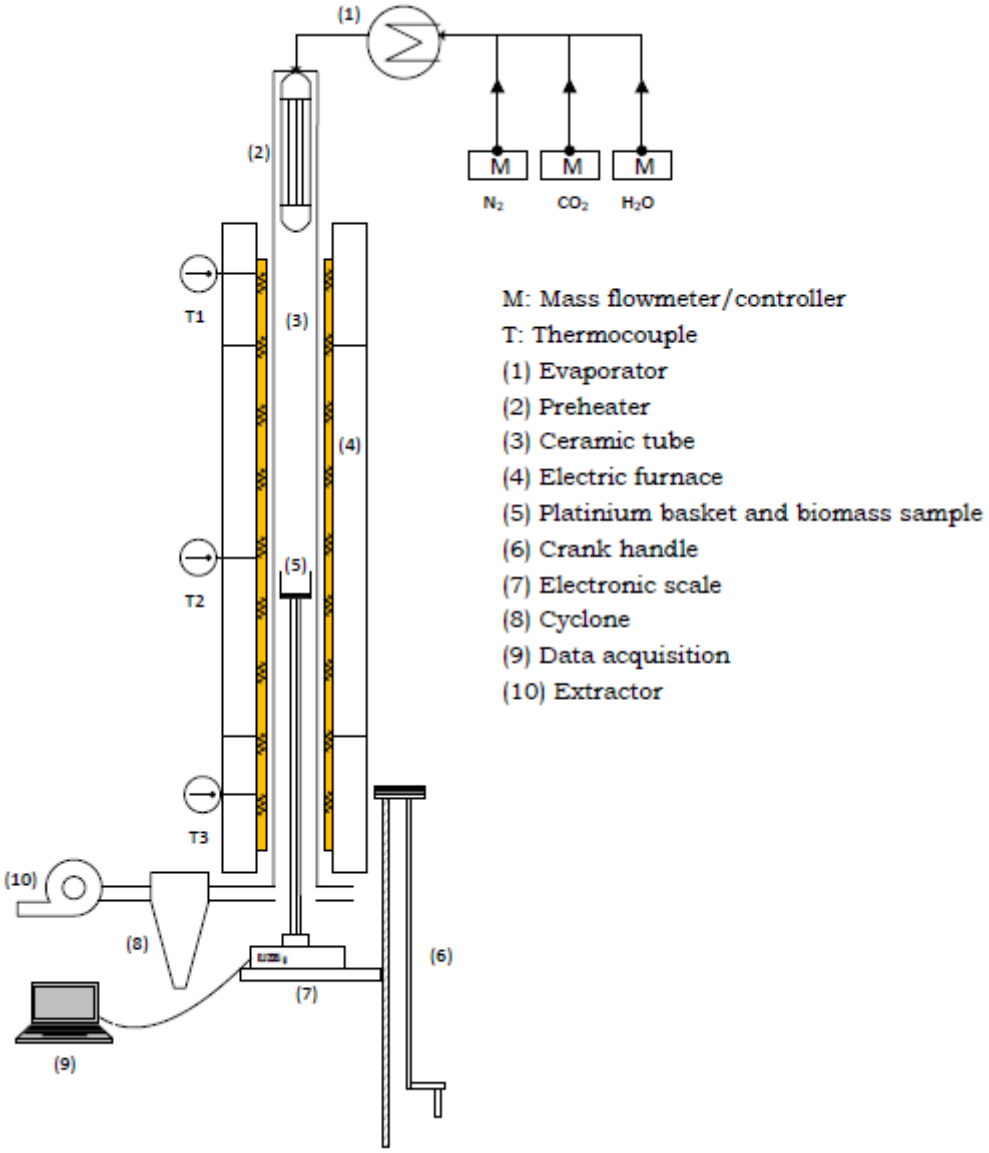

Figure 4.1: Macro TG experimental device scheme

The reacting gas flow inside the reactor is laminar and flowing at an average velocity of 0.2 m/s. The weighing system comprises an electronic scale having an accuracy of ± 0.1 mg, a metallic stand placed over the balance on which are fixed three ceramic hollow tubes having a length of 1 m and a 2.4 mm external diameter. These ceramic tubes hold up a platinum basket having a 50 mm diameter, a solid bottom and a side wall made from a 500 μm grid to allow the gas to pass through it. The

biomass samples are placed into it to be afterwards pyrolysed and gasified in the hot furnace.

The weighing system can be moved in the vertical direction using a crank handle. The platinum basket can be hence introduced into the hot furnace within less than 15 s. Altogether, the macro-TG experimental device has the advantage of being in an experimental scale far greater than the conventional TG-devices. This makes sample representativity better because an average result for several wood-chips is obtained for each run. The wood chips or char particles are not grinded as they use to be when the gasification is performed in a classic TG device. The size reduction process leads indeed to structural and chemical composition modifications, loss of fibrous texture and heterogeneous dispersion of catalytic minerals which vary according to the biomass particle size range [165]. This would affect the biomass reactivity data which may not be representative of the raw biomass. Moreover, the biomass particles are submitted to a thermal shock similarly as when they are introduced in a fluidized bed. Moreover, the biomass particles are submitted to a thermal shock similarly as when they are introduced in a fluidized bed. Finally, to our best knowledge, it is not possible to perform isothermal gasification experiments in a classical TG device without preheating the char sample to the desired temperature over a quite long time. This thermal treatment has an impact on the char reactivity. In fact, It has been widely demonstrated for several biomasses such as maize stalk, rice straw, cotton straw, rice husk, Brazil Nut shells and eucalyptus that the char reactivity decreases with thermal treatment as a result of morphological modifications encompassing the evolution of the level and type of porosity and the average pore size [40] [89] [90] [88] [86]. The char structure becomes increasingly condensed and ordered when increasing the heat treatment temperature and duration. This thermal annealing phenomenon would surely distort the real char reactivity data. On the contrary, in our case the biomass sample is introduced into the reactor within 10 s. The pyrolysis takes less than 1 minute to be fulfilled.

4.2.2 Biomass feedstock and char preparation

Biomass feedstock

The beech feedstock was firstly sieved to select particles with a size ranging between 4 and 5 mm and a thickness of 1 to 2 mm. The size and thickness of biomass particles may greatly influence the rate of the gasification reaction if they impact the heat and mass transfer inside the particle [23] [146]. In a recent study [166] [103], the authors demonstrated that the gasification rate was not influenced when varying the char particle size in the range of 10.5 to 15 mm. The influencing characteristic dimension was rather the particle thickness as it slowed down the reaction rate by 1.6 times when it was increased from 1.5 to 6 mm for a constant size of 10.5 mm. No differences were observed between thicknesses of 2.5 and 1.5 mm, which suggests that the reaction is chemically controlled below a 2.5 mm particle thickness. Leaning on these observations and owing to the similarities between the raw biomasses (beech wood chips) and the experimental devices (Macro-TG), we performed the gasification reactions with biomass and char particles having a size in the range of 4 to 5 mm and a thickness of about 1 to 2 mm.

Experimental procedure for char preparation and gasification

A mass of wood chips of 0.8 to 1 g is introduced in the platinum basket; the biomass particles are spaced enough to avoid chemical and thermal interactions. After heating the reactor to the desired temperature, the weighing system is lifted up using the crank handle; the platinum basket -containing the wood chips- is introduced into the hot furnace in less than 15 s. The biomass is firstly pyrolysis in a flow of nitrogen until reaching a constant mass, that of char. This procedure allows obtaining special chars prepared at a high heating rate. When the mass of char is stabilized, the displayed

weight on the electronic scale is reinitialized to zero and the reactant gas flow is established marking the beginning of the char gasification stage. The mass of char begins to decrease progressively until it reaches a plateau corresponding to the end of the experiment. The weighing system is then moved downward using the crank handle and the residual ashes are weighed after cooling. Following this procedure, we can accurately know the mass of char that was converted during the gasification reaction. The study focuses mainly on the gasification of biomass chars prepared at a high heating rate in the Macro-TG device as described in the previous paragraph. However, in order to highlight the specificity of these 'HHR-chars', we also conducted gasification experiments with chars prepared at a low heating rate 'LHR-chars'. These LHR-chars were obtained after a slow pyrolysis in a retorting furnace with a heating rate of 5°C/min up to 550°C and a residence time at the final temperature of 30 min. With a low heating rate, the char yield was about 24.8 %, whereas it was much lower with a high heating rate. It decreased slightly when increasing the reaction temperature from 9.89 % at 850°C to 7.87 % at 950°C. These results were expected regarding previous studies on biomass pyrolysis [74] [90] [14]. Table 1 lists the results of the proximate and ultimate analysis of the raw biomass wood chips, the LHR-chars and the HHR-chars obtained at 3 temperatures.

Table 4.1: Proximate and ultimate analysis of the beech wood-chips (dry basis)

	Proximate analysis			**Ultimate analysis**			
	VM	Ash	FC	C	H	O	N
Wood-chips	88.1	0.4	11.6	46.1	5.5	48.1	0.1
LHR-char	20.03	1.88	78.09	82.06	2.85	12.88	0.30
HHR-char 850°C	–	3.75	–	83.51	0.86	11.60	0.28
HHR-char 900°C	–	4.14	–	85.56	0.80	8.42	1.04
HHR-char 950°C	–	4.15	–	85.83	0.91	8.07	1.05

The ash content increased with increasing the pyrolysis heating rate due to lower char yields and little devolatilisation of the mineral species. One can note that the fuel-nitrogen remained in the char. The concentration of hydrogen and oxygen decreased with increasing the temperature.

4.2.3 Experimental conditions and method of data analysis

The gasification experiments were performed at atmospheric pressure with operating conditions similar to those encountered in fluidized bed gasifiers. The reactor temperature was in the range of 800 to 950°C and the gasifying medium partial pressure in the range of 0.1 to 0.3 atm. Table 2 gives the operating conditions for the different gasification experiments.

Table 4.2: Operating conditions of the gasification experiments

Reacting medium	Reacting gas partial pressure (atm)	Temperature (°C)
H_2O	0.1, 0.2, 0.3	800, 850, 900, 950
CO_2	0.1, 0.2, 0.3	850, 900, 950
H_2O/CO_2	0.1/0.1;0.1/0.2; 0.2/0.1	900

Method of data analysis

The normalized mass or conversion ratio X during the gasification reaction is calculated according to:

$$X_{(t)} = \frac{m_0 - m_{(t)}}{m_0 - m_{ash}} \tag{4.1}$$

Where m_0,m_t and m_{ash} are respectively the initial mass of char, the mass at a time t and the mass of the residual ash. The gasification experiments were reproduced 2 to 5 times and showed a good repeatability with deviation less than 12% which is considered acceptable regarding the heterogeneity of the wood material. Mass loss data curves were firstly smoothed using a polynomial least square function covering a fixed time period before and after each point. Precautions were taken for restoring smoothed data with high fidelity to the experimental ones. These data are afterwards used to calculate the char instantaneous reactivity throughout the gasification. Reactivity data were obtained following the next equation:

$$R_{(X)} = \frac{1}{1 - X_{(t)}} \times \frac{dX_{(t)}}{dt} \tag{4.2}$$

The char undergoes structural modifications throughout the gasification reaction due to phenomena such as pore enlargement, coalescence or blocking. This leads to more or less available carbon active sites $C_{t\,(X)}$ for the gasifying agents. The reactivity, which is a function of temperature, gas partial pressure and available reactive surface, is therefore continuously changing during the gasification. It is consequently expressed by means of a chemical kinetic term accounting for temperature and partial pressure effects $R(X)_{(T,P_i)}$, and a reactivity profile $F(X)$ that aims to describe the effects of available reactive surface. The reactivity must therefore refer to a specific conversion level. Reactivities at 10 or 50 % of char conversion are often used for the determination of the kinetic parameters; the latter is actually the most selected one in several similar investigations [99] [116] [139]. In our study the reactivity at 50 % conversion level is taken as reference. Assuming that the structural function does not depend on the temperature and pressure ranges of the gasification experiments, the reactivity can be expressed as follows:

$$R(X)_{(T,P_i)} = R(50)_{(T,P_i)} \times F(X) \tag{4.3}$$

A n^{th} order kinetic model following the Arrhenius law for the reactivity-temperature dependence and a power law for the reactivity-gas partial pressure dependence is considered for the determination of the kinetic parameters of the steam and carbon dioxide gasification reactions. The reactivity at 50 % conversion level is given by:

$$R(50)_{(T,P_i)} = k_{(T)} \times P_i^n \tag{4.4}$$

$$k_{(T)} = A \times exp(-E/RT) \tag{4.5}$$

The reactivity profile expression can be developed from general structural models such as uniform conversion models, shrinking core models, grain models or random pore models that may contain one or more parameters to adjust for the fitting with experimental data [23]. It is however worth noting that not only the structural modifications are responsible for the reactivity change throughout the gasification, but rather other factors intervene such as the char inner mineral species concentration and types [70] [74] [71] [167], the thermal annealing phenomena occurring in parallel with the gasification reaction [85] and also the type of the gasifying media as it has been demonstrated that the char contact with steam change drastically its structure into a more ordered one [42] [41] [158].

Owing to those observations and to the difficulties to determine the singular contribution of each of these parameters on the gasification reactivity, we opted for a determination of an empirical formulation for the structural term F(X) which is assumed to encompass all the influencing parameters that cause the reactivity change along the gasification reaction.

The structural function F(X), which is a normalized reactivity, can be calculated at any conversion level as follows:

$$F(X) = R(X)/R(50) \tag{4.6}$$

In the literature, the ratio (R(X))/(R(ref)) is calculated within a conversion level range where experimental errors are acceptable and still on the author's appreciation. For instance, some authors chose a (0.2-0.8) conversion range with a reference at X=0.2 [134], others chose ranges between (0.2 to 0.8) and (0.15 to 0.9) with a reference reactivity at X=0.5 [99] [166]. In our study, F(X) is determined in the conversion level range of 0.2 to 0.9. This range was selected to minimize weight measurement uncertainties at the small mass loss in the early stages of the reaction ($X = 0 - 0.2$), and to avoid high reactivity values as the mass goes to zero in the final stages of the gasification reaction ($X = 0.9 - 1$). A 5^{th} order polynomial regression is applied to the experimental X and F(X) data to determine the reactivity profile.

4.3 Results and discussion

In this section we will first present results of HHR-char gasification in single atmospheres containing H_2O or CO_2 and determine the intrinsic kinetic parameters and the reactivity profiles for each case. The specificity of the HHR-chars will be also highlighted through a comparison with LHR-chars. Finally we will get into an experiment based comprehensive approach on the understanding of the mechanisms involved in the char gasification in mixed atmospheres of steam and carbon dioxide.

4.3.1 HHR-char gasification in single atmospheres of steam and carbon dioxide

To determine the kinetic parameters and the reactivity profiles for the H_2O and CO_2 char gasification reactions, we performed experiments in which we varied the gas partial pressure at constant temperatures and vice versa. Although all the possible combinations of temperature and gas partial pressure were tested, we present in the next sections only some results of reference experiments.

Char-H_2O gasification experiments

Influence of the temperature and H_2O partial pressure on the char-H_2O gasification reaction

Figures 4.2.a and 4.2.b illustrate respectively the effect of the temperature and steam partial pressure on the H_2O-char gasification rate. The influence of temperature was evaluated in the range of 800 to 950°C. Figure 2.a shows the char conversion versus time in gasification experiments with 20% H_2O in the gasifying medium at 800, 850, 900 and 950°C.Increasing the temperature from 800 to 950°C reduced the time required for 90% conversion in a ratio of more than fivefold.

Temperature of 900°C was taken as reference to evaluate the role of H_2O partial pressure in the char-H_2O gasification reaction. A conversion level of 90 % was reached respectively after 220, 330 and 580 s with H_2O concentrations of 30, 20 and 10 % in the gasifying medium. That is to say, increasing the H_2O concentration from 10 to 30 % results in 2.5 times higher char reactivity.

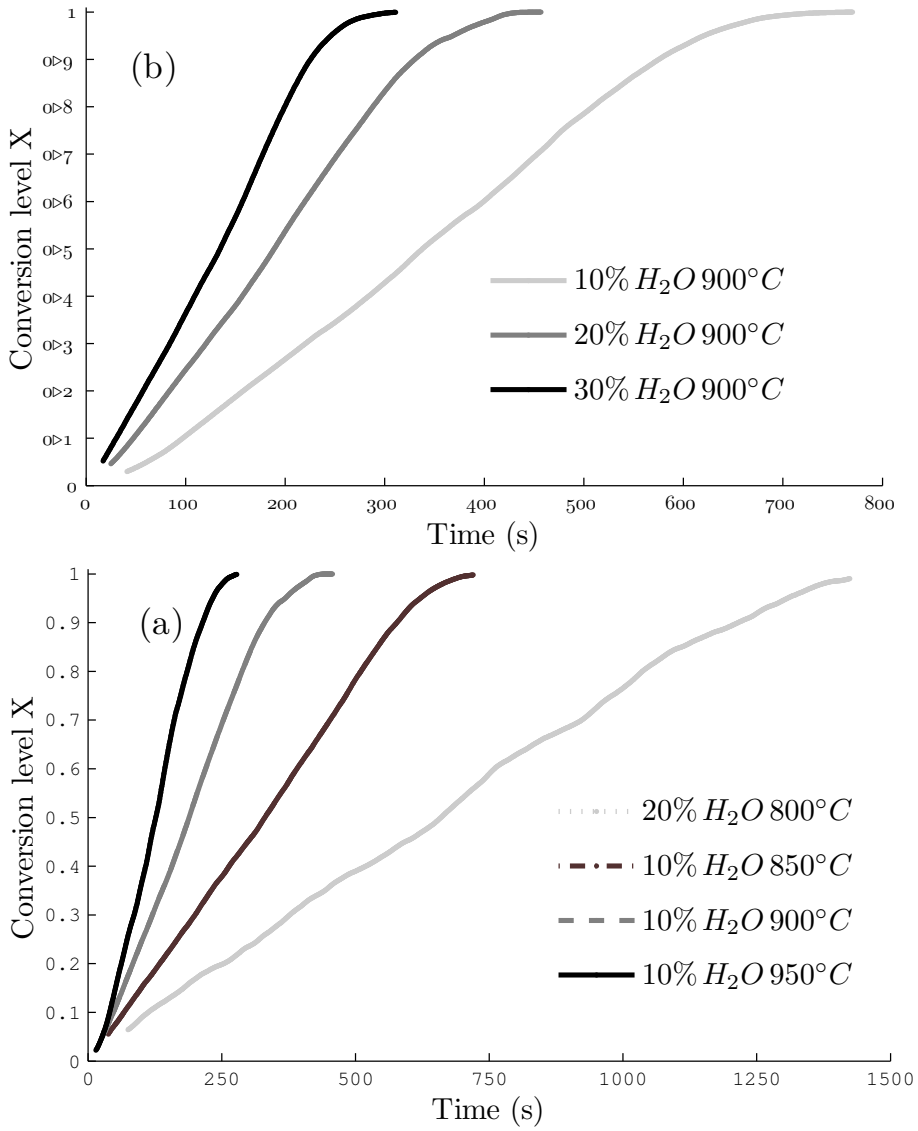

Figure 4.2: Influence of the temperature (a) and steam partial pressure (b) on the char gasification rate

Determination of kinetic parameters for the H_2O-char gasification reaction

Adopting a n^{th} order model and a reference reactivity at 50 % of conversion provides a set of linear equations when taking the logarithm of both sides of equation 4 for the different temperatures and H_2O partial pressures.

$$Ln(R(50)) = ln(A) - \frac{E}{R} \times \frac{1}{T} + n \times ln(P_{H_2O}) \tag{4.7}$$

The set of equations was put in a matrix form to determine A, E and n with a minimization of the error according to the least squares method. The logarithm of R(50) is plotted versus the inverse of the temperature in figure 4.3 to illustrate the temperature dependence of the reactivity following an Arrhenius law for the different steam partial pressures. The linear dependence of the logarithm of R(50) on the inverse of the temperature is verified with a good correlation. Similarly, the dependence of the logarithm of R(50) on the steam partial pressure for the different gasification temperatures

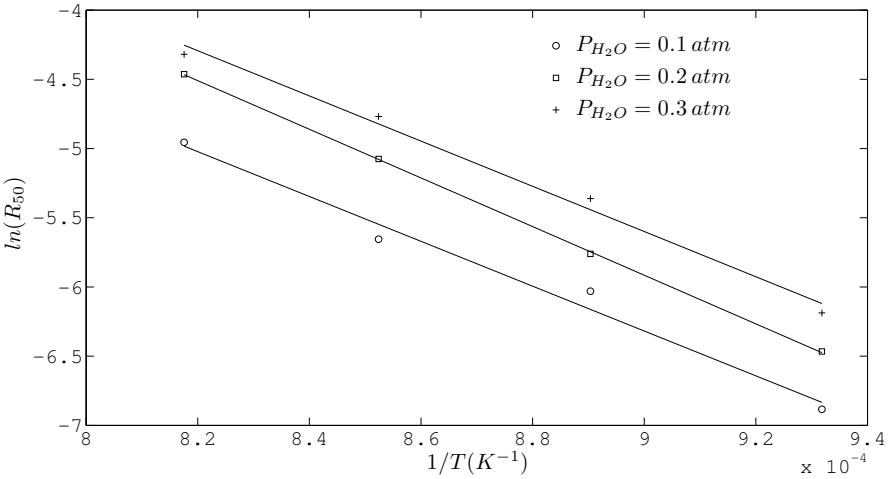

Figure 4.3: Arrhenius plots for H_2O gasification of HHR-chars

was also verified. The correlation coefficient is superior to 0.99 validating thus the proposed model. The derived kinetic parameters are reported in table 3 with a comparison with data found in the literature.

Table 4.3: Comparison of kinetic parameters for H_2O- beech chars gasification reaction

$E(kJ/mol)$	$A(s^{-1}.bar^{-n})$	n	$Reference$
139	2.63 10^4	0.64	This study
211	1.71 10^7	0.51	[134]
167	8.77 10^4	0.6	[72]
149	2.18 10^5	0.7	[56]

The derived kinetic parameters are in accordance with recent studies on steam-beech char gasification. Moreover, the activation energy and the reaction order are in the range of the values reported in Di Blasi's review for biomass char-steam gasification reaction, i.e. 40-240 $kJ.mol^{-1}$ for E and 0.4 to 1 for n [14].

Determination of the reactivity profile F(X)-H_2O

Reactivity profiles for the different H_2O-char gasification experiments are plotted in figure 4.4. Except few irregularities probably due to the measurement uncertainties, all reactivity profiles are monotonically increasing functions and almost superposed.

The temperature and H_2O partial pressure would not therefore affect the reactivity evolution tendency in the studied range of parameters. The average of the functions obtained for the different gasification experiments can be expressed through:

$$F_{(X)}^{H_2O} = -0.00823\,X^5 + 0.02038\,X^4 + 0.11367\,X^3 + 0.23074\,X^2 + 0.56013\,X + 1.12488 \quad (4.8)$$

The weak influence of the temperature and H_2O partial pressure on the shape of the reactivity profile was also observed by [166] whereas in Barrio's study there was a clear influence of the temperature on the reactivity profile especially in the final stages of conversion as the function decreased with increasing the temperature. This can be imputable to mineral species loss or accentuated thermal annealing of the char which exhibited a lower reactivity [134].

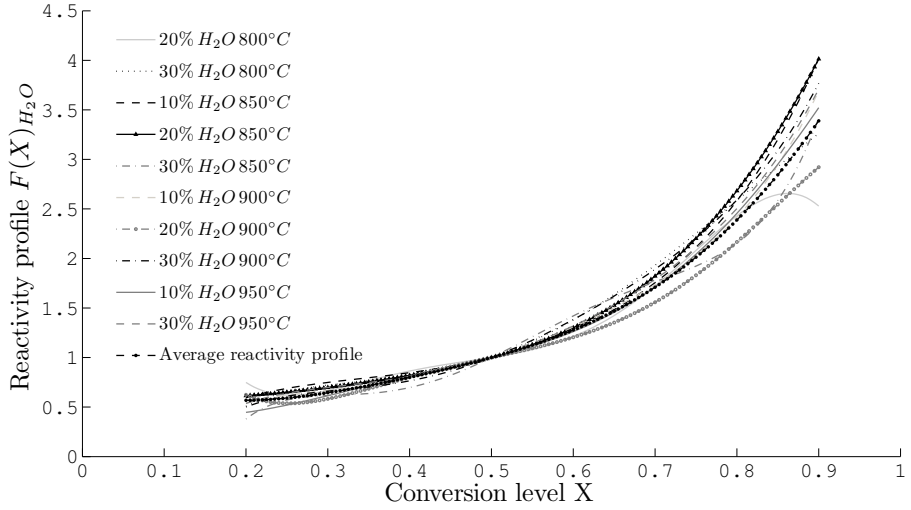

Figure 4.4: Reactivity profile F(X) in the H_2O-char gasification experiments

Char-CO_2 gasification experiments

Influence of the temperature and CO_2 partial pressure on the char- CO_2 gasification reaction

Figures 4.5.a and 4.5.b illustrate respectively the effect of the temperature and CO_2 partial pressure on the CO_2-char gasificationrate. Experiments with CO_2 partial pressure of 0.2 atm were taken as references to evaluate the role of the temperature. As shown in figure 4.5.a, increasing the temperature by 100°C reduced the time required for 90% of conversion by more than 3.5 times.

Char gasification experiments results at a reference temperature of 900°C with CO_2 partial ranging from 0.1 to 0.3 atm illustrate the effect of the CO_2 partial pressure on the gasification rate. Increasing the CO_2 concentration in the gasifying medium from 10% to 30% allows reaching 50% of char conversion in almost half of the time. 90% conversion times are respectively 800, 590 and 460 in gasifying atmospheres containing 10, 20 and 30% of CO_2. Similar trends were found at 850°C and 950°C.

Determination of kinetic parameters for the CO_2-char gasification reaction

The same procedure as for steam gasification was followed to determine the kinetic parameters for the char-CO_2 gasification reaction. Figure 4.6 shows the Arrhenius dependence of the char reactivity on the temperature for the different CO_2 partial pressure. The linear dependence between the logarithm of R(50) and the reciprocal temperature is verified with a good correlation.

Likewise, we obtained a linear dependence of the logarithms of R(50) and CO_2 partial pressure at the different gasification temperature. The results are not plotted here. The model is also verified for CO_2 gasification experiments with a very good determination coefficient $R^2 = 0.996$. The derived kinetic parameters are: E=154 kJ/mol, A=55.18 103 $s^{-1}.bar^{-n}$ and n=0.55, which are in the respective value ranges reported in Di Blasi's review for biomass char-CO_2 gasification reaction [14].

Determination of the reactivity profile F(X)-CO_2

Figure 4.7 shows the reactivity profiles obtained for the CO_2-char gasification experiments at different temperatures and CO_2 partial pressure. The char reactivity increases along the gasification;

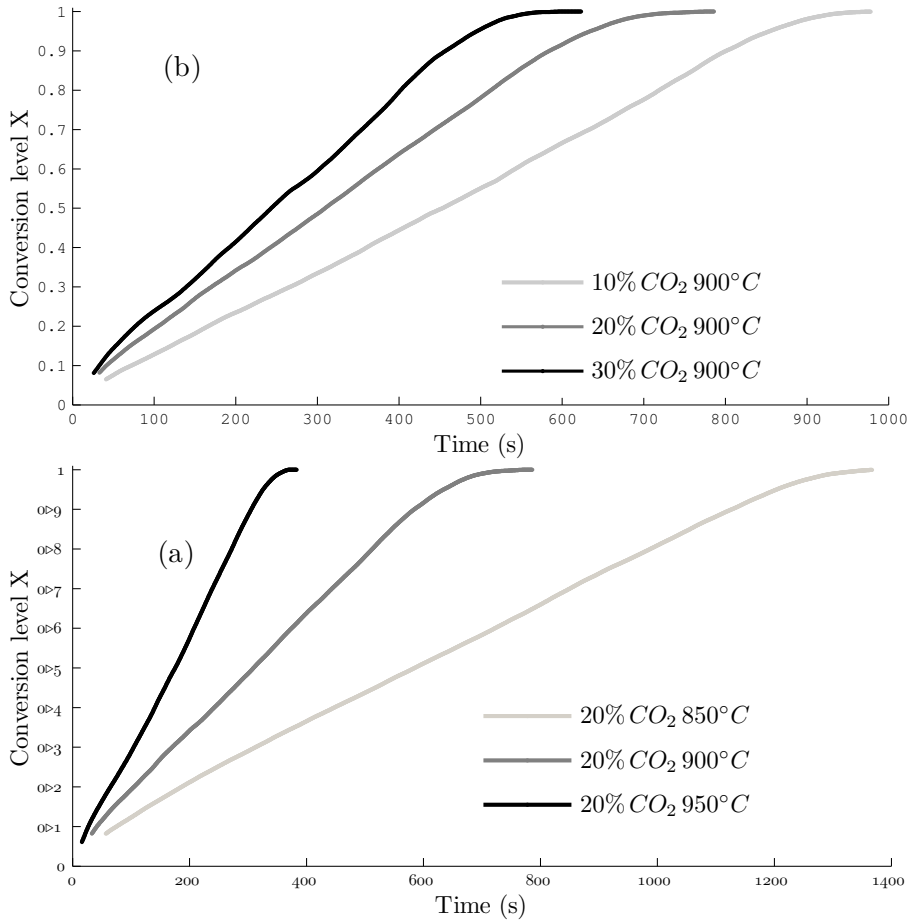

Figure 4.5: Influence of the temperature (a) and CO_2 partial pressure (b) on the char gasification rate

this reactivity tendency is typical of the majority of biomass char in contrast with that of coal chars which decreases as the conversion level increases.

Apart from small discrepancies, all the reactivity profiles are superposed. Neither the temperature nor the CO_2 concentration affects the reactivity profile. The reactivity profile is clearly related to other phenomena such as the structural modifications and the increasing concentration of minerals in the biomass char as suggested in many similar studies. Weak effects of the temperature and CO_2 partial pressure on the reactivity profile were observed in the work of [166] while the temperature clearly affected the reactivity profile for birch char gasification experiments as exposed elsewhere [134]. The average of the obtained functions in the different gasification experiments and has the following expression:

$$F_{(X)}^{CO_2} = 0.01442\,X^5 + 0.08102\,X^4 + 0.1379\,X^3 + 0.2142\,X^2 + 0.5254\,X + 1.1175 \tag{4.9}$$

Specificity of the HHR-chars

In order to highlight the specificity of the HHR-chars, we performed gasification experiments under respectively 20% of steam and 20% of CO_2 at 900°C with the beech char particles prepared with a low heating rate (5°C/min). The results are plotted in figure 4.8 in terms of average reactivity

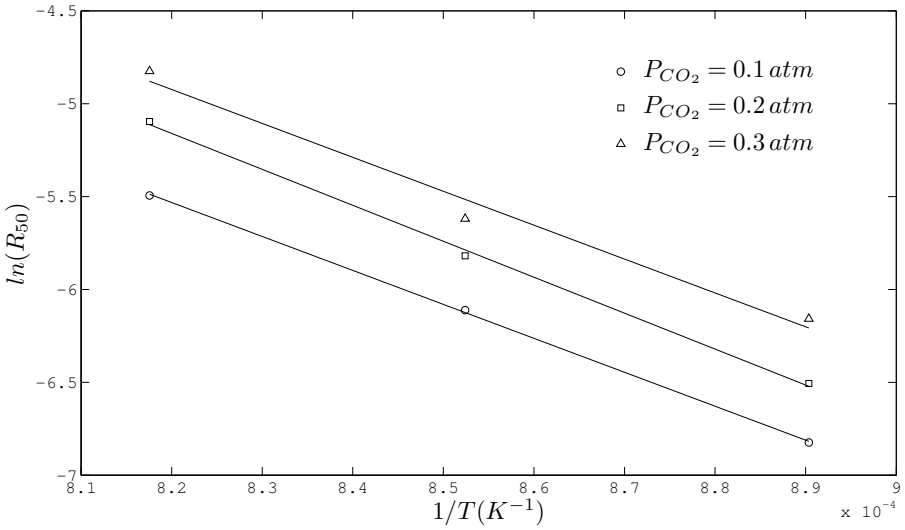

Figure 4.6: Arrhenius plots for CO_2 gasification of HHR-chars

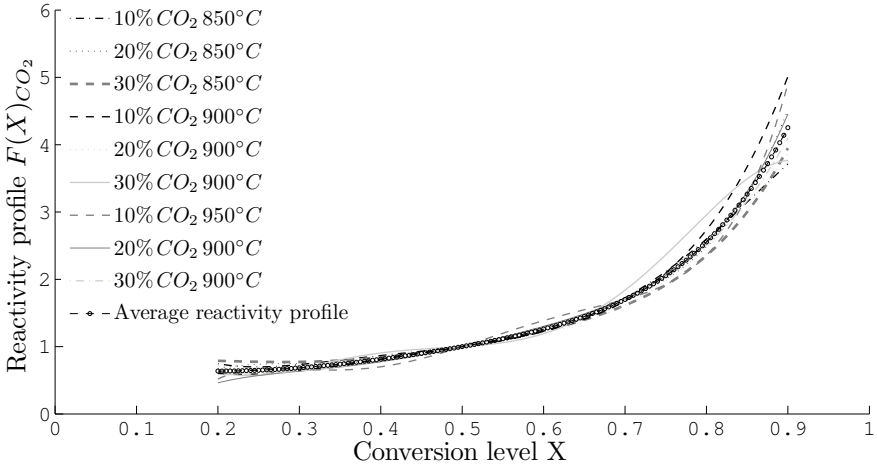

Figure 4.7: Reactivity profile F(X) in the CO_2-char gasification experiments

calculated in the conversion range of 20 to 90%. The effect of the heating rate is clear as the HHR-char reactivity was more than 3.5 times higher in 20% of steam than for the LHR-char in the same operating conditions. Similarly, the LHR-char reactivity in an atmosphere containing 20% CO_2 was estimated at 0.001g/(g.s) while it was 4.3 times higher for the HHR-char in the same operating conditions. These results are in accordance with the literature [74] [90] [81], still the effect of the heating rate on the char reactivity is much more pronounced in the present study than in that of [90] for eucalyptus char gasification and come close to the observations made by[74]. In the work of [90], the increase in the char reactivity with the HR was not so marked as in the present work or that of [74]. Despite that the LHR and HHR chars were respectively obtained after pyrolysis in a fixed bed reactor at 10°C/min and in a fluidized bed reactor, the char yields were not so different, 18.3% for LHR-char and 21.4% for HHR-char at 900°C; one would expect a larger difference owing to the operating conditions. The high char yield in the HHR conditions may be explained by re-polymerisation phenomena corresponding to secondary char formation by tar condensation inside the char particle. This would lead to a less porous structure which makes the gas access to the

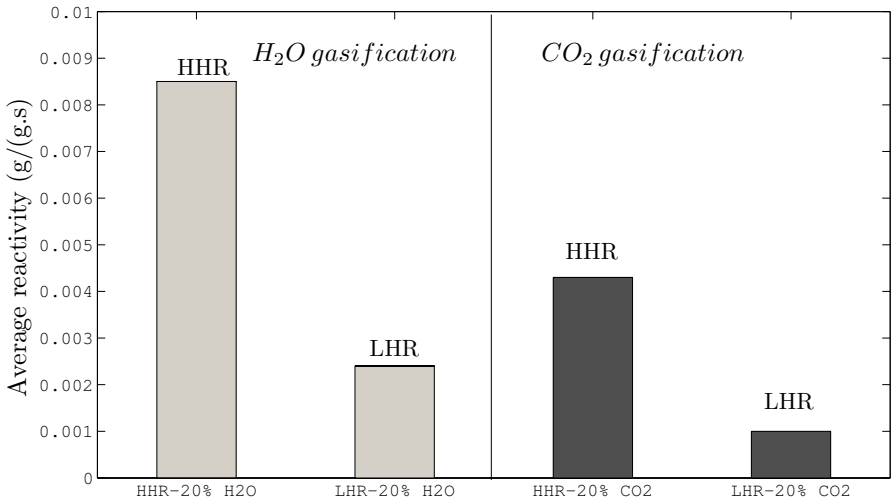

Figure 4.8: HHR and LHR char average reactivity at 900°C

carbon active site more difficult. Even more, this secondary char can encapsulate the mineral species and hinders them to play their catalytic role. Another explanation would be related to a possible mineral species devolatilisation during the rapid pyrolysis which reduces the char reactivity [168]. The char ash content is unfortunately unavailable in the work of [90] to state on the validity of this assumption. In the work of [74], the char yields under low and high heating rates were respectively 24.3% and 14.2% with an increase in the ash amount when increasing the heating rate. The effect of the heating rate on the char reactivity with steam was as important as in the present work as the HHR-char reactivity was 2.6 times higher than that of the LHR char. The authors concluded that besides the more porous structure obtained in HHR-chars, the mineral species would play a crucial role. In the present work, the HHR-chars exhibited high gasification rates which may be imputable to two main factors: the small particle thickness and the high pyrolysis heating rate. The former factor allows minimizing the mass transfer limitations while the second leads to a highly porous char having a mineral content over two times greater than that of LHR char. These combined parameters are known to greatly enhance the char reactivity.

4.3.2 Char gasification in mixture of H_2O + CO_2

In order to study the effect of introducing the CO_2 as a co-reactant next to steam, we performed gasification experiments at 900°C with a steam concentration of 10% and a CO_2 concentration increasing from 0 to 30%. Conversion levels versus time plots are shown in figure 4.9.

The CO_2 introduction clearly enhances the reaction rate. 90% conversion time was about 580 s with 10% H_2O and no CO_2 in the gasifying medium and decreased with increasing the CO_2 concentration in the input gas to 215 s with a CO_2 molar fraction of 30%. The evolution of the char average reactivity, calculated in the conversion range of 20 to 90%, with the increasing CO_2 concentration is illustrated in figure 4.10. The average reaction rate with 20% of CO_2 introduced next to steam was twice that of free-CO_2 gasification experiments with only 10% steam in the gasifying medium. It is clear that the introducing the CO_2 would not inhibit the gasification reaction as proposed elsewhere [139]. This assumption is not valid for the present gasification experiments. To go further on the understanding of the gasification reaction in the CO_2/H_2O mixture, we compared the char reactivity obtained in mixed atmospheres with the sum of the reactivities obtained in single atmosphere experiments for the same steam and carbon dioxide partial pressures.

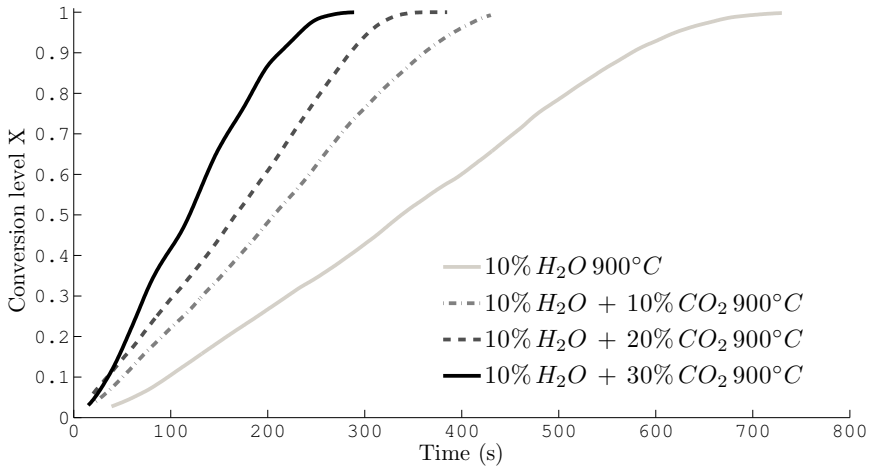

Figure 4.9: Effect of the CO_2 co-feeding next to steam on the gasification reaction rate

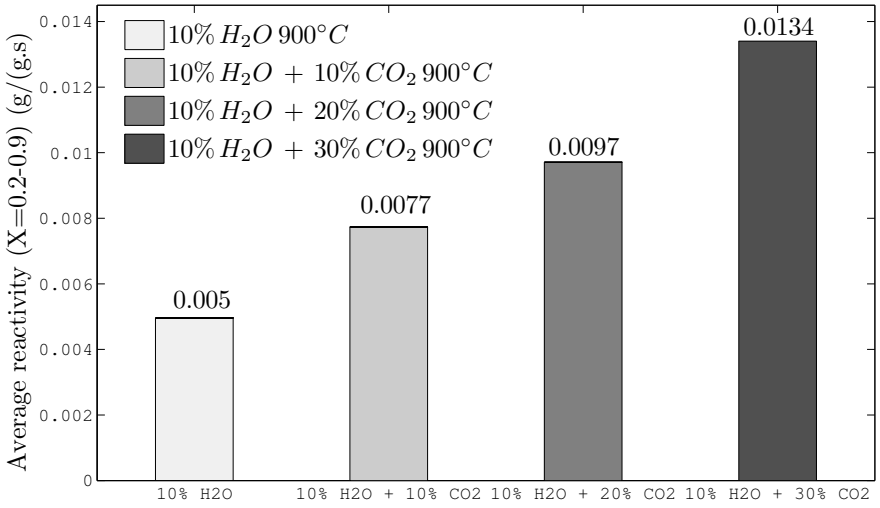

Figure 4.10: Char average reactivity evolution with the increasing amount of CO_2 introduced next to 10% steam

Reactivity curves in the conversion range of 20-90% are plotted in figure 4.11. Apart from small discrepancies probably due to experimental errors, an additive law is valid to describe char gasification under mixed atmospheres.

A first a priori conclusion would be that H_2O and CO_2 are operating on separate active sites (Passive cooperation). Nevertheless, this observation may be due to two opposed actions resulting in an apparent additive law. To further interpret this result, we propose in the next section a detailed reflexion based on a literature review and on additional gasification experiments.

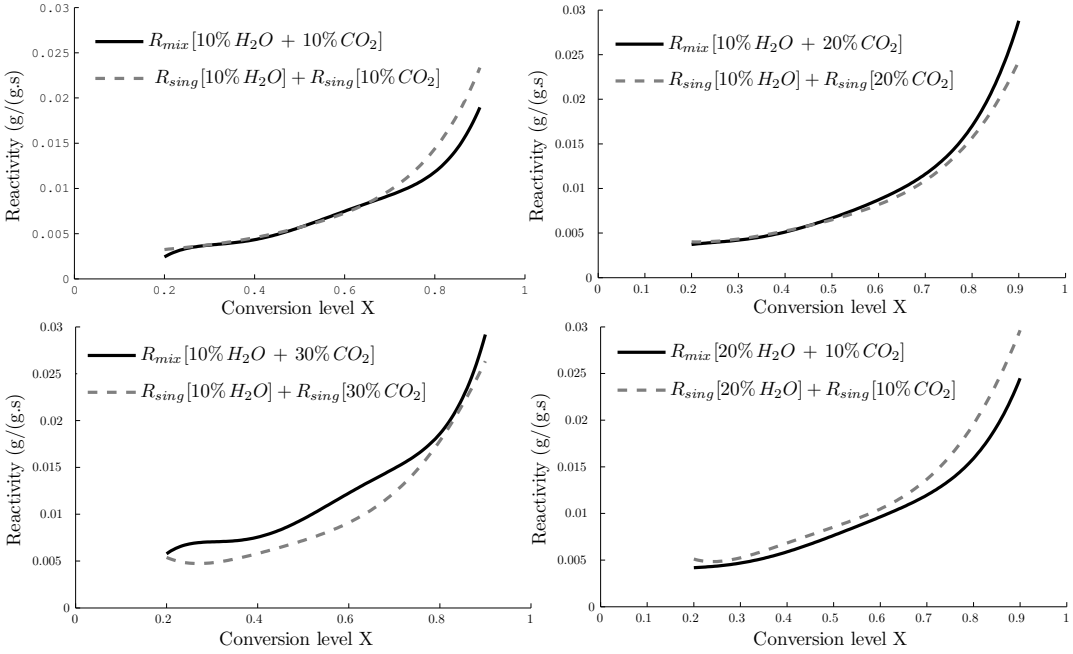

Figure 4.11: Comparison of the HHR-char reactivity in mixed atmosphere with the sum of the single reactivities for different gasifying medium composition at 900°C

4.3.3 On the understanding of the char gasification reaction in mixed atmospheres of CO_2+H_2O

Literature review and discussion

Concerning the mechanisms involved in the char gasification reaction in mixed atmospheres, three main assumptions are held in the literature:

- **CO_2 and H_2O gasification reactions occurring on common active sites (Inhibition)**;

In a previous study on coal char gasification, the authors observed that the char reactivity decreased when adding CO_2 next to steam and concluded that there was a competition between the two gases for the access to the carbon active sites [139]. Despite that the chars are different (coal and biomass chars), which may lead to different results, the authors limit their observations to the first 10% of char conversion which is not representative of the overall gasification reaction. The coal char may exhibit a different behaviour beyond 10% of conversion, mainly when pores become more opened and gasification spreads homogeneously through the particle. In a more recent study, the authors found the char-H_2O gasification reaction was independent on the char-CO_2 reaction, while this latter is inhibited by the former one [164]. Others proposed a model based on a partial sharing of active sites. The two gases are competing in part of the active sites, while reacting separately in their own ones [163]. This assumption is clearly not valid regarding the result of the present study. Other studies on coal char gasification showed that there was no inhibition between the gasifying agents, but rather a passive cooperation on separate active sites [140] [141] [41]. This will be discussed in the next paragraph.

- **CO_2 and H_2O gasification reactions on separate active sites (Passive cooperation)**;

The model of passive cooperation assumes that the two gases react on separate active sites without influencing each other. In their study on coal char gasification, [115] found that the overall carbon

conversion rate in the presence of CO_2 and H_2O is the sum of the single char reactivities. This assumption was also held by (Tay et al. 2011) for coal char gasification. The authors found that the gasification rate in mixed atmospheres of O_2 + H_2O + CO_2 was approximately equal to the sum of the gasification rates in the respective single atmospheres. They suggest that the additivity in char conversion rates means that O_2, H_2O and CO_2 do not compete for the same active sites on the coal char but are rather operating on separate active sites. Similar conclusions can be found elsewhere for the coal char gasification reaction in mixed atmospheres containing CO_2 and H_2O [140] [141]. In both of the studies 2 models based on the assumptions of char-CO_2 and char-H_2O reactions occurring on common and separate active sites were tested. The model assuming reactions on separate active sites well fitted the experimental results whereas the model assuming competition for the same carbon active sites under predicted the experimental results. [135] also performed gasification experiments of birch wood, straw and miscanthus pellets in non-isothermal conditions (HR=10°C/min) up to a temperature of 750°C with a residence time of 2 h and found that the yield of solid product is lower in a mixed atmosphere of CO_2+H_2O than with steam only which means that the CO_2 is also participating in the global gasification reaction. They also observed that the CO_2+H_2O gasification environment lead to a more developed pore structure and surface area which is a mere result of an advanced stage of the biomass gasification reaction. In a more recent study on sewage sludge gasification in a fluidized bed, the authors found that the reaction rate in a mixture of CO_2+H_2O is well represented by the sum of the individual reaction rates obtained with CO_2 and H_2O individually [169].

- **Synergy between CO_2 and H_2O (Active cooperation)**;

This model assumes that besides reaction on separate active sites, there is an active cooperation between the gases for the accessibility to the carbon active sites. At least one of the reactant is supposed to act in a certain way to enhance the char reactivity toward the second gas. Such an action can be for example the creation of additional porosity as proposed by [8] or the retention of catalytic mineral species inside the char as mentioned elsewhere [41]. Recently, in their study on the pine char gasification,[103] proposed a model where the CO_2 and H_2O cooperate together for the accessibility to the carbon active sites. The authors found that the char reactivity in a mixed atmosphere was higher than the sum of the reactivities obtained in single atmospheres of CO_2 and H_2O. They concluded on a cooperative effect of the two reactants with char gasification reactions occurring on separate active sites but did not go further on the understanding of the mechanisms involved in. [8] also think that the CO_2 next to steam may lead to an enhanced reactivity as it could develop further the porosity inside the char particle and provide a greater reactive surface. The authors performed gasification experiments of several biomasses in a TG apparatus with a heating rate of 10°C/min and observed that the total number of pores during CO_2 thermal treatment was an order of magnitude greater than that observed during H_2O/N_2 processing. Even the range in pore sizes was much more extended with CO_2 (2-50 μm) than with steam (10-20 μm). They also observed that the gasification was completed when introducing 30% of CO_2 next to steam, while a black char residue remained when using only steam as a gasification medium. Regarding the results obtained in the present study, the most plausible assumption would be that the two reactants are operating in separate active sites without any kind of synergy. Still, we cannot definitely conclude in that way without taking into consideration the observations of [103] and [8]. For that reason, we performed two other types of char gasification experiments: **(i)** with LHR-chars to come closer to Tagutchu's experimental conditions in terms of HR, **(ii)** char gasification experiments with gas transition wherein the char is firstly operated with CO_2 till a defined conversion level and afterwards gasified with steam to evaluate if the CO_2 influences the char physical properties and consequently impacts its reactivity toward steam.

Reactivity of LHR-chars in mixed atmospheres of H_2O+CO_2

Contrary to our experiments, Tagutchou et al used char particles having a greater thickness (5 mm) and prepared with a relatively low heating rate (60°C/min) in a screw pyrolysis reactor. The differences in operating conditions for the char preparation certainly lead to chars with different reactivities and morphological features (available reactive surface and pore opening). Chars prepared at a high heating rate have already their pores opened and present a high surface area, whereas those prepared at a low heating rate have a less developed reactive surface and a narrower porous network [81][90][74]. We performed additional gasification experiments with LHR-char in mixed atmospheres of steam and carbon dioxide to see if the additivity of single reactivities is valid for LHR-chars. The results are plotted in figure 4.12.

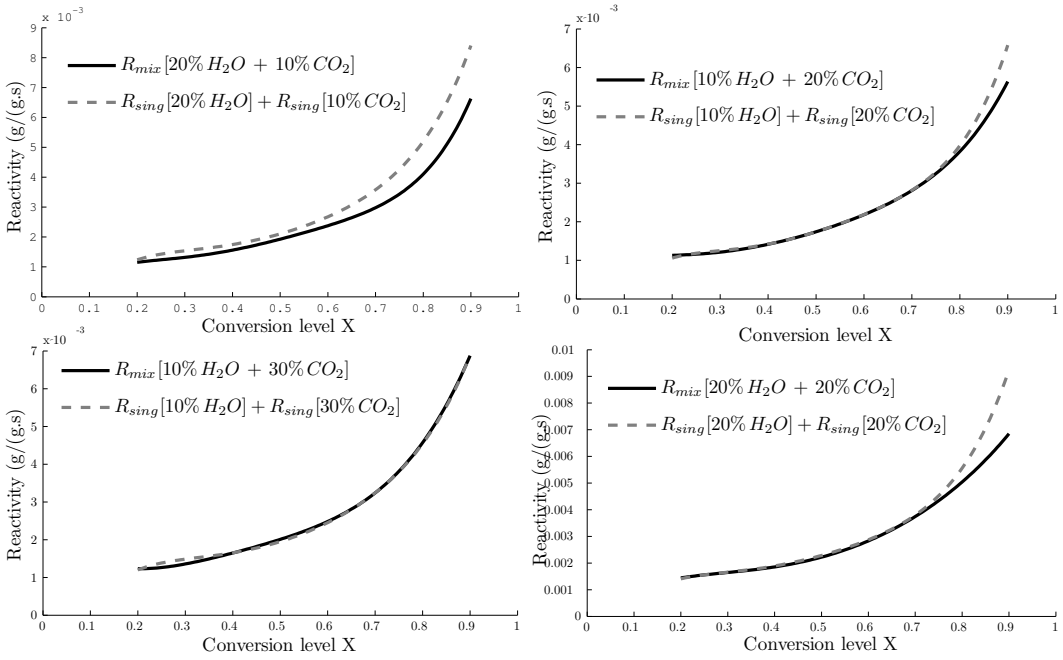

Figure 4.12: Comparison of the LHR-char reactivity in mixed atmosphere with the sum of the single reactivities for different gasifying medium composition at 900°C

The reactivity curves obtained in mixed atmospheres match very well with those of the added single reactivities except a small deviation observed for the gasifying atmosphere composed of 10% CO_2 + 20% H_2O. Additivity of reactivities is again a valid assumption for the LHR-char. The heating rate would therefore only impact the reaction rate but not on the reaction mechanisms in a mixed atmosphere. Other authors found that the contributions of the char-H_2O reaction and char-CO_2 reaction in the global mixed atmosphere reaction rate remained the same independently of the pyrolysis heating rate [164].This is in accordance with our findings. If we assume that there is no influence of the type of biomass (pine and beech wood), we believe that in Tagutchu's work, it would rather be the char particle thickness that influences the global reaction rate and the mixed atmosphere gasification mechanisms. Because of internal diffusion limitations for the CO_2 molecules, due to a greater particle thickness (5 mm) in comparison with the present case, the enhancement of the gasification reaction observed by [103] in mixed atmosphere conditions may be due to the fact that the steam gasification reaction developed further the char internal porosity and ameliorated the access of the CO_2 molecules to the heart of the char particle which resulted in an apparent reactivity that was greater than the sum of the respective single reactivities. The additive law would be therefore

valid as long as the char particle is thin enough to prevent internal diffusion limitations toward the CO_2 molecules. This possible explanation must be further investigated by comparing the effect of the particle thickness respectively on the H_2O and CO_2 gasification reaction rates. Another worth noting fact is that the average reactivity profiles for H_2O, CO_2 and mixed atmospheres gasification experiments for HHR and LHR chars are practically the same except some deviations for higher conversion levels that can be attributed to measurement uncertainties as depicted in figure 4.13.

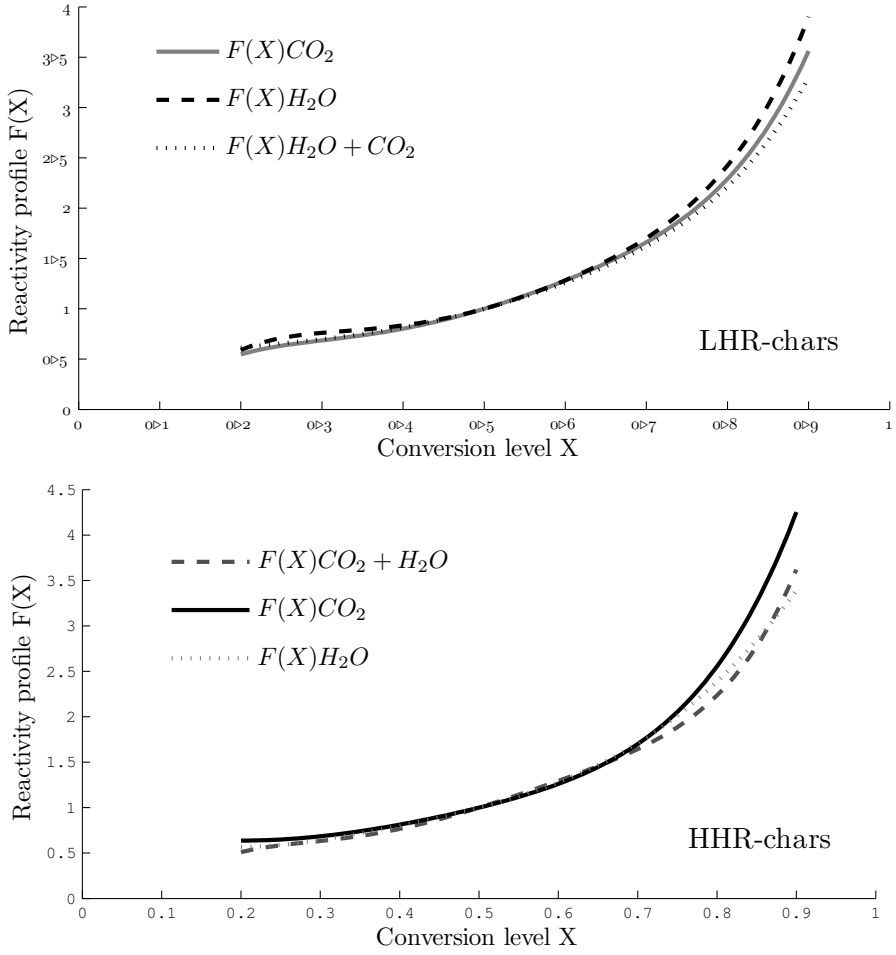

Figure 4.13: Comparison of the average reactivity profiles for steam and carbon dioxide gasification experiments

This tendency was not observed for example by [103] and [166] who found different reactivity profiles for CO_2 and H_2O gasification experiments. The authors observed that the H_2O reactivity profile showed a continuous increase throughout the conversion while the CO_2 reactivity profile did not go beyond the value of 1 until a conversion level of 80% from which it began to increase. In other words the char reactivity did not increased in the range of 50 to 80% of conversion. This may be due to the limited access of the CO_2 molecules to the heart of the char particle despite the advanced gasification stage. In the present study, the similarity of the reactivity profiles may be imputed to the absence of internal diffusion limitations due to the particle small particle size. Once again, this assumption has to be further investigated.

Gas alternation gasification experiments

The aim of such an experiment is to verify whether or not there is a kind of synergy as claimed by [103] and [8] that leads in the present case to an apparent additive law. The CO_2 is firstly introduced as a gasifying reagent to establish whether or not it creates additional porosity and develops further the reactive surface for H_2O. The unfolding of this type of experiment comprises three stages:

- char gasification with CO_2 up to a certain conversion level;
- stopping the CO_2 flow, stabilisation of the mass and purge of the reactor under N_2;
- introduction of steam and pursuance of the gasification reaction up to total conversion.

The first experiment was performed on a HHR-char that was gasified with 20% CO_2 up to a conversion level of 28% and afterward operated with 10% of steam. The second one, on a LHR-char, was performed with 20% of CO_2 up to a conversion level of 35% followed by steam gasification with a steam concentration of 20% in the gas flow. Figures 14.a and 14.b illustrate the unfolding of these experiments. On these figures are plotted reference char reactivities obtained in single atmospheres of steam and carbon dioxide (grey and black solid lines) and the char reactivity in the gas-alternation experiment (black dashed line).

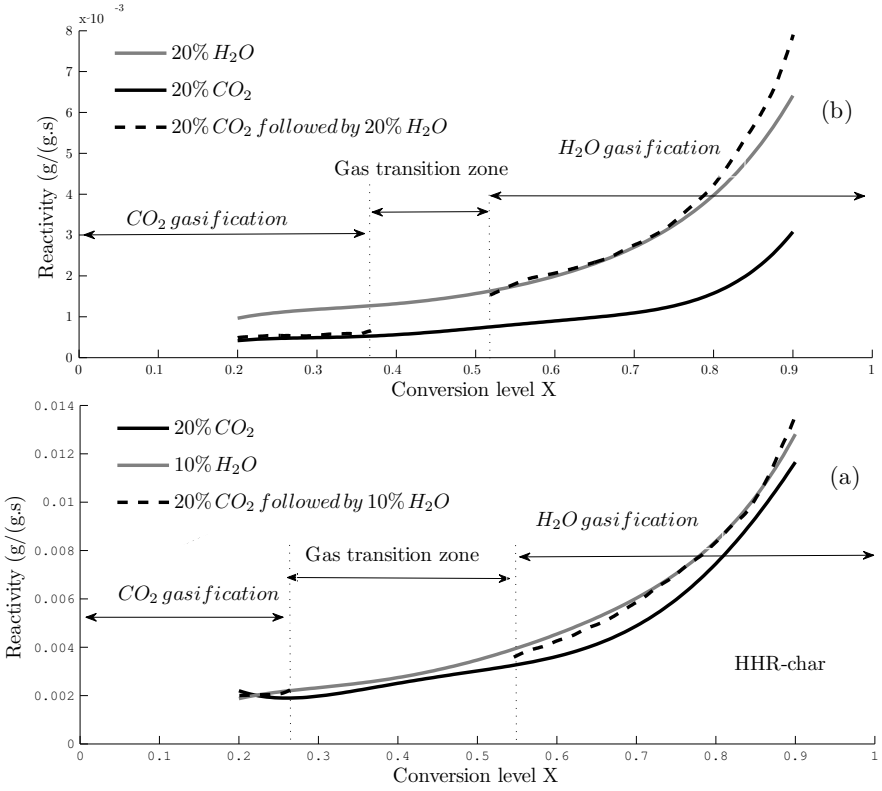

Figure 4.14: HHR-char (a) and LHR-char (b) gasification experiments with alternation of CO_2 and H_2O at 900°C

For the HHR and LHR-chars, in the first stage of the gas-alternation experiment, the char reactivity curve naturally follows the reference one obtained under a CO_2 containing atmosphere. No results are reported during the gas transition zone. We can then clearly see on the two figures that the char reactivity curve in the H_2O gasification stage re-joins the reference curve obtained in the

reference steam containing atmosphere. If the CO_2 had changed the char properties, we would have seen an enhancement or a decrease of the char reactivity towards H_2O; it is not the case here. Leaning on these observations, the most likely explanation for the observed additive law would be that the CO_2 and H_2O are operating on separate active sites without any kind of synergy.

This conclusion is to be taken with precaution, as there can be other phenomena when the two gases are reacting simultaneously, nonetheless it constitutes a step forward into the understanding of the mechanisms involved in the char gasification in mixed atmospheres. Finally, the observation of [8] concerning the incomplete char burnout with only steam as reactant may be a consequence of an ordering of the carbon structure due to the thermal annealing which is promoted by the contact with steam as proposed elsewhere for coal and biomass char gasification [42] [41]. Introducing 30% of CO_2 would have overcome the structural ordering of the carbon matrix as the rate of the gasification reaction became higher than that of the carbon ordering and resulted in complete char burnout. Owing to the obtained results and literature review and discussion, for our study, the char reactivity in a mixed atmosphere of CO_2 + H_2O can be written as the sum of the single reactivities:

$$R_{(H_2O+CO_2)} = R_{(H_2O)} + R_{(CO_2)} \tag{4.10}$$

4.4 Conclusion

The new macro-TG experimental device allowed us to perform gasification experiments on beech chars prepared at high heating rates. These experimental conditions are of interest as they come close to those encountered in fluidized beds. The fast pyrolysis was followed directly by gasification experiments without additional heating of the char particle to the gasification temperature as usually done in conventional TG devices. Reliable kinetic data are obtained for HHR-char gasification reactions with H_2O and CO_2 and can be used for the design and optimisation of fluidized bed gasifiers. The heating rate greatly affects the char reactivity toward H_2O as well as toward CO_2. The HHR-char reactivity was 3.5 times higher in H_2O gasification and greater than four folds with CO_2 in comparison with LHR-chars. Introducing CO_2 next to steam resulted in a higher reactivity of the beech char whatever the pyrolysis conditions (low or high heating rate). For a HHR-char increasing the CO_2 concentration from 0 to 30% in a 10% steam containing atmosphere resulted in a 2.7 times higher char reactivity. A comprehensive approach was established in order to clarify further the mechanisms involved in mixed atmosphere gasification reactions. The present work demonstrates the validity of an additive law reflecting a passive cooperation of steam and carbon dioxide in the gasification reaction. Specific experiments carried in this work showed that converting a char under CO_2 to approximately X=30% does not affect its reactivity during further conversion under H_2O. The additive law would be valid as long as the particle is thin enough to prevent diffusional limitations phenomena toward the CO_2 molecules. We believe that the steam gasification reaction would facilitate the access of CO_2 molecules to the heart of the char particle in the case of thick particles, which results in an apparent enhanced reactivity.

Acknowledgements

The authors acknowledge the national research agency ANR-France for its financial support in the project RECO2. They also wish to express their appreciations to Mr. Brenard Auduc for his technical support.

Chapter 5

High-temperature pyro-gasification of woody biomass in pure CO_2: experiments and modelling

Abstract

An increasing number of studies focus on the CO_2 as a gasifying media for thermochemical conversion of biomass and coals. The present paper focuses on the pyro-gasification of thin wood particles in pure CO_2 at 850°C under high heating rate conditions (similar to fluidized bed gasifiers). The aim is to assess the potential use of CO_2 as gasifying medium and to learn more about its effects on the pyrolysis as well as on the char gasification stages. Experimental and numerical modelling results provide answers on the unfolding of the whole CO_2 biomass pyro-gasification process. It was found that despite the CO_2 is present inside the particle during the pyrolysis stage, it has no noticeable impacts on the reaction rate nor on the char yield due to the relatively low temperature inside the particle. The CO_2 char gasification is the rate limiting step of the global pyro-gasification reaction as its duration is near to 95% of the entire biomass conversion time.

Keywords: Biomass, Pyrolysis, Gasification, CO_2, High heating rate, numerical modelling.

Résumé

Un nombre croissant d'études traitent de l'utilisation potentielle du CO_2 comme média gazéifiant pour la conversion thermochimique de biomasses ou de charbons. La présente étude se focalise sur la pyro-gazéification de fines plaquettes de bois dans du CO_2 pur à 850°C sous des conditions de chauffe rapide similaires à celles rencontrées dans des lits fluidisés. Le but étant d'évaluer l'usage potentiel de CO2 en tant que média gazéifiant et d'apprendre sur les impacts qu'il peut avoir sur les phases de pyrolyse et de gazéification du char. Au moyen de résultats expérimentaux et numériques, nous apportons des éléments de réponse sur le déroulement de la pyro-gazéification de la biomasse sous CO_2. Le présent travail montre que malgré la présence de CO_2 dans la porosité durant la phase de pyrolyse, ce dernier n'a pas d'impacts notables sur la vitesse de perte en masse ou sur le rendement en char à cause d'une faible température au sein de la particule. La gazéification du char au CO_2 est l'étape limitante de la réaction de pyro-gazéification. La durée de cette dernière correspond environ à 95% de la durée totale de la réaction.

Mots clés: Biomasse, Pyrolyse, Gazéification, CO_2, Chauffe rapide, Modèle numérique

5.1 Introduction

Biomass to biofuels is considered to be one of the promising routes to cope with the fossil fuel depletion and to mitigate the green house gas emissions (mainly CO_2) causing numerous environmental problems such as the global warming [6] [170]. The CO_2 emissions are on the centre stage of the debate due to their continuously increasing amount in the atmosphere. Many research focus on possible ways to reduce them. Alternate fuels and value-added products can be obtained from the conversion of carbon dioxide from simple molecules to higher hydrocarbon fuels and polymers following several techniques such as photo-reduction, electrolysis, plasma, electro-catalysis, dry-reforming etc [171]

Thermochemical conversion of biomass involves processes such as combustion, pyrolysis, liquefaction and gasification among others. The biomass pyro-gasification encompasses two distinct stages: biomass pyrolysis and char gasification. Biomass pyrolysis corresponds to the thermal decomposition of the fresh biomass into gas, tars and char. The pyrolysis product distribution depends on the biomass characteristics (biomass type, chemical composition, particle size...) and process conditions (temperature, heating rate...) [7]. Char is a solid product of the biomass pyrolysis. It contains in major part carbon atoms with some hydrogen, oxygen, nitrogen and some minerals. The formed char reacts with the surrounding gasifying medium, O_2, H_2O, CO_2 or mixtures, yielding additional gases, namely CO_2, H_2 and CO, which amounts depend on the gasifying medium composition [8] [172] [14].

Biomass pyro-gasification is conventionally operated with steam or air as gasifying medium but can also be performed using CO_2. Increasing number of studies dealing with coal and biomass thermochemical conversion are paying attention to CO_2 molecule as a gasifying agent [132] [8] [172]. For instance, it was demonstrated that introducing CO_2 with steam as a gasifying medium leads to an enhanced CO production [8] [172] [124]. Indeed, in the gas phases CO_2 can potentially react in the gas phase with hydrocarbons, such as methane, via a dry reforming reaction:

$$CO_2 + CH_4 \longrightarrow 2H_2 + 2CO \quad \Delta H = +246.9\,kJ/mol \tag{5.1}$$

CO_2 can also react with hydrogen molecules according to the reverse water gas shift reaction (rWGS):

$$CO_2 + H_2 \longrightarrow H_2O + CO \quad \Delta H = +41.2\,\mathrm{kJ/mol} \tag{5.2}$$

Finally, in a biomass gasifier, CO_2 can react with the carbon of the char formed by the pyrolysis step, via the heterogeneous Boudouard reaction:

$$C + CO_2 \longrightarrow 2CO \quad \Delta H = -179.5\,\mathrm{kJ/mol} \tag{5.3}$$

Several authors also focused on the char gasification reaction under mixed atmospheres of H_2O and CO_2. Conclusions differ from a study to another on whether CO_2 inhibits the H_2O-char gasification reaction, accelerates it or that the two reactants operate separately on the char surface [123] [139] [169]. In a previous study, we found experimentally that the CO_2 does not inhibit the H_2O-char gasification reaction, but rather that the two gases cooperate and that the gasification rate in mixed atmospheres is the sum of the individual reactivities [154].

Renganathan et al. [117] performed a thermodynamic analysis of carbonaceous feedstocks gasification using CO_2 or mixtures of carbon dioxide with steam or oxygen and identified a universal optimal operating temperature of 850 °C for minimum energy input.

Other researchers [125] found that the use of CO_2 in biomass gasification in a fluidized bed gasifier increased substantially the carbon and energy conversion efficiency and decreased the amount of tars in the produced gas. The highest cold gas efficiency was achieved when gasifying biomass with CO2.

The introduction of CO_2 as a reacting gas in biomass gasifier was also studied in [124] in the case of rice straw gasification. The authors studied the effect of the different gasification atmosphere compositions in H_2O, CO_2, O_2 and N_2 on the thermal efficiency of the gasification process, and came to the conclusion that the introduction of CO_2 has a positive effect on the thermal efficiency of a gasifier at temperature of 850°C and above.

Other studies rather focused on the char gasification reaction with the aim of determining the kinetic parameters of the CO_2-char gasification reaction, or comparing the char gasification rates obtained with CO_2 and steam [94] [99] [57]. The effects of CO_2 on the pyrolysis process was also studied but less extensively than for the char gasification. CO_2 was found to influence the gas yield and composition as well as the char yield, properties [129] [119] [130]. In our previous work, we found that the major effects of CO_2 on the biomass pyrolysis are the increase of gas yield and modification of the char textural properties. However, the char reactivity to O_2, H_2O and CO_2 were practically the same as for char prepared under N_2 atmosphere [173].

Most of the modelling studies in the literature on biomass thermochemical conversion deal either with the sole pyrolysis step, or with the char gasification step only [146] [174] [175] [108] [99] [176] [57]. To the authors best knowledge, no previous studies deals with the entire pyro-gasification process of biomass in pure CO_2. In the present work, we focus on the whole woody biomass pyro-gasification process in the presence of pure CO_2 at a temperature of 850°C. The objective of this paper is to learn more about the effect of CO_2 on the heterogeneous reactions of char formation and gasification respectively during the pyrolysis and gasification steps experimentally and theoretically. We focus particularly on high heating rates conditions typically encountered in fluidized bed gasifiers. In section 5.2, we will present the experimental device and procedure. Section 5.3 and 5.4 will be dedicated to the numerical model and its implementation in COMSOL software. Experimental and modelling results will be presented in section 5.5.

5.2 Experimental study

5.2.1 Parent wood sample

Biomass samples are beech wood-chips provided by SPPS Company (France). Raw samples were initially sieved. Biomass particle having a parallelepipedic shape with a characteristic length L of 6 mm and a thickness Th of 1 mm were selected. Proximate and ultimate analysis of the biomass samples are presented in table 5.1. The results are given on a dry basis. The moisture content of the wood-chips was estimated to 10% ± 1 %.

Table 5.1: Proximate and ultimate analysis of the beech wood-chips (% dry basis)

Proximate analysis			**Ultimate analysis**			
VM	Ash	FC	C	H	O	N
88.1	0.4	11.5	46.1	5.5	47.9	0.1

5.2.2 The macro-thermogravimetry experimental device and procedure

The macro-thermogravimetry M-TG device is described in detail in our previous work on char gasification in mixed atmospheres of CO_2 and H_2O [154]. In general terms, the experimental apparatus consists of a 2-m long, 75 mm internal diameter alumina reactor electrically heated and a weighing system of ± 0.1 mg accuracy. A metallic stand is placed over the scale on which a 1 m-length

and 2.4 mm external diameter hollow ceramic tube is fixed. The ceramic tube holds up a platinum basket in which the biomass particles are placed. The gas flow rates are controlled by means of mass flow-meters/controllers. The gas flow inside the reactor is laminar and flowing at an average velocity of 0.20 m/s at 850°C. About 0.5 g of biomass particles is introduced in the platinum basket. The particles are spaced enough to avoid thermal and chemical interactions. The platinum basket bearing the biomass particles is introduced in the hot reactor zone within 13 s. This procedure allows fast heating of the biomass particles and reproduces the conditions encountered in a fluidized bed gasifier. The pyrolysis experiments were performed at $850°C$, a typical temperature of a fluidized bed gasifier.

External heat transfer The M-TG reactor was characterized in terms of global heat transfer coefficient. The heat transfer coefficient was determined following a lumped heat capacitance method using a drilled steel sphere having a diameter of 5 mm and a Biot number inferior to 0.1. The heat transfer coefficient at $850°C$ was found to be around 140 $W/m^2.K$ [173] which is in the range of values for external heat transfer coefficients reported in the literature for fluidized bed gasifiers [146].

Reactor temperature profile When introduced into the reactor, the biomass particles are not submitted directly to the hot zone temperature. The surrounding temperature increases along the z axis from the ambient to the final temperature. We measured the temperature along the reactor. The results are shown in figure 5.1.

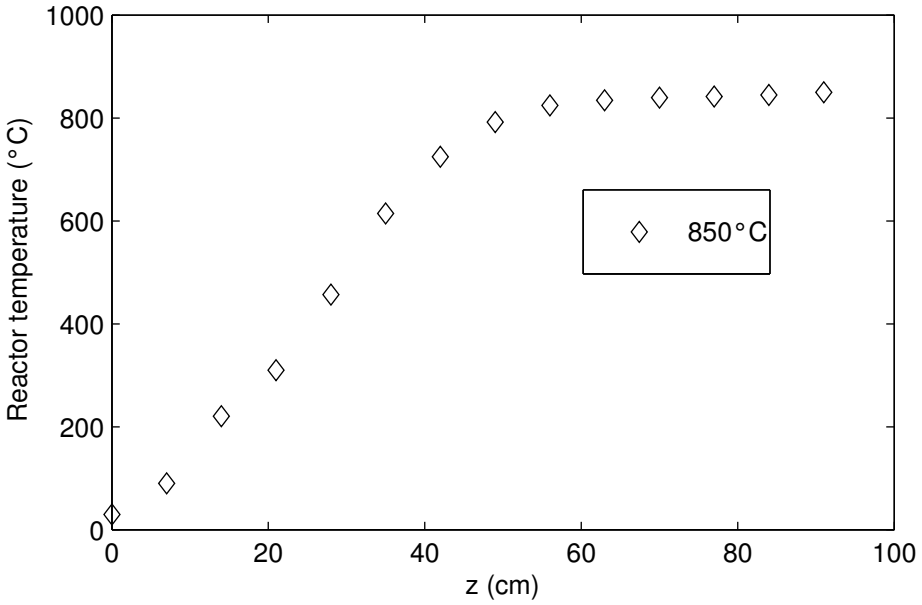

Figure 5.1: Temperature profile in the M-TG reactor

As the introduction speed is known (v=7 cm/s), the temporal variation of the temperature surrounding the biomass particles reads:

$$\frac{dT_\infty}{dt} = \frac{dT_\infty}{dz}\frac{dz}{dt} = v\frac{dT_\infty}{dz} \tag{5.4}$$

$\frac{dT_\infty}{dz}$ is known from the temperature profile. The surrounding temperature is afterwards expressed as a polynomial function of the time $T_\infty(t)$ and is implemented in the model as an external condition related to reactor temperature.

Blank tests are performed prior to the pyrolysis experiment to account for the flowing gas dynamic pressure (force exerted on the basket) in addition to the drag forces along the ceramic tubes. Blank data are afterwards subtracted from the pyrolysis experiment ones. The blank tests as well as the experiments show a very good repeatability [173].

5.3 Numerical modelling of the CO_2 pyro-gasification

During the biomass CO_2 pyro-gasification process, several phenomena are involved, including convective and radiative heat transfer between the biomass particle, the surrounding gas and the reactor walls, conductive and internal radiative heat transfer respectively through the particle solid phase and in the pores, chemical reactions, chemical species transport, shrinking etc... To model the physics underlying the process, we established mass and energy balance equations and considered several assumptions to render the model tractable:

- A 2D geometry is used due to similarity between the tangential and radial properties in the wood/char
- Local thermodynamic equilibrium between the solid and the gas phase
- No particle shrinking is taken into account
- Char is assimilated to pure carbon
- Darcy's law is used to determine the gas velocity in the solid matrix
- In Darcy's law, we use an isotropic permeability, since the large difference of permeabilities between the radial and the fibre direction induces numerical convergence problems.
- All gaseous species are assumed to follow a Fick diffusion law, with the same isotropic diffusion coefficient.
- Chemical reactions follow Arrhenius law and are first order reactions with respect to the reactants.

5.3.1 Kinetic scheme

The CO_2 pyro-gasification reactions scheme is shown in figure 5.2. It gathers the pyrolysis and the char gasification steps. The pyrolysis stage includes three parallel reactions where the initial wood decomposes into gas (R1), tars (R2) and char (R3), with defined mass stoichiometric coefficients. Tars are afterwards cracked into gas following the secondary reaction (R4). The mass stoichiometric coefficients are noted ω_C, ω_G and ω_T for char, gas and tars respectively.

$$\omega_C + \omega_G + \omega_T = 1 \tag{5.5}$$

The char yield was fixed at 0.12 (according to our experimental data). The tar yield was fixed to 0.05 and the gas yield is given by the difference to the unity. The char gasification corresponds to the reaction (R5) where the surrounding CO_2 reacts with the char following the Boudouard reaction to form CO.

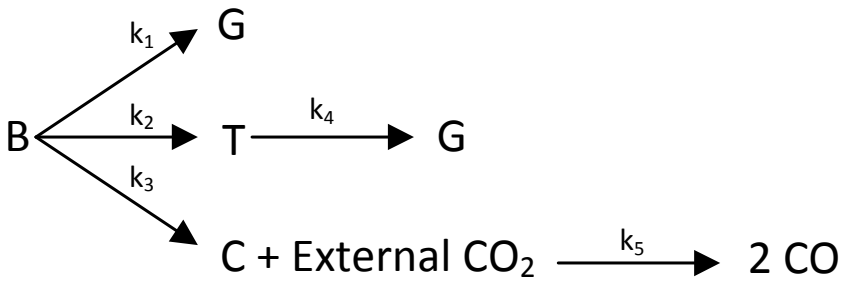

Figure 5.2: CO_2 pyro-gasification reaction scheme

5.3.2 Mass conservation equations

Solid species

Biomass and char are solid species. The conservation equations for these latter do not include transport terms.

Biomass decomposition is described by the following equation:

$$\frac{\partial \rho_B}{\partial t} = -(\omega_G k_1 + \omega_T k_2 + \omega_C k_3)\rho_B \tag{5.6}$$

Char formation and gasification is given by:

$$\frac{\partial \rho_C}{\partial t} = \omega_C k_3 \rho_B - k_5 \rho_C P_{CO_2} \tag{5.7}$$

The first term on the right hand side accounts for char formation while second accounts for the char gasification reaction.

Gaseous species

Four gaseous species are considered:

- CO_2, which is the surrounding gas in the reactor. The particles void is considered to be initially filled with CO_2.
- Gas, representing the pyrolysis gas emitted by the wood decomposition reaction. An average molecular weight of 22 g/mol was calculated for the pyrolysis gas based on the work of Couhert et al [177].
- Tars, the heavy condensible gases assumed to have a molecular weight of 78 g/mol.
- CO, which is the product of the CO_2-char gasification reaction (R5).

The CO_2 conservation equation reads:

$$\frac{\partial \epsilon \rho_{CO_2}}{\partial t} + \nabla.(\rho_{CO_2}\mathbf{v} - D_{eff}\,\nabla \rho_{CO_2}) = -k_5 \rho_C P_{CO_2} \tag{5.8}$$

The pyrolysis gas conservation equation reads:

$$\frac{\partial \epsilon \rho_G}{\partial t} + \nabla.(\rho_G \mathbf{v} - D_{eff} \nabla \rho_G) = \omega_G k_1 \rho_B + \omega_T \epsilon k_4 \rho_T \tag{5.9}$$

The tars conservation equation reads:

$$\frac{\partial \epsilon \rho_T}{\partial t} + \nabla.(\rho_T \mathbf{v} - D_{eff} \nabla \rho_T) = \omega_T (k_2 \rho_B - \epsilon k_4 \rho_T) \tag{5.10}$$

The CO conservation equation reads:

$$\frac{\partial \epsilon \rho_{CO}}{\partial t} + \nabla.(\rho_{CO} \mathbf{v} - D_{eff} \nabla \rho_{CO}) = +k_5 \rho_C P_{CO_2}^n \tag{5.11}$$

5.3.3 Momentum conservation

The gas phase momentum equation in the porous media is expressed through A Darcy's Law. The superficial velocity is expressed as:

$$\mathbf{v} = -\frac{K}{\mu} \nabla P, \tag{5.12}$$

where K and μ are respectively the average permeability and the gas viscosity. As the permeability in the grain direction is far greater than in the radial direction we considered an average permeability for the two directions to ensure the numerical convergence. The total pressure is expressed by using the ideal gas law. Summing the pressure contribution of all the gas species:

$$P = \left(\frac{\rho_G}{M_G} + \frac{\rho_{CO_2}}{M_{CO_2}} + \frac{\rho_T}{M_T} + \frac{\rho_{CO}}{M_{CO}} \right) RT \tag{5.13}$$

5.3.4 Energy conservation equation

The energy conservation equations is formulated with the assumptions of constant particle volume and a local thermal equilibrium between solids and gases:

$$\frac{\partial \mathcal{H}}{\partial t} + \nabla.\sum_i h_i \mathbf{N}_i = -\nabla.\,\mathbf{q} \tag{5.14}$$

The first term on the left hand-side of the equation represents the time derivative of the total enthalpy per unit volume with:

$$\mathcal{H} = \sum_{i=B,C,G,T,CO_2,CO} \rho_i h_i$$

The total enthalpy time derivative can be expressed in a more extended form as:

$$(\rho_B C_{pB} + \rho_C C_{pC} + \epsilon \rho_G C_{pG} + \epsilon \rho_T C_{pT} + \epsilon \rho_{CO_2} C_{pCO_2}) \frac{\partial T}{\partial t} + \nabla.\sum_i h_i \mathbf{N}_i = -\nabla.\,\mathbf{q} + \dot{Q} \tag{5.15}$$

The second term on the left hand-side of the equation represents the convective and diffusive transport of energy, with:

$$\sum_{i=G,T,CO_2,CO} h_i \mathbf{N}_i = \mathbf{v} \left(\sum_{i=G,T,CO_2,CO} \rho_i h_i \right) - D_{eff} \left(\sum_{i=G,T,CO_2,CO} h_i \nabla \rho_i \right)$$

$\mathbf{q}$ is the conductive heat flux inside the porous media expressed by Fourier's law:

$$\mathbf{q} = -\overline{\overline{\boldsymbol{\lambda}}}\nabla T$$

where $\overline{\overline{\boldsymbol{\lambda}}}$ is the effective thermal conductivity tensor $W.m^{-1}.K^{-1}$ taking into account the radiative heat transfer inside the pores.

$\dot{Q}$ accounts for the energy released/consumed by the different reactions R(1-5) as well as for the differences of sensible heats between the products and reactants of these reactions. This formulation of the source term was introduced by Haseli et al. [175].

$$\begin{aligned}\dot{Q} = -(\omega_G\rho_B k_1(\Delta H_{B-G} + \int(C_{p_B} - C_{p_G})dT) + \omega_T\rho_B k_2(\Delta H_{B-T} + \int(C_{p_T} - C_{p_B})dT)\\ +\omega_C\rho_B k_3(\Delta H_{B-C} + \int(C_{p_C} - C_{p_B})dT) + \omega_T\epsilon\rho_T k_4(\Delta H_{T-G} + \int(C_{p_G} - C_{p_T})dT)\\ +k_5\rho_C P_{CO_2}(\Delta H_{Boudouard} + \int(C_{p_{CO_2}} - C_{p_{CO}})dT))\end{aligned}$$

5.3.5 Initial and boundary conditions

Initial conditions

Seven initial conditions are identified for the model variables including the density of the different species and the temperature. The temperature is initially uniform in the particle and fixed to 293 K. The particle porosity is assumed to be filled with CO_2 at the atmospheric pressure.

$$\begin{aligned}\rho_B(\mathbf{r}, t=0) &= {\rho_B}^0 && (5.16)\\ \rho_C(\mathbf{r}, t=0) &= 0 && (5.17)\\ \rho_G(\mathbf{r}, t=0) &= 0 && (5.18)\\ \rho_T(\mathbf{r}, t=0) &= \rho_T^0(\mathbf{r}) && (5.19)\\ \rho_{CO}(\mathbf{r}, t=0) &= 0 && (5.20)\\ \rho_{CO_2}(\mathbf{r}, t=0) &= M_{CO_2}(\frac{P^0(\mathbf{r})}{RT^0}) && (5.21)\\ T(\mathbf{r}, t=0) &= 293K && (5.22)\end{aligned}$$

Boundary conditions

At the particle surface For gas, tars and CO, a flux condition is considered at the particle surface: the gas flux at the particle surface is proportional to the difference between the concentration $\rho_i^{\partial\Omega}$ at the particle surface and that in the surrounding ρ_i^{∞}.

$$\mathbf{N}_i^{\partial\Omega}.\mathbf{n} = k_m(\rho_i^{\partial\Omega} - \rho_i^{\infty}) \qquad i = G, T, CO \tag{5.23}$$

where k_m is the convective mass transfer coefficient, and the total gas flux $N_i^{\partial\Omega}$ is the sum of convective and diffusive terms:

$$\mathbf{N}_i^{\partial\Omega} = (\rho_i\mathbf{v} - D_{eff}\nabla\rho_i)^{\partial\Omega} \tag{5.24}$$

Since the surrounding gas is assumed to be pure CO_2, we set $\rho_i^{\infty} = 0, i =$ G, T, CO.

For the surrounding gas (CO_2), the boundary condition is obtained by fixing the total pressure at the particle surface as $P^{\partial\Omega} = P_\infty$. Using equation (5.13) gives the concentration of the CO_2 specie at the particle surface:

$$\rho_{CO_2}^{\partial\Omega} = M_{CO_2}\left(\frac{P_\infty}{RT^{\partial\Omega}} - \frac{{\rho_G}^{\partial\Omega}}{M_G} - \frac{\rho_T^{\partial\Omega}}{M_T} - \frac{\rho_{CO}^{\partial\Omega}}{M_{CO}}\right) \tag{5.25}$$

The heat flux continuity at the particle surface leads to the following boundary condition:

$$\mathbf{q}^{\partial\Omega}.\mathbf{n} = h_{conv}(T_\infty - T) + \sigma\xi(T_\infty^4 - T^4) \tag{5.26}$$

where h_{conv} $(W.m^{-2}.K^{-1})$is the convective heat transfer coefficient.

k_m as well as h_{conv} are determined by using correlations based on Nusselt and Sherwood numbers for a flow over a thin slab:

$$Nu = 0.644\, Re^{0.5}\, Pr^{0.343} \tag{5.27}$$

$$Sh = 0.644\, Re^{0.5}\, Sc^{0.343} \tag{5.28}$$

where Re, Pr and Sc are respectively the Reynolds, Prandlt and Schmidt numbers, functions of the surrounding gas (CO_2) properties and flow characteristics. Finally, σ is the Stephan-Boltzmann coefficient and ξ is the particle emissivity.

At the particle mid-planes A symmetry condition is considered at the particle mid-planes $(x, y = Th/2)$ and $(x = L/2, y)$:

$$\mathbf{N}_i^{mid}.\mathbf{n} = 0 \tag{5.29}$$

$$\mathbf{q}^{mid}.\mathbf{n} = 0 \tag{5.30}$$

5.3.6 Kinetic parameters, heat of reactions and thermo-physical properties

Kinetic parameters, heat of reactions and thermo-physical properties (porosity, permeability, thermal conductivity, pore diameter, emissivity) were identified from the literature based on biomass pyro-gasification studies. The data are summarized in table 5.2, 5.3 and 5.4. The physical properties of the solid blend biomass + char during the pyrolysis are calculated as linear combinations of the properties of char and biomass following:

$$\text{Prop} = \text{Prop}_B\frac{\rho_B}{\rho_{B0}} + \text{Prop}_C(1 - \frac{\rho_B}{\rho_{B0}}) \tag{5.31}$$

5.4 COMSOL Modelling

5.4.1 The geometry

A two-dimensional model is considered for the CO_2 pyro-gasification model. The biomass particle is assimilated to a rectangle which corners are reshaped for a better numerical convergence. The biomass particle has a thickness Th=1 mm and a length L=6 mm. Because of the symmetry at the particle centre, only a quarter of the biomass particle can be considered. The particle geometry and

Table 5.2: Thermophysical properties

Thermophysical property	Value/correlation	References
Thermal conductivity (W/m.K)	$\lambda_{B-grain} = 0.25$ $\lambda_{B-radial} = 0.1$ $\lambda_{C-grain} = 0.1$ $\lambda_{C-radial} = 0.07$	[175]
Permeability (cm^2)	$K_{B-grain} = 510^{-12}$ $K_{B-radial} = 510^{-12}$ $K_{C-grain} = 10^{-9}$ $K_{C-radial} = 10^{-9}$	[175]
Viscosity (Pa.s)	$\mu = 4.3510^{-5}$ for all the gas species	[74]
Pore diameter (cm)	$dp_B = 510^{-3}$ $dp_C = 10^{-2}$	[175]
Porosity	$\epsilon_B = 0.3$ $\epsilon_C = 1 - (1 - \epsilon_B)\omega_C$	[175]
Tortuosity	$\tau = 3$	[17]
Heat capacity (J/kg.K)	$C_{p_B} = 1.5 + 10^{-3}T$ $C_{p_C} = 0.44 + 2\,10^{-3}T - 6.7\,10^{-7}T^2$ $C_{p_G} = 0.761 + 7\,10^{-4}T - 2\,10^{-7}T^2$ $C_{p_T} = -0.162 + 4.6\,10^{-3}T - 2\,10^{-6}T^2$ $C_{p_{CO_2}} = 24.997 + 55.186\theta - 33.691\theta^2 + 7.948\theta^3 - 0.1366/\theta^2$ $C_{p_{CO}} = 25.567 + 6.0961\theta + 4.0546\theta^2 - 2.6713\theta^3 + 0.1310/\theta^2$ $\theta = 1000/T(K)$	[175]
Emissivity	$\xi_B = 0.6$ $\xi_C = 1$	[174]
Molecular diffusivity (m^2/s)	$D_{eff} = \frac{\epsilon}{\tau}\frac{1}{(\frac{1}{D_{Knudsen}} + \frac{1}{D})}$ $D = (1.67\,10^{-5}\frac{T}{298})^{1.75})$ for all the gas species $D_{Knudsen} = 0.97(d_p/2)(T/M_i)^{0.5}$	[74]

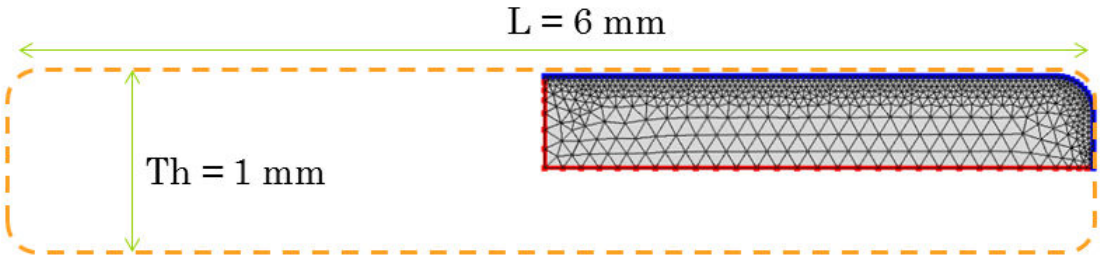

Figure 5.3: Geometry and meshing of a quarter of the biomass particle

meshing is shown in figure 5.3. The mesh size is reduced near the surface for a better numerical convergence. The model sensitivity to the mesh size was tested by reducing the mesh size by a half.

CO_2 pyro-gasification experiments were modelled using 3 modules in COMSOL software: *"Mathematics"*, *"Transport of diluted species"* and *"Heat transfer in fluids"*. The first one is used to define the ordinary differential equations (ODEs) related to the conservation of solid species (wood + char).

Table 5.3: Kinetic parameters

Reaction rate constant (s^{-1})	Pre-exponential factor, A (s^{-1})	Activation energy (kJ/mol)	References
k_1	$1.3\,10^8$	140	[178]
k_2	$2\,10^8$	133	[178]
k_3	$1.08\,10^7$	121	[178]
k_4	$3.2\,10^4$	72.8	[175]
k_5	$1.04\,10^2$	200	adjusted

Table 5.4: Heat of reactions

Reaction	Heat of reaction (kJ/kg)	References
1	418	[178]
2	418	[178]
3	418	[178]
4	-42	[178]
4	179.5	[172]

The second and third modules are used to describe mass and heat transfer inside the porous media. The former is used for the mass conservation of the gaseous species and the latter is used to set the energy conservation equation. COMSOL software has pre-defined forms for the conservation equations which are not consistent with the above-described set equations. Some mathematical transformations of the latter are therefore needed so that it fits into the COMSOL formalism.

5.4.2 Mathematical transformation of the conservation equations

For the *"Transport of diluted species"* COMSOL module, the mass conservation of a gaseous specie "i" is described as:

$$\frac{\partial C_i}{\partial t} + \nabla.(C_i\mathbf{V} - D\nabla C_i) = R_i \tag{5.32}$$

In our case, the model variables, there are the densities of the different gaseous species. For the i^{est} gas specie, the conservation equation reads:

$$\frac{\partial \epsilon\rho_i}{\partial t} + \nabla.(\rho_i\mathbf{v} - D_{eff}\nabla\rho_i) = r_i \tag{5.33}$$

We define therefore:

$$C_i = \epsilon\frac{\rho_i}{M_i} \quad , \quad \mathbf{V} = \frac{\mathbf{v}}{\epsilon} \quad , \quad D = \frac{D_{eff}}{\epsilon} \quad , \quad R_i = r_i/M_i$$

For the *"Heat transfer in fluids"* COMSOL module, the energy conservation equation is written as:

$$\rho C_p\frac{\partial T}{\partial t} + \rho C_p\mathbf{u}\nabla T = -\nabla.\mathbf{q} + \tilde{Q} \tag{5.34}$$

In the present case, the energy conservation equation reads:

$$(\rho_B C_{pB} + \rho_C C_{pC} + \epsilon\rho_G C_{pG} + \epsilon\rho_T C_{pT} + \epsilon\rho_{CO_2} C_{pCO_2})\frac{\partial T}{\partial t} + \nabla.\sum_i h_i\mathbf{N}_i = -\nabla.\,\mathbf{q} + \dot{Q}$$

Heat transported by the gas species entering and exiting from a volume dV is expressed by:

$$\nabla.\sum_i(h_i\,\mathbf{N}_i) = \sum_i \nabla.(h_i\,\mathbf{N}_i)$$

For the i^{est} gas specie, we have:

$$\nabla.(h_i\,\mathbf{N}_i) = h_i\nabla.\,\mathbf{N}_i + \nabla h_i.\,\mathbf{N}_i \qquad \text{and} \qquad \nabla h_i = Cp_i\,\nabla T + T\,\nabla Cp_i$$

As the specific heat is only temperature dependent, it gives:

$$\nabla Cp_i = \mathbf{0}$$

Therefore:

$$\nabla.\sum_i(h_i\,\mathbf{N}_i) = \sum_i(Cp_i\,\mathbf{N}_i\,\nabla T) + T\sum_i(Cp_i\,\nabla.\,\mathbf{N}_i)$$

We define here "A" as:

$$A = \sum_i(Cp_i\,\nabla.\,\mathbf{N}_i)$$

The energy conservation equation becomes:

$$(\rho_B C_{p_B} + \rho_C C_{p_C} + \epsilon\rho_G C_{p_G} + \epsilon\rho_T C_{p_T} + \epsilon\rho_{CO_2} C_{p_{CO_2}} + \epsilon\rho_{CO} C_{p_{CO}})\frac{\partial T}{\partial t} + T\,A + \sum_i(Cp_i\,\mathbf{N}_i).\,\nabla T = -\nabla.\,\mathbf{q} + \dot{Q}$$

By identification with the COMSOL formulation we can set:
An equivalent ρCp

$$(\rho Cp)_{eq} = (\rho_B C_{p_B} + \rho_C C_{p_C} + \epsilon\rho_G C_{p_G} + \epsilon\rho_T C_{p_T} + \epsilon\rho_{CO_2} C_{p_{CO_2}} + \epsilon\rho_{CO} C_{p_{CO}})$$

An equivalent velocity $\mathbf{u}$:

$$\mathbf{u}_{eq} = \frac{\sum_i(Cp_i\mathbf{N}_i)}{(\rho Cp)_{eq}}$$

and finally an equivalent heat source term $\tilde{Q}_{eq}$:

$$\tilde{Q}_{iden} = \dot{Q} - TA$$

5.5 Results and discussion

5.5.1 CO_2 pyro-gasification experimental results

Figure 5.4, which represents the normalized mass loss vs. time, shows three repeatability tests of the CO_2 pyro-gasification. The experiments are very reproducible and the plots are almost superposed. The biomass pyro-gasification in CO_2 shows two major steps, namely the wood pyrolysis and the char gasification. The pyrolysis stage lasts 30 times less than the char gasification one. The former takes 20 s (including the heating stage) while the latter lasts for near to 600 s. Clearly, the char gasification is the rate limiting step in the total pyro-gasification process.

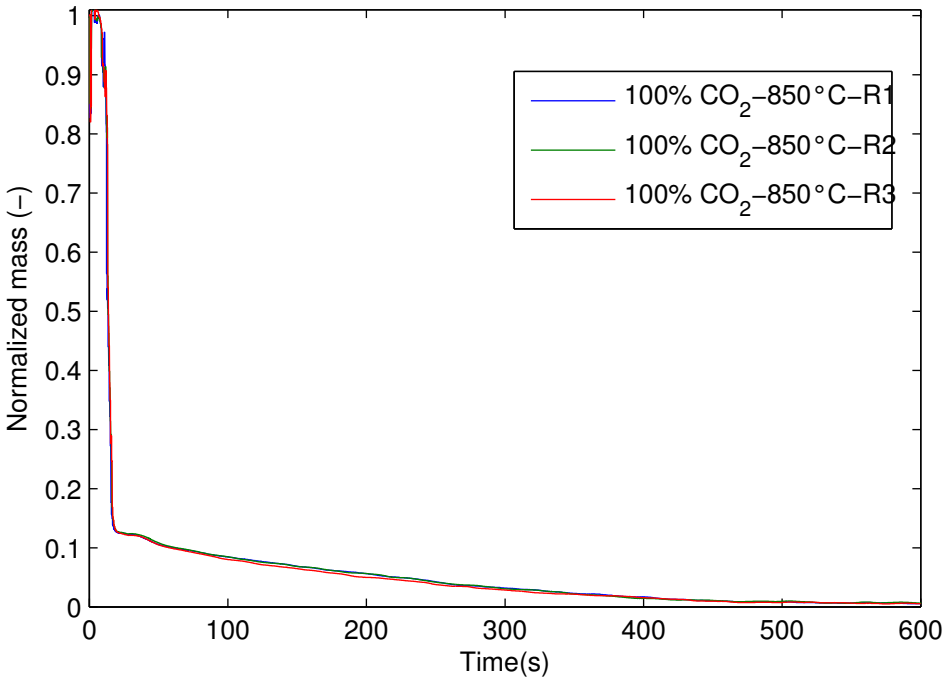

Figure 5.4: Pyro-gasification in pure CO_2: normalized mass VS time

In order to assess the effect of using pure CO_2 on the pyrolysis step, it is suitable to compare the CO_2-pyrolysis with a reference one in a N_2 atmosphere. The results are shown in figure 5.5. The time scale was reduced to 200 s to highlight the pyrolysis stage and the beginning of the char gasification. During the pyrolysis active phase the rate of mass loss is almost the same in the N_2 and CO_2 pyrolysis atmospheres. No influence of the CO_2 can be perceived during this stage. We observed also that the char yield is almost the same. We expected that less char would be formed during the pyrolysis in pure CO_2 since we had found previously that in a that in a mixture of 20% CO_2 in N_2 pyrolysis atmosphere, the char yield decreased by near to 1% and imputed it to the gasification of the nascent char among the plausible explanations [173]. Other researchers have found that the coal char yield decreases in a pure CO_2 atmosphere compared to the pyrolysis in a He atmosphere [132], and was also attributed to the gasification of the nascent char. For biomass chars, the routes may be different for high CO_2 concentrations. Indeed, Watanabe et al. [130] found that in the case of lignin pyrolysis, the pure CO_2 atmosphere induces the formation of more char than in an argon atmosphere. The CO_2 was found to react with metal salts present in the lignin structures (K, Na) and forms carbonates (Na_2CO_3 or K_2CO_3). For metal depleted lignin, the char yield in an Ar or a CO_2 atmosphere were the same. The gasification of nascent char, and the formation of carbonates on the char surface have opposite effects which may lead, in our case, to a similar char yield as in an N_2 atmosphere.

The major mass loss occurs between t=10 s and t=16 s. In this time interval, the particle loses near to 80% of its mass. Follows a slower mass decay until 25 s after which the char mass was constant. The pyrolysis stage can be divided into two phases: the active phase where the major mass loss occurs, and the passive phase where the mass loss rate is far smaller than in the active phase. Under the N_2 and CO_2 atmospheres, the char mass reached respectively an almost constant value at t=25 s:0.116 and 0.123. In a CO_2 atmosphere, there is an almost constant plateau followed by the char gasification stage which started at 35 s while the char mass remained constant in the N_2 atmosphere. The char gasification and pyrolysis steps seems to be independent and not overlapping.

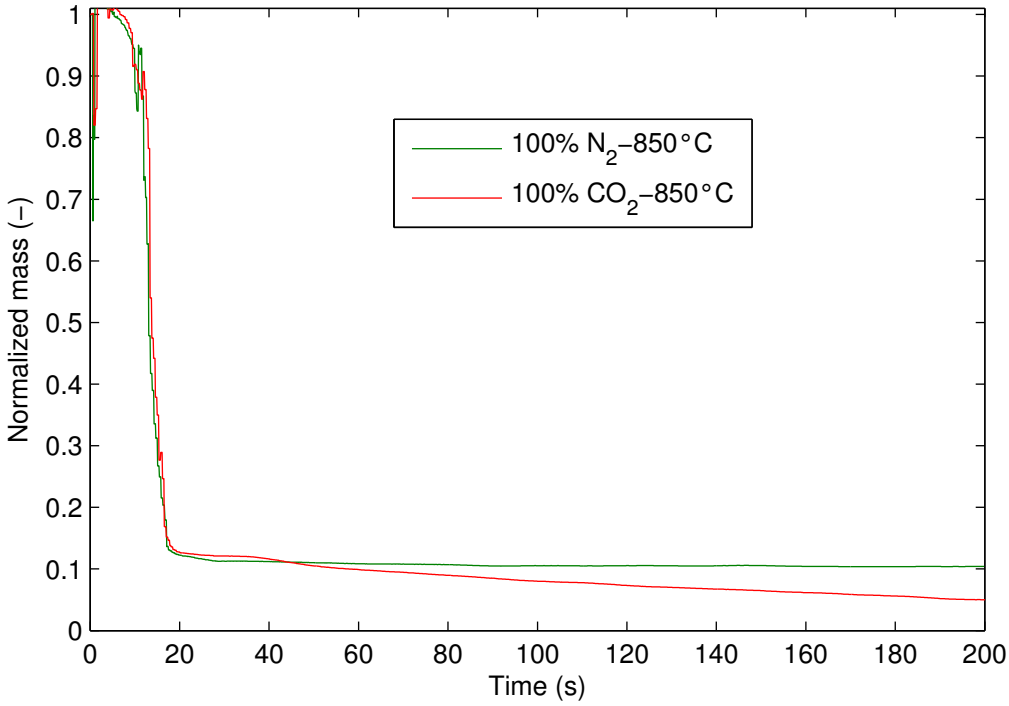

Figure 5.5: Pyro-gasification in pure CO_2 VS N_2 pyrolysis

The presence of the 10 s plateau before the starting of the gasification will be discussed in the next sections.

5.5.2 Modelling results

Figure 5.6 shows the modelling results in terms of normalized mass versus time compared to the experimental data. As visible on the figure, the model predicts very well the experimental data. Some small discrepancies are nonetheless observable. In order to highlight the agreement of the numerical model with the experimental data, we made a focus on the pyrolysis stage in Fig.5.7 and another one on the char gasification stage in Fig.5.8. In the very beginning of the normalized mass vs. time curve (at around 2-3 s), we can note an abrupt mass decrease followed by an increase. This artefact has nothing to do with the pyrolysis reaction, but is related to the mechanical forces when moving the weighing system upward. Only the very beginning of the weighing device introduction process is poorly reproducible. The numerical model describes correctly the heating stage as well as the pyrolysis stage. There are small discrepancies between the model and the experimental data in the beginning and in the end of the pyrolysis, still, they are acceptable. The model captures well the transition (25 to 35 s plateau) between the end of the pyrolysis (at 25 s) and the beginning of the char gasification (at 35 s) as shown in figure 5.7. The char gasification is correctly described by the model (figure 5.8) but with a lower accuracy. The activation energy for the CO_2-char gasification reaction was adjusted to 200 kJ/mol and is in the range of values presented in Di Blasi's review on combustion and gasification rates of lignocellulosic chars [14].

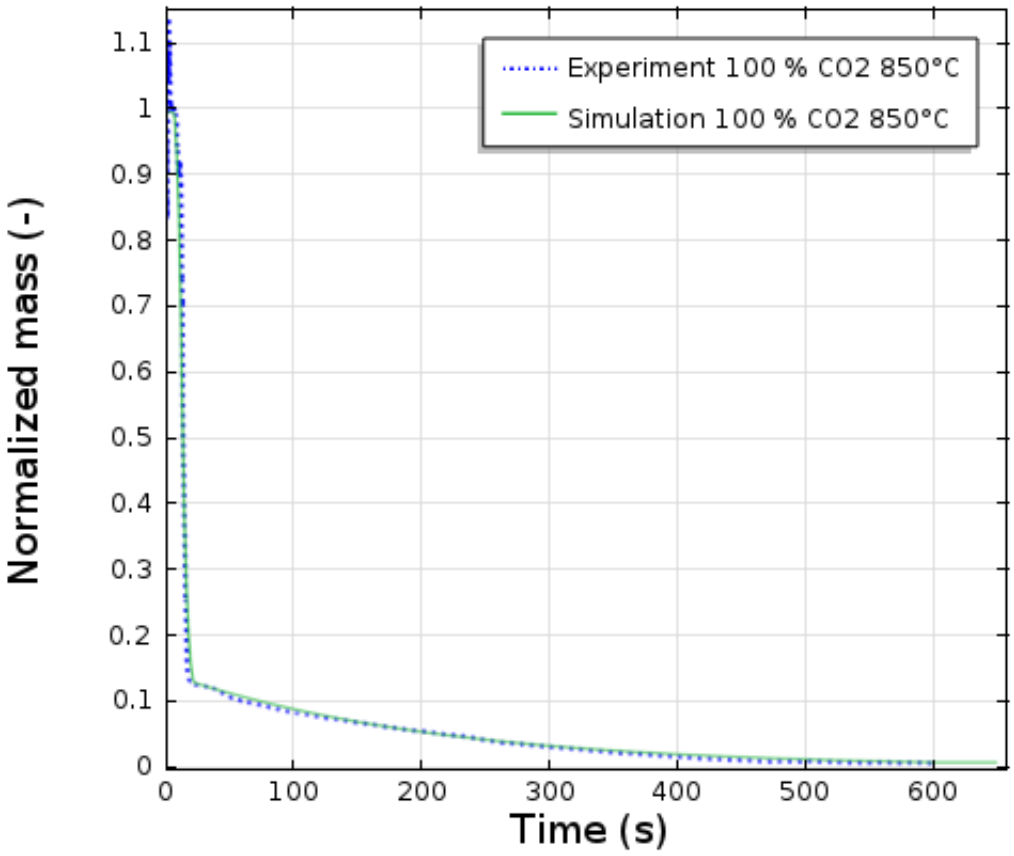

Figure 5.6: CO_2 pyro-gasification modelling results

Pyrolysis stage analysis

When introduced into the hot reactor, the wood particles are heated by radiation with the hot gas and the reactor wall and by convection with the surrounding hot gas. As the wood particles are not thermally thin bodies (Biot number $\simeq 0.1$), there exists a temperature gradient between the surface and the particle centre. This temperature difference would become smaller and smaller as the particle becomes thinner. To illustrate this spatial temperature difference, the time variations of the temperatures on the particle surface and in the center is shown in figure 5.9. A semi-log scale is adopted to enhance readability. It can be seen that the temperature increases differently at the particle surface and centre. During the heating stage, the energy received from the surroundings heats the particle surface, and heat is transported by conduction towards the center. As the biomass pyrolysis reaction starts, part of the energy received is consumed by the endothermic pyrolysis reaction as chemical bonds are disrupted. A temperature near-plateau is observed around 11 s. The temperature plateau observed corresponds to a steady-state phase where the energy extracted from the hot surroundings exactly balances the energy sucked by the reaction in the whole particle This temperature evolution behaviour was noticed in previous studies [179] [180] [181]. This has to be taken with caution, since no experimental measure of the surface temperature was performed. Contour plots of the fresh biomass mass fraction are shown in figure 5.10 at different reaction times. The black regions correspond to pure char, whereas the white ones correspond to fresh wood. The region where the fresh biomass mass fraction is equal to zero (black coloured) denotes that the solid corresponds only to char. While the outer regions of the particle are pyrolysed with production gas and char, the inner regions can contain fresh wood. At 18 s almost all the initial fresh biomass is

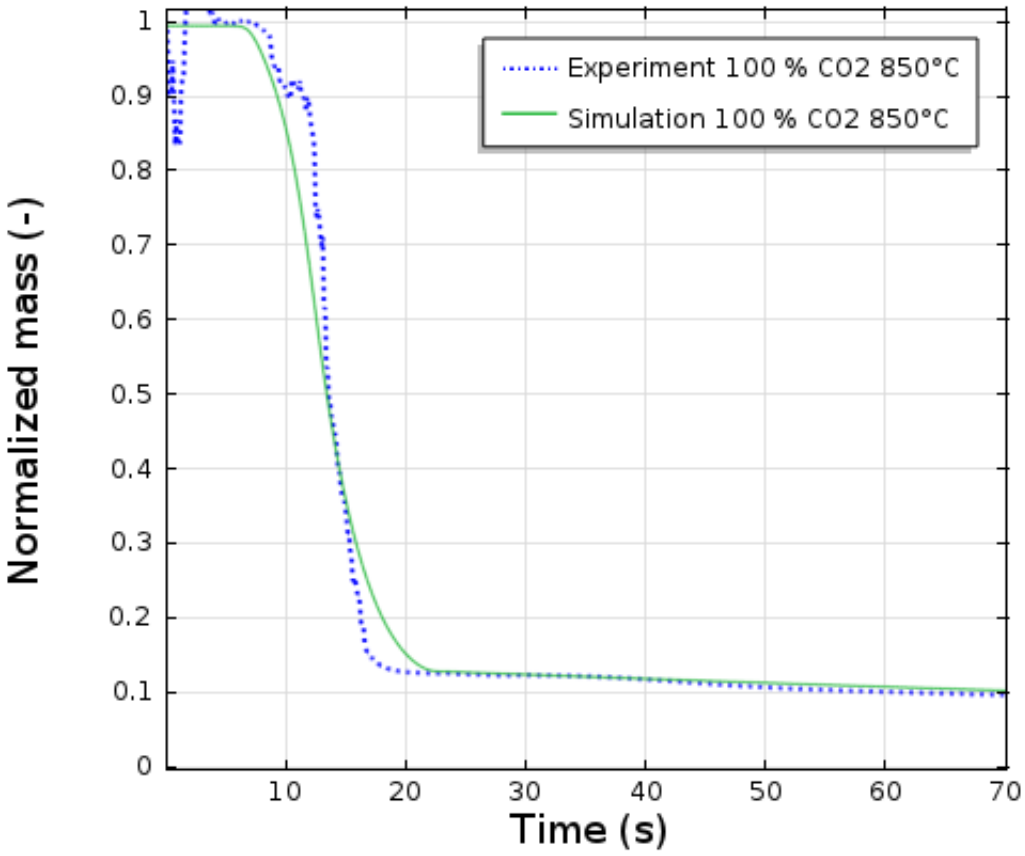

Figure 5.7: A zoom on the pyrolysis stage and of the beginning of the char gasification

pyrolysed.

When the biomass decomposes, the solid porosity increases and the released gaseous compound fill the porous void. The porosity evolution at the particle surface as well as in the centre predicted by the model is shown in figure 5.11. The same time delay as for the temperature increase is noticed for the porosity evolution. As the chemical reaction rate is not uniform throughout the particle due to the non uniformity of the temperature, less wood is dissociated near the centre than near the surface. This impacts the porosity which increases more rapidly at the surface. It can be also noticed that the difference between the porosity evolution at these two respective locations vanishes as soon as the gasification of the char begins. This attests of the homogeneity of the char gasification reaction throughout the char particle.

During the wood pyrolysis, the presence of gaseous species inside the pores induces a pressure increase. As for temperature, the total pressure evolution at the particle surface and centre is plotted in figure 5.12. The pressure at the surface remains constant as it is a fixed boundary condition. At the particle centre, the pressure initially decreases. The temperature gradient between the particle surface and center induces a CO_2 concentration gradient, leading to a CO_2 flow toward the surface. Afterwards, the pressure increases as the pyrolysis begins with the production of gaseous species. Two pressure peaks can be noticed. This phenomena is due to the competition between the two mechanisms of Darcy and Fick diffusion which govern the gas species transport inside the particle. Simulation results show that the pressure reaches a maximum of 128 kPa at the centre of the particle. Similar values are reported in the literature [175] [182]. During the gasification stage the pressure remains constant throughout the particle. This will be discussed latter on.

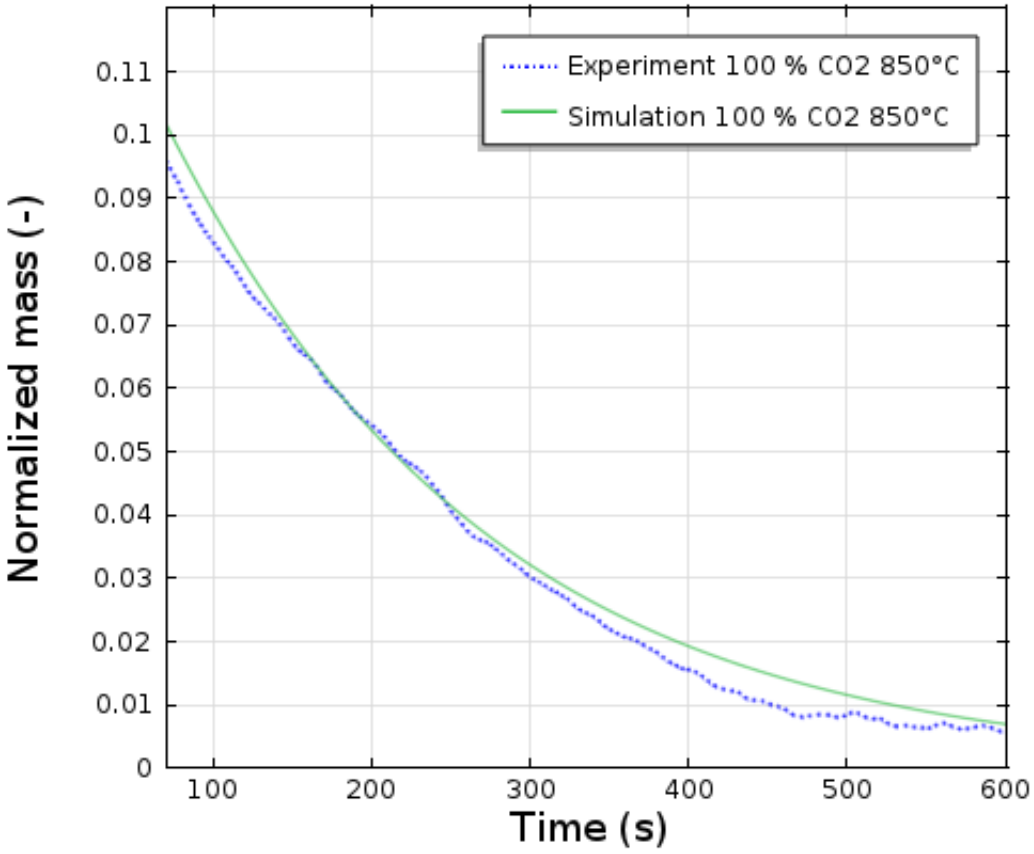

Figure 5.8: A zoom on the char gasification stage

Colour map plots of the gas+tar mass fraction $\frac{(\rho_G + \rho_T)}{(\rho_G + \rho_T + \rho_{CO} + \rho_{CO_2})}$ in the pore space are shown in figure 5.13 at 12 s, 14 s, 16 s, 18 s and 20 s. The difference to the unity represents the CO_2 + CO mass fraction in the pore space. Initially, part of the CO_2 leaves the particle during the heating stage as discussed before. During the heating stage, the temperature gradient inside the particle causes a concentration gradient leading to a CO_2 flux toward the surface according to Fick's law. Part of the CO_2 remains in the particle porosity during the heating stage. When chemical reactions start with production of gas and tars, the CO_2 remaining in the particle becomes mixed with these latter inside the particle porosity. Due to the concentration difference and pressure gradients, gas and tars leave the particle. Simultaneously, the CO_2 concentration difference between the particle surface and the internal regions induces an inward CO_2 diffusive flux. The CO_2 concentration increases with time inside the particle.

What is the impact of CO_2 during the pyrolysis stage?

According to the previous observations and discussion about the presence of CO_2 inside the particle during the pyrolysis stage, even if non-uniformly distributed, one can expect that it begins to react with the char as soon as formed. Nevertheless, the Boudouard reaction has a very low rate at low temperature, so that even if CO_2 is present in certain regions, without a sufficiently high temperature the reaction term accounting for CO_2 consumption would be negligible. To highlight this assertion, colour map plots of CO_2 partial pressure as well as contour plots of the temperature are plotted in figure 5.14. Despite the CO_2 is present in the particle, even with a considerable partial pressure, the char gasification reaction can not take place as the temperature is not high enough. For

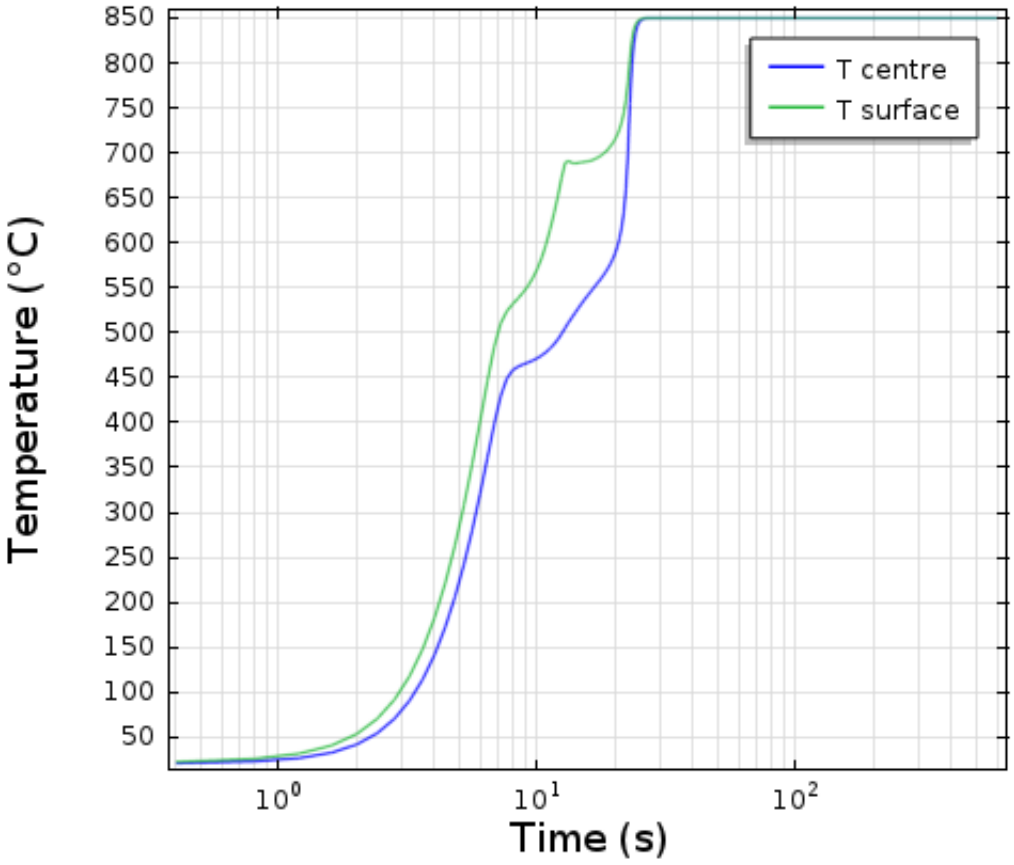

Figure 5.9: Temperature evolution at the particle surface and centre during the pyro-gasification process

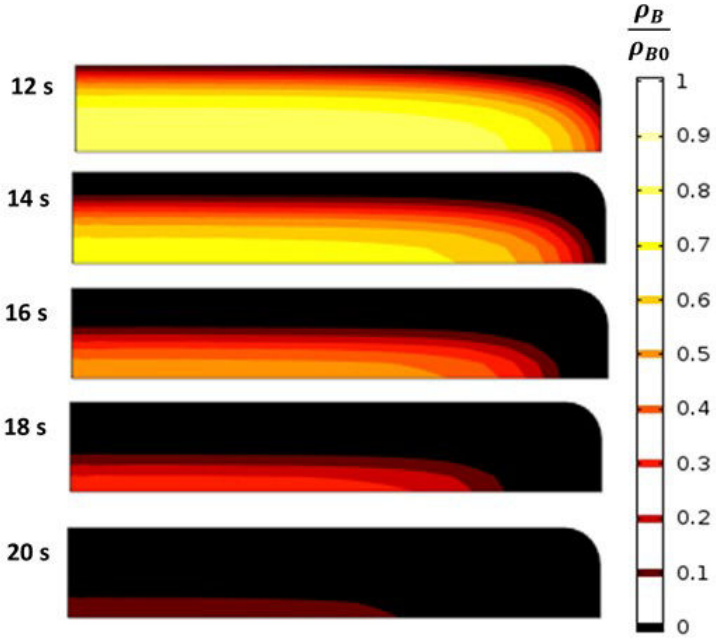

Figure 5.10: Contour plots of the fresh wood mass fraction along the conversion at 12 s, 14 s, 16 s, 18 s and 20 s

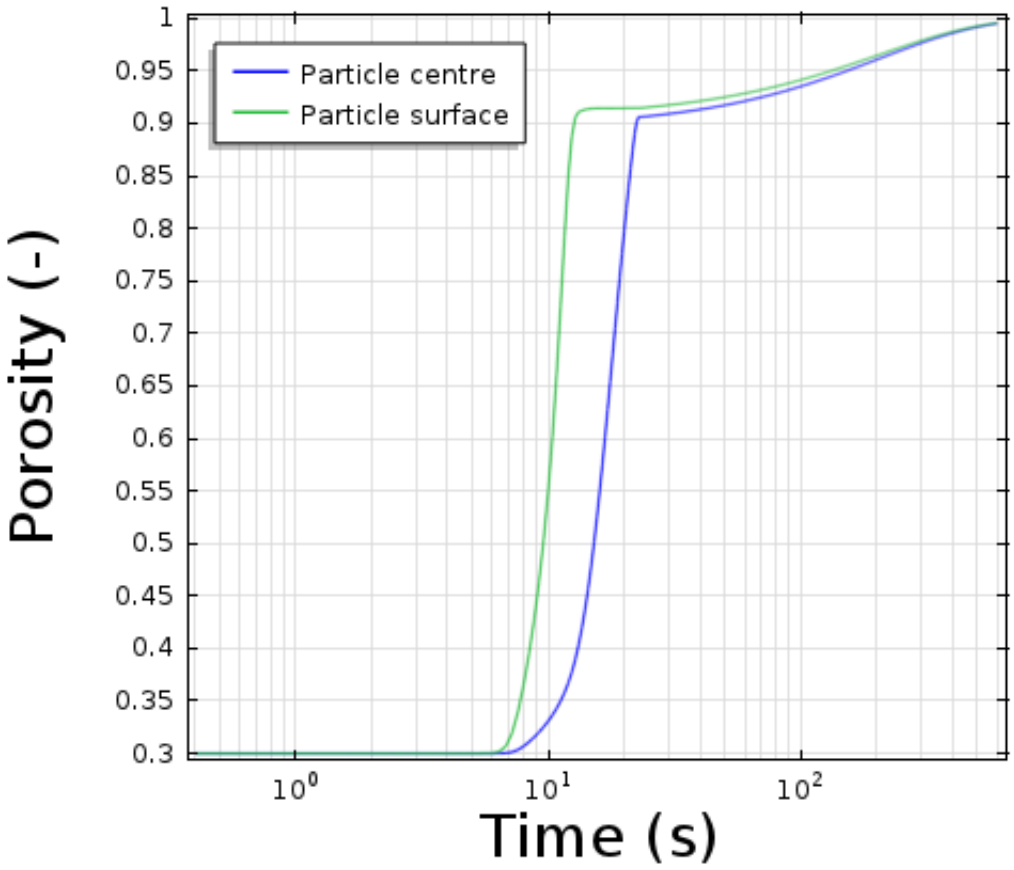

Figure 5.11: Porosity evolution at the particle surface and centre during the pyro-gasification process

instance, at t=18 s, one can notice that in a part of the particle, the CO_2 partial pressure reaches 50 kPa at a temperature of 650°C while in an other outer region, it reaches 90 kPa at a temperature of 790°C. The gasification reaction rate is not sufficiently high to induce a noticeable mass loss in these conditions.

Analysis of the char gasification stage

The char gasification stage is the rate limiting step in the pyro-gasification process. The temperature, and the pressure as shown in figure 5.9 and 5.12 are uniform throughout the particle and constant along the conversion. Once the pyrolysis stage is finished, all the the remaining char porosity is filled with CO_2. This latter reacts with the char to produce CO via the Boudouard reaction. The char void remains all mostly filled with CO_2 along the char conversion. The CO_2 mass fraction in the char porosity is very close to unity. The CO produced diffuses out of the particle while the decrease in the CO_2 concentration is constantly adjusted by diffusion due to the imposed constant CO_2 pressure at the particle surface. The CO diffuses out of the particle so rapidly that it has no time to accumulate and cause a pressure increase. In such operating conditions, the gasification reaction characteristic time is far greater than that of reactants/products diffusion [56].

The porosity evolution in the gasification stage is uniform throughout the particle which is synonym of the uniformity of the reaction in the particle. While transfer limitations exists for the the pyrolysis stage, the char gasification is performed in a chemically controlled regime.

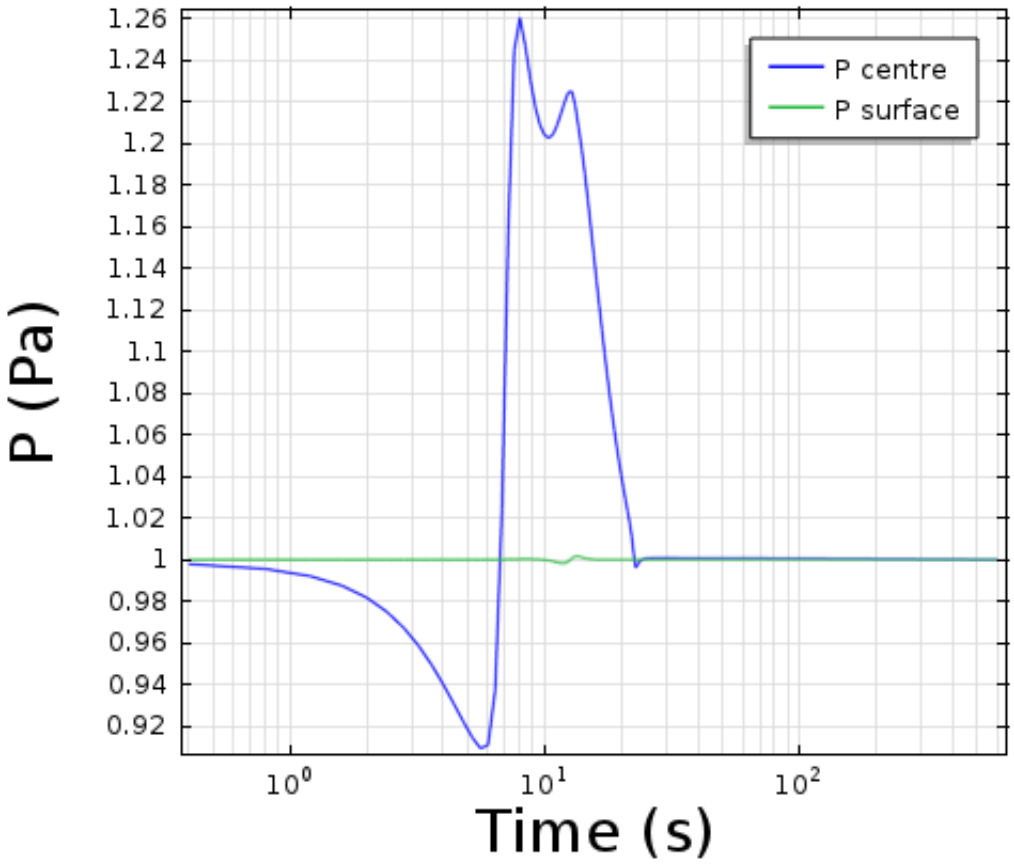

Figure 5.12: Pressure evolution at the particle surface and centre during the pyro-gasification process

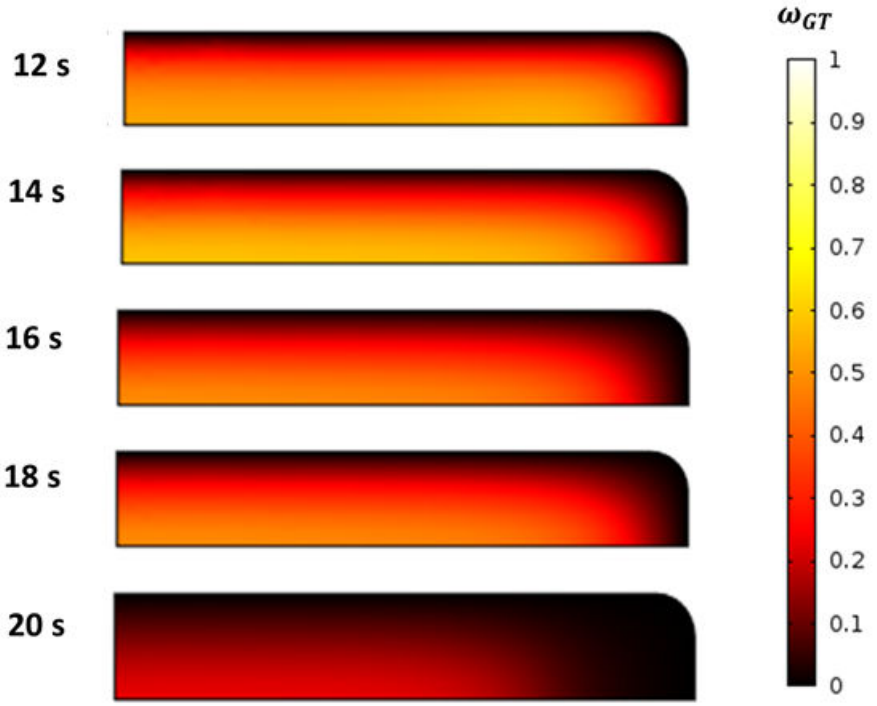

Figure 5.13: Colour map plots of the gas+tar mass fraction in the gaseous phase at 12 s, 14 s, 16 s, 18 s and 20 s

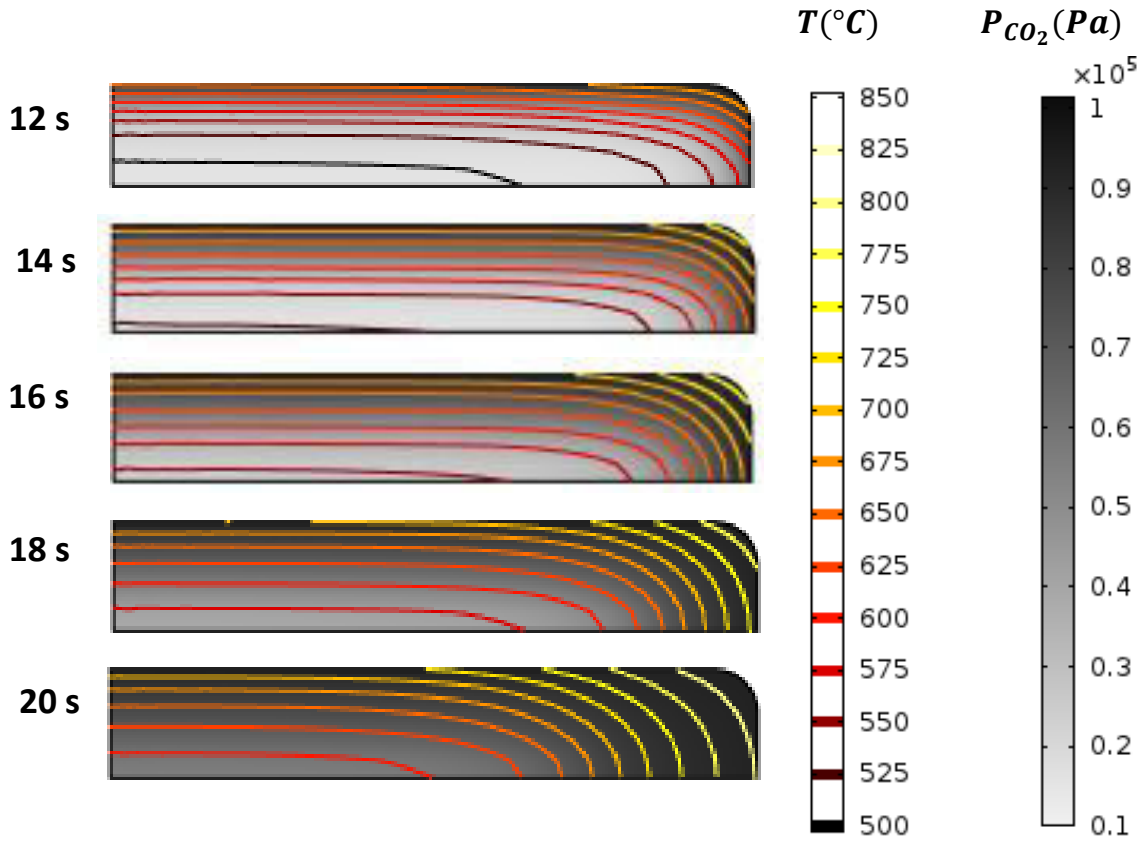

Figure 5.14: Colour map plots (Gray scale) of the CO_2 partial pressure in the particle and contour plots (yellow to red contours) of the temperature at 12 s, 14 s, 16 s, 18 s and 20 s

Model sensitivity

The modelling results can be affected by the meshing size as well as by the model parameters. We first assessed the model sensitivity to the mesh size. Figure 5.15 shows the experimental vs. modelling results for three mesh sizes. As depicted on the figure, decreasing the maximum mesh size by 3 folds or doubling it does not influence the modelling results.

The sensitivity of normalized mass vs. time results to several model parameters was investigated by modifying them, one at a time. The results are shown in figure 5.16 and 5.17.

The main results are that the model sensitivity to the $\int(Cp_i - Cp_j)dT$ term is quite low. Omitting this term does not modify the modelling result. The model sensitivity to the heat of pyrolysis, convective heat transfer coefficient, wood thermal conductivity as well as particle emissivity is not very marked. However, we found that the model is quite sensitive to the stoichiometric coefficients. The model is not able to capture the end of the pyrolysis reaction when doubling ω_C. Keeping ω_T constant, ω_G varies when ω_C is changed, but with no marked influence on the pyrolysis rate. Increasing k5 impacts on the gasification rate as depicted in figure 5.17.

5.6 Conclusion

The CO_2 pyro-gasification of biomass was studied with the aim to assess the potential of CO_2 valorisation as a gasifying medium in fluidized bed gasifiers. Experimental results obtained for 1 mm thick particles, show that the gasification stage is the rate limiting step in the pyro-gasification process. The pyrolysis ended at about 25 s while near to 600 s were necessary to achieve the

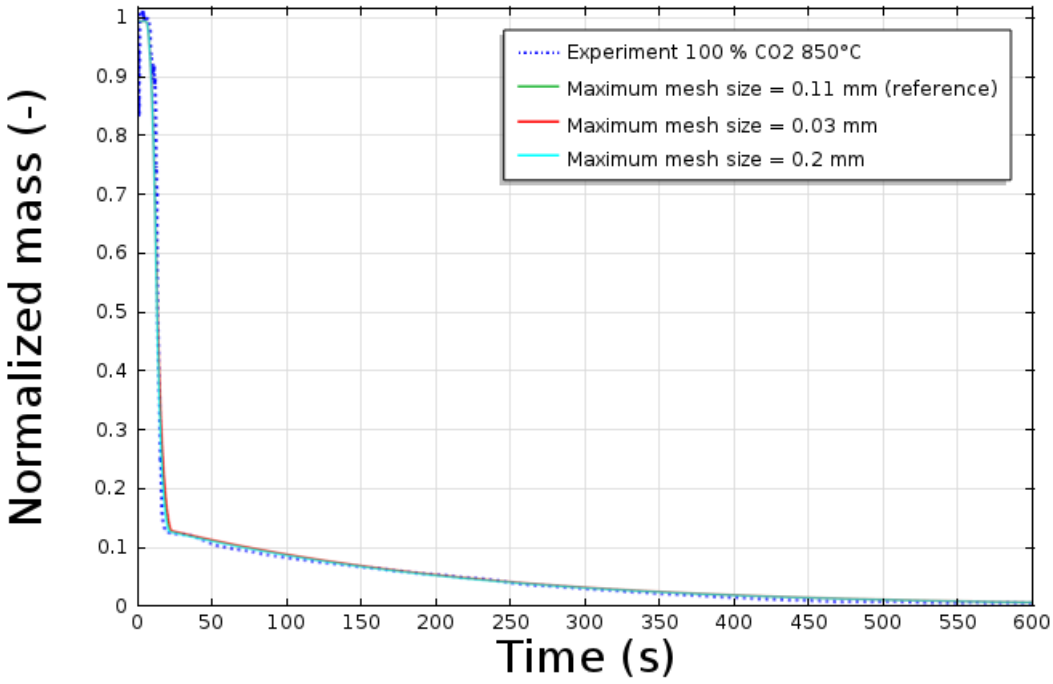

Figure 5.15: Influence of the mesh size on the modelling results

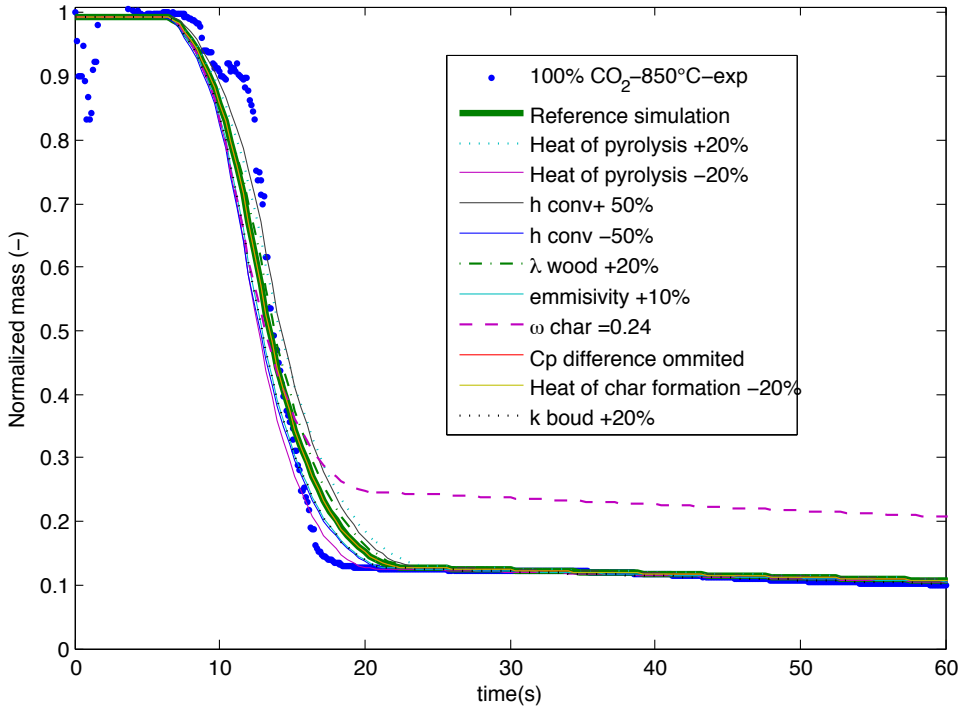

Figure 5.16: Sensitivity analysis: focus on the pyrolysis stage

char gasification reaction. The CO_2 had no major effects on the pyrolysis rate compared to reference pyrolysis in an N_2 atmosphere. After the pyrolysis stage, a 10 s duration plateau was observed before the starting of the char gasification. This plateau was captured by the model. The modelling results show that during this plateau, the CO_2 was present inside the char particle, but the temperature was quite low to induce a starting of the gasification and a noticeable mass loss. The numerical model

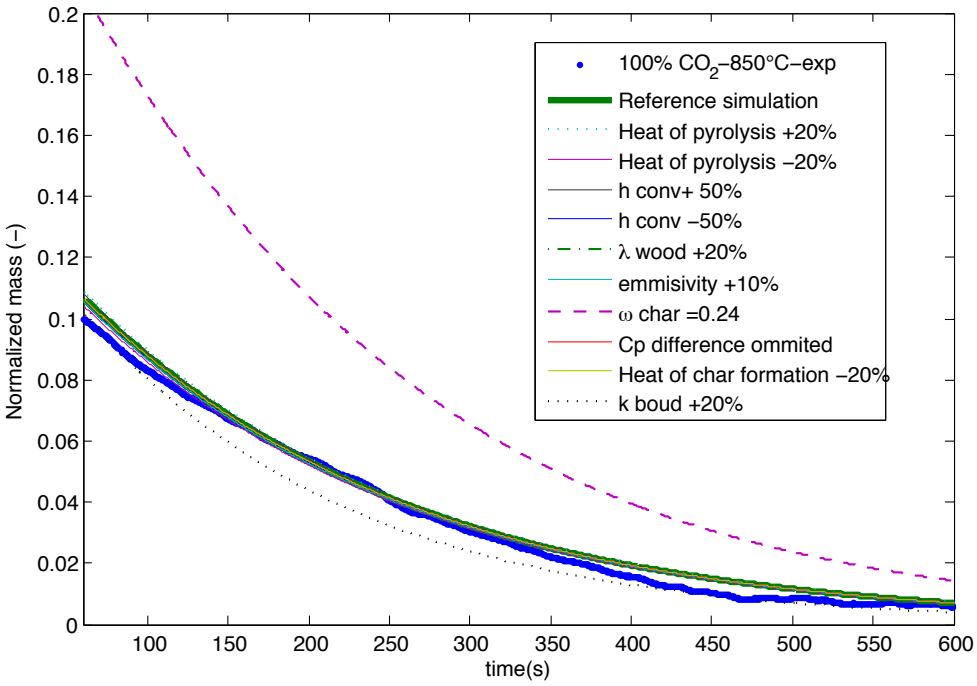

Figure 5.17: Sensitivity analysis: focus on the char gasification stage

developed in this work shed light on the unfolding of the whole pyro-gasification of 1 mm thick wood-chips. This global approach, for high heating rate conditions, is not tackled in the literature. However, the model still a simplified one. It can be further improved by considering a more extended pyrolysis scheme and considering the interaction of CO_2 with the pyrolysis gas products.

Acknowledgements

The authors acknowledge the national research agency ANR France for its financial support in the RECO2 project. They also wish to express their appreciation to Diago Hermano for his help.

Chapter 6

Influence of temperature and particle size on the single and mixed atmospheres gasification of biomass char with H_2O and CO_2

Abstract

The paper focuses on the gasification of Low Heating Rate chars in H_2O, CO_2 and their mixtures. The first part is dedicated to the study of the influence of particle size and temperature respectively on H_2O and CO_2 gasification reactions. Thiele approach was adopted to assess the extent of diffusional limitations when varying the char particle size and the temperature. We found that at 900°C, the gasification reaction with H_2O or CO_2 is performed in the chemical regime for powdery particle of 0.04 mm. The reaction rate constant as well as the effectiveness factors for the different particle size were determined for both gasification reactions. We also studied the mixed atmosphere gasification of 0.2 mm chars at various temperature and found that the char reactivity is fairly represented by an additive law at relatively low temperatures of 800°C and 900°C but not at 1000°C and 1100°C for which the char reactivity was lower than the sum of the individual contributions. Similarly, we assessed the effect of particle size on the mixed atmosphere gasification reactivity and found that at 900°C, additive law was quite representative of the experimental reactivities in char particle size range from 0.2 mm to 13 mm. A linear combination model to calculate the reactivity in mixed atmospheres is proposed and discussed along. Finally, we studied the effects of a prior gasification with CO_2 on the char reactivity towards H_2O and vice versa. It was found that for 0.2 mm and 13 mm char particle size, the historic of gasification does not impact on the char reactivity towards a gas. This latter is only conversion-dependent. The present work provides useful and worthy information on the char gasification reactivity in H_2O and CO_2 as well as in their mixtures in conditions close to practical operating ones encountered in biomass gasifiers.

Keywords: Biomass char, CO_2, H_2O, Reactivity, Mixed atmospheres, Thiele modulus, Cyclic atmospheres.

Résumé

Le présent chapitre porte sur la gazéification au CO_2 et à H_2O de chars obtenus par pyrolyse lente de bois. La première partie est consacrée à l'étude de l'influence de la taille des particules de chars et de la température sur la cinétique de gazéification sous CO_2, H_2O et leur mélange. Une approche basée sur le module de Thiele est adoptée pour évaluer l'étendue des limitations diffusionelles dans diverses conditions de gazéification. On a trouvé qu'à 900°C, la réaction de gazéification à l'eau ou au CO_2 est opérée en régime chimique pour des particules de char de 0.04 mm. Les constantes cinétiques des réactions de gazéification ainsi que les facteurs d'éfficacité ont été déterminés. On a aussi étudié la gazéification en atmosphères mixtes de particules de char de 0.2 mm à plusieurs températures et on a trouvé que la réactivité du char sous atmosphères mixtes est correctement représentée par une loi d'additivité à 800°C et à 900°C mais pas à des températures plus hautes de 1000°C et 1100°C pour les quelles la réactivité en atmosphère mixte est inférieure à la somme des réactivités individuelles. Nous avons aussi étudié l'effet de la taille des particules sur la gazéification en atmosphère mixte et avons trouvé qu'à 900°C, une loi d'additivité représentait bien les réactivités expérimentales dans une large gamme de taille de 0.2 à 13 mm. Un modèle simple pour le calcul de réactivité est proposé et discuté. Finalement, nous avons aussi étudié l'effet d'une gazéification du char au CO_2 sur sa réactivité à l'eau et vice versa et avons trouvé que la réactivité du char ne depend pas de l'historique de gazéification. La présente étude comporte des données importantes sur la réactivité de char à H_2O, CO_2 et leurs mélanges dans des conditions rencontrées dans les réacteurs de gazéification.

Mots clés : Char de biomasse, CO_2, H_2O, Reactivité, Atmosphéres mixtes, Module de Thiele, Atmosphéres cycliques.

6.1 Introduction

Char gasification is an important step the global operation of biomass gasification. Indeed, when a biomass particle is gasified, it dries first, pyrolyses in second lieu, resulting in emission of gas species and formation of a solid char containing mainly carbon with some oxygen, hydrogen and mineral species in a far lesser amount. The produced char reacts with the gasification medium resulting in the production of additional gaseous species mainly composed by CO and H_2. The gasification reaction is the limiting step in the global gasification reaction and is of major importance in the sizing of gasifiers [7]. Inside a gasifier, the solid char can react with various gasifying agents such as O_2, H_2O, CO_2 and H_2. The gasifying agents have two origins: either they are provided by an external supply into the gasifier or are produced inside the gasifier by the drying and pyrolysis reactions. In most of practical situations, the char reacts with a mixture of these species following the reaction of char combustion and gasification:

Char combustion

$$Partial\,combustion\ : C + 1/2\,O_2 \longrightarrow CO\,(-111kJ/mol) \tag{6.1}$$

$$Complete\,combustion\ : C + O_2 \longrightarrow CO_2\,(-394kJ/mol) \tag{6.2}$$

$$\tag{6.3}$$

Char gasification

$$Steam\,gasification\ : C + H_2O \longrightarrow CO + H_2\,(+131kJ/mol) \tag{6.4}$$

$$Boudouard\,reaction\ : C + CO_2 \longrightarrow 2CO\,(+173kJ/mol) \tag{6.5}$$

$$Hydrogen\,gasification\,(Methanisation)\ : C + 2H_2 \longrightarrow CH_4\,(-75kJ/mol) \tag{6.6}$$

Huge literature exists on biomass char combustion and gasification with O_2, H_2O and CO_2. The reader can refer to Di Blasi's review on combustion and gasification rates of biomass chars [14]. Wide range of gasification kinetic data of various char biomasses is reported. On the contrary, few studies deal with the gasification of biomass char in complex atmospheres containing more than one gasifying agent- in particular CO_2 + H_2O)- while it is of practical interest to study the effects of mixing the gases on the char gasification reaction, as it is representative of practical situation in gasifiers. For instance, inside a fixed bed gasifier, a char particle can be gasified simultaneously by more than a gasifying agent. It can also react at first with a gas "A", for instance CO_2, and then reacts with another one, a gas "B", H_2O for example, and vice versa. It's therefore of interest to study the mixed atmosphere gasification of chars as well as the mutual effects of gases on the char reactive properties, providing thus worthy information for near-practical conditions encountered in such processes.

In mixed atmosphere gasification reactions, H_2O and CO_2 can react separately (**passive co-operation or additivity**), the reactivity in mixed atmosphere of CO_2 and H_2O can be therefore expressed as the sum of the single reactivities. The two gases can also compete and react on shared active sites (**Competition**). The reactivity in mixed atmosphere of CO_2 and H_2O is therefore lower than the sum of the single reactivities. The third case, there can be synergy between the two gases (**Synergy or active cooperation**) and the char reactivity in mixed atmosphere gasification experiments is higher than the sum of the single reactivities.

An overview on the literature focusing on complex atmosphere gasification of biomass chars shows for instance that Groeneveld and Van Swaaij [104] studied the wood char gasification reaction in a mixture of H_2O and CO_2. The authors proposed a n^{th} order model for wood char gasification in a mixed atmosphere of H_2O and CO_2. The two reactions were assumed to have the same activation energy and the global reaction rate was dependant on the sum of the partial pressures of H_2O and CO_2.

Maria Barrio and co-workers [134] performed experiments of wood-char gasification in steam-carbon dioxide mixtures. The authors found that the carbon conversion is mainly due to steam gasification meanwhile the carbon dioxide, which is less reactive, has potentially another role when it is injected as a co-reactant with steam but in any case would inhibit the gasification reaction.

In 2008, Tagutchu et al [103] observed a synergy between H_2O and CO_2 when mixed together as a gasifying agent. They found that the char reactivity in mixed atmospheres of CO_2+H_2O was higher than the sum of the single reactivities and concluded to synergy effects between the two gases. They proposed a model based on the work of Robert and Harris [139] in which the H_2O and CO_2 react on separate active sites. As suggested in [103], the authors think that CO_2 creates additional micro-porosity and enhances the access of H_2O to the active sites.

The gasification of large variety of biomass samples was investigated in a TG apparatus with a heating rate of 10°C/min up to 1000°C using steam, carbon dioxide or a mixture of both reactant as a gasification medium [8]. The authors observed that regardless of the biomass type, introducing CO_2 with a minimum amount of 30 % next to steam into the flow stream resulted in a complete char burnout with a light mineral film remaining in the crucible, whereas a black char residue remains when using only steam as a gasification medium. In a complementary study, the same authors reported several facts related to the CO_2-addition as co-gasifying medium with steam such as the enhanced char micro-porosity [123].

Susana Nilsson et al studied the gasification of dried sewage sludge (DSS) chars in a pilot fluidized bed reactor under CO_2, H_2O and their mixtures [136]. The experiments were performed in the temperature range of 800-900°C and gas partial pressure of 0.1-0.3 bar. The authors demonstrated that the DSS char reactivity in mixed atmospheres of H_2O and CO_2 can be expressed as the sum of the single atmosphere gasification reactivites.

Susana Nilsson et al studied the gasification reactivity of olive tree pruning [137] in the same fluidized bed apparatus. The experiments were done in the temperature range of 760-900°C in mixtures of CO_2, H_2O, H_2, CO and N_2. The authors determined the reaction kinetic constants respectively for the CO_2 and the H_2O gasification reactions. Afterwards, they performed gasification experiments in mixtures of H_2O and CO_2 and found that their experimental results are correctly described by summing the two single rates.

In our previous work on the gasification of HHR-chars and LHR-chars at 900°, we found that regardless of the pyrolysis conditions, and for various CO_2 + H_2O concentrations in the gasification medium, that the char reactivity in mixed atmospheres can be fairly described by summing the single reactivities obtained respectively under H_2O and CO_2 [154].

The main results on biomass char gasification in mixed atmospheres of CO_2 and H_2O as discussed before are summarized in table 6.1.

Study on mixed atmosphere gasification of chars originating from coal or lignite are more numerous than those performed on biomass chars. It is of great interest to refer to them as the chars have several common features, but without forgetting that they are not identical to avoid hasty conclusions and non reliable comparisons. For instance, Liliedahl and Sjostrom [138] studied the gasification of finely ground lignite char samples of 0.5-1 g in a thermo-balance at atmospheric and elevated pressures, at temperatures between 750 and 850°C, using a number of CO-CO_2-H_2O-Ar mixtures. The authors found that the mixed atmosphere char gasification reactivity can be modelled following a common active sites reaction mechanism.

Roberts and Harris [139] performed a comparative study on the gasification of a charcoal in single atmospheres of H_2O and CO_2 and in a mixture of the two gases. In a mixed atmosphere, the char conversion rate decreased comparatively with that obtained in a pure steam gasification medium which led the authors to conclude on the inhibiting effect of CO_2 on the steam-gasification reaction. They proposed the model bellow assuming that there is a competition between steam

Table 6.1: Literature review on biomass chars gasification in mixed atmospheres of CO_2 and H_2O

Reference	Char	Pyrolysis conditions	Mixed atmosphere mechanism
[104]	Wood char (4 cm)		Same activation energy and dependance on the sum of partial pressure
[134]	Birch wood char (45-63 μm)	Slow pyrolysis 24°C/min	Competition
[103]	Pine wood char (5.5 mm)	Medium rate pyrolysis in a screw reactor at 60°C/s	Synergy
[8]	Various biomasses	Slow pyrolysis 10°C/min	Synergy
[136]	Dried Sewage sludge char (1.2 mm)	Fast pyrolysis in FBR	Additivity
[137]	Olive tree prunning char (1.9 mm)	Fast pyrolysis in FBR	Additivity
[154]	Beech wood char (1 mm)	Fast pyrolysis 100°C/s Slow pyrolysis 5°C/min	Additivity

and carbon dioxide for the same surface reaction sites. The authors made the assumption that the CO_2-carbon gasification reaction rate is so low that the reduction in the available surface area by adsorbed C(O) species from the CO_2 reaction is likely behind the decrease in steam gasification reaction upon addition of CO_2. These conclusions are nonetheless hasty as they were drawn for a 0-10% char conversion level. The carbon dioxide seems to inhibit the steam-carbon reaction in the earlier stage of gasification, yet there is a lack of evidences to conclude on a permanent inhibiting effect throughout the gasification reaction.

Everson et al [140] also investigated the effect of a mixture of carbon dioxide and steam on the gasification of char-coals. Firstly, they conduct gasification experiments in binary gas mixtures (H_2O+H_2 and CO_2+CO) for the determination of the rate constants. The gasification reaction was best described with the assumption that the reactions occurred on separate sites.

More recently, Huang et al [141] carried the same gasification experiments as Everson et al. They determined the different gasification constants by studying the char gasification with binary gas mixtures H_2O+H_2 and CO_2+CO. Experiments with multi-component gasifying mixtures (H_2O + H_2 + CO_2 + CO) were also carried out showing results that fit well with the "separate reactive sites" reaction model given above. The comparison was based on the char reactivity at the conversion level of 50%. The calculated predictions according to the model were very close to the experimental values.

The assumption of reaction on separate active sites was also held by Tay H.L et al [41] for coal char gasification. The authors performed gasification experiments at 800°C with different gasification atmospheres (15 % H_2O balanced with Ar; 4000 ppm O_2 balanced with CO_2; 4000 ppm O_2, 15 % H_2O balanced with CO_2) and gasification holding times. Char conversion rate calculations show that the degree of char conversion during the gasification in an O_2 + H_2O + CO_2 mixture was approximately equal to the sum of those during the gasification in 15% H_2O (balanced with argon) and in O_2 + CO_2 mixture. They suggest that the additivity in char conversion means that O_2, H_2O and CO_2 do not compete for the same active sites on the coal/char.

More recently, Chao Chen et al [142] investigated the effect of the pyrolysis conditions on the gasification reactivity of lignite chars in mixtures of H_2O + CO_2. Two kinds of char were prepared from a lignite by fast pyrolysis using a drop tube furnace and by slow pyrolysis using a fixed-bed

furnace at the temperature of 1273 K. Char gasification reaction with CO_2, H_2O and their mixtures were performed in a thermogravimetric analyser (TGA) system. The gasification rate equations derived from TGA were afterwards validated by fluidized-bed gasification experiments. The authors found that both fast-chars and slow-chars were dense. The shrinking core model was able to predict both gasification of fast-char and slow-char, which means that the reaction occurs mainly in the external surface. The authors found that the char gasification rate in the mixtures of CO_2 and H_2O was lower than the sum of the two single reaction rates, but higher than the rate of each independent reaction, for both fast-char and slow-char gasification. The gasification rate in mixture of H_2O and CO_2 was linearly dependant on the CO_2 single gasification rate. The gasification rate in mixtures of both gases could be written as a linear combination of the two single gasification rates. The regressed coefficient of $R_{(CO_2)}$ is about 0.65 and the coefficient of $R_{(H_2O)}$ is about 1 for both fast-char gasification and slow-char gasification. Both of the results from the TGA and the fluidized-bed reactor showed that char-H_2O reaction was independent on char-CO_2 reaction, while char-CO_2 reaction was inhibited by char-H_2O reaction.

Umemoto et al [143] studied the coal gasification reaction in mixed atmospheres of CO_2 and H_2O. The coal chars were prepared in a drop tube furnace at 1673 K. The authors performed gasification reaction in a TG apparatus. They found that the gasification reaction rate in mixed atmospheres was neither well described by a model were the H_2O and CO_2 react on separate active sites (the model over-predicted the experimental data), nor by a common active sites model as it under-predicted the gasification rate. The authors proposed that the two reactant, H_2O and CO_2, share partially their respective active sites. The authors modified the LH expression for the chemical reaction rate term proposed by Everson et al and introduced new parameters to account for the sharing of the active sites. The authors found the greater contribution to the char gasification was from the steam gasification reaction. They think that this fact is due to the lower molecular size of the H_2O molecule which can penetrate in all the pores.

Bai et al [144] studied recently the char coal gasification reactivity with CO_2, H_2O and their mixtures. The coal samples were pyrolyzed under an argon atmosphere at temperatures of 800°C, 900°C, 1000°C and 1100°C adopting slow pyrolysis operating conditions. Then gasified isothermally in CO_2 and H_2O environments ranging from pure CO_2 to pure H_2O in 20 vol% increments. The authors found that at temperatures of 900°C, 1000°C and 1100°C, the coal char has a maximum reactivity in a 100% H_2O atmosphere. Its reactivity decreases with CO_2 addition. However, at a temperature of 800°C, the coal char has a higher reactivity in a mixed atmosphere than in pure H_2O or pure CO_2. Evenmore, the reactivity in mixed atmosphere of CO_2 and H_2O was higher than the individual reactivities in H_2O and CO_2 respectively. The same results were obtained at 750°C. The mixed atmosphere gasification showed competition beyond 800°C and synergy at 800°C and below [144]. These differences were found to be linked to catalytic effects due to calcium species.

The main results on coal and lignite char gasification in complex atmospheres are summurized in table 6.2.

As reported in tables 6.1 and 6.2, mixed atmosphere gasification reactions were tested for various biomasses and coal chars with various particle size going from several tenth of millimetre to several millimetres. The char preparation conditions as well as the gasification temperature and gas pressure were different from a study to another. The mechanisms proposed for the mixed atmosphere gasification also differ from a study to another. These observations mean that the validity of a mechanism (additivity, competition or synergy) depends on the experimental conditions as well as on the nature of the char.

One ambiguous issue is still non well clarified is the issue of intrinsic conditions. In fact, the size of a char particle and the reaction temperature are determining factors in whether the gasification rate is controlled by the rate of chemical reactions, heat and mass transfer or both of them. It

Table 6.2: Literature review lignite and coal chars gasification in complex atmospheres

References	Fuel type	Pyrolysis	Mixed atmosphere mechanism
[138]	lignite char (200-900 μm)	Slow pyrolysis	Competition
[139]	coal char (600 μm)	Slow pyrolysis 10°C/min	Competition
[140]	coal char (20-70 μm)	Slow pyrolysis 20°C/min	Additivity
[141]	coal char (20 μm)	Fast pyrolysis in FBR 1000°C/s at 840°C	Additivity
[41]	Coal char (63-150 μm)	Fast pyrolysis in FBR at 800°C	Additivity
[142]	lignite char (70-106 μm)	Slow pyrolysis 10°C/min Fast pyrolysis in FBR at 800°C	Competition
[143]	Coal char (40 μm)	Fast pyrolysis in DTF at 1400°C	Competition
[144]	Coal char (125 μm)	Slow pyrolysis 10°C/min	Synergy below 800°C and inhibition beyond

is acknowledged that the smaller is the particle the more uniform is the gas concentration and temperature inside it. In the case of concentration and temperature uniformity inside the char particle, gasification would be chemically-controlled and heat and mass transfer limitations would not influence the reaction rate. Increasing the char particle size introduces heat and mass transfer limitations, until reaching a critical size above which heat and mass transfer limitations predominate. In several studies [57], [74], authors pointed out that biomass apparent reactivity decreases when increasing the particle size, which is due to an increasing diffusional resistance.

Many authors propose a maximal particle size below which the gasification rate is constant and is consequently performed in the chemical regime, however the values are quite disparate from a study to another. For instance, Mermoud et al proposed 1 mm as a critical size below which char steam gasification is chemically-controlled at 900°C [75]. Van De Steene et al [77] found that the particle thickness was the characteristic dimension for parallelepiped shape pine char. They also found that for particle thickness below 2.5 mm, the char steam gasification is chemically controlled at 900°C. Gomez Barea et al [57] found that the CO_2 gasification reaction of char from pressed-oil stone is chemically controlled for powder char particles of 0.06 mm, in a temperature range of 800 to 950 °C which is quite different from the values given above. Klose et al. proposed that H_2O-char and CO_2-char gasification reactions are performed in the intrinsic regime for particle size below 0.125 mm in a temperature range of 750 to 780 °C and 10 mg of sample mass. Isothermal gasification experiments were done in a thermogravimetric apparatus [55].

This variety of statement about intrinsic conditions shows well that it is quite difficult to state with insurance on the nature of the gasification regime. It depends highly on the experimental conditions as well as on the texture of char. This issue will be discussed in the frame of the present work. The first aim of the present work is to provide data on char reactivity to H_2O, CO_2 and their mixture in practical gasification operating conditions. We aim also to evaluate the extent of diffusional limitations when varying the temperature and particle size. The aim is also to shed light on the influence of temperature and char particle size on the multi-components gasification reaction with CO_2 and H_2O.

6.2 Material methods

6.2.1 Low Heating-rate char preparation

The raw biomass samples are beech wood spheres of a 20 mm diameter. Proximate and ultimate analysis of the wood samples are given in table 6.3. Low Heating-rate chars were prepared by a slow pyrolysis of the wood spheres under nitrogen. The pyrolysis was performed in a batch reactor. The wood spheres were placed in a metallic plateau, spaced enough to avoid chemical and thermal interactions. The plateau was introduced in the furnace heated zone which was progressively heated under nitrogen from room temperature to 900°C at 5°C/min. The chars were kept for 1 h at the final temperature, cooled under nitrogen and stored afterwards in a sealed container. The low heating rate is expected to ensure a good temperature uniformity in the wood particle and to lead to a quite homogeneous wood-char, from the structural and chemical viewpoints, as demonstrated by [92] and pointed out by [78] and [80]. During the pyrolysis reaction, the char particles shrink and get an ovoid form. The mean particle diameter, calculated as the average of the three particle dimensions was estimated at 13 mm.

Table 6.3: Proximate and ultimate analysis of the beech wood-chips (% dry basis)

Proximate analysis			**Ultimate analysis**			
VM	Ash	FC	C	H	O	N
88.1	0.4	11.5	46.1	5.5	47.9	0.1

Some of the 13 mm char particles were afterwards ground with a mortar and a pillar. Several particle size fractions, on a wide particle size range from 0.04 mm to 13 mm, were retained for gasification experiments: char particles of 0.04 mm (char004), 0.2 mm (char02), 0.35 mm (char035) and 1 mm (char1) screen size. Char particles of 5 mm characteristic length and 1 to 2 mm thickness (char5), and finally the 13 mm (char13) char particles.

To ensure of the chemical and structural homogeneity inside the 13 mm char particle, the char structure and chemical composition were analysed at three location: at the surface, at half the distance from the centre and at the centre. Elemental composition and Raman spectroscopy were used to check the particle homogeneity. Raman spectra of the chars were recorded with a WITec Confocal Raman Microscope (WITec alpha300 R, Ulm, Germany) equipped with a Nd-YAG excitation laser at 532 nm. Table 6.4 shows the mean elemental composition of the char sample at the three locations (surface, half distance from the core and particle core). The standard deviation are quite low showing the chemical composition homogeneity through the char particle.

Table 6.4: Ultimate analysis of the wood-char samples

C (wt.%)	H (wt.%)	O (wt.%) (by difference)	N (wt.%)	Ash (wt.%)
90.83± 0.93	0.676±0.07	7.03	0.21± 0.027	1.25±0.13

Normalized Raman spectra with respect to the G peak height are shown in figure 6.1.a. The normalized Raman signals are identical at the three locations attesting of the structural homogeneity of the char particles. The Raman spectra show in the first order region (800-2000 cm^{-1}), two main broad and overlapping peaks with maximum intensities at 1350 cm^{-1} and 1590 cm^{-1} [43]. In the literature, we frequently refer to these two peaks as respectively the D and G bands. Deconvolution of the Raman signal into five bands corresponding to five carbon structures composing the char show that the prepared char contains an amorphous phase (D3 band). D3 band area decreases as the carbon gets ordered at higher temperatures. The D3 band is typical of disordered carbonaceous

materials like coke, coal and biomass chars. These results are in accordance with those of [92] who evidenced the large char particle homogeneity when prepared in low heating rate conditions.

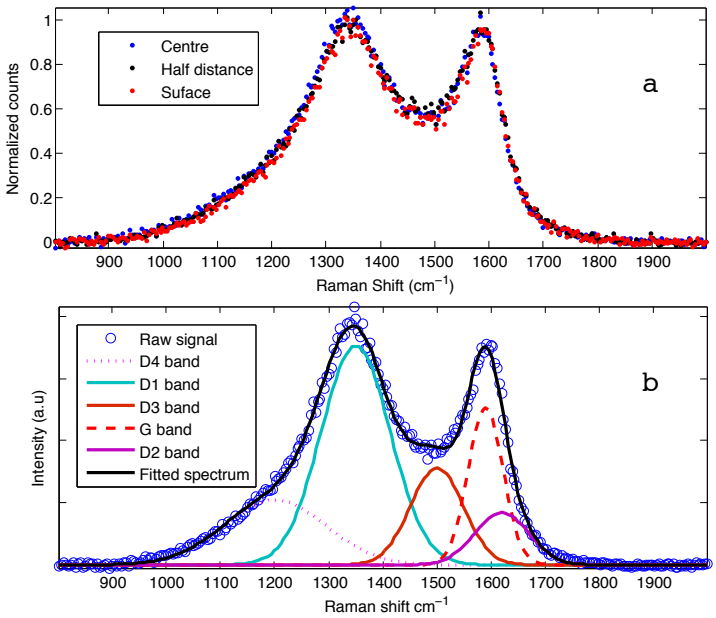

Figure 6.1: Normalized Raman spectra (a) of the parent char at three locations of the particle(surface, half distance from the core and particle core) and spectrum deconvolution (b)

6.2.2 Char gasification experiments in H_2O, CO_2 and their mixture

The Macro-TG experimental device and procedure

The M-TG device is described in detail in our previous work on char gasification in mixed atmospheres of CO_2 and H_2O [154]. In general terms, the experimental apparatus consists of a 2-m long, 75-mm i.d. alumina reactor that is electrically heated, and a weighing system comprising an electronic scale having an accuracy of $\pm$ 0.1 mg, a metallic stand placed over the scale on which a 1 m long, 2.4 mm external diameter hollow ceramic tubes is fixed. The ceramic tube hold the platinum basket in which the biomass particles are placed. The gas flow rates are controlled by means of mass flow-meters/controllers. The gas flow inside the reactor is laminar and flowing at an average velocity of 0.20 m/s.

Gasification of char004 and char02

Char004 and char02 are in the form of powders. A char mass of 100 to 130 mg is spread-out on the whole surface of the 50 mm diameter platinum basket in the form of a very thin layer. The char mass may seems important compared to what is introduced in classical TG devices but the surface of the crucible is large enough (0.002 m^2) to allow spreading this mass in the form of a thin layer. The char is directly exposed to the surrounding atmosphere as the platinum basket is simply in the form of a circular plane without any side wall.

Gasification of char035, char1, char5 and char13

Char035 and those of greater size can be distinguished and placed individually. The char particles are spread over the platinum basket and spaced enough to avoid thermal and chemical interaction.

Table 6.5: Char gasification experiments

Samples	CO_2 gasification	H_2O gasification	Mixed atmospheres	Gas alternation
Char004	900°C 0.2 atm	900°C 0.2 atm	- -	- -
Char02	850-900-950 1000-1100 °C 0.2 atm	800-850-900 1000-1100 °C 0.2 atm	900°C 0.2 + 0.2 atm -	900°C 0.2 / 0.2 atm -
Char035	900°C 0.2 atm	900°C 0.2 atm	- -	- -
Char1	900°C 0.2 atm	900°C 0.2 atm	- -	- -
Char5	900°C 0.2 atm	900°C 0.2 atm	900°C 0.2 + 0.2 atm	- -
Char13	900°C 0.2 atm	900°C 0.2 atm	900°C 0.2 + 0.2 atm	900°C 0.2 / 0.2 atm

For the char sample char035, char1 and char5, about 20 to 40 particles are spread on the platinum basket. For the char13 samples, 2 particles are placed in the platinum support for a total mass of nearly 1.2 g.

The gasification procedure

The platinum support containing the char is introduced in the furnace under a nitrogen flow. The char is kept 5 min under nitrogen before starting the gasification. During this period the char loses mass, probably in the form of water vapour and light gases which are released due to the thermal shock. The mass loss was less than 6%. This period is sufficient for the establishment of a thermal equilibrium between the weighing system, the furnace and the surrounding gases. Afterwards, the gasification medium is introduced. The char gasification experiments were performed with CO_2, H_2O and their mixtures.

Operating conditions

The operating conditions in terms of temperature and atmosphere composition for the different char gasification reactions including single atmosphere gasification reactions, mixed atmosphere gasification and gas alternation experiments are listed in table 6.5.

Theoretical modelling of the single atmosphere gasification reactions

The char apparent reactivity towards a gas can be expressed following:

$$R(X)^{app} = \frac{1}{1 - X_{(t)}} \times \frac{dX_{(t)}}{dt} \tag{6.7}$$

Where X is the conversion level given by:

$$X_{(t)} = \frac{m_0 - m_{(t)}}{m_0 - m_{ash}} \tag{6.8}$$

Where m_0, m_t and m_{ash} are respectively the initial mass of char, the mass at a time t and the mass of the residual ash. If the gasification reaction is performed in the chemical regime (relatively

low temperature and small particle size), the calculated reactivity would be the intrinsic one. As stated above, the char reactivity depends on the operating conditions (temperature and reactant gas pressure), and char properties (texture, mineral content, structure). It is thus commonly expressed as the product of a reference reactivity $R(Xref)_{(T,P_i)}$(depending on the temperature and reactant gas pressure) and a structural term $f(X)$ accounting for the char properties evolution along the conversion. Owing to the difficulties in the monitoring of the intrinsic char properties along the conversion, the structural term is usually an empirical correlation where the conversion level appears as the sole variable. Changes in the char intrinsic properties are implicitly described by this empirical term. The reference reactivity corresponds to a specific conversion level. Reference reactivity at 10% or 50% of conversion have been used in the literature [57] [99] [100]. The reactivity at 50% conversion level R(50) is the most frequently used as a reference value. The reactivity at any gasification stage can be thus expressed as:

$$R(X)^{int}_{(T,P_i)} = R(50)^{int}_{(T,P_i)} f(X) \tag{6.9}$$

Where $R(50)^{int}_{(T,P_i)}$ is the intrinsic reactivity at X=50% and $f(X)$ is the structural function expression describing the evolution of the char properties during the gasification.

nth-order kinetics are often used to express the temperature and CO_2 pressure dependence of $R(50)^{int}_{(T,P_i)}$ By assuming an Arrhenius-type kinetics for the kinetic constant, the intrinsic reactivity can have the following expression:

$$R(50)^{int}_{(T,P_i)} = M_C \, S_r \, k_{(T)} \, P_g^n \tag{6.10}$$

Where M_C is the carbon molecular weight, S_r is the reactive surface ($m^2.kg^{-1}$), $k_{(T)}$ the kinetic rate constant of char gasification ($mol.s^{-1}.m^{-2}.atm^{-n}$) and P_g the reacting gas partial pressure at the particle surface(atm)

$k_{(T)}$ is expressed following an Arrhenius-type law:

$$k_{(T)} = A exp \frac{-E}{RT} \tag{6.11}$$

Where A is the pre-exponential factor ($mol.s^{-1}.m^{-2}.atm^{-n}$), E is the char gasification activation energy (J/mol), R is the universal gas constant ($J/(mol.K)$) and T is the temperature (K).

For macroscopic char particles, there exist diffusional limitations [57]. One can no longer speak about a volumetric reaction rate (intrinsic) as the gas concentration inside the particle is not uniform. In this kind of situation there is a competition between gas diffusion and reaction inside the char particle. To model such a situation, one must solve the gas mass and energy conservation equations along the reaction to obtain the gas concentration profiles at any time and any location in the particle [74]. Although it is rigorous, numerical modelling requires too high computing capacities. There exist alternative methods for formulating the apparent gasification reaction rate. The simplest method is using the pseudo-activation energy which changes with temperature. However, this method cannot express the effect of the particle size and is poorly describing the physical phenomena. The evolution of the gasification rate with particle size can be described through a semi-empirical expression, where the apparent reaction rate is expressed as a function of the intrinsic reaction rate and the particle size [105]. The third method consists in the effectiveness factor approach to take into account the diffusion-reaction competition [110] [112] [113] [108]. We will use this method in the present work to account for diffusional limitations when varying the char particle size or temperature.

The effectiveness factor approach originates from the catalyst theory. In the presence of diffusion-reaction competition, Thiele [114] defined an effectiveness factor η which is the ratio of the apparent reaction rate to the intrinsic one. It allows to take into account the consumption of the reactant gas

while it diffuses inside the porous particle. It is equal to unity in the absence of diffusional limitations and tends toward zero in the presence of high diffusional limitations. Using the effectiveness factor, the apparent reactivity reads:

$$R(50)^{app}_{(T,P_i)} = \eta\, R(50)^{int}_{(T,P_i)} \tag{6.12}$$

With η being the Thiele effectiveness factor.

Reaction order of biomass char gasification differs from a study to another. In Di Blasi's review, CO_2 char gasification reaction order varies between 0.36 and 1.2. That of H_2O char gasification is comprised between 0.4 and 1 [14]. When using the effectiveness factor approach to model the effect of LHR char gasification, we will consider the gasification reactions as first order reactions. The definition of the effectiveness factor is rigorous only for a first order reaction. The effectiveness factor expression is obtained by volume integration of the reactant gas balance equation and has the following expression for spherical particles:

$$\eta = \frac{3}{\phi}\,(\frac{1}{tanh\phi} - \frac{1}{\phi}) \tag{6.13}$$

The Thiele modulus ϕ has the following expression:

$$\phi = \frac{d_{part}}{2}\sqrt{\frac{\beta\, S_v\, k_{(T)}\, P_g}{M_g\, Di_{eff} C_g}} \tag{6.14}$$

Where d_{part} is the particle diameter (m), β is a stoichiometric coefficient equal to ratio between the gas molar mass and that of carbon, S_v is a volumetric surface (m^2/m^3), M_g is the molecular weight of the reactant gas $(kg.mol^{-1})$, C_g the bulk concentration of the reactant gas$(mol.m^{-3})$, Di_{eff} is the effective diffusion coefficient (m^2/s).

For a gas "i" (CO_2 or H_2O), Di_{eff} is expressed through the the molecular diffusion coefficient Di_{mol} and the Knudsen diffusion coefficient $Di_{Knudsen}$:

$$Di_{eff} = \frac{1}{\frac{1}{D_{Knudsen}} + \frac{1}{Di_{mol}}} \tag{6.15}$$

$$Di_{mol} = a_i\, 10^{-5}\left(\frac{T}{298}\right)^{1.75} \tag{6.16}$$

$$Di_{Knudsen} = \frac{\epsilon}{\tau} 0.97 \frac{d_{pore}}{2}\left(\frac{T}{M_i}\right)^{0.5} \tag{6.17}$$

Where a_i is a constant taken to 1.67 for CO_2 and 2.1 for H_2O [113], d_{pore} is the pore diameter (m), ϵ is the char porosity and τ is the char tortuosity

Several authors used the effectiveness factor approach to model the char combustion and gasification reaction for different temperature and particle size [115] [57] [110] [108] [116] [97] [113]. The effectiveness approach render the calculation of the char reactivity straightforward. Despite it does not gather all the physics of the gasification reaction, it is a simple method allowing to predict the char apparent reactivity without enormous computational effort.

Modelling procedure

At 50% of conversion we adopted a char porosity of 0.95, a tortuosity of 3 and an apparent density of $250(kg/m^3)$ (the initial density after pyrolysis is around $500(kg/m^3)$). We measured the Total Surface Area of char02 at X=0.5 by N_2 adsorption at 77 K. The values were 1230 (m^2/g) for H_2O

gasification and 840 (m^2/g) for the CO_2 gasification. We used these values for the parameter S_r as well as in the calculation of S_v which is the product of S_r by the apparent density.

In the Thiele modulus expression, there are three unknown parameters that will be determined by best fitting the model to the experimental data. These parameters are d_{pore} in the effective diffusivity expression, A and E in the rate constant expression. d_{pore} and k_{900} are determined first by fitting the experimental R(50) data obtained at 900°C for char004, char02, char035, char1 and char13 with the model. A and E are afterwards determined by best fitting the experimental R(50) data obtained for the char02 at different temperatures: 800°C, 850°C, and 900°C for H_2O gasification, and 850°C, 900°C, 950°C and 1000°C for CO_2 gasification.

d_{pore}, A and E are determined by the minimisation of the following objective function:

$$OF = \sum_{j=1}^{n} (R(50)_j^{model} - R(50)_j^{exp})^2 \tag{6.18}$$

Mixed atmosphere gasification reaction modelling

In the present work, we propose to model the mixed atmosphere reactivity as a linear combination of the single reactivities with CO_2 and H_2O following:

$$R(mix) = \alpha\, R_{(H_2O)} + \beta\, R_{(CO_2)} \tag{6.19}$$

In the case of passive cooperation, the char reactivity in mixed atmosphere is equal to the sum of the individual reactivities, and α and β would be both equal to 1. In the case where the two gases compete for the same active sites, the global reactivity is lower than the sum of the individual ones. α and β would vary between 0 and 1 without reaching both the unity (case of passive cooperation). If α or β equals zero, only one gas is operating while the other is a spectator. Intermediate values depict the contribution of the gases to the global reaction. If there is a synergy, the global reactivity is higher than the sum of the individual ones. One or both coefficients will be higher than 1.

In the present work, we study the variation of these coefficients with the temperature (800°C, 900°C, 1000°C and 1100°C) for the 0.2 mm size particles, as well as the variation with the char particle size considering the char02, char5 and char13 samples gasification at 900°C.

α and β are determined by the minimisation of the following objective function:

$$OF = \sum_{j=1}^{n} (R(mix)_j^{model} - R(mix)_j^{exp})^2 \tag{6.20}$$

This approach assumes that the contributions of H_2O and CO_2 gasification reactions are constant along the reaction.

6.3 Results and discussion

6.3.1 Effects of particle size on the char gasification reactivity in single atmospheres of H_2O and CO_2

Figure 6.2 shows the influence of particle size on the char gasification reactivity towards H_2O (a) and CO_2 (b) gasification. It can be clearly seen that the char reactivity decreases when increasing the particle size due to increasing diffusional limitations. Char02 reactivities are quite close to that of char004 for both H_2O and CO_2 gasification. This means that at 900°C and for these particle size the gasification conditions approaches the intrinsic ones. Figure 6.2 also shows that for high

conversion levels and low particle size (0.04 mm and 0.2 mm), the char reactivity shows unexpected trends. For instance, considering steam gasification, the reactivity of char004 becomes very similar to that of char02 at X=0.5 but then dropped below it. In the same way, considering CO_2 gasification, char004, char02 and char035 exhibited the same reactivity at X=0.7. The reactivity of char004 and char02 were equal for higher conversion levels while that of char02 was lower. These observations are difficult to explain as for higher conversion levels, the presence of minerals highly catalyses the gasification reaction [14] [73]. There can be loss of minerals for the smallest particles at the end of conversion which impacts on the gasification reactivity.

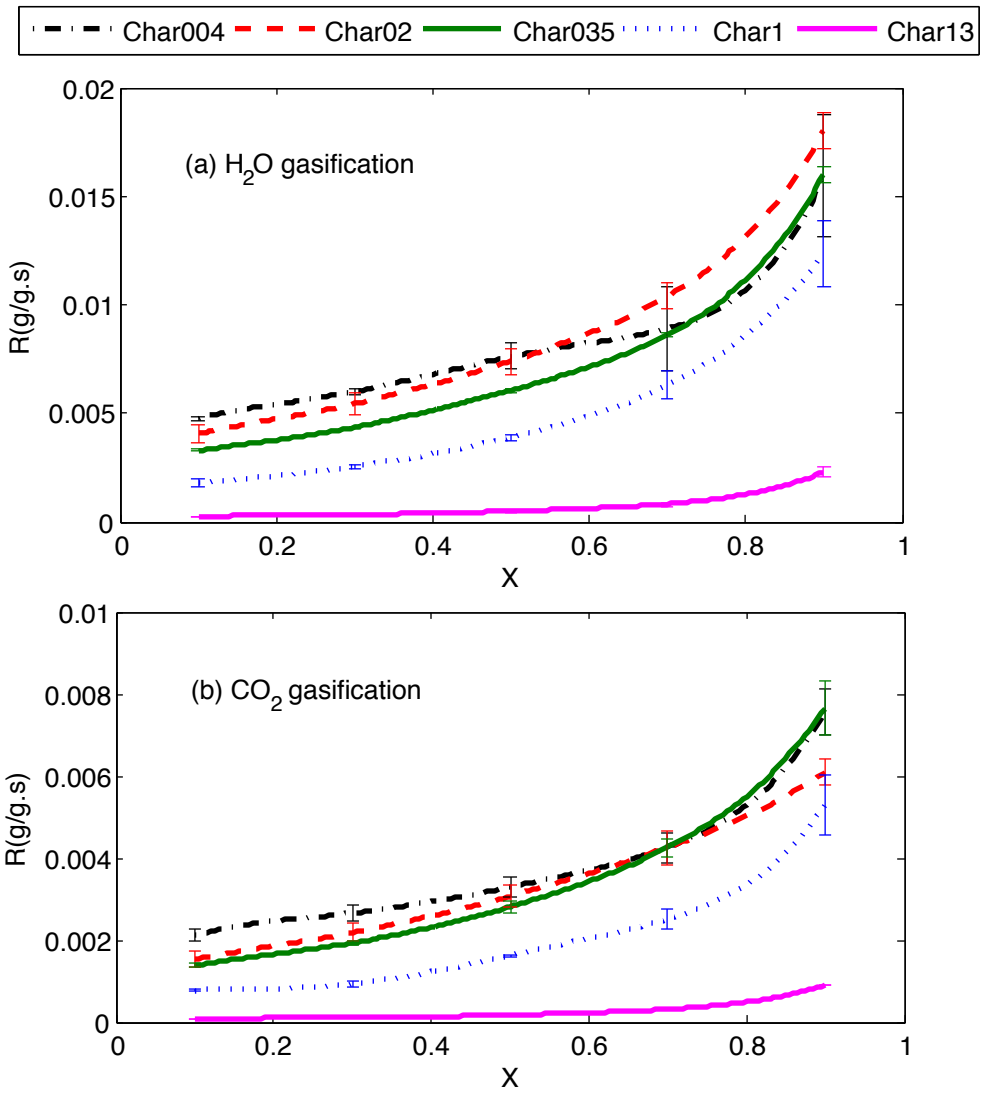

Figure 6.2: Influence of particle size on the char gasification reactivity at 900°C with 20% H_2O (a) and with 20% CO_2 (b)

The normalized R(50)for the different particle size with respect to the R(50) of char004 is illustrated in figure 6.3. A semi-log scale is adopted for a better representation. For the two gasification reactions, increasing the char particle beyond 0.04 mm induced nearly the same relative reactivity decrease.This result indicates the equivalence of the reaction-diffusion competition for the two gasification reactions. This will be discussed with more details in the next paragraphs.

Figure 6.4 shows the experimental R(50) as well as the Thiele model predictions for H_2O (a) and CO_2 (b) char gasification at 900°C. As explained above this first step allows to determine the best

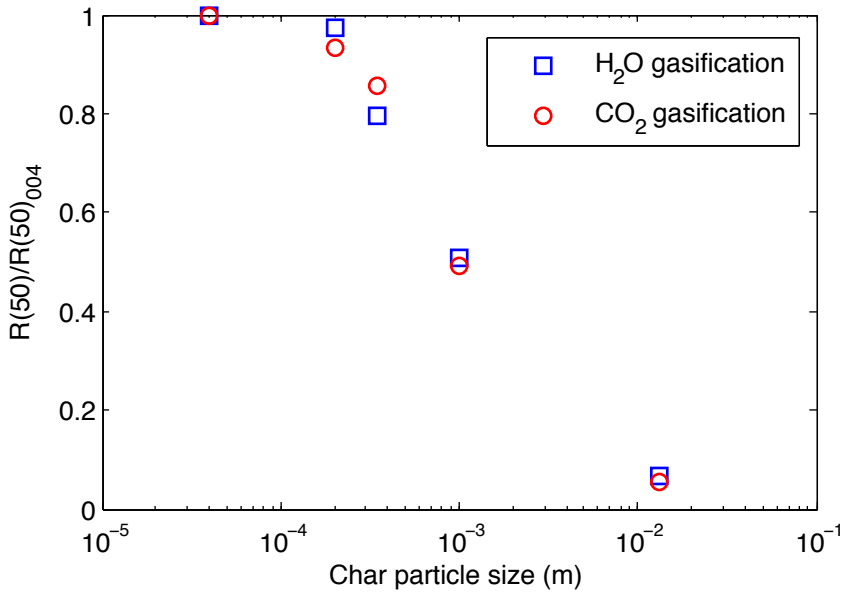

Figure 6.3: Normalized R(50) with respect to that of char004 for H_2O and CO_2 gasification

average pore diameter to fit with experimental results. For both H_2O and CO_2 gasification, the pore size for which we obtain the best fit is in the macropore size range. For H_2O gasification, we found that the best fit is given for a very high pore diameter (a value that has no physical meaning), but when plotting the sum of squared residuals between the experimental data and model prediction as a function of the pore diameter, we observed that this error is constant for pore sizes higher than 1μm. As shown on figure 6.4 fixing the pore diameter to 1μm or 5μm gives quite satisfactory results. In the case of H_2O gasification the pore size would be higher than 1μm. For CO_2 gasification, the best fit was obtained for a pore size of 1.5μm. Similarly, when plotting the sum of squared residuals between the experimental data and model prediction as a function of the pore diameter, we obtained a minimum around this value but the experimental data still well represented for pore sizes in the range of 0.5 to 5μm. This range of pores would be the most influencing during CO_2 gasification. These results mean that the gasification reactions are mainly occurring in macropores. Some authors think that the mesopores and macropores are better indicators of the char reactivity. Contribution of micropores to the active surface area is thought to be negligible compared to that of macropores and large mesopores [80]. To assess if the model captures the experimental data for other pore sizes, we fixed the pore size at some specific values: 1 nm (micropores), 30 nm (mesopores) and 1000 nm (macropores) and searched for k_{900} that allows the best fitting to the experimental results. As shown in figure 6.4, neither pore size representative of micropores nor one representative of mesopores allows to capture the experimental R(50). It can also be seen that for the char004, both gasification reactions are performed in the chemical regime. The experimental R50 points for the char004 are located in the plateau given by the model so that reducing further the char particle size will not modify the char reactivity.

Diffusional limitations increase with increasing particle size. To illustrate the extent of the diffusional limitations, we present in figure 6.5, the evolution of the effectiveness factor with the char particle size for H_2O and CO_2 gasification at 900°C. The similarity in the evolution if η with the particle size means that the reaction-diffusion competition is similar for both gasification reaction. However, H_2O is found to react and diffuse faster than CO_2 molecule which have a lower chemical reactivity and diffusivity due to its bigger molecular size. The ratio of H_2O and CO_2 reactivities is

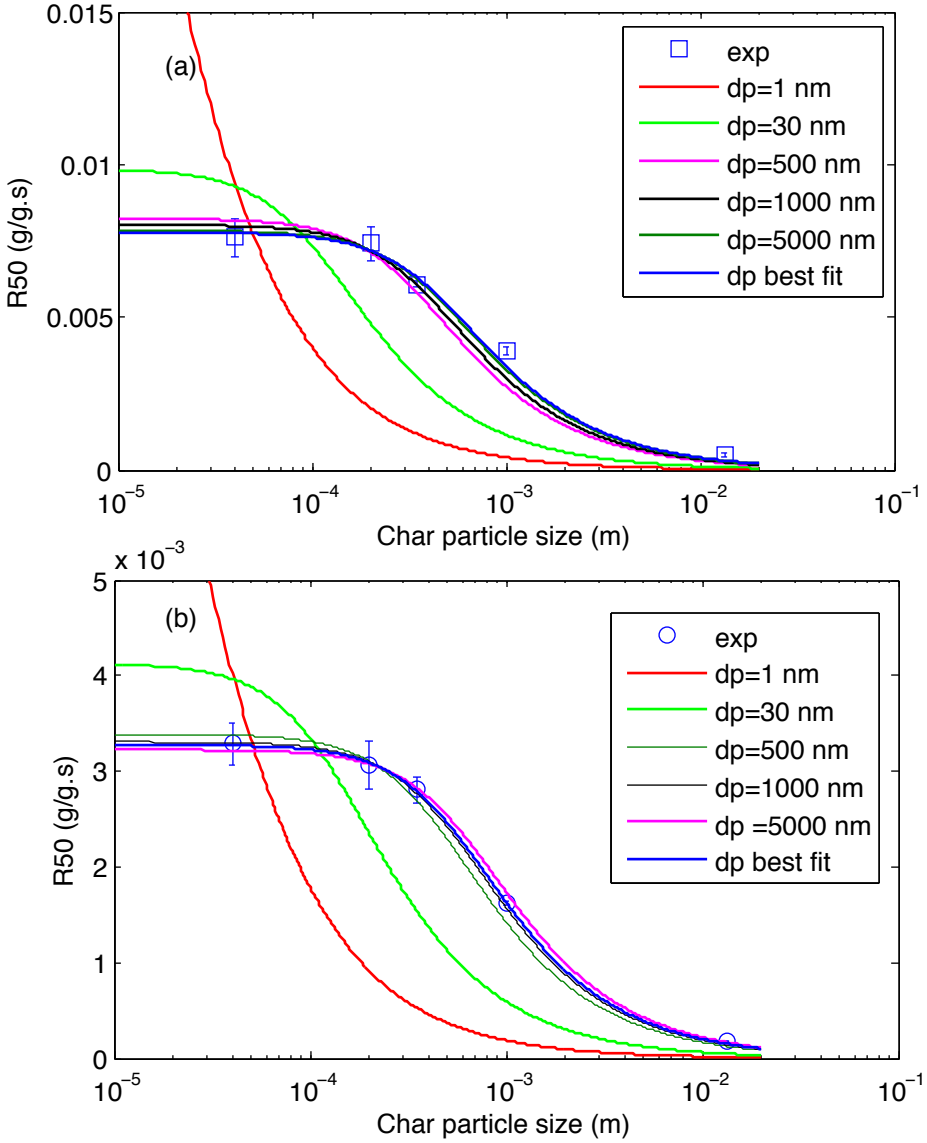

Figure 6.4: Experimental R(50) and Thiele model for H_2O (a) and CO_2 (b) char gasification at 900°C

around 2 while the effective diffusive coefficients are 5.10^{-5} m^2/s for H_2O and 3.10^{-5} m^2/s for CO_2. It can be seen on this figure that for both reactions increasing the particle size from 0.04 mm to 13 mm induced the reactivity to decrease by more than twenty folds.

The kinetic parameters, namely A and E were determined by fitting the R(50) data for the char02 with the Thiele model at various temperatures for H_2O and CO_2 gasification reactions. Arrhenius plots are shown in figure 6.6 for both reactions. The model fits quite well to the experiments. The values of A and E are given in table 6.6. They match well with the values given in Di Blasi's review on lignocellulosic biomass char gasification with CO_2 and H_2O [14]. The activation energies for both reactions are around 200 kJ/mol which is quite close to the findings of [55] who found equivalent values for beech wood-char gasification with H_2O and CO_2.

We found that for 0.2 mm particle size, both gasification reactions would be performed in the chemical regime at 800°C with η being very close to one. Diffusional limitations becomes non negligible at 900°C with an effectiveness factor around 0.92. At 1000°C, the effectiveness factors for both reactions are around 0.7 for 0.2 mm sized char particles.

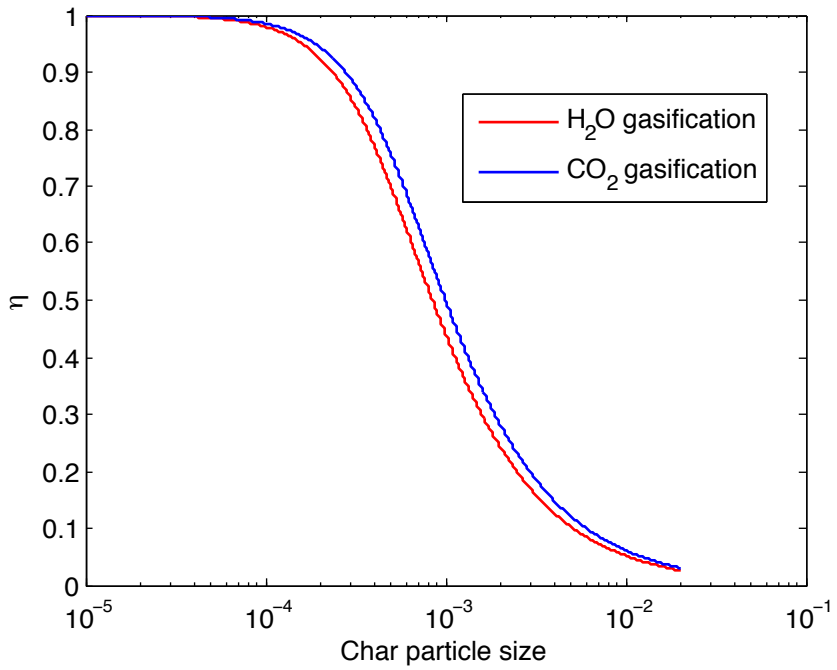

Figure 6.5: Evolution of the effectiveness factor with the char particle size for H_2O and CO_2 gasification at 900°C

Table 6.6: Kinetic parameters

	E ($kJmol^{-1}$)	A ($kg.s^{-1}.m^{-2}.atm^{-1}$)
H_2O gasification	207.95	4.16 10^3
CO_2 gasification	202.19	1.56 10^3

6.3.2 Gasification experiments in mixed atmospheres of H_2O and CO_2

Effect of temperature on the mixed atmosphere gasification

The effect of temperature on mixed atmosphere gasification was studied for char02 sample. Char02 gasification reactivities in single and mixed atmosphere of H_2O and CO_2 at 800°C, 900°C, 1000°C and 1100°C are shown in figure 6.7. It can be seen in the figure that the char reactivity towards H_2O is higher than that towards CO_2 at all temperatures, except in the very beginning of the reaction at 1100°C where the reactivity to CO_2 was a little bit higher. We think that this observation is related to morphological modifications or loss of catalysts occurring at high temperatures. With the reaction unfolding, the H_2O reactivity was higher than the CO_2 reactivity.

Concerning the mixed atmosphere gasification, we can observe that the reactivity in mixed atmosphere of 20% H_2O +20% CO_2 is higher than the reactivity towards steam. An exception is observed at 1000°C were an inhibition effect is observed. The reactivity in mixed atmosphere is lower than with steam alone but higher than that of CO_2. At 1100°C, the char reactivity at the very beginning is similar to that obtained at 1000°C. This observation can be explained by structural modifications at higher temperatures, thermal annealing by an ordering of the carbonaceous matrix and loss of functional groups constituting the active sites [183]. A reduced catalytic effect can also at the origin of this observation, as the catalytic species like *K, Ca, Mg* or *Na* may volatilize or sinter at high temperature [184]. The High temperature reaction can contribute to increase the volatility of catalytic species [185]. The 5 min soaking time at 1100°C can also induce structural and chemical

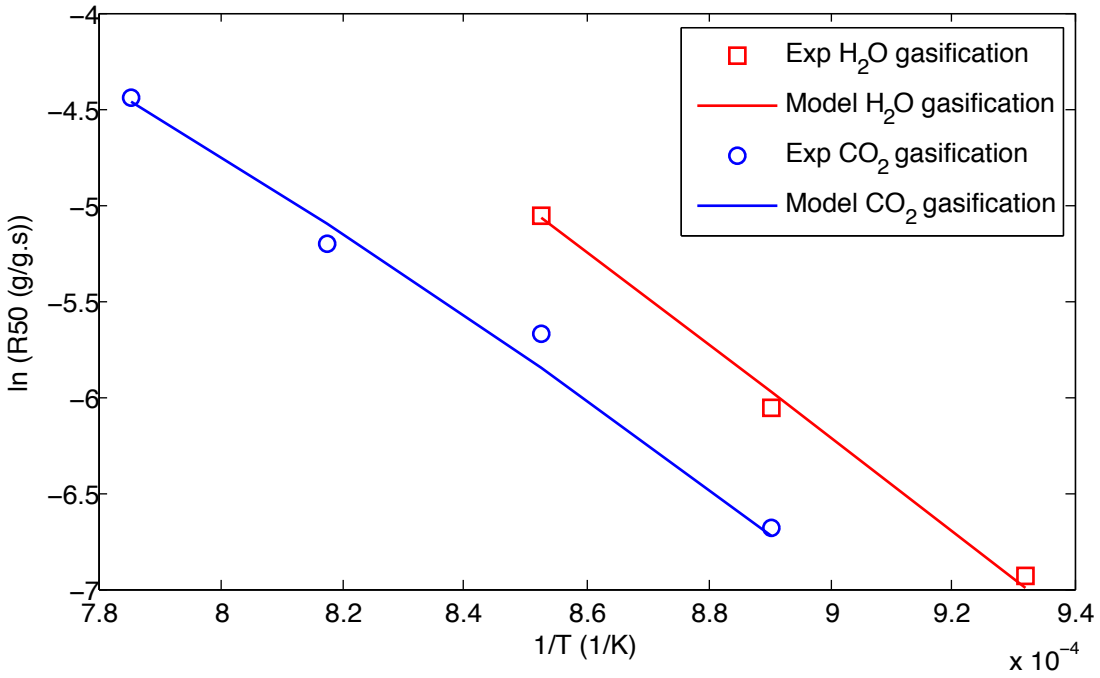

Figure 6.6: Arrehnius plots for H_2O and CO_2 gasification: experimental data and models

modifications of the char matrix, expressed in an accentuated ordering, loss of catalytic species and shrinkage. But these modifications seem to vanish with the reaction progress, by the continuous oxygenation of the char surface due to steam and Boudourad gasification reactions as well as by the porosity development with gasification.

The experiments as well as the modelling results are shown in figure 6.8. The linear combination model reproduces well the experiments. At 800°C, the gasification reaction is thought to be performed in the chemical regime as seen above. The reactivity in mixed atmosphere is fairly described by an additive law since $\alpha = \beta = 1$. In the modelling procedure, we fixed at first a lower boundary for α and β at 0 as a negative contribution would have no physical meaning. α and β were however allowed to take values beyond 1. At 900°C, the best fit was obtained for α=1.61 and β=0.11. This result means that in the presence of CO_2, the activity of H_2O in the char gasification reaction was enhanced while the contribution of CO_2 was relatively poor. At 1000°C, the tendency was reversed. The CO_2 was found to have a full contribution to the gasification reaction while the steam gasification appears to be inhibited by the presence of CO_2. The values of α and β were respectively 0.14 and 0.96. At 1100°C, there was also a competition between the two molecules, but H_2O gasification is found to be the most predominant. The values of α and β were respectively 0.96 and 0.25.

These results have to be considered with more care concerning the accuracy of the determined α and β values. In the modelling procedure, α and β that ensure the best fit to the experiments are given for lowest value of the objective function. However, there may be several combinations of α and β that may give satisfactory results. In order to check if the solutions obtained for the different temperatures are unique, we fixed manually, in a second modelling run, the value of α and searched that of β that gives the best fit to the experimental data. α was varied between 0 and 2 by a step of 0.4. The modelling results as well as the experimental results are shown in figure 6.9.

At 800°C, regardless of the combination of α and β, the modelled reactivity is found in the range of the experimental standard deviations zone. For β to remain positive, α must be in the range of 0 to 1.35 which is a quite wide range to state about the mechanism of mixed atmosphere gasification

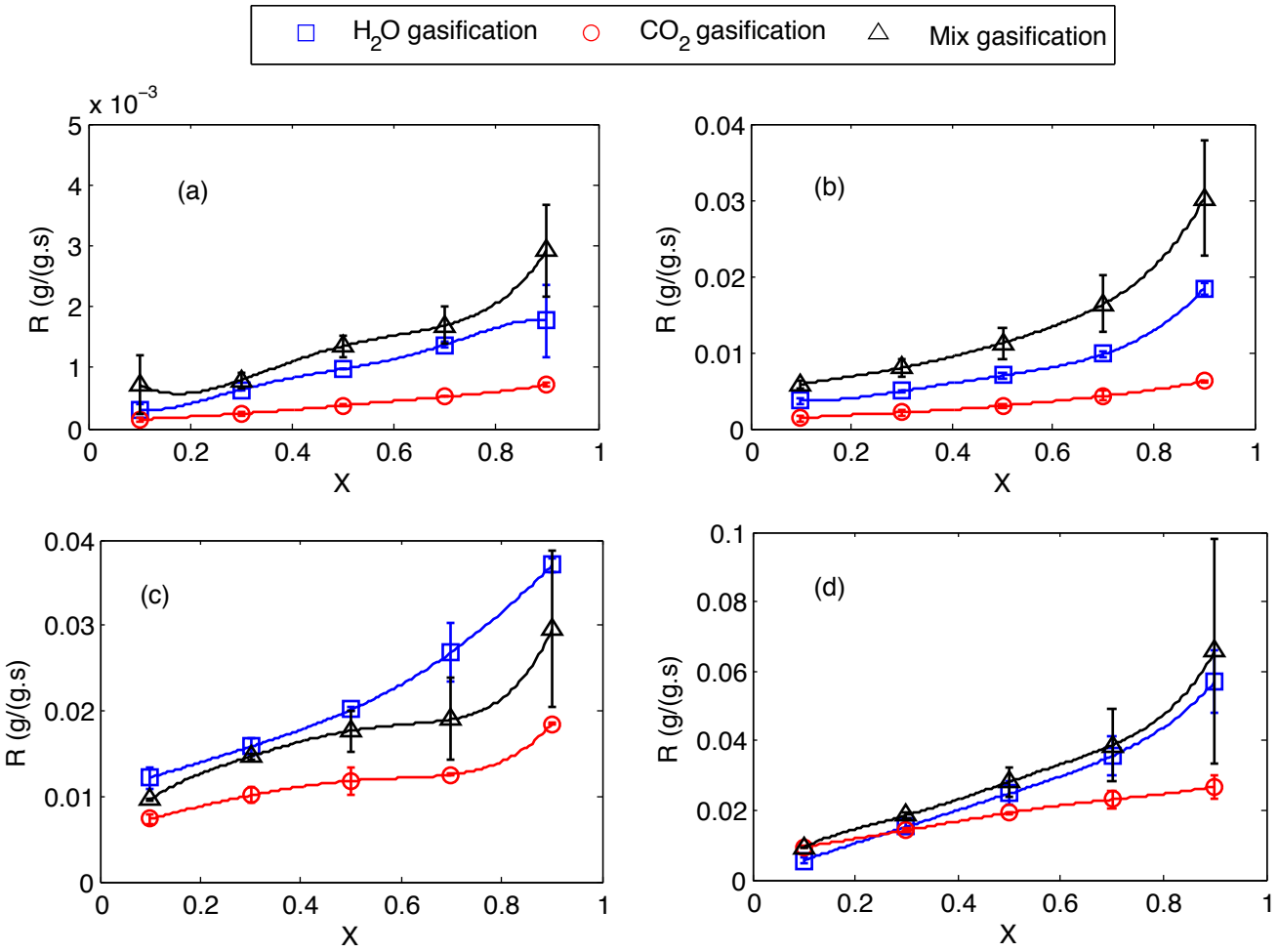

Figure 6.7: Char02 gasification reactivity in 20% H_2O, 20% CO_2 and 20% H_2O + 20% CO_2 at 800°C (a), 900°C (b), 1000°C (c) and 1100°C (d)

at 800°C. Similarly at 900°C, while α is comprised between 0 and 1.65, all combinations of α and β give satisfactory results. The reactivity curve is in the experimental standard deviations zone.

At 1000°C, the situation is a bit different as only values of α below 0.2 and beta between 1.1 and 1.5 allow to correctly describe the experimental reactivity without being out of the standard deviation zone in the conversion level range of 0 to 0.4. At 1100°C, α is found to be in the range of 0.8-1.1 with β in the range of 0 to 0.48 for the modelled reactivity to be in the standard deviation zone for levels of conversion between 0.1 and 0.3. Beyond X=0.3, all possible combination of α and β give correct predictions. These results indicate that it is not possible to state on the gasification mechanism in mixed atmosphere gasification at 800°C and 900°C as wide ranges of α and β are found to reproduce the experimental results. At 1000°C and 1100°C, the situation is a bit different as only particular α and β value give correct representations of the reactivity, yet they are limited to defined conversion ranges out of which it is not possible to define which gas is the most reacting with the char. In the literature, as seen in the introduction of the present paper, many studies state on the gasification mechanism as it is a passive cooperation from the observation that there is an additive law representing well the reactivity in mixed atmosphere. This statement has to be taken with caution regarding the results of the present studies. What appears to be an additive law may in fact be a more complex mechanism involving competition and synergy effects that result in an additive-like mechanism.

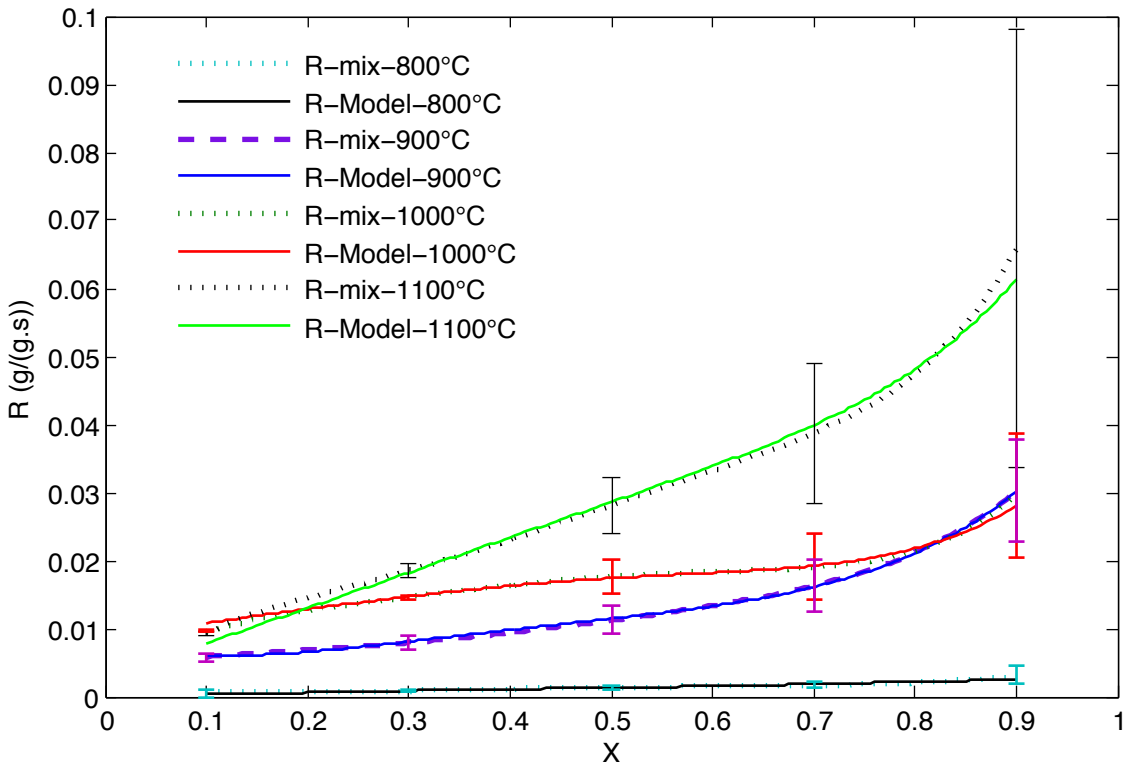

Figure 6.8: Char02 gasification reactivity in 20% H_2O, 20% CO_2 and 20% H_2O + 20% CO_2 at 800°C (a), 900°C (b), 1000°C (c) and 1100°C (d)

Effect of the char particle size on the mixed atmosphere gasification

Figure 6.10 shows the char reactivity at a temperature of 900°C, in mixed atmosphere of 20% H_2O + 20% CO_2 for the char02, char5 and char13 samples. Decrease in reactivity with size is related to mass transfer limitations as discussed previously. In figure 6.10.a, we plotted the experimental reactivities along with an additivity model for which α=β=1. As it can be seen on the figure, the additivity model represents quite fairly the char reactivity in mixed atmospheres of H_2O and CO_2. For high diffusional limitations (char13) as well as for quite low ones (char02), the mixed atmosphere char reactivity in 20% H_2O + 20% CO_2 at 900°C can be fairly considered as the sum of the individual reactivity contributions. The best fit modelling results give values for α and β different from 1. The values of α and β equal respectively 1.61 and 0.1 for char02, 1.58 and 0.1 for char5 and 0.9 and 0.8 for char13. The tow gases are likely competing for the biggest chars while H_2O seems to have an enhanced activity in the presence of CO_2 for the char02 and char5 samples. However, there exist a wide range of α/β combinations that ensure a good representation of the experimental results, so that we can not state on the contribution of each reaction to the char gasification. This modelling approach allows only to calculate the reactivity in mixed atmosphere but not to understand the gasification mechanism. Another approach is needed to go deeper on this issue.

Does the char reactivity toward H_2O changes when the char is gasified with CO_2 or vice versa?: cyclic gasification experiments

In the situation of a mixed atmosphere gasification, it's legitimate to ask if a the CO_2, for instance, interact with the active sites on the char matrix, reacts on, creates other active sites and develops further the porosity, does this modify the char reactivity towards H_2O? We have seen in our previous

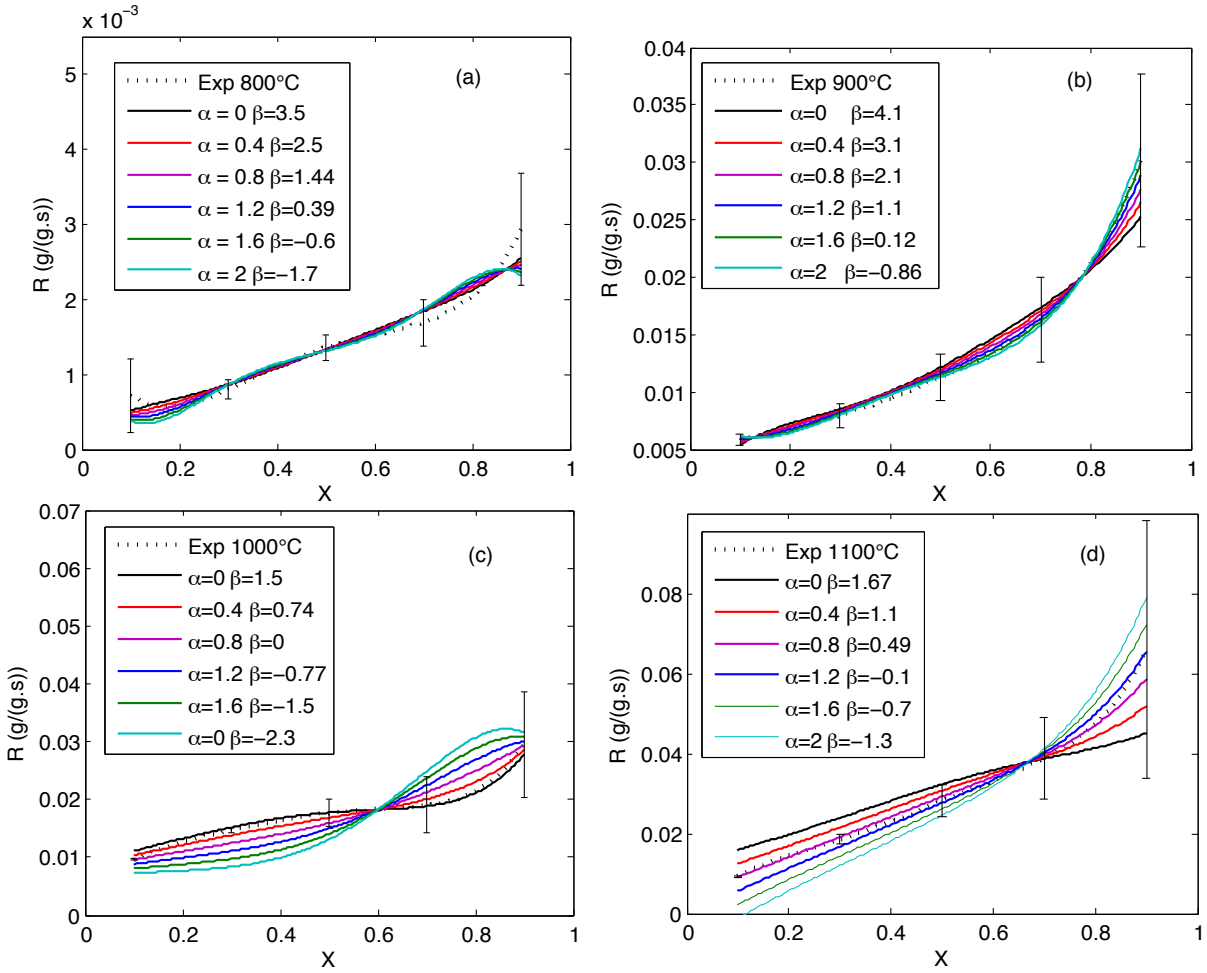

Figure 6.9: Modelled mixed atmosphere reactivities for different combination of α and β and their confrontation to the experimental results at 800°C (a), 900°C (b), 1000°C (c) and 1100°C (d)

studies [154] that for 1 mm thick chars prepared under low and high heating rate that the gasifying the char under CO_2 to a certain conversion level does not modify its reactivity towards H_2O. The same test is done for the char02 sample. These results are shown in figure 6.11.

In this figure, the reference char reactivities with CO_2 and H_2O are shown with that obtained in the gas alternation experiments. Converting the char up to 20% of conversion with CO_2 does not modify its reactivity towards H_2O. The char reactivity follows in the beginning the reference reactivity curve with CO_2, then joins that obtained in H_2O when switching the gases. The active surface complex or free carbon sites formed during CO_2 gasification would exhibit the same reactivity toward steam. Also, we have seen in the previous sections that internal transfer in macropores would be the most influencing for both gasification reactions. The macroporosity may evolve similarly under the tow gases to lead to such results. Further investigations are needed to characterise the chemical, structural and textural properties of the char during the gasification reactions under CO_2 and H_2O to elucidate such observations.

Tagutchu and al [103] found in their study that there was synergy between CO_2 and H_2O leading to a char reactivity in mixed atmosphere higher than the sum of single reactivities. The authors argued that CO_2 should create additional porosity that facilitates the H_2O access to the reactive sites and thus result in a higher reactivity. Logically, if it was the case, we would have seen an enhanced reactivity of the char toward H_2O after gasification with CO_2. This was not observed neither for 0.25

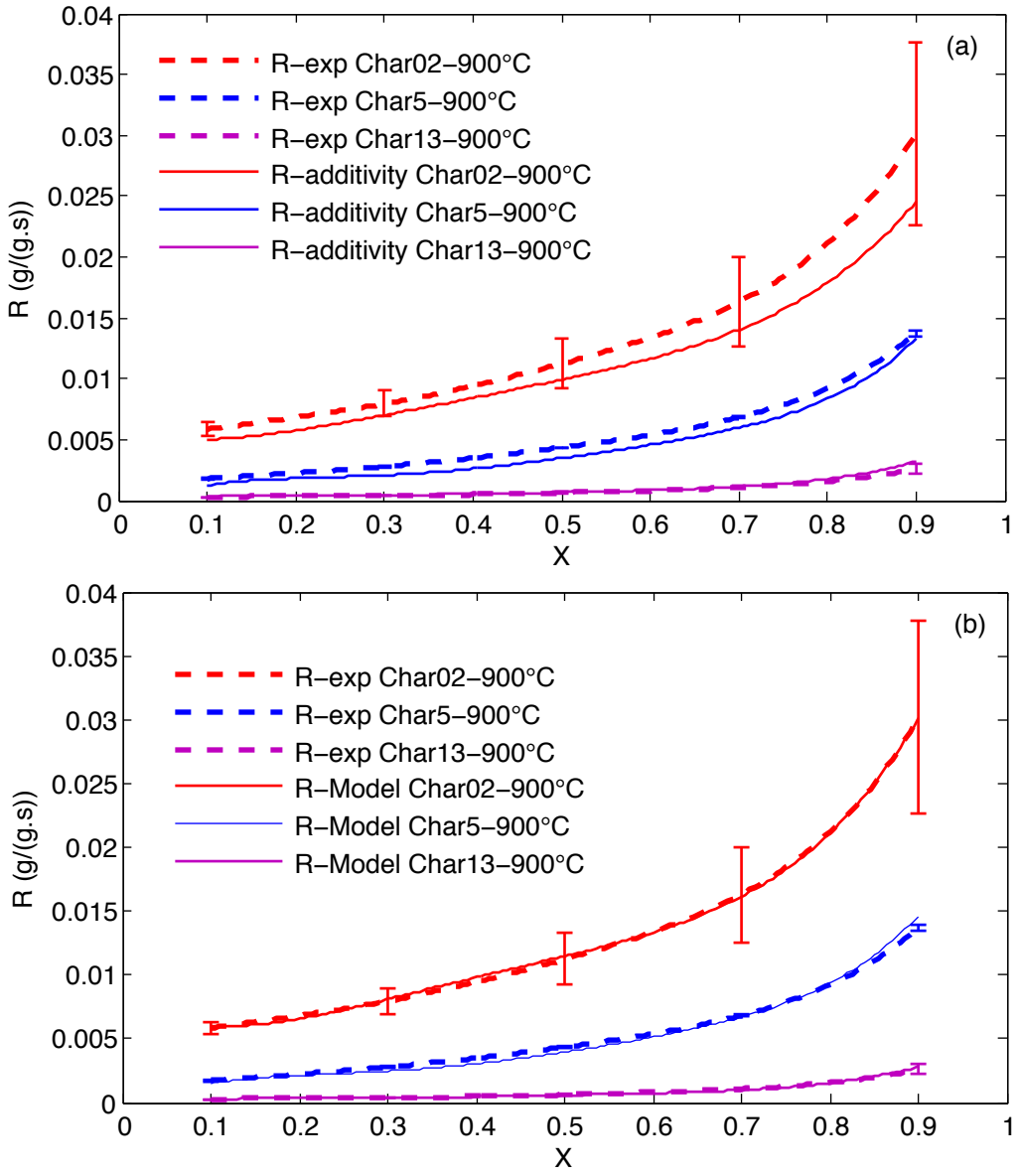

Figure 6.10: Experimental char gasification reactivity in 20% H_2O + 20% CO_2 at 900°C for char02, char5 and char13 and modelling results (a) additivity model, (b) best fit

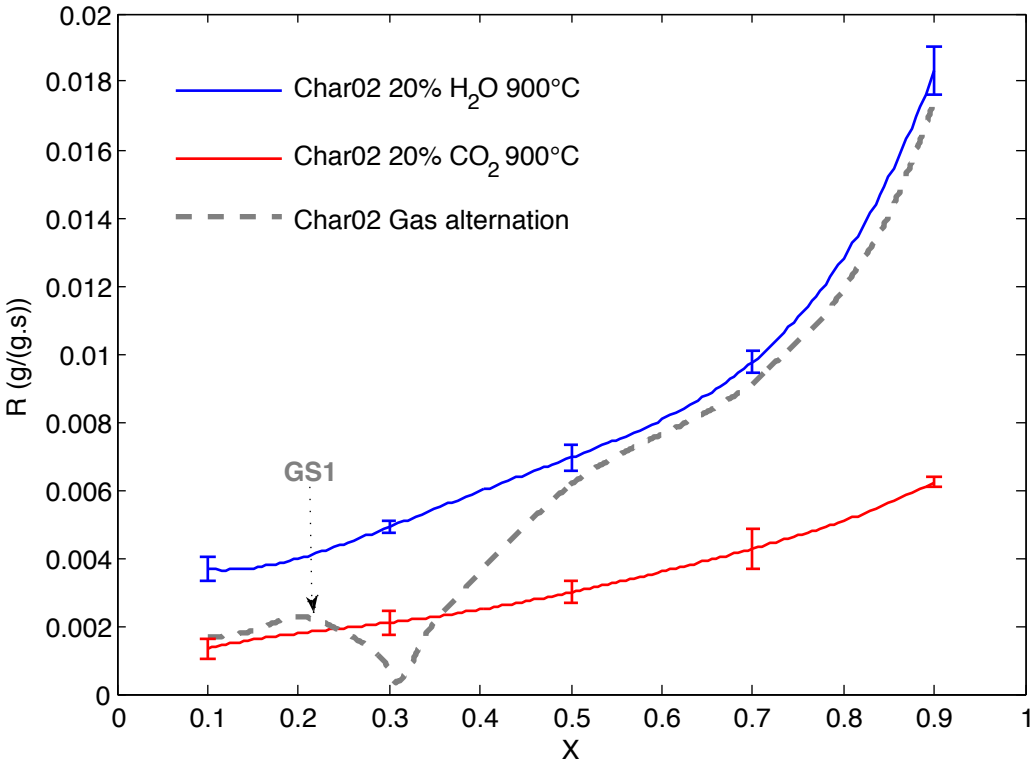

Figure 6.11: Gas alternation gasification experiments for 0.2 mm char particles at 900°C (GS: Gas Shift)

mm LHR chars, nor for 1 mm LHR and HHR chars. As the authors performed their gasification on thicker char particles (5 mm thick pine char particles), the suggested effects of porosity enhancement by CO_2 could take place for thick particles. For this purpose, we checked not only the effect of CO_2 on the H_2O-char reaction, but rather the mutual effects of both gases on the char reactivity towards each other. The experiments were done for the biggest char particles of 13 mm size. As the full gasification time was long, we were able to perform cyclic gasification experiments and alternating many times H_2O and CO_2 gases. The results are shown in figure 6.12. In this figure, the char reactivities in single atmospheres (20 % CO_2 and 20 % H_2O) as well as the cyclic gasification experiments are plotted. The reactivity curve in the cyclic gasification experiment jumps from a reference curve to the other one when switching the gases whatever is the conversion level. The reactivity curve in the cyclic experiment superposes to the reference reactivity curves each time the gasification atmosphere is switched. Small deviations are observed in the advanced conversion level but they still in the standard deviation zone of the experiments. It can be clearly seen that the char reactivity does not depend on the historic of gasification. Gasifying the char with CO_2 to a defined conversion level does not modify its reactivity towards H_2O when switching the gases. This effect is reciprocal. Altogether, the char reactivity towards a gas is here only conversion dependent. It is as if there is a kind of a char "gasification memory loss": at a defined conversion level the char reactivity is constant whatever is the gasification history. The char reactive surface would evolve similarly for the two gases to observe such kind of results. To the authors best knowledge such findings are not presented in the literature were the mutual influences of two gases on the char reactive properties are studied. The reactivity is conditioned by several char physical (porosity, specific area, particle size...) and chemical (elemental composition, carbon forms, mineral matter content...) characteristics. In order to understand this reactivity behaviour in cyclic gasification experiments as well as to go deeper into the understanding of the mixed atmosphere gasification mechanisms, deep structural, chemical

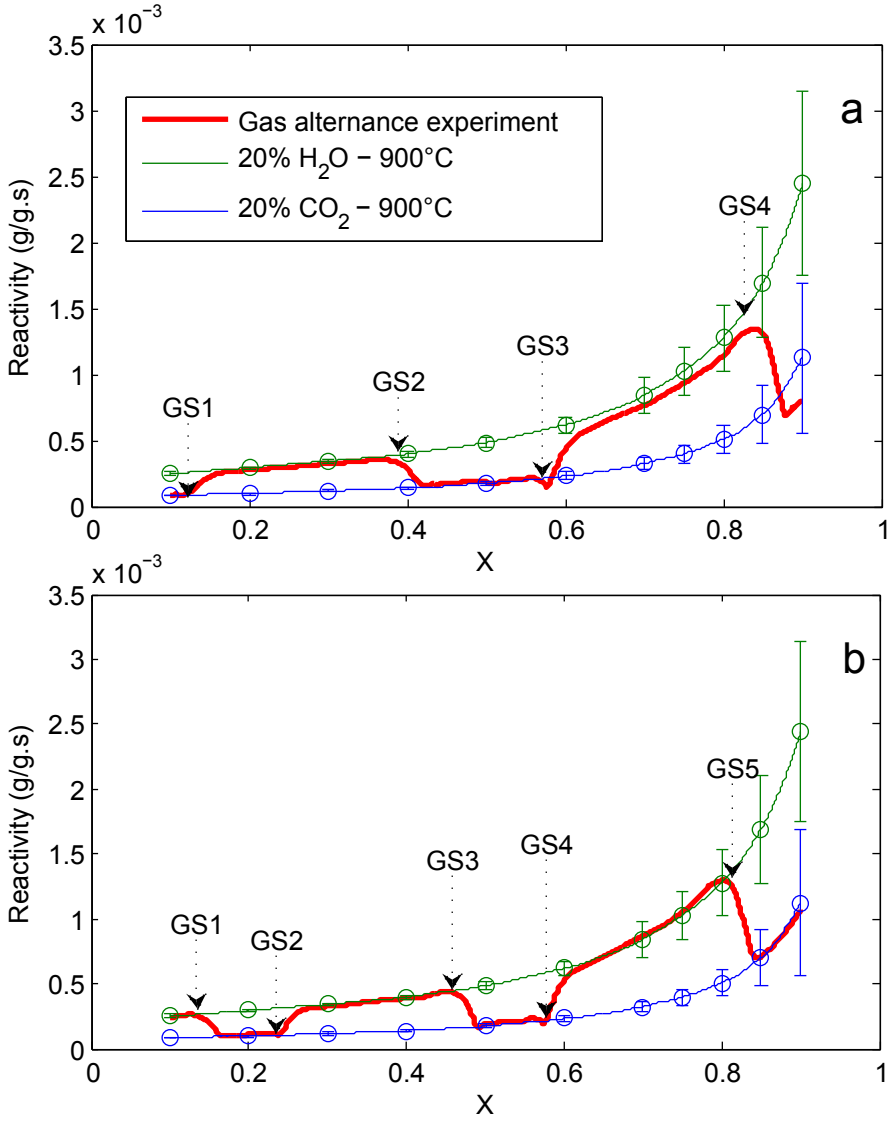

Figure 6.12: Gas alternation gasification experiments for 13 mm char particles at 900°C (GS: Gas Shift)

and textural characterisation of the chars during the gasification reaction are required. This will be our focus in the next studies.

6.4 Conclusion

The objective of the present work was to evaluate the extent of diffusional limitations when varying the temperature and char particle size and also to shed light on the influence of temperature and char particle size on the multi-components gasification reaction with CO_2 and H_2O.

Adopting an effectiveness factor approach, we quantified the extent of the internal diffusional limitations in a large char particle size range going from 0.04 mm to 13 mm for both H_2O and CO_2 gasification reactions. We found similar effectiveness factor evolution with particle size for both reactions. The diffusion-reaction competition for both gasification reactions was nearly the same for both molecules. However, H_2O was found to have an almost twice higher reactivity and diffusivity than CO_2 explaining the equivalence of the diffusion-reaction competition. At 900°C, the

char gasification H_2O or CO_2 would be performed in the chemical regime for char particles of 0.04 mm and below.

In a second part, we assessed the effect of temperature and particle size on the mixed atmosphere gasification. The char02 reactivity in mixed atmosphere of H_2O and CO_2 was nearly equal to the sum of the individual reactivity at 800°C, a little bit higher at 900°C and lower than it at 1000°C and 1100°C for 0.2 mm sized char particles. Despite that the reactivity in mixed atmosphere is well represented by a linear combination of the two individual reactivities, it is not possible to state on the gasification mechanism due to the wide range of α and β combinations that allow to reproduce correctly the char reactivity, especially at 800°C and 900°C. Similar conclusions were drawn when varying the particle size as it was not possible to determine the gasification mechanism due to various linear coefficient combinations allowing to correctly model the char reactivity.

Another worth noting result is that the char reactivity at 900°C, for particle size range of 0.2 mm and 13 mm, does not depend on the historic of gasification: the char reactivity to H_2O or CO_2 at a defined conversion level is constant whatever the gas has the char anteriorly reacted with.

To best authors knowledge, these results are quite new in the literature on biomass char gasification in complex atmospheres. Further investigations are needed, especially concerning the char properties evolution along the gasification reactions in H_2O, CO_2 and in CO_2+H_2O in order to understand the reaction mechanisms. This issue will be tackled in future works.

Acknowledgements

The authors acknowledge the national research agency ANR-France for its financial support in the RECO2 project. They also wish to express their appreciation to Bernard Auduc for his technical support.

Appendix

To check the accuracy of the thermogravimetric data obtained at 900°C, so that the reaction rate is effectively determined for a reactant concentration of 20% at the char bed surface, we considered a monodimensional diffusion model involving the external diffusion of the reactant gas (H_2O or CO_2) from the environment where the molar concentration is C_{env}=20% to the char bed where the concentration is C_{bed}, and a diffusion within the char bed with a volumetric reaction term (source term) corresponding to the carbon consumption. The study was applied to the case of the 0.04 mm char particles for which the reaction rate is the highest compared to the other bigger particles. The source term is determined from the experimental reactivity obtained at X=0.5. The external diffusion height (h2=0.4 mm) is fixed to 10 times that of the internal diffusion inside the char bed (h1=0.04 mm).

A schematic representation of the gasification reaction in is shown in figure 6.13.

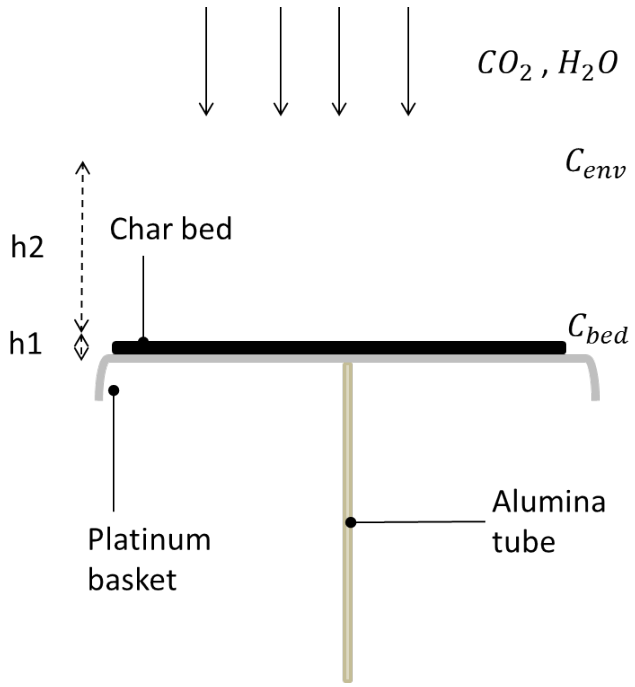

Figure 6.13: A schematic representation of the char04 gasification at 900°C with H_2O or CO_2

FickâĂŹs second law in a steady state regime gives:

$$\nabla . J_i = R_i \tag{6.21}$$

The suffix "i" designates the gas species involved in the gasification reaction (CO_2, CO and N_2 in the Boudourad reaction, and H_2O, CO, H_2 and N_2 in the steam gasification reaction).

J_i ($kg/m^2.s$) is the diffusive flux calculated by the Fick's law:

$$J_i = \rho \, D_i \, \nabla \omega_i \tag{6.22}$$

Where:

- *rho*: the total gas density (kg/m^3)
- D_i: molecular diffusion coefficient (m^2/s). The effective diffusion coefficient in the char bed is corrected by the ratio $\frac{\epsilon}{\tau}$.

- ω_i: gas specie "i" mass fraction

R_i $(kg/m^3.s)$ is the source term determined from the experimental carbon consumption in the char bed at X=0.5. Stoichiometric considerations allow to calculate the source term for each gas specie considering the two chemical reaction of Boudouard and steam gasification.

$$Boudouard\,reaction\ : C + CO_2 \longrightarrow 2CO \tag{6.23}$$

$$Steam\,gasification\ : C + H_2O \longrightarrow CO + H_2 \tag{6.24}$$

The modelling results are shown in figure 6.14. It can be seen on this figure that the gas concentration at the bed surface is very close to that in the surroundings. A quite small decrease is found, and thus external diffusional limitations can be assumed to be negligible.

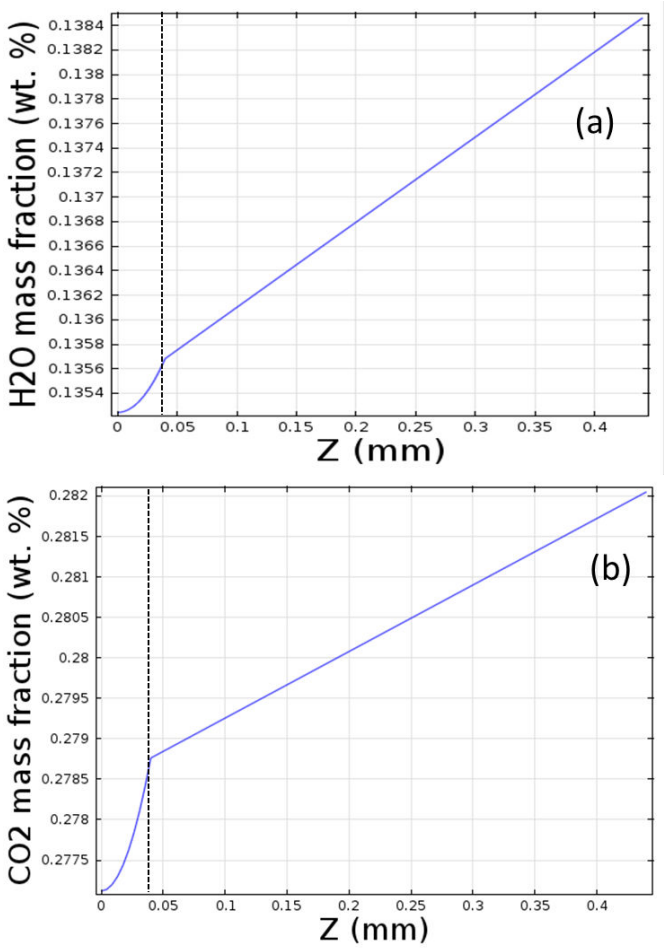

Figure 6.14: H_2O (a) and CO_2 (b) mass fractions in the surrounding and in the char bed. The dashed black line represents the interface between the char bed surface and the surroundings

Chapter 7

Evolution of chemical, textural and structural properties of biomass chars during gasification under H_2O, CO_2 and their mixture

Abstract

Char gasification reaction phenomenology is not so well understood due to its complexity as well as to the numerous factors conditioning the char reactivity. Classical char reactivity studies deal about kinetics of gasification and most of the time use black box functions to account for the structural modification occurring inside the char through the gasification reaction. The present study is rather axed on the understanding of the char gasification reaction phenomenology by monitoring the chemical, structural and textural char characteristics through the reaction. Low heating chars from beech wood were gasified under 20% H_2O, 20% CO_2 and 20% H_2O + 20% CO_2 in nitrogen at 900°C. The gasification reactions were stopped at 20%, 50% and 70% of conversion to analyse the char properties evolution. The char surface functional groups were analysed by temperature programmed desorption coupled to mass spectrometry. The char active surface area was measured by oxygen chemisorption. The structural evolution of the chars was monitored by Raman spectroscopy while their textural properties were analysed by scanning electron microscopy imaging as well as by nitrogen adsorption at 77 K. Mineral species behaviour through the gasification reactions was analysed by scanning electron microscopy coupled to energy dispersive X-ray analysis as well as by X-ray fluorescence. We provide, thanks to these analysis, valuable information on the unfolding of the gasification reactions with H_2O, CO_2 and their mixtures. H_2O and CO_2 gasification reactions were found to follow different pathways. We also found that despite the char reactivity in mixed atmosphere can be fairly expressed by summing the two individual reactivities, the situation is in fact more complex, as this additivity-like mechanism is the result of several competitions and synergy interactions between H_2O and CO_2 molecules.

Keywords: Biomass char, CO_2, H_2O, Reactivity, Raman spectroscopy, Temperature programmed desorption, Mass spectrometry, Active Surface Area, Total surface area, Pore size distribution, Mineral species, Scanning electron microscopy, X-ray fluorescence.

Résumé

La phénoménologie de la réaction de gazéification reste un sujet ouvert au vu de la complexité des phénoménes qui la régissent et des facteurs conditionnant la réactivité du char. Les études classiques de gazéification de chars visent à évaluer et à modéliser la réactvité d'un char en usant de fonctions structurales qui traduisent la variation de la structure, de la texture et de la chimie du char lors de la conversion. Ces fonctions sont la plupart du temps des "boites noires" qui ne décrivent pas la physique et la chimie sous-jacentes à la réaction de gazéification. La présent travail se veut être une étude compréhensive de la réaction de gazéification en suivant l'évolution des propriétés chimiques, structurales et texturales du char lors de la conversion. Pour ce faire, des chars ont été préparés par pyrolyse lente de bois et gazéifiés partiellement jusqu'à 20%, 50% et 70% de conversion sous 20% H_2O, 20% CO_2 et leur mélange à 900°C. On a ainsi pu suivre l'évolution de la chimie de surface du char en quantifiant les fonctions de surface par thermodésorption programée couplée à la spectrométrie de masse. On a également suivi l'évolution de la structure du char par spectrométrie Raman et analysé l'évolution de la texture du char par microspcopie électronique à balayage et adsorption d'azote à 77 K. Enfin, on a aussi suivi le comportement de certains minéraux se trouvant dans le char par spectrométrie de fluorescence X. Grace à ces analyses, nous apportons de précieuses informations quant au déroulement des différentes réactions de gazéification. On a pu ainsi trouver que les réactions de gazéification du char par H_2O et CO_2 suivent des voies différentes. Bien que la réactivité du char sous atmosphères mixtes puisse être décrite comme la somme des réactivités individuelles, la situation est en réalité beaucoup plus complexe qu'une simple réaction sur des sites séparés. Ce qui nous apparait comme additivité est en fait le résultat de plusieurs interactions de compétition et de synergie entre les deux gaz.

Mots clés: Char de biomasse, CO_2, H_2O, Reactivité, Spectroscopie Raman, Désorption en temperature programmée, Spectrométrie de masse, Surface active, Surface totale, Distribution de taille des pores, Eléments minéraux, Microspcopie électronique à balayage , Spectrométrie de fluorescence X.

7.1 Introduction

Fossil fuel depletion, climate change as well as environmental and human health problems are urging humanity to reconsider its relationship with natural resources, change its energy policy and adopt a more sober way of living. Renewable energies are undoubtedly part of the solution, at least to cope with fossil fuel depletion and mitigate the CO_2 emissions in the atmosphere [1]. Biomass constitutes a renewable energy resource when used with parsimony. Biomass resources are various and can be classified into two main categories of dry and wet biomasses. The thermochemical routes of biomass conversion depends mainly on the nature of this latter, including combustion for thermal energy generation, pyrolysis for the production of bio-oil and bio-char, liquefaction (mainly for wet biomasses) and gasification for the production of Syngas and bio-fuel synthesis.

Biomass gasification allows to convert biomass into Syngas mainly composed of CO and H_2. These two molecules can be used afterwards as starting blocks for bio-fuel synthesis in processes such as Fisher-Tropsh. Biomass gasification is operated at high temperatures and includes several steps of drying, pyrolysis and residual char gasification. The char gasification is the rate limiting step of the process. Biomass char can be viewed as a highly porous, carbonaceous, non-organised material. It contains in majority carbon (up to 90%), oxygen hydrogen, nitrogen and mineral species such as potassium, calcium, sodium, silicon and magnesium. The proportion of these chemical species as well as the textural and structural properties of the char depend on the parent biomass and on the operating conditions.

The char reactivity is conditioned by all these parameters which are highly coupled. In biomass gasifiers, the char gasification reaction take place when the solid char reacts with the surrounding gas molecules of O_2, H_2O, CO_2, and H_2 following the reaction of combustion, steam gasification, Boudourad reaction and methanation. The gasification reaction is a heterogeneous reaction that implies the reactant gas diffusion inside the char, reaction with the active sites and diffusion of the gas product out of the particle.

The char texture, including total surface area (TSA), pore size distribution as well as pore shape, influence the gas diffusion inside the particle. C. Avila et al. [79] established links between reactivity and morphology of 10 biomass chars. They observed that biomasses giving the thickest walled char had the lowest reactivities while those having the thinnest walled char had the highest ones because of a lower resistance to mass and heat transfer. The initial porosity and TSA depend on the pyrolysis conditions [80] [81]. Mermoud et al [80] observed that High Heating Rate chars exhibiting a higher reactivity have a higher porosity consisting mainly of mesopores and macropores, while Low Heating Rate chars exhibit a lower porosity mainly consisting of micropores. Attempts to correlate the initial reactivity (at X=5%) of the different char with their respective TSA were unsuccessful. The authors found that the mesopore and macropore areas are better indicators of the char reactivity [80].

Reactivity of biomass char can increase by near to 10 folds at the end of the reaction compared to the initial stages [72]. Several authors explain this reactivity increase by the increase in the reactive surface during the gasification, however, the reactivity increase is not proportional to the increase in the TSA. For instance, Fu et al. [31] investigated the evolution of char textural and chemical features during steam gasification. The char was produced from fast pyrolysis of rice husk. The authors found that the highest TSA was obtained at X=49%. TSA decreased beyond this conversion level, probably because of pore coalescence and collapse. Similarly, Laine et al [64] observed that coal chars with nearly the same TSA, have quite different reactivity.

Klose et Wolki [55] measured a "Reactive Surface Area" (RSA) corresponding to the amount of desorbed CO complex from the char surface during H_2O and CO_2 gasification reaction by means of Temperature Programmed Desorption. The authors established a good correlation between the evolution of the char reactivity and the RSA. The TSA is likely a good parameter for estimating the

char porosity but not its reactivity. The functional groups on a char sample can be determined by Temperature Programmed Desorption and gas analysis by Mass spectrometry (TPD-MS) [51] [53] [54] [55]. This technique consists of heating the char sample in vacuum at a low heating rate. The decomposition of the surface functional groups leads to the emission of CO_2, CO, H_2O and H_2 in major part. According to the temperature and to the nature of the emitted gas, the nature of the surface functional groups can be determined. For instance, Figueiredo et al [51] as well as Zhuang et al [54] used this technique to follow the evolution of coal char functional groups during oxidation with O_2, while Klose et Wolki [55] measured the evolution of the CO surface complex for CO_2 and H_2O gasification reaction. Another concept to approach the intrinsic reactivity of a carbon material is the Active Surface Area measurement, which consists roughly in cleaning the char surface by a thermal treatment and adsorbing on O_2 at a low temperature in the range of 200-300°C [64] [65]. The quantity of adsorbed Oxygen on the char surface is an index of the carbon reactivity as it can be related directly to the number of active sites on the char surface. The ASA represents a small part of the TSA. Not all the surface participates to the gasification reaction. The ASA is more representative of the char reactivity as it is directly linked to the structural units composing the carbonaceous material. Laine et al measured the evolution of the TSA and ASA of chars during combustion with oxygen and showed the high difference that exists between TSA and ASA [64]. The ASA would be more representative of the char reactivity than the TSA.

The char structure is also a governing parameter in char reactivity as more ordered structures are less reactive. Char structural ordering is promoted at high temperatures and long soaking time. The char structural ordering is accompanied by a loss of oxygen functional groups which are thought to be the major and most reactive sites on the char surface [40]. The elemental composition of the biomass char changes with temperature. Oxygen and hydrogen continue to be released out of the char porous matrix as the pyrolysis temperature increases. The chars obtained at the highest temperatures, have the highest carbon content. The high levels of oxygen content in biomass fuels foster cross-linking of the carbon chains and inhibits ordering of the char matrix [87]. The loss of oxygen and hydrogen by elimination of functional groups are clear indicators of subsequent coalescence, ordering and rearrangement of aromatic rings. Gaseous emissions become insignificant beyond 900°C, showing that this temperature is sufficient to evacuate most of the volatiles and to obtain a char with low amount of hydrogen and oxygen [88] [86]. Asadullah at al. [40] found that the reactivity to oxygen of chars obtained from a mallee wood decreased with increasing the temperature from 700°C to 900°C. The increase of temperature was also accompanied by a loss of oxygen functional groups and ordering of the char which are likely behind the decrease in reactivity. Tay et al. [66] studied the structural features of partially gasified char, in different atmospheres containing reducing (H_2O) and oxidising (CO_2 and O_2) gasifying agents, using FT-Raman spectroscopy followed by spectral deconvolution. The authors found that the presence of H_2O during gasification at 800°C plays a decisive role in the evolution of char structure, in particular by decreasing the relative ratio of small and large aromatic ring structures in char. Keown et al. made similar observations as the structure of cane trash chars changes drastically after contact with steam [42]. Li et al. [46] also studied the evolution of the char structure during gasification with CO_2, H_2O and their mixtures using FT-Raman spectroscopy followed by spectral deconvolution. Drastic changes in char structure were perceived during the reactions. The structural changes were different respectively in CO_2 and H_2O atmospheres. The char char obtained in mixed atmosphere showed a very close structure to that obtained in single H_2O atmosphere. The authors came to the main conclusion that CO_2 and H_2O gasification reactions follow different pathways. For a defined gasification reaction, the char structural features did not vary in the temperature range of 800-900°C.

Mineral species highly impacts the char reactivity as they catalyse or inhibit the gasification reaction depending on their nature. *K*, *Ca* and *Na* were found to be catalytic species while *Si*

and P were shown to inhibit the gasification reaction [78] [71] [80] [72] [73] [50]. These latter were found also to migrate during the reaction, form cluster or stay evenly dispersed throughout the char particle [29]. For instance Henriksen et al. [78] show that the presence of *Si* hinders the gas from penetrating into the char particle as they form clusters and block the pores access. More recently Dupont et al [72] found that the char reactivity towards steam for various samples can be expressed as the product of kinetic term accounting for temperature and steam partial pressure dependence, and an empirical correlation bearing the concentration of K and *Si* which respectively catalyse and inhibit the gasification reaction. Hognon et al [73] also show that the increase or decease of the char reactivity at the end of the reaction is directly related the the K, *Si* and P contents of the char. Their effects are mainly observed at the end of the reaction by the reactivity increase for high K content and decrease for high *Si* and P contents. Tay et al. [66] demonstrated that the presence of steam during the gasification was also seen to greatly improve the retention of *Mg* and *Ca* during gasification, possibly by changing the physico-chemical forms of *Mg* and *Ca*. The retention of mineral species has likely to do with the presence of O-containing functional groups. H radicals can change the chemical form of mineral species so that they do not volatilize even with the loss of O-containing functional groups. Tay et al. [44] observed that the concentrations of *Ca* and *Mg* in coal char remained roughly constant with char yield during gasification in pure CO_2. However, they increased more significantly with decreasing char yield for gasification performed in H_2 and H_2O containig atmospheres. Tay et al. [44] also showed in a more recent work that a catalyst tends to encourage the oxidation of char during gasification and makes the consumption of char less selective during gasification in contrast with metal depleted chars. Authors also show that the presence of O-containing structures in char tends to increase the observed Raman intensity due to a resonance effect between O and the aromatic ring structure connected to the O-containing structure. The O-containing structures were much more present in the raw chars containing minerals. Fu et al[31] found also that the steam gasification favoured the volatilization of *Na*. *K*, *Mg* and *Ca* showed a similar behaviour as their concentrations increased up to 60.3% and decreased afterwards. The authors think that loss of O-containing structures caused significant volatilization of *K*, *Mg* and *Ca*.

Altogether, this brief literature review shows that the char reactivity is highly conditioned by the char textural, structural and chemical features. These characteristics are also highly coupled which makes the task of understanding the gasification reaction mechanisms even more difficult. Char gasification models are for the great part semi-empirical ones, as they include a term accounting for the structural, chemical and textural properties change along the gasification which is function of the degree of conversion. These char properties are not so straightforward to measure [14] which justify such a global reactivity approach. Nevertheless, further understandings of the gasification reaction mechanisms can be achieved by monitoring the char characteristics evolution during the gasification. Gathering information on the the evolution of the different textural, structural and chemical parameters will undoubtedly shed light on the reaction unfolding and allow the establishing of a gasification reaction scenario.

The present work tackle the issue of the gasification reaction using a comprehensive approach. The aim is to understand the gasification reaction unfolding with CO_2, H_2O and their mixtures through deep characterization of the chars along the gasification. The char surface chemistry, the structural and textural properties as well as the mineral species content are monitored in the conversion range of 0-70%.

7.2 Material methods

7.2.1 Low Heating-Rate char preparation

The raw biomass samples are beech wood spheres of a 20 mm diameter. Low Heating-rate chars were prepared by pyrolysing the wood spheres under nitrogen. The pyrolysis was performed in a batch reactor. The wood spheres were placed in a metallic plateau, spaced enough to avoid chemical and thermal interactions. The plateau was introduced in the furnace heated zone which was progressively heated from room temperature to 900°C at 5°C/min. The chars were kept for 1 h at the final temperature, cooled under nitrogen and stored afterwards in a sealed recipient. The low heating rate ensure a good temperature uniformity in the wood particle and leads to a quite homogeneous wood-char, from the structural and chemical viewpoints, as demonstrated by [92] and pointed out by [78] and [80]. With high heating rate there can be heterogeneity among the char layers from the surface to the particle centre due to the temperature gradient and heat transfer limitations during the pyrolysis stage. After the pyrolysis reaction, the char particles shrink and get an ovoid form. The mean particle diameter, calculated as the average of the three particle dimensions was estimated at 13 mm.

Some of the char particles were afterwards ground with a mortar and a pillar. Char particle having size of 0.2 mm were retained for gasification experiments at 900°C. To ensure of the chemical and structural homogeneity of the char particle, the char structure and chemical composition were analysed at three location: at the surface, at half the distance from the centre and at the centre. Elemental composition and Raman spectroscopy showed that the char sample is homogeneous.

Table 7.1: Proximate and ultimate analysis of the beech wood-chips (% dry basis)

Proximate analysis			**Ultimate analysis**			
VM	Ash	FC	C	H	O	N
88.1	0.4	11.5	46.1	5.5	47.9	0.1

7.2.2 Char gasification experiments in H_2O, CO_2 and their mixture

The Macro-TG experimental device

The M-TG device is described in detail in our previous work on char gasification in mixed atmospheres of CO_2 and H_2O [154]. In general terms, the experimental apparatus consists of a 2-m long, 75-mm i.d. alumina reactor that is electrically heated, and a weighing system comprising an electronic scale having an accuracy of ± 0.1 mg, a metallic stand placed over the scale on which a 1 m long, 2.4 mm external diameter hollow ceramic tubes is fixed. The ceramic tube hold the platinum basket in which the biomass particles are placed. The gas flow rates are controlled by means of mass flow-meters/controllers. The gas flow inside the reactor is laminar and flowing at an average velocity of 0.20 m/s.

The gasification reaction procedure and operating conditions

A wood-char mass of 130-150 mg is spread-out on the whole surface of the 50 mm diameter platinum basket in the form of a char mono-layer. The char mass may seems important compared to what is introduced in classical TG devices but the surface of the crucible is large enough (0.002 m^2) to allow spreading this mass in the form of a mono layer. The char is directly exposed to the surrounding atmosphere as the platinum basket is simply in the form of a circular plane without any

side wall. The platinum crucible containing the char is introduced in the furnace under a nitrogen flow. The char is kept 5 min under nitrogen before starting the gasification. During this period the char loses mass, probably in the form of water vapour and light gases which are released due to the thermal shock. We estimated the mass loss to be less than 6%. This period is sufficient for the establishment of a thermal equilibrium between the weighing system, the furnace and the surrounding gases. Afterwards, the furnace atmosphere is switched and the gasification medium is introduced. The char gasification experiments were performed with CO_2, H_2O and their mixture. The gasification reaction were performed at 900°C with 20% H_2O, 20% CO_2 and 20% H_2O + 20% CO_2 in nitrogen.

Table 7.2: Ultimate analysis of the wood-char samples

C (wt.%)	H (wt.%)	O (wt.%) (by difference)	N (wt.%)	Ash (wt.%)
90.83± 0.93	0.676±0.07	7.03	0.21± 0.027	1.25±0.13

Reactivity calculation

The char conversion level is given by:

$$X_{(t)} = \frac{m_0 - m_{(t)}}{m_0 - m_{ash}} \tag{7.1}$$

Where m_0, m_t and m_{ash} are respectively the initial mass of char, the mass at a time t and the mass of the residual ash.

The char reactivity was calculated over time following the relation:

$$R_{(t)} = \frac{1}{1 - X_{(t)}} \times \frac{dX_{(t)}}{dt} \tag{7.2}$$

7.2.3 Partially gasified char preparation

To follow the evolution of char during the gasification reaction, partially gasified chars were prepared at 20%, 50% and 70% of conversion. Knowing the initial char mass that was introduced in the crucible, the gasification reaction was stopped after reaching the desired conversion level. The gasifying medium flow was directly switched to pure nitrogen and the platinum basket bearing the sample was quickly pulled out to the reactor cool zone (180°C). The reacted char was kept there during 4 min to cool and avoid burnout when taken out completely to the ambient atmosphere. Afterwards, the chars were kept in an inert atmosphere to avoid chemical transformations of the surface functional groups in air. To do so, the chars were introduced in small glass recipients which were put in a plastic bag under a flow of nitrogen. After insuring that no oxygen still in the bag atmosphere (by analysing the leaving gases with gas chromatography), the containers were sealed under nitrogen.

7.2.4 Monitoring the evolution of the char properties along the gasification

Char surface chemistry characterisation by Temperature Programmed Desorption and Mass Spectrometry TPD-MS

The TPD-MS technique allows a quantification of the surface functional groups located on the char surface and their evolution during gasification. The TPD-MS experimental bench comprises a quartz

tubular reactor electrically heated in which is introduced a quartz crucible containing near to 20 mg of the char sample, a pumping system to create vacuum and a mass spectrometer for gas analysis. The reactor is first out-gased in a primary vacuum down to 1 mm Hg of pressure, and then in a second step to a secondary vacuum down to 10^{-4} mm Hg of pressure by means of a turbo-molecular pump. The char sample in the crucible is afterwards heated up to 900°C at constant rate of 5°C/min and kept at this final temperature during 1 h. During the analysis, the functional groups are removed from the char surface which results, depending on the nature of the functional groups, in the emission of H_2O, CO_2, CO and H_2. The rate of emission as well as the quantities emitted depends on the temperature as well as on the abundance of functional groups in the char surface. The gases evolved during the heating process were continuously analysed quantitatively by a mass spectrometer which is calibrated using commercial H_2, CO, CO_2, and N_2. The total pressure of the gas released during the heat treatment was also measured as a function of the temperature using a Bayard Alpert gauge. From the TPD analysis, the desorption rate of each gas as a function of temperature was determined. The total amount of each gas released was computed by time integration of the TPD curves.

Active Surface Area of chars

O_2 chemisorption

The Active Surface Area (ASA) of the biomass chars was determined following the method of Laine and Co-workers [64] consisting on O_2 chemisorption on the char sample at 200°C. The ASA experiments were done in the same experimental bench as in the TPD-MS experiments. The char sample surface was first cleaned by heating the sample up to 900°C with a constant heating rate of 5°C/min and kept 1 h at this final temperature (classical TPD-MS experiment). Afterwards, the char sample is cooled down to 200°C, keeping the reactor under vacuum. When the temperature stabilizes, oxygen is introduced (pressure close to 0.5 mm Hg) and chemisorbed on the char surface for a period of 15 h leading to the formation of surface oxygen complexes.

After the chemisorption step, a TPD experiment is performed and the char sample is heated up to 900°C with a constant heating rate of 10°C/min and kept for 20 min at this final temperature. The ASA (m^2/g) of a char sample may be calculated using the equation:

$$ASA = \frac{n_O \sigma_O N_{Avo}}{m_{char}} \tag{7.3}$$

n_O is the total number of oxygen moles calculated from the relation:

$$n_O = n_{CO} + 2n_{CO_2} \tag{7.4}$$

n_{CO} and n_{CO_2} are obtained from the time integration of the TPD curves:

$$n_{CO} = \int_{t_0}^{t_{end}} Q_{CO}\, dt \tag{7.5}$$

$$n_{CO_2} = \int_{t_0}^{t_{end}} Q_{CO_2}\, dt \tag{7.6}$$

Q_{CO} and Q_{CO_2} are the molar emission rate of CO and CO_2 (mol/s).
N_{Avo} is Avogadro number and σ_O is the cross sectional area of an oxygen atom (0.083 nm^2).

Char structural evolution by Raman spectroscopy

Raman spectroscopy is a powerful characterisation technique for carbonaceous materials. It allows a differentiation of the different carbon allotropes (pyrolytic carbons, graphitic carbon...) in the char

sample due to their different carbon bonds type and orientations. Raman spectroscopy have been used to determine the structural features of the chars during gasification with CO_2, H_2O and their mixtures. Raman spectroscopy can provide information about an 'average structural composition' of the chars and thus allows a comparison between the different char sample at the different conversion levels.

Acquisition and deconvolution of the Raman spectra of the char samples Raman spectra of the chars were recorded with a BX40 LabRam, Jobin Yvon/Horiba spectrometer. Several char particles were sampled and deposited on a rectangular glass slide for the Raman analysis. Raman spectra were obtained by a backscattered configuration with an excitation laser at 635 nm. The Raman spectra at each position gives an average structural information of a large number of carbon micro-crystallites. The Raman spectra were recorded at 6 locations of the char sample. A representative spectrum of the char sample was afterwards calculated as the average of the Raman spectra at the different char locations. Mean values as well as relative standard deviations are calculated for the different parameters related to the Raman spectrum, taking thus into account the heterogeneity among the char sample.

The Raman spectra of heterogeneous carbon materials shows in the first order region (800-2000 cm^{-1}), two main broad and overlapping peaks with maximum intensities at 1350 cm^{-1} and 1590 cm^{-1} [149] [43]. In the literature, we frequently refer to these two peaks as respectively the D and G bands. In the case of highly ordered carbon materials, the Raman spectra can be expressed as the result of these two bands. The G band corresponds to an in-plane bond-stretching motion of pairs of sp^2 carbon atoms in the graphitic structure (aromatic ring breathing mode) while the D band corresponds to the defects in the graphitic structure and is forbidden in pure graphitic ordered materials.

For heterogeneous carbon materials such as biomass or coal chars, we can no longer speak about those two peaks. The Raman spectra is rather the combinations of several bands corresponding to different carbonaceous structures. The Raman spectrum can be deconvolved into five main bands as proposed by Jawhari [38] or more recently by Sadezky [43], Sheng [39] and by Chabalala [150]. The five bands correspond to well defined carbon structures are summarized as follows:

- G band at 1590 cm $^{-1}$: stretching vibration mode with E2g symmetry in the aromatic layers of the graphite crystalline
- D1 band at 1350 cm^{-1}:graphitic lattice vibration mode with A1g symmetry and in-plane imperfections such as defects and hetero-atoms
- D2 band at 1620 cm^{-1}:lattice vibration similar to that of the G band. The D2 band results from graphene layers which are not directly sandwiched between two other graphene layers. Sheng [39] reported that the D2 band is always present when the D1 band is present and that its intensity decreases with the increase of the degree of organization in the char.
- D3 band at 1500 cm^{-1}: Related to amorphous carbon structures and appears as a very broad band. It is suggested to originate from the amorphous sp^2-bonded forms of carbon (organic molecules, fragments or functional groups, in poorly organised materials).
- D4 band at 1200 cm^{-1}: appears only in very poorly organised materials, such as soot and coal chars [39] [43]. It is attributed to sp^2 - sp^3 mixed sites at the periphery of crystallites and to C - C and C=C stretching vibrations of polyene-like structures.

The D3 and D4 bands are suggested to be responsible of the reactive sites in the char and thus determine the char reactivity. The deconvolution procedure was performed with a MATLAB program. Spectrum fitting was performed following a least square minimization procedure between the raw signal and the calculated one. The Raman signal was deconvolved into 5 Gaussian bands with the above mentioned fixed positions. The objective function to be minimized is:

$$OF = \sum_{i=1}^{i=n} (I_i^{cal} - I_i^{exp})^2 \tag{7.7}$$

I_i^{cal} and I_i^{exp} are respectively the experimental recorded intensity (photon counts) and the calculated one.

Mineral species analysis by X-Ray Fluorescence (XRF)

Mineral content of the different chars was measured by X-ray fluorescence (XRF) spectrophotometer (PHILIPS PW2540) equipped with a rhodium target X-ray tube and a 4 kW generator. 100 mg of char were priorly ground and mixed with 200 mg of boric acid, and then pressed into a pellet under a 9 tons pressure for 45 minutes. The XRF analysis was seen to overestimate the mineral content of the char despite attempts to calibrate the apparatus with a known composition char sample. Matrix effects seem to change with the conversion degree. However, despite the amount of minerals is overestimated, the relative abundance of a mineral specie in the total ash would be accurate [186].

Char textural characterisation by N_2 adsorption

The textural properties of the materials were investigated with a Micromeritics ASAP 2020 instrument using N_2 adsorbate at 77 K. Prior to the analysis the char samples were out-gassed overnight in vacuum at 300. The Total Surface Area (TSA) was calculated for the linear plot in the relative pressure range of 0.05 to 0.15 while the micropore volume (Vmicro) was estimated by using the αs-plot method. The mesopore volume (Vmeso) was obtained by subtracting the micropore volume from the total pore volume of N_2 adsorbed at relative pressure of 0.95. The pore size distribution was determined using the DFT model on carbon slit pores. For the reader's convenience as well as for the text structure, we adopted annotations for the different char samples. The char sample name will be composed by: 'The gasifying agent'-'level of conversion'. For instance, the char sample obtained after CO_2 gasification at 50% of conversion will be named as: CO_2-X50 char. The reference char is named Ref-char.

7.3 Results and discussion

7.3.1 Char reactivity

The char reactivity in 20% CO_2, 20% H_2O and their mixture at 900°C is shown in figure 7.1. The char reactivity in H_2O is nearly twice as faster as that in CO_2 atmosphere. The char reactivity in 20% CO_2 + 20% H_2O is higher than that in single atmospheres denoting the non-inhibiting character of CO_2 when it is co-reacting with steam in such operating conditions. The char reactivity in mixed atmospheres can be fairly described by adding the reactivities obtained in single atmospheres as shown by the dashed line curve on the figure. The experimental mixed atmosphere reactivity is slightly higher than the one obtained by the additive law, however the approximation is reasonable as this latter is located in the standard deviation zone of the experimental results. The intent of

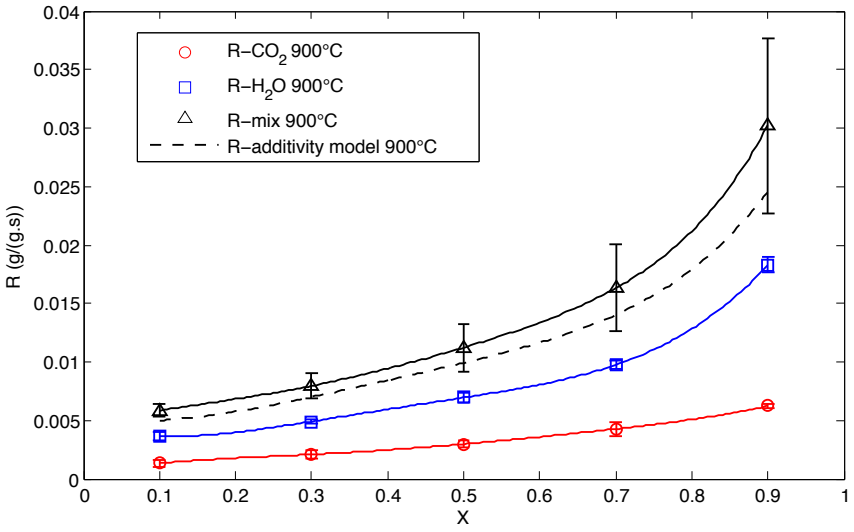

Figure 7.1: Char reactivity in 20% CO_2, 20% H_2O and their mixture at 900°C

coming sections is to try to explain the reactivity trends as well as the apparent additive rates obtained in mixed atmosphere experiments.

In a parallel study that we are performing in our laboratory on the effect of particle size on the evolution of the char apparent reactivity, we found that for the relatively small 0.2 mm char particle there exist diffusional limitations for the three gasification reactions performed with 20% CO_2, 20% H_2O and their mixture at 900°C. In the present case, the char reactivity is an apparent one.

7.3.2 Evolution of the char surface chemistry during gasification: TPD-MS results

Figures 7.2.a, 7.2.b and 7.2.c show respectively the evolution of the CO_2 signal of the CO_2-char, H_2O-char, Mix-char along the gasification. A first overview show that the rate of CO_2 emission from the char surface globally increases with conversion for the regardless of the gasifying agent. This observation denotes the increase of surface functional groups responsible of CO_2 emission, with the extent of the gasification.

For all partially gasified chars, the CO_2 desorption begins at a relatively low temperature of 60-70°C, while it begins at a higher temperature of 110°C for the the Ref-char. The Ref-char shows a broad CO_2 signal in which two peaks can be distinguished, the first at 260°C and the second at 500°C. In several TPD studies on the surface functional groups of carbon materials, authors attribute the low temperature CO_2 peak to carboxylic acid functions and the higher temperature one to anhydrides and lactones [51] [53]. For the CO_2-char, three principal peaks can be distinguished: The first peak around 90-130°C (varying with the conversion level)and a second one at nearly 300°C are attributed to the decomposition of carboxylic acid functions, the third one at 490°C probably resulting from carboxylic anhydrides and lactones decomposition [51]. One can note that the CO_2-X20 char shows a peak at 540°C which vanishes at higher conversion levels. Also, that the first peak is observed at a lower temperature at 70% of conversion. Structural and textural modifications, as well as the nature of neighbouring functional groups can impact on the decomposition temperature of R-COOH groups.

Similarly, we can distinguish three main peaks for H_2O-chars: a first peak at 100°C and a second one at 300°C which are probably resulting from the decomposition of R-COOH groups. The third one

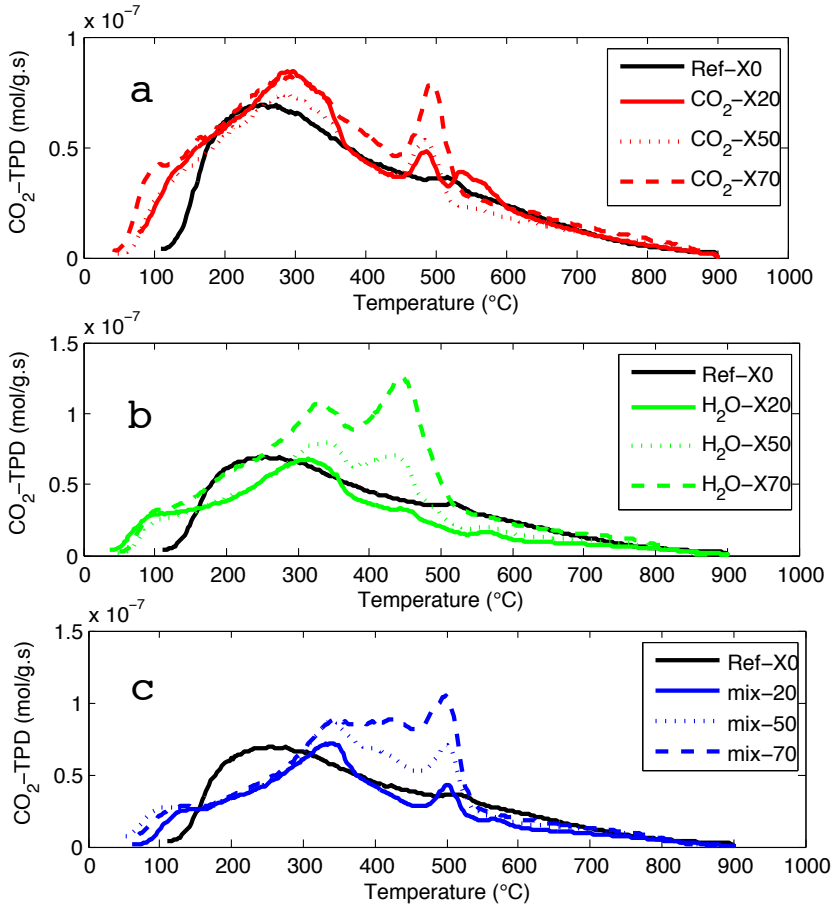

Figure 7.2: CO_2 desorption profile during TPD experiments over the char samples

at 450°C corresponds to the decomposition of more stable forms like anhydrides and lactones. The first obvious observation is that the third peak is observed at a lower temperature than for the CO_2-chars. The second one is that the relative intensity of the second and third peaks changed with extent of conversion. Below 50% of conversion, the presence of RCOOH functional groups predominates over that of more stable forms like anhydrides and lactones, while the tendency reversed beyond 50% of conversion.

The mix char samples shows also the presence of three main peaks: a first peak at a relatively low temperature of 100-130°C and a second one around 330°C. The third one is observed at 500°C. One can note that the second peak is somewhat shifted to higher temperatures compared to single atmospheres. The Mix-X50 char shows a shouldering corresponding to a new peak at nearly 420-430°C, which has likely to do with H_2O gasification. At 70% of conversion, the Mix-X70 char shows a net intensity increase in the temperature range of 390-440°C and appearance of new peaks. The 340°C peak intensity remained unchanged while that at 500°C increased drastically. The Mix-char CO_2 profile shows clearly a complex profile with the rise of new peaks at 50% of conversion and beyond. At 70% of conversion the Mix-X70 char shows a CO_2 emission profile that is likely a mixture of the two profiles obtained respectively in H_2O and CO_2 atmospheres. In the early stages of gasification the peak at 430°C is not observable, probably due to its low intensity denoting potentially a higher contribution of CO_2 to the global gasification reaction. At 50% and beyond its intensity increased, showing the higher contribution of the H_2O gasification reaction.

Figures 7.3.a, 7.3.b and 7.3.c show respectively the evolution of the CO_2 signal of the CO_2-char,

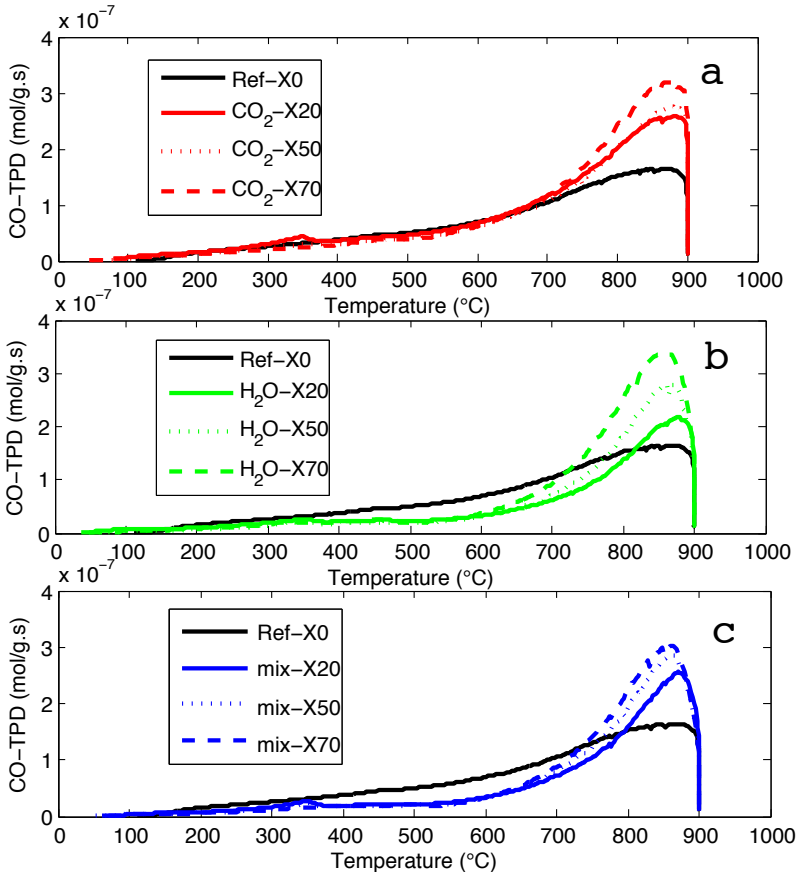

Figure 7.3: CO desorption profile during TPD experiments over the char samples

.

H_2O-char, Mix-char along the gasification. For all the char samples, the CO signal exhibited a single peak with a maximum at around 880°C-890°C. The CO peak intensity increases with the conversion level. For a given char, H_2O char, CO_2 char or mix char, the CO signal is the same in the temperature range of 20-600°C at all the conversion level. The variation with the conversion level are noticed beyond 600°C where the peak intensity increases with the conversion level. However, it is worth-noting that the CO signal for the CO_2 chars fits with that of the Ref-char, while less CO is emitted between 200°C and 600°C for the H_2O-chars and Mix-chars. It is likely that the functional groups responsible of the CO emission in this temperature range reacted with steam at the early stage of gasification (0-20% of conversion). The functional groups emitting CO at low temperatures are thought to be ethers, anhydrides and phenols while at high temperatures quinones are responsible of the CO emissions [53]. Steam would react with these groups at the early stage of gasification (0-20% of conversion).

Figures 7.4.a, 7.4.b and 7.4.c show respectively the evolution of the H_2 signal of the CO_2-char, H_2O-char, Mix-char along the gasification. For the Ref-char, the H_2 began to be emitted at 400°C and strated to increase sharpely at 750°C. The peak intensity is recorded at 900°C. H_2 peak intensity decreased with the conversion for the CO_2 chars. Even the starting of the peak was at higher temperatures for the 50% and 70% converted chars. However, for the H_2O-chars and Mix-chars, the H_2 signal increases with the conversion. The starting of the peak was at lower temperature (680-700°C) than for the CO_2-chars. Also, the peak intensity was greater for H_2O-chars and Mix-

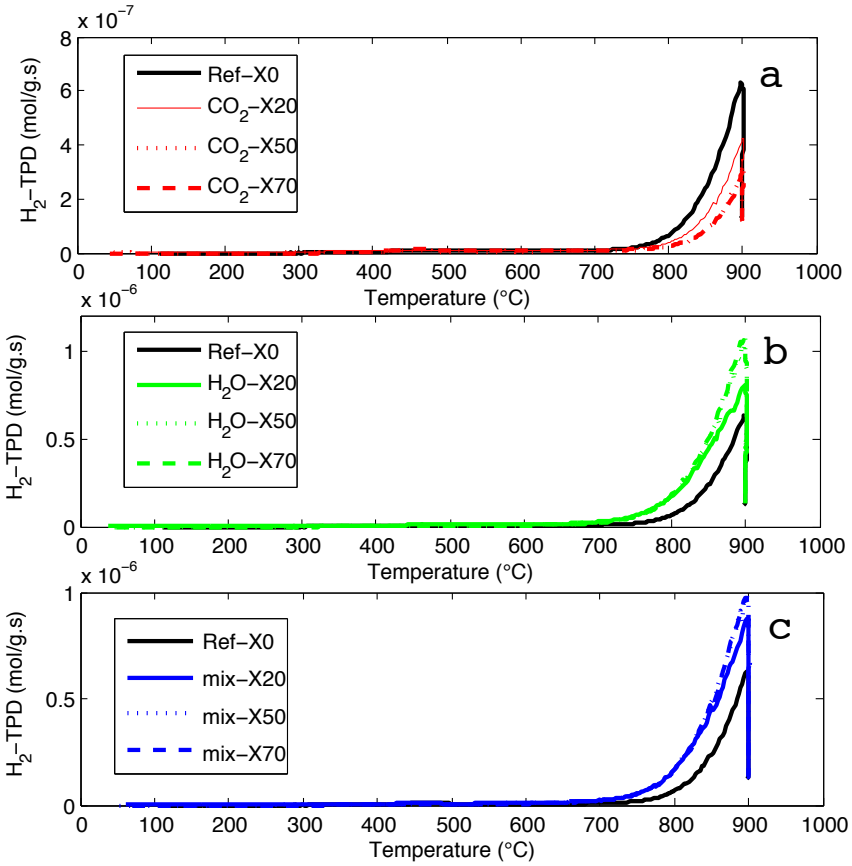

Figure 7.4: H_2 desorption profile during TPD experiments over the char samples

.

chars than for the CO_2-chars. A clear difference is thus noticed on the H_2 emissions when CO_2 is the gasifying medium. It is likely that CO_2 reacts on H sites and reduces consequently the H concentration in the char. The increasing quantity of H_2 emitted from H_2O-chars and mix-chars is related to the continuous hydrogenation of the char surface by the steam gasification reaction.

Figures 7.5.a, 7.5.b and 7.5.c show respectively the evolution of the H_2O signal of the CO_2-char, H_2O-char, Mix-char along the gasification.

For the Ref-char , the water release begins from room temperature and shows a peak at 220°C, very close to the CO_2 peak observed at 250°C. H_2O continue to be emitted up to 900°C. H_2O and CO_2 can come from the carboxylic acid groups decomposition. The dehydration of two neighbouring carboxylic acids leads to the formation of anhydride and water. At a higher temperature, H_2O can be emitted by the dehydration of a phenol and a carboxylic acid, leading to the formation of lactones. H_2O can also be emitted by the dehydration of a phenol and a carboxylic acid, leading to the formation of lactones. It can also result from the dehydration of two phenol groups forming thus an ether [51] [53].

It is of interest to have a look on the integrated signal of H_2O, CO_2, CO and H_2. The total quantities of these gases is an index of the reactive functional groups on the char surface. Figure 7.6 shows the evolution of the total emitted amount of H_2O, CO_2, CO and H_2 from the different char samples along the gasification. H_2O emitted quantity increased a bit for the three chars at 20% of conversion and remained almost constant along the conversion except for the mix char where it decreased beyond 50% of conversion. The CO_2 emitted shows a global trend of increase. The H_2O-

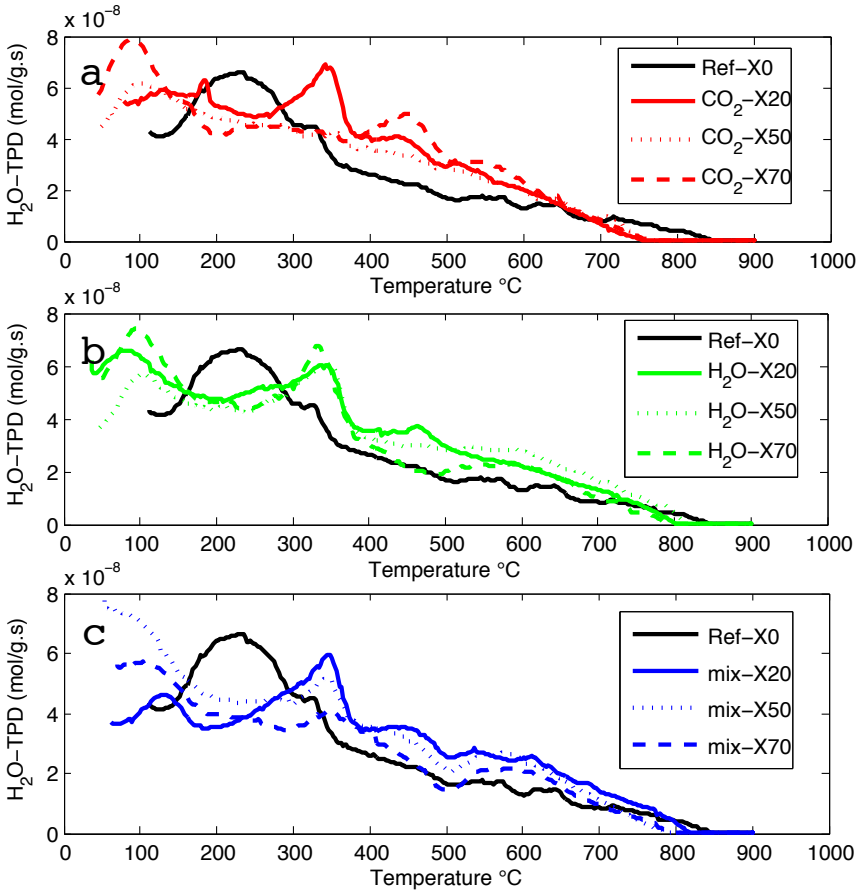

Figure 7.5: H_2O desorption profile during TPD experiments over the char samples

.

char and Mix-char show a decrease in the emitted CO_2 quantities at 20% of conversion compared to the reference state. This can be related to the preferential reaction of H_2O with phenols, ethers and anhydride functional groups in the first stages of the reaction. Afterwards, the CO_2 emitted quantity increased steadily with conversion. CO_2 and H_2O were the minor emitted species while H_2 and CO emissions were greater by almost 1 order of magnitude. The H_2 emissions decreased with the conversion for the CO_2-char, from 1.4 μmol/g for the Ref-char to 0.83 μmol/g at 70% of conversion. On the contrary, it increased for the H_2O-char and Mix-char along the conversion up to 1.9 μmol/g at 70% of conversion. The CO emitted quantity was always higher for the CO_2-char than in the 2 other chars. It increased a bit from 0.8 μmol/g to nearly 1 μmol/g at 20% of conversion and remained almost constant afterwards. On the contrary, it decreased from 0.8 μmol/g to 0.6 μmol/g for the H_2O-char and Mix-char at 20% of conversion and then showed an increase trend up to 70% of conversion. These two trends concerning H_2 and CO shows the difference between H_2O and CO_2 gasification reactions.

What can be noticed when having a global view on the different trend is that the gas evolution for the mix-char followed always the trend of the H_2O-char. In mixed atmosphere gasification, if we consider that the the H_2O and CO_2 react independently, near to 70% of the char is converted by the steam gasification reaction as this latter is twice as fast as the Boudouard reaction. This may explain the fact that the mix-char surface functions tends towards that of the H_2O-char. The fact that the H_2O-chars and Mix-chars contained more H may be explained by the steam gasification reaction.

The water molecule dissociation over the char surface is at the origin of the continuous hydrogenation of the surface and the formation of C(H) sites by various possible intermediate reactions:

$$2C() + H_2O \longrightarrow C(H) + C(OH) \tag{7.8}$$
$$C(OH) + C() \longrightarrow C(H) + C(O) \tag{7.9}$$

The emission of H_2 is due to the dehydrogenation of two neighbouring C(H) or C(OH) sites following the possible reactions of:

$$C(H) + C(H) \longrightarrow 2C() + H_2 \tag{7.10}$$
$$C(OH) + C(H) \longrightarrow C(O) + C() + H_2 \tag{7.11}$$
$$C(OH) + C(OH) \longrightarrow 2C(O) + H_2 \tag{7.12}$$

The decrease of in the H_2 quantities in the CO_2-chars has likely to do with the absence of hydrogenation reaction and/or reaction of CO_2 on these H sites. The fact that the CO_2-chars contain more CO emitting groups may be explained by the Boudouard reaction which is constantly providing CO intermediate species on the char surface:

$$C() + CO_2 \longrightarrow C(O) + CO \tag{7.13}$$
$$C() + CO_2 \longrightarrow C(O) + C(CO) \tag{7.14}$$

Intermediate surface complex are of C(O) and C(CO) type with no external hydrogen supply, while in H_2O gasification, intermediate surface groups are more various: C(O), C(CO), C(H) and C(OH). This is probably why the CO emissions are greater for the CO_2-chars than the H_2O-chars at the same conversion level. The same reasoning can be held for the H_2 emissions.

The total oxygen moles emitted from the char surface can be calculated from a simple balance based on the emitted gas quantities:

$$n_O = n_{H_2O} + 2n_{CO_2} + n_{CO} \tag{7.15}$$

Similarly, the total Hydrogen moles emitted from the char surface can be calculated from a simple balance based on the emitted gas quantities:

$$n_H = 2n_{H_2O} + 2n_{H_2} \tag{7.16}$$

Oxygen and hydrogen moles emitted from the chars are given in table 7.3. The emitted oxygen quantity show a global increasing trend along the conversion for the three chars. The major difference is perceived on the H emitted which decreases for the CO_2-chars and increases for the two others by the continuous hydrogenation of the chars via the steam gasification reaction. Another possible explanation for the H leaving the char is that the CO_2 gasification reaction mechanisms induces structural modifications that promote hydrogen emissions.

7.3.3 Evolution of the Active Surface Area during gasification

Figure 7.7 shows the evolution of the ASA of the CO_2-char, H_2O-char, Mix-char along the gasification. The ASA shows a global trend of increase with conversion for the three chars. It increased from 45 m^2/g at the reference state to 58m^2/g, 59m^2/g and 67m^2/g at 70% of conversion respectively for

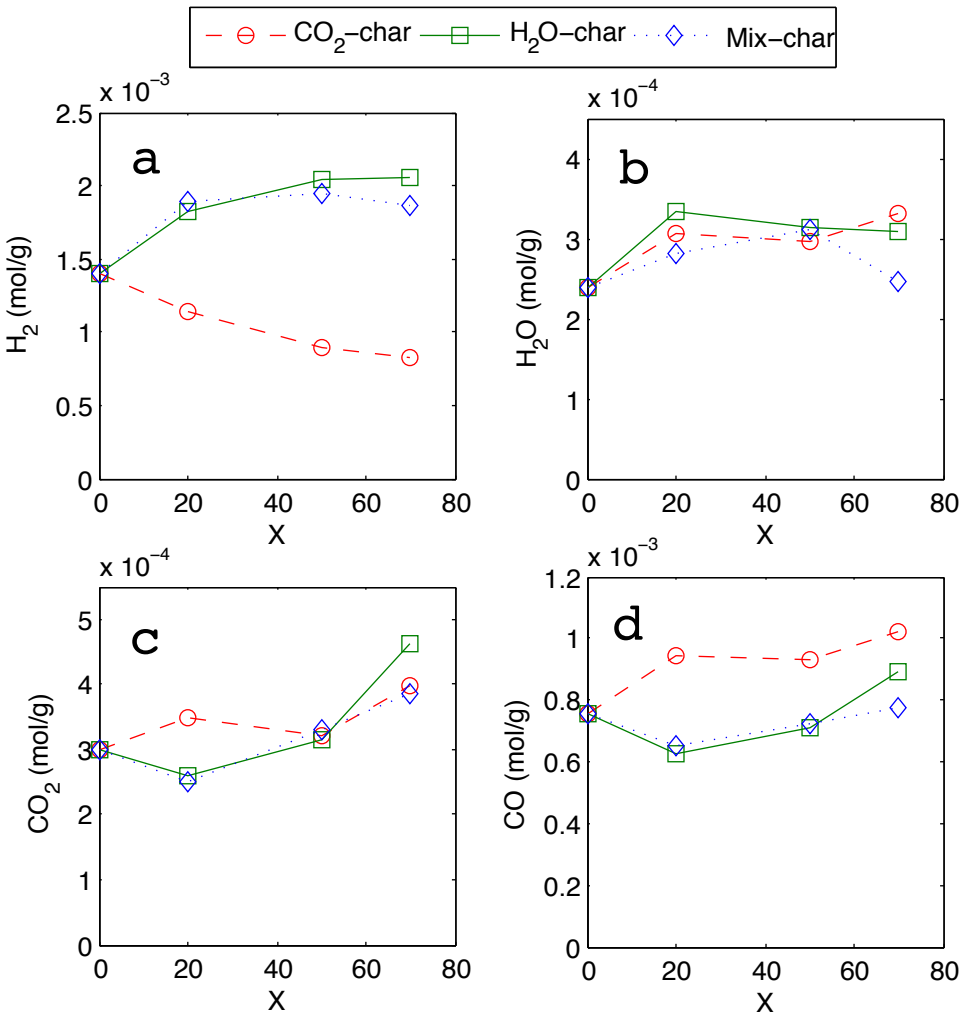

Figure 7.6: Cumulated gas quantities emitted during TPD experiments

.

CO_2-char, H_2O-char and Mix-char. At a defined conversion level, the ASA values of the different chars were very close to each other. Reactivity of beech-chars shows increases along the reaction. The increase becomes very marked from 60-70% of conversion and beyond. The increase of reactivity may be caused in a part by the increase of ASA, but this latter would not be the sole governing parameter as the reactivity and ASA do not increase by the same proportions.

In our previous work, we found that after gasifying the char with CO_2 up to 20% or 40 % of conversion and switching the gasification atmosphere to H_2O, the char reactivity towards H_2O does not change and the char behave as if it was gasified with steam from the very beginning of the reaction. This observation can be explained by the ASA results. In fact, the ASA is representative of the available active site at a defined conversion level. The proximity of CO_2-char ASA and H_2O-char ASA at a defined conversion level can be related to the fact that the char reactivity towards H_2O does not change when the char is gasified priorly with CO_2. When switching the atmosphere H_2O molecules would have a similar number of active site to react on and consequently the reactivity is preserved.

This explanation must be taken with caution as the ASA is an index of the char reactivity towards O_2. However, one can not make abstraction of the obtained results and their eventual link with the

Table 7.3: Evolution of total moles of oxygen and hydrogen emitted from the char surface during TPD-MS experiments

Char	O (μmol/g)	H (μmol/g)
Ref	1.6	3.29
CO_2-X20	1.94	2.9
CO_2-X50	1.87	2.38
CO_2-X70	2.12	2.32
H_2O-X20	1.44	4.34
H_2O-X50	1.69	4.5
H_2O-X70	1.79	4.72
mix-X20	1.44	4.34
mix-X50	1.69	4.5
mix-X70	2.12	4.2

char reactivity. The TPD results shows a similar oxygenation of the different chars which can also explain the non-variability of the char reactivity towards H_2O after a gasification with CO_2.

7.3.4 Char structural evolution: Raman spectroscopy results

Raman spectra of the char samples were very well represented by the five bands deconvolution procedure. Example of Raman spectrum is given in figure 7.8. Over the 60 fitted spectra, the highest error obtained following this fitting procedure was 3%.

The ratios between some major band intensities were used to investigate the char structure evolution during the gasification with CO_2, H_2O and mixture of the gases and to approach the reaction mechanisms. Different peak intensity ratios are plotted in figure 7.9.

For instance when considered the ratio of the D3 intensity and D1 intensity $\frac{I_{D3}}{I_{D1}}$, one can observe that this ratio is almost constant along the gasification reaction with CO_2, only a slight decrease is observed at the end of reaction. On the contrary, in a H_2O containing atmosphere this ratio decreased markedly denoting the preferential reaction of H_2O with the D3 type carbonaceous structures (organic molecules, fragments of functional groups and amorphous sp^2 forms) and/or the growth of small rings to bigger ones of D1 type. Indeed, H radicals generated by H_2O gasification can penetrate into the char matrix and induce the ring condensation. Consequently, small aromatic ring systems condense into large ones in addition to their reaction with H_2O. This assumption is corroborated by the TPD results showing a marked increase of the H atoms at the char surface as well as the decrease of phenol, anhydride and ethers functional groups (belonging to the D3 band) at 20% of conversion after steam gasification. Similarly when plotting $\frac{I_{D3}}{I_G}$, the peak intensity ratio is constant along the conversion for the CO_2 gasification while it decreased in a H_2O-containing atmosphere. Similar results are reported in the literature on the drastic change of the char structure upon contact with steam [42] [46]. The Mix-char structure evolution is similar to that of H_2O-char due to the preponderance of steam gasification reaction in the global carbon gasification.

$\frac{I_{D1}}{I_G}$ increases during the CO_2 gasification denoting the reaction of CO_2 with G type carbons and/or the condensation of small rings into bigger ones of D1 type. However, the trend was in the opposite way for the H_2O gasification as the $\frac{I_{D1}}{I_G}$ decreased along the conversion. These two opposite

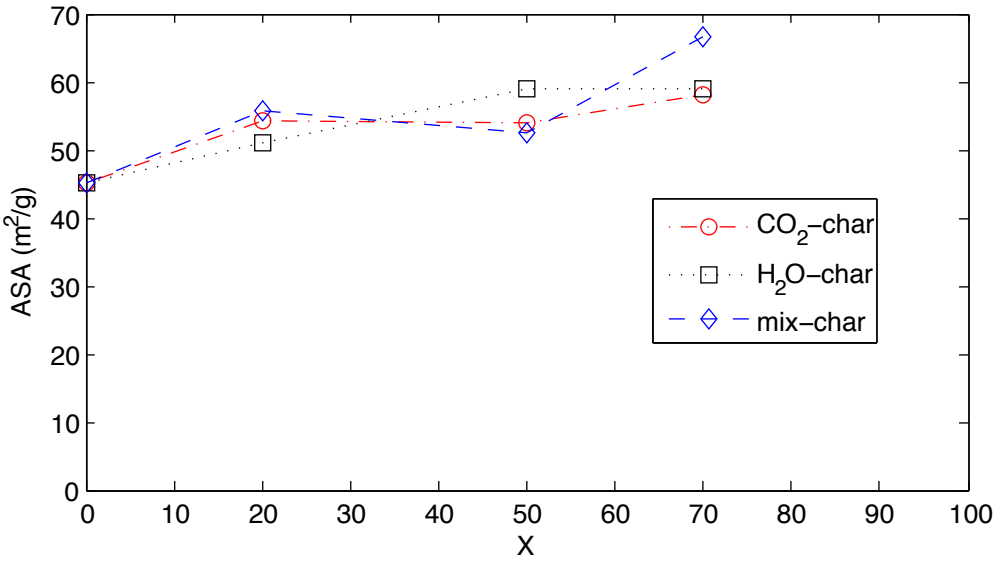

Figure 7.7: Active Surface Area evolution with conversion for the CO_2-char, H_2O-char and mix-char

trends clearly state on the different reaction pathways for the CO_2 and H_2O gasification reactions.

Similar observations are made concerning the $\frac{I_{D4}}{I_G}$ which shows a decreasing trend for the H_2O gasification reaction and an opposed increasing one for the CO_2 gasification reaction. For the mix-char, the trend was to a slight decrease and the curve as located between the single atmosphere ones. The D4 forms are thought to be sp^2-sp^3 sites at the periphery of crystallites and C-C, C=C stretching vibrations of polyene-like structures. Regarding these results, a possible explanation is that CO_2 is likely reacting with the G forms, while D4 forms increases during the conversion by the reaction of CO_2 with G forms and creation of sp^2-sp^3 sites at the periphery of these reacting graphitic structures.

$\frac{I_{D2}}{I_G}$ evolution was similar for the three chars. This ratio increased along the gasification denoting the increase of graphene layers which are not sandwiched between two other ones.

Altogether, these data shows that CO_2 and H_2O reaction follows different pathways. The results obtained for mix-char indicate that steam greatly influence on the char structure which tends to that of H_2O chars due to the predominance of the steam gasification reaction. CO_2 would react in similar ways with the different forms of carbons while H_2O reacts more preferably with amorphous D3 forms.

7.3.5 Evolution of the char textural properties during gasification

Analysisng the char texture evolution at a micrometric level: SEM imaging during gasification

Despite its limited resolution at the micrometer level, SEM imaging allows a direct visualisation of the char texture during gasification. SEM images gather valuable information on the state of the char surface, the development of macropores as well as on the nature and localization of minerals by chemical mapping of char surface using Energy Dispersive X-ray analysis (EDX). Indeed, we observed different evolutions of char texture upon gasification with CO_2 and H_2O. For instance, considering CO_2 gasification, we observed that the gasification reaction affected almost all the surface in an

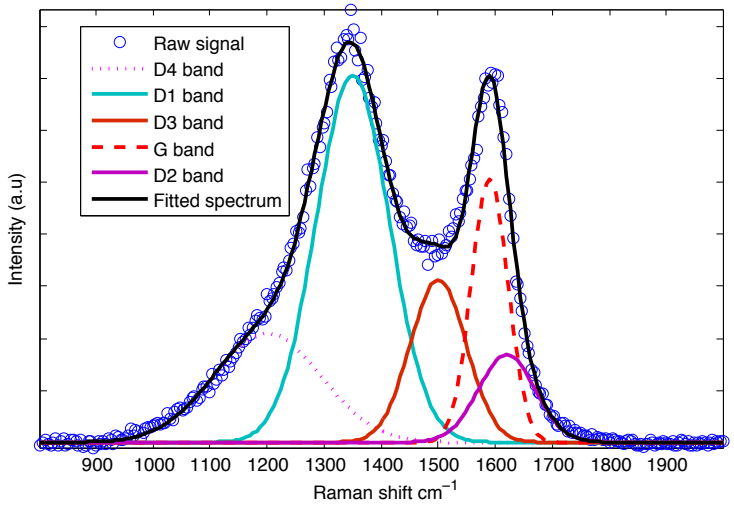

Figure 7.8: Example of Raman fitted spectrum

equivalent way. SEM images of the char along CO_2 gasification are shown in figure 7.10. Considering the non-gasified char (ref-char X=0), SEM images at the level of cells show a quite smooth surface with the presence of mineral particles evenly dispersed. When gasifying the char with CO_2, alteration of the char surface is observed at the cell level as well as on its surroundings. The char surface shows clearly an accentuated porosity along the gasification with CO_2. The char gets a spongelike surface at an advanced gasification conversion level as shown in figure 7.10.

Considering H_2O gasification, we observed some differences compared the the gasification with CO_2. Similarly as with CO_2 gasification, we assessed the porosity development at the level of the wood cells and their periphery. As shown in figure 7.11, the char surface was altered at the level of cells and their near periphery while the rest of the surface was almost as intact and smooth as that of the non gasified char, even at X=0.5. At X=0.7, we could observe the alteration of the whole surface which, as for CO_2 gasification, took a spongelike appearance.

This difference can be explained by a limited diffusion of CO_2 molecules inside the char particle and an accentuated surface reaction, while H_2O, which has a better diffusivity and a smaller molecular size, can get inside the char matrix and have a more developed volumetric reaction. Indeed, SEM is unable to provide information on micro and mesopores which are unobservable. We suspect a high microporosity at the cell surroundings in which H_2O can diffuse and reacts inside while it is inaccessible to the CO_2 molecules which react at the external surface causing its alteration as shown in figure 7.10.

The mix-char show a texture at X=0.2 similar to that obtained under H_2O with a porosity mainly appearing around the cell region. At X=0.5, we observed the alteration of the external surface probably due to CO_2 gasification. As for the two precedent char, at X=0.7, the char surface was quite well damaged with a marked spongy appearance (see figure 7.12).

Evolution of the char textural properties during gasification

N_2 adsorption isotherm of the Ref-char, CO_2-chars, H_2O-chars and mix-chars along the conversion are shown in figure 7.13. The N_2 uptake increases with the extent of conversion for all chars indicating the extension of porosity due to the gasification reaction. The Ref char, and CO_2-chars isotherms are of type I, indicating that those chars are almost exclusively microporous and that the TSA resides in the micropores [187]. Moreover, CO_2-char adsorption isotherms show that the "knee" of the isotherm

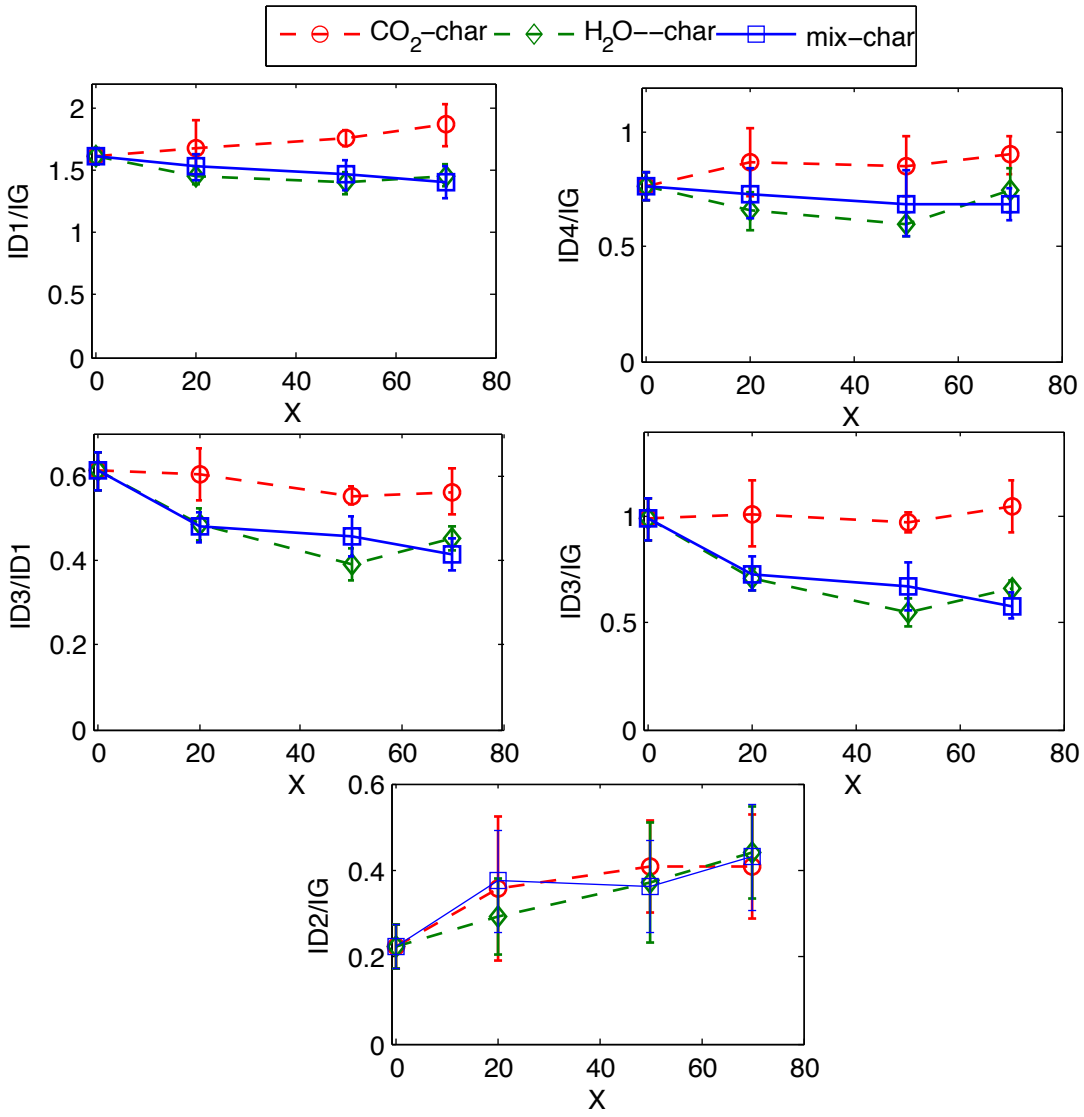

Figure 7.9: Peak intensity ratios evolution during the char gasification in CO_2, H_2O and their mixture

tends to open as the conversion increases indicating the widening of microporosity. This is logical as the pores become wider by carbon removal. According to these results, CO_2 gasification produces two effects, i.e. the development of new micropores together with the widening of the existing ones.

H_2O-chars are also highly microporous regarding the N_2 volume adsorbed at low relative pressure range. For an equivalent conversion level, the N_2 volume adsorbed for H_2O-chars is higher than for CO_2-chars. This indicates that the gasification with H_2O is more volumetric than CO_2 gasification. H_2O molecules would diffuse much more easier inside the char matrix than CO_2 molecules which reacts more on the surface. These findings are corroborated by the SEM observations.

H_2O-chars show the presence of mesopores especially at 50% and 70% of conversion were the adsorption and desorption isotherm show hysteresis loops (P/P0=0.42-1) [187]. The presence of mesopores is accentuated at 50% and 70% of conversion. H_2O gasification produces the development of new micropores as well as the creation of mesopores by pore enlargement and/or coalescence.

Isotherm plots of mix-chars show also that these latter are quite microporous. The increase of the micropore width can also be noted. The hysterisis loops on the isotherms denotes the presence of mesopores which are due most probably to steam gasification of the chars. The mixed atmosphere

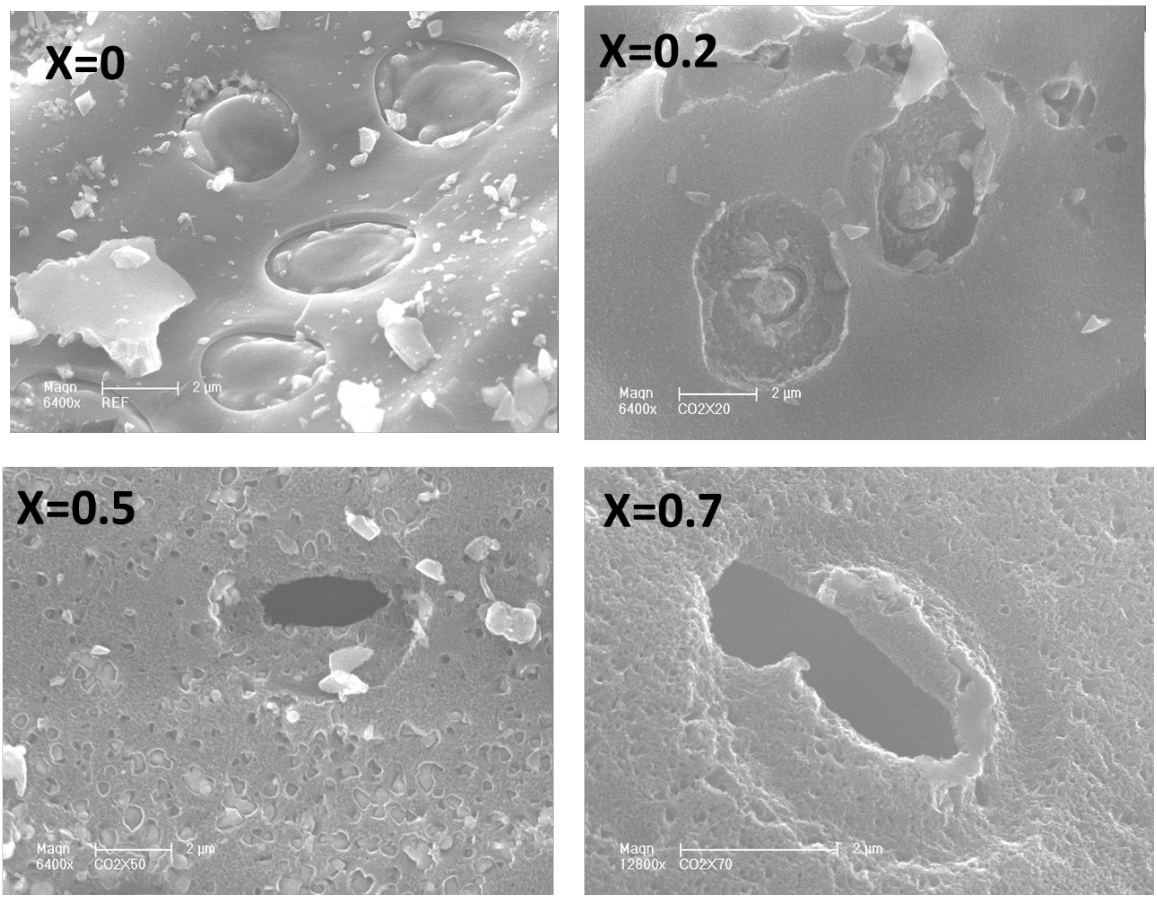

Figure 7.10: SEM images of the char along CO_2 gasification

chars show a higher porous volume than the single atmosphere chars for equivalent conversion levels. This is somewhat surprising as it underlies that the gasification reaction occurs in more volumetric way in mixed atmospheres than in single atmospheres.

The TSA of chars calculated according to the BET theory are shown in figure 7.14. For the three chars, the TSA increases almost linearly with conversion. At equivalent conversion levels, the TSA of CO_2 chars is always lower than that of the H_2O chars. This indicates that the two gases develop different porosity when reacting with the char. H_2O molecule are smaller than CO_2 molecules and can thus access to smaller micropores and open new pores that are inaccessible for the CO_2 molecule. This results in a more developed porosity.

The TSA of mix chars is quite close to that of H_2O chars along the conversion. When considering separately the contribution of H_2O-char and CO_2-char gasification reactions, near to 66.6% of the TSA is created by the steam gasification while 33.3% of the TSA is created by the CO_2-char gasification reaction. A theoretical TSA according to separate gasification reaction reads:

$$TSA(mix)_{the} = 0.66TSA(H_2O) + 0.33TSA(CO_2) \tag{7.17}$$

The theoretical mix-char TSA is plotted in figure 7.14. One can see that this consideration does not reproduce the TSA obtained in mixed atmosphere, which is found to be higher.

Density functional theory (DFT) has been proposed as a good approach to characterize microporous solids using either N_2 a probe molecule. Grossly speaking, The DFT approach models the real isotherm by combining theoretical isotherms (kernels) calculated for individual pores for a given adsorbent - adsorbate system. This kernel of theoretical isotherms can then be used to estimate the

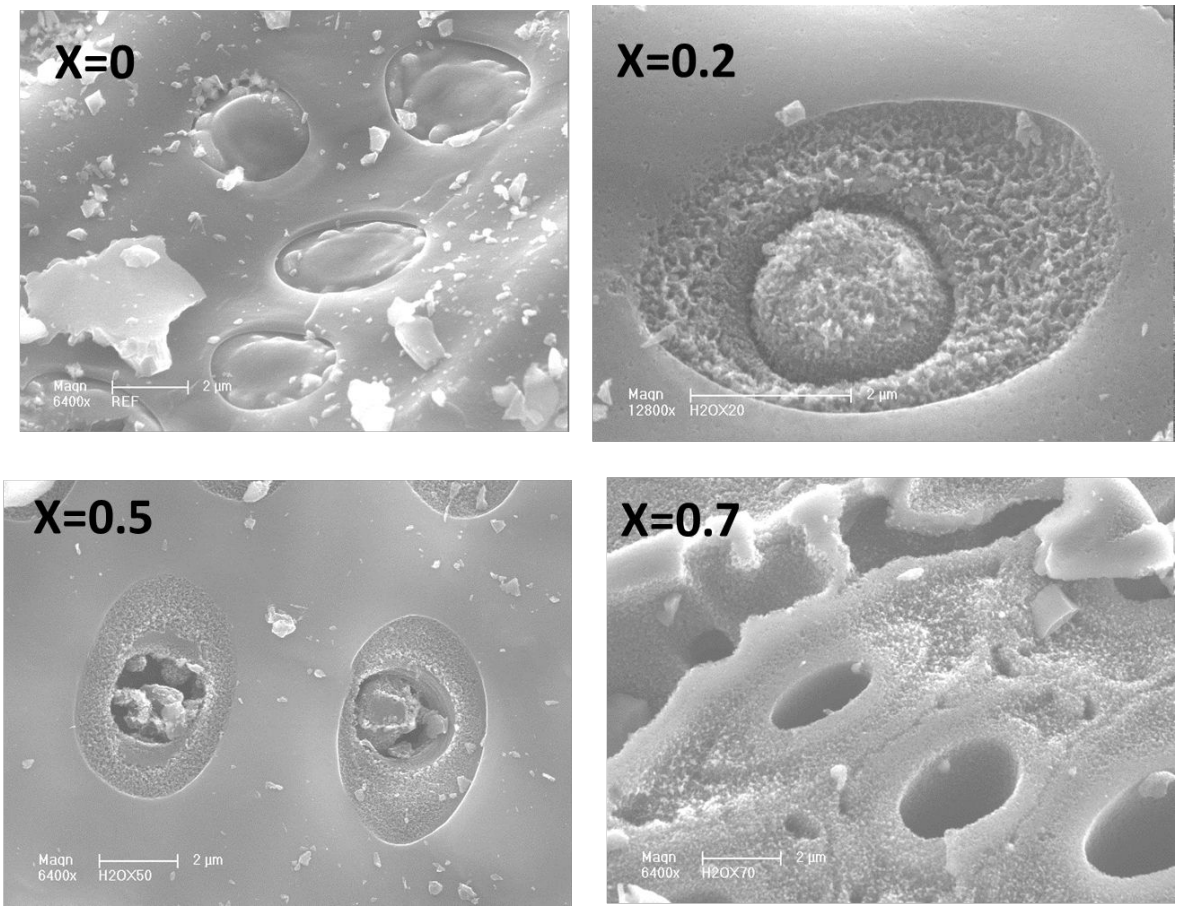

Figure 7.11: SEM images of the char along H_2O gasification

pore size distribution (PSD) for a given porous solid, i.e. the volumetric contributions of pores with different sizes whose theoretical isotherms best fit the experimental data. For the low conversion level of 20%, there is a development of ultra-micropores of 6 angstroms for the the three chars. The development of narrow microporosity (pores less than 8 angstroms) with the extent of reaction for all chars demonstrates the presence of diffusional limitations during the gasification reactions. Beyond 20% of conversion, one can notice the development of 11 angstroms micropores in the case of H_2O gasified chars, while we notice a larger microporosity and the formation of small mesopores for the CO_2 gasified chars. The mix chars show a pore size distribution similar to that of the CO_2 chars (bimodal distribution), however the pore volume is much more developed in mixed atmosphere gasification as noticed above.

What is surprising in the PSD of mix-chars is the absence of the 11 angstroms micropores developed in steam gasification. This may be related to the fact that H_2O, when reacting with the char, facilitates the CO_2 access to the pores which reacts on and induces the micropores widening. H_2O would therefore enhance the gasification of char by CO_2 by facilitating its access to the reactive area. Owing to these results, there can be a synergy between the two molecules for the access to the internal surface area of the char. One one hand, CO_2 and H_2O can compete for the same active sites, which tends to lower the reaction rate while in the other hand, H_2O can facilitate the CO_2 diffusion to other active sites, which tends to increase the reaction rate, the whole leading to an observed near-additivity. These results indicate the situation of mixed atmospheres is more complicated than considering a simple additive law.

The increase in O_2-ASA is somewhat small with the extent of conversion compared to that of

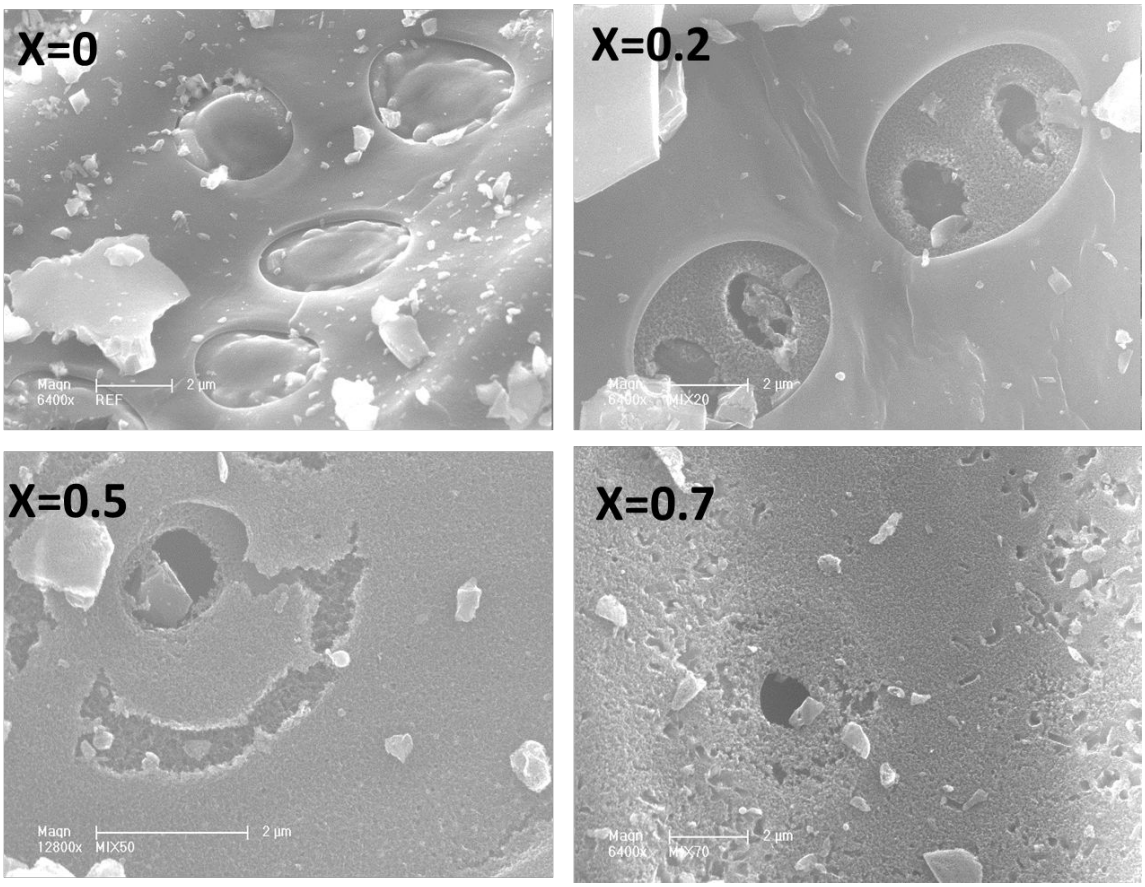

Figure 7.12: SEM images of the char along gasification in mixture of H_2O + CO_2

TSA. The TSA and ASA-O_2 evolution along the conversion as well the normalized values with respect to the reference char (X=0) are summarized in table 7.4. The ASA represent clearly a small portion of the TSA. Not all the char surface is participating to the reaction. The increase of TSA and ASA are far from being identical. The values of normalized ASA and TSA indicate that for instance, the ASA of H_2O-char increased by a factor of 1.3 at 70% of conversion, while its TSA increased by three folds. Laine et al made similar observations as they noticed that the TSA of coal char increased by more than 15 folds at 35% of conversion when reacting with O_2, while its ASA increased nearly by 1.8 folds [64]. Similar observations were also made by [65]. The ratio $\frac{ASA_X}{TSA_X}$ was seen to decrease with conversion as the ASA represented near to 10% of the TSA for the Ref-char and decreased respectively to 5.7%, 4.4% and 4.4% for the CO_2-char, H_2O-char and mix-char at 70% of conversion.

The decrease of oxygen atoms per unit of TSA is on the opposite trend of the reactivity increase along the conversion. There would therefore another influencing factor compensating the decrease of oxygen atoms per unit of TSA and leading to the reactivity increase. This will be discussed in the next sections.

7.3.6 Evolution of minerals during gasification

EDX analysis performed along with the SEM observations revealed quite interesting information about the type of mineral contained in the chars as well as their dispersion on the char surface. Potassium and magnesium were found to be present in a very diffuse state in the char matrix while

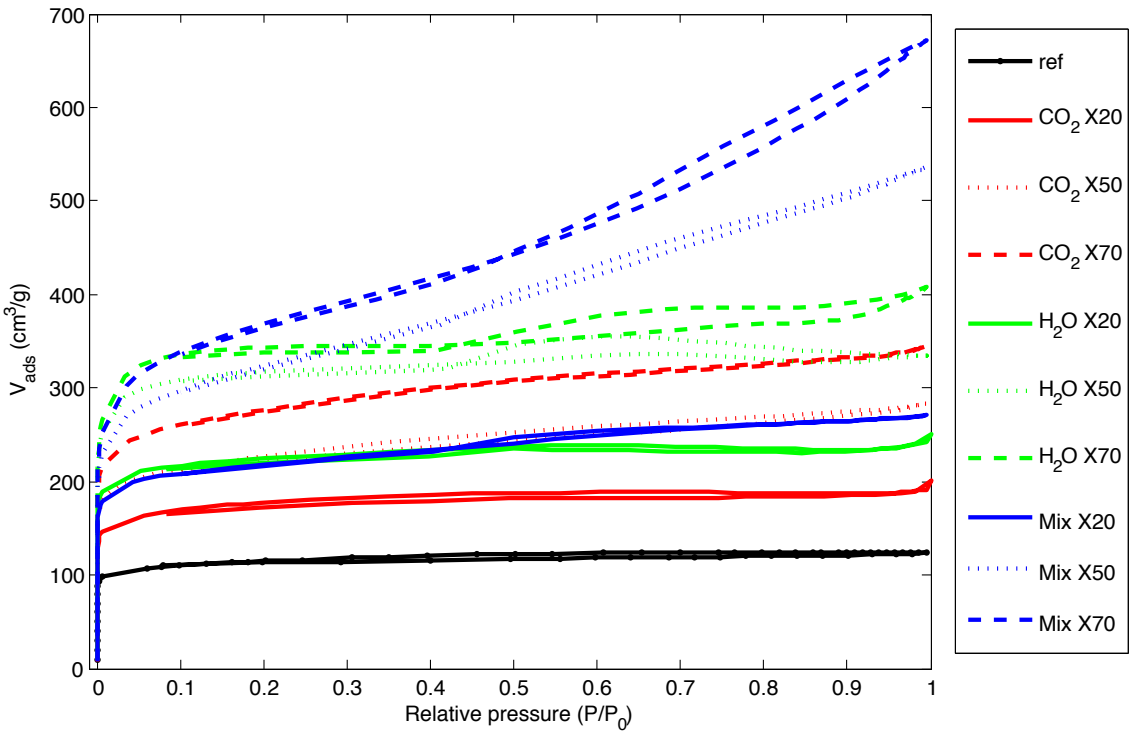

Figure 7.13: N_2 adsorption isotherm of the CO_2-chars, H_2O-chars and mix-chars along the conversion

calcium was found in the form of bigger clusters located at the char surface. Similarly, silicon was found in the form of big clusters located at the mouth of pores. Clearly, we could distinguish two different behaviour for the mineral species: those who are evenly dispersed through the char matrix like potassium and those who migrate to the surface and form clusters like calcium and silicon. The clusters were seen to contain a mixture of metals, and high concentrations of oxygen are present, indicating that the minerals are in the oxide or carbonate form. These results are in accordance with the findings of [29]. Dispersion of minerals as well as their nature and concentration play a crucial role in the heterogeneous gasification reactions [50].

The relative concentration of mineral species in the total mineral phase of the chars along the gasification reactions is shown in figure 7.16. We can see on this figure that the main constituents of the char mineral part are Alkali and Alkaline Earth Metals (AAEM). Potassium, calcium and magnesium form near to 60% (molar basis) of the total minerals in the ref-char. Follows then transition metals like iron, manganese, aluminium and zinc with a molar concentration of about 30% and finally non-metals like sulphur, silicon and phosphor with a molar concentration of 10%. Along the gasification and depending on the reacting gas, some minerals were retained in the char while others left went to the gas phase. For instance, the relative concentration of K in the mineral part increased during CO_2 gasification from 27 to 43% while that of Ca remained almost constant. Mg concentration also increased along CO_2 gasification. A concentration decrease is observed for Zn and Al which are likely removed from the solid matrix during CO_2 gasification. Fe content also decrease while Mn, S and P concentration were relatively constant. During H_2O gasification, AAEM species behaviour was almost the same as for CO_2 gasification. In a similar way the Zn content in ash decreased markedly along the conversion. However, Al was more retained with H_2O than with CO_2 and so was Si which concentration increased with conversion. Fe concentration increased up to 50% of conversion and then decreased. S and Pcontent were almost constant. For mixed atmosphere gasification, AAEM species concentration increased with gasification and

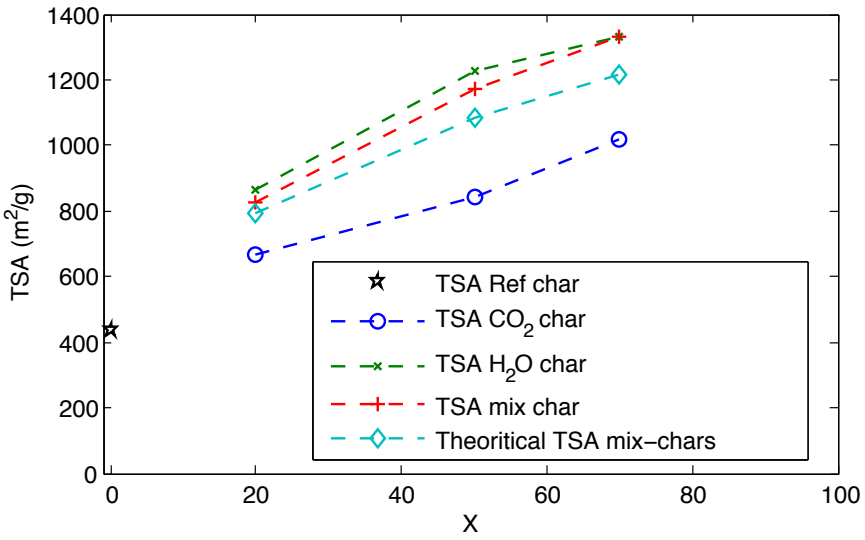

Figure 7.14: TSA evolution of the CO_2-chars, H_2O-chars and mix-chars along the conversion

Table 7.4: Summary of the O_2-ASA and TSA evolution along the conversion

Char	ASA-O_2	TSA	$\frac{ASA_X}{ASA_{X=0}}$	$\frac{TSA_X}{TSA_{X=0}}$	$\frac{ASA_X}{TSA_X}$
Ref	45	437	1	1	0.1
CO_2-X20	54	669	1.2	1.5	0.081
CO_2-X50	54	842	1.2	1.9	0.064
CO_2-X70	58	1020	1.3	2.3	0.057
H_2O-X20	51	866	1.1	2	0.058
H_2O-X50	59	1225	1.3	2.8	0.048
H_2O-X70	59	1332	1.3	3	0.044
mix-X20	56	824	1.2	1.9	0.067
mix-X50	53	1173	1.2	2.8	0.048
mix-X70	66	1332	1.5	3	0.044

remained almost constant for higher conversion levels. *Zn* was highly removed as in the case of single atmospheres. *Si* concentration was almost constant while that of *Al* decreased as for CO_2 gasification. *Fe*, *Mn*, *P* and *S* content were relatively constant along the conversion. The main difference between CO_2 and H_2O gasification is seen on the behaviour of *Al* and *Si* species which are removed in the presence of CO_2 and concentrated in steam gasification.

The relative abundance of mineral species is of high importance as some of them play a well admitted catalytic role in H_2O and CO_2 gasification [70] [72] [73]. The catalytic species such as *K*, *Ca*, *Mg* and *Fe* constitutes active sites inside the char on which gasification occurs via several steps including carbonation, de-carbonation and formation of metal oxides among others [50]. While catalytic active species concentrates into the char, the number of active sites increases consequently which may explain the increasing trend of the char reactivity along conversion. The relative abundance of catalytic active species may also be perceived through the TPD results as these latter constitute potential sites for oxygenation and hydrogenation. Other species inhibit the gasification reaction such as *Si* and *P* [72][73]. Hognon et al. [73] reported two typical behaviour of biomass

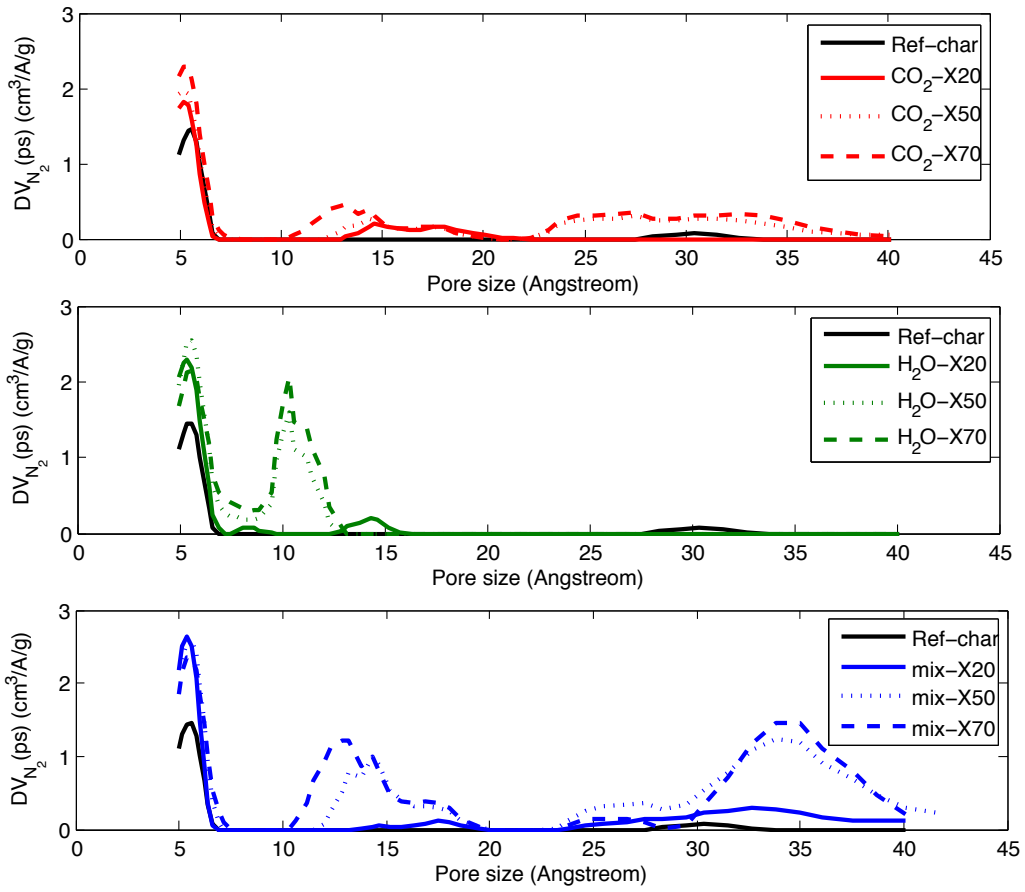

Figure 7.15: DFT pore size distribution for the CO_2-chars, H_2O-chars and mix-chars along the conversion

char, those which reactivity decrease along the conversion having a K/Si ratio below one, and those having a K/Si ratio above one exhibiting a constant reactivity or slight decrease followed by reactivity increase beyond 70% of conversion. Si is thought to encapsulate catalytic active species such as K reducing consequently its activity. Our results show quite interesting potential synergy between CO_2 and H_2O during gasification as the presence of CO_2 induces the departure of Si from the char which is an inhibitor in steam gasification.

7.3.7 Discussion on the relationship between the char reactivity and the char properties

"What is (are) the most influencing factor(s) conditioning the char reactivity ?" is a question for which we attempt to provide an answer. If the char reactivity is conditioned by one or more of the char properties, there must be a proportionality relation between them. We tried to search for correlation between the char reactivity and the different structural, chemical and textural parameters that we measured in the conversion level range of 20-70%. We found no proportionality with the structural parameters obtained by Raman analysis. The increase of TSA and ASA were not proportional to the char reactivity increase as discussed before.

We found, however, that the char reactivity is reasonably proportional to the product of 2 of the analysed properties, namely the TSA and the amount of oxygen in CO and CO_2 desorbed from

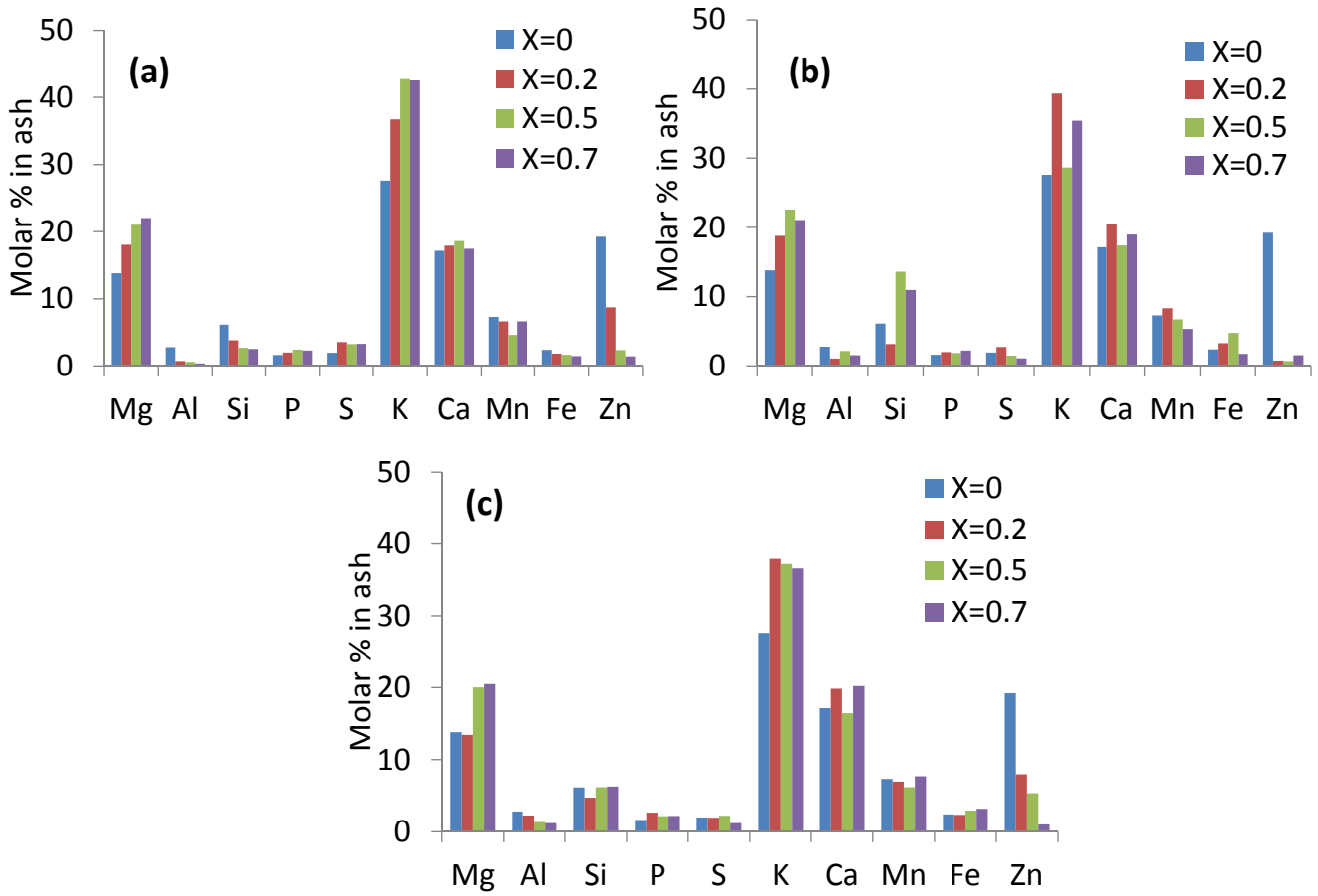

Figure 7.16: Concentration of minerals in ash (molar %) along the gasification:(a) CO_2 gasification, (b) H_2O gasification and (c) mixed atmosphere

the char species. Dividing the char reactivity by the product of these two quantities leads to a relatively constant value, specially for the CO_2-char and H_2O-char. The results are less accurate for the mix-char as shown in figure 7.17.

According to these results there would be two governing parameters for the char reactivity: a chemical parameter related to the presence of the oxygenated functional groups on the char surface and the TSA of the chars which is more related to the species diffusivity inside the porous char. In our case, the gasification reactions are performed with slight diffusional limitations.

7.4 Conclusions and discussion on the gasification reaction unfolding in H_2O, CO_2 and their mixture

Owing to the different observed results, one can clearly see that H_2O and CO_2 gasification reactions have different pathways. The Raman spectra show different char structural evolution during the two reactions. H_2O reacts preferentially with D3 carbon form and probably induces ring condensation due to the presence of mobile H on the char surface, while CO_2 is likely reacting preferably with more ordered carbon forms (D1 and G). The emission profiles of the different gases during TPD experiments are also different. H_2O appears to react preferably with ethers, phenols and anhydrides in the first stages of the reaction as revealed by the TPD analysis. This observation can be correlated with

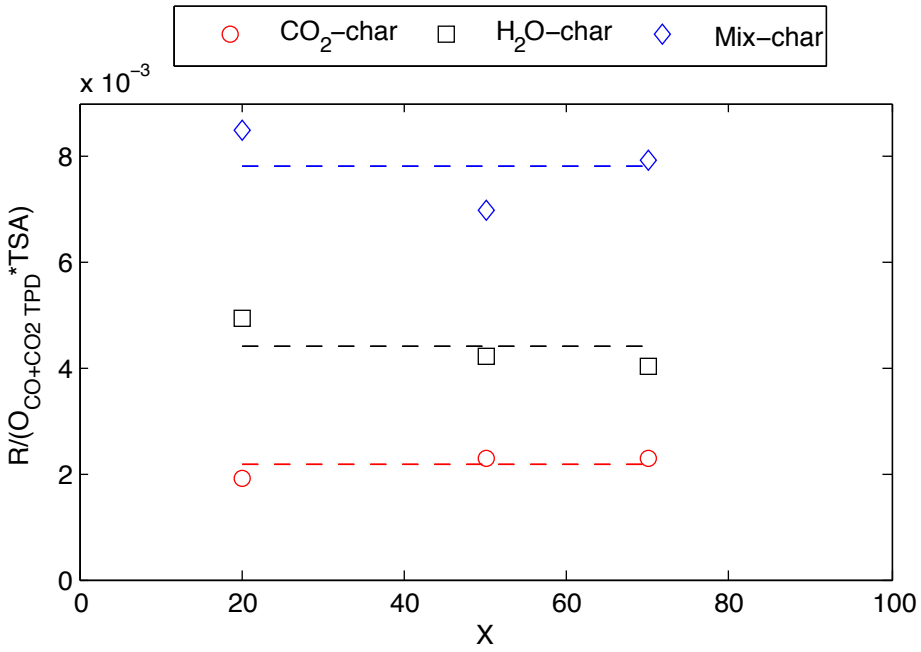

Figure 7.17: $\frac{Rapp(X)}{(TSA(X)\,[O(X)_{(CO+CO_2)TPD}])}$ for the CO_2-chars, H_2O-chars and mix-chars along the conversion

the decrease of the $\frac{ID3}{ID1}$ ratio, as these functional groups belong to the D3 form in poorly organised carbonaceous materials. Moreover, the marked increase of surface H atoms due to steam gasification, as revealed by TPD, is accompanied by the decrease of the $\frac{ID3}{ID1}$ ratio. The decrease of $\frac{ID3}{ID1}$ ratio is less marked beyond 20% of conversion and corroborated by the lower increase of H atoms on the char surface. The char surface chemistry is different for the two reactions as CO_2 chars contains more emitting CO surface functions, while H_2O gasified chars are much more hydrogenated.

The textural properties also differ. H_2O gasification leads to a higher internal char porosity at the same conversion level due to the more volumetric gasification reaction, develops preferentially 10 Angstroms micropores and creates mesoporosity along the conversion. The CO_2 gasification develops mainly micropores, but with a larger pore size distribution, and a very low mesoporosity. CO_2 gasification affects more the char surface than the particle core as revealed by SEM imaging and porosity measurements.

What is noticed in the case atmosphere gasification is that the mix char properties tend to those of the H_2O char. This is quite logical as the steam gasification reaction participates by near to 70% to the global gasification reaction. The CO_2 TPD profile of mix chars especially denotes the contribution of the two reactions as it appears as a blend of the CO_2 TPD profiles obtained for single atmosphere chars. However, it was found that the micropore size distributions of mix chars tend toward those of CO_2 char. The microporosity in the range of 10 to 40 Angstroms is better developed in mixed atmosphere gasification. Micropores of 25 to 40 Angstroms are exclusively developed in the case of CO_2 gasification. H_2O may thus enhances the access of CO_2 to these kind of micropores to react on. The other case is also possible, as the developed micropores by CO_2 may become the preferential reactive sites for H_2O, explaining thus the enhanced development of these latter. It is therefore not excluded that there may be a competition between CO_2 and H_2O for the reaction on a part of the active surface and simultaneously a mutual synergy effect by an enhancement of the

internal diffusivity. Besides, CO_2 was seen to enhance the departure of Si from the char matrix while it was retained with steam. There may be thus synergistic effects in mixed atmosphere gasification due to the action of CO_2 on Si which is known to be an inhibitor of the steam gasification.

In conclusion, CO_2 and H_2O reactions follows different pathways. However, in mixed atmosphere gasification, these two molecules do not react independently from each other. There are in fact several competition and synergy interactions that lead to an additivity-like mechanism.

Acknowledgements

This work results from the contribution of many researchers. The authors want to thanks gratefully Joseph Dentzer for his help in TPD-MS experiments and Habiba Nouali for her help in char textural analysis. They also want to thank Laure Michelin and Ludovic Josien for their help in SEM and X-ray fluorescence analysis. The authors also acknowledge the national research agency ANR-France for its financial support in the RECO_2 project. They also wish to express their appreciation to Bernard Auduc for his technical support.

General conclusion and prospects

The present work was performed in order to analyse the effects of CO_2 enriched atmospheres on biomass pyrolysis and char gasification reactions in High Heating Rate and Low Heating Rate conditions. The study was performed at the particle level scale (biomass and char particles) with the aim to answer to two main objectives belonging to different spheres:

- The first one is to provide practical data on pyrolysis and char gasification reaction in the presence of CO_2. The aim is to analyse the effects of CO_2 on the above-mentioned reactions from a macroscopic view point. That means to analyse the effects of CO_2 on the biomass pyrolysis rate as well as on the char reactivity. This part of the work belongs to the sphere of chemical engineering.
- The second objective was to understand the unfolding of the char gasification reactions with CO_2, H_2O and their mixtures. To do so, the chemical, structural and textural features of the char were monitored along the gasification reaction. This part of the work is rather performed at the level of the char basic structural units, the porosity formed by their spatial disposition as well as their surface chemistry. This part of the work belongs to the sphere of analytical and solid state chemistry.

As we studied the impacts of CO_2 on chars prepared by slow and fast pyrolysis, it comes out in a general view that for the same operating conditions of temperature and gas partial pressure, HHR-char gasification reactivity is near to 4 times higher than that of LHR-chars. The introduction of CO_2 alongside steam enhances the char gasification rate for both heating rates. The mixed atmosphere char reactivity can be fairly expressed by an additive law reflecting an "apparent" passive cooperation of steam and carbon dioxide in the gasification reaction. Specific experiments carried out in this work showed that converting a char under CO_2 to a defined conversion level did not affect its reactivity during further conversion under H_2O. We will develop further the main conclusions in the following paragraphs.

In the first big part of the thesis we were interested in High Heating Rate conditions such as encountered in fluidized bed gasifiers. We performed biomass pyrolysis reaction in CO_2 containing atmospheres at 850°C and analysed the effects of CO_2 on the pyrolysis rate, gas yield ans char reactive properties. Afterwards, we studied the HHR-chars gasification with CO_2, H_2O and their mixtures varying the reacting gas molar fraction between 0.1 and 0.4 in a temperature range of 800 to 950°C typical of practical gasification conditions. We compared then the reactive properties of these chars with those prepared with LHR. Then, we studied for both cases the effects of CO_2 as a co-reactant with steam on the char gasification reactivity at 900°C for various CO_2 and H_2O concentrations and tried to learn more on the mixed atmosphere gasification mechanism. The last part in the frame of HHR conditions was dedicated to the study of the global pyro-gasification reaction in pure CO_2 at 850°C. The intent was to analyse the unfolding of the global transformation of a biomass particle to gas (including the pyrolysis and char gasification steps) when introduced quickly in a hot reactor

containing pure CO_2. The Macro-TG device used in the present work allows to monitor the mass loss accurately in such HHR conditions. We developed in parallel a numerical model with the aim to better understand the global pyro-gasification reaction in pure CO_2.

The main conclusions related to the effects of CO_2 on the HHR pyrolysis and char gasification are:

- CO_2 does not influence the biomass pyrolysis rate in HHR conditions at 850°C.
- The CO_2 is thought to react with radicals on the char surface formed during the fast pyrolysis and impacts slightly the char yield
- The presence of CO_2 induces a higher CO production. The CO_2 may have reacted with the char, in the gas phase via reverse water gas shift reactions or participates to other reactions of tar reforming leading to more CO.
- The char obtained after pyrolysis in a CO_2 is different from the one obtained after nitrogen as they have different TSA and temperature programmed oxidation profiles. Nevertheless, their reactivities towards CO_2, H_2O or O_2 were nearly the same.
- Introducing CO_2 along steam induces an increase of the char gasification reaction rate.
- Mixed atmosphere gasification experiments on HHR-chars at 900°C for various CO_2 +H_2O concentrations in the gasifying medium show that the char gasification reactivity in mixed atmosphere could fairly be expressed as the sum of the individual reactivity.
- The experimental results of 1 mm thick biomass particles pyro-gasification in pure CO_2 at 850°C, showed that the char gasification stage is the rate limiting step in the pyro-gasification process. The pyrolysis ended at about 25 s while near to 600 s were necessary to achieve the char gasification reaction. A pure CO_2 atmosphere had no major effects on the pyrolysis rate compared to reference pyrolysis in an N_2 atmosphere. After the pyrolysis stage, a 10 s duration plateau was observed before the starting of the char gasification. This plateau was captured by the numerical model: the CO_2 was present inside the char particle, but the temperature was too low to induce a starting of the gasification. The numerical model developed in this work sheds light on the unfolding of the whole pyro-gasification of 1 mm thick wood-chips. This global approach, for high heating rate conditions, is not tackled in the literature.

The second big part of the thesis was dedicated to the gasification of chars prepared in Low Heating Rate conditions such as in fixed bed or staged gasifiers. In first place, we focused on the issue of intrinsic conditions as well as the influence of the char particle size on its gasification reactivity. This issue was tackled using the Thiele modulus approach. We performed CO_2 and H_2O char gasification experiments at 900°C on a large particle size range from powdery particles of 0.04 mm size to relatively big ones of 13 mm. Thanks to this, we evidenced the extent of diffusional limitations when increasing the particle size and determined conditions for which the reaction is performed in the chemical regime. In second place, we studied the influence of temperature and char particle size on the char gasification reactivity in mixed atmospheres of CO_2 and H_2O and tackled also the issue of cyclic atmosphere gasification for which we analysed the effects of alternating CO_2 and H_2O on the char gasification reactivity. This part of the study provides valuable information on the char reactivity in practical operating conditions as a wide temperature and particle size ranges are covered. Finally, we studied -for the case of LHR chars- the evolution of the char chemical, structural and textural properties along the gasification with 20%H_2O, 20% CO_2 and their mixture at 900°C for the sake of understanding the unfolding of the char gasification reaction. This issue is still not

totally clarified in the literature as the gasification reaction is generally tackled from a macroscopic view point with the aim to have char reactivity data. The char structure, surface chemistry, mineral content, texture and ASA were monitored along the gasification reaction at conversion levels of 20%, 50% and 70%. This part of the work provides worthy information on the unfolding of the gasification reactions.

The main conclusions related to the effects of CO_2 on the LHR-char gasification are:

- The apparent char gasification reactivity depends highly on the particle size. Increasing the particle size from 0.04 mm to 13 mm reduced by more than 20 times the char gasification reactivity both for H_2O and for CO_2 reactions at 900°C.
- At 900°C, the char gasification by H_2O or CO_2 is performed in the chemical regime for 0.04 mm sized char particles or smaller.
- For both H_2O and CO_2 gasification reactions, we found similar effectiveness factor evolution with particle size. The ratio of diffusion-reaction was nearly the same for both molecules. However, H_2O was found to have a higher reactivity and a higher diffusivity than CO_2. The equivalence of the diffusion-reaction competition is "fortunate".
- For 0.2 mm sized char particles, the char reactivity in mixed atmosphere of H_2O and CO_2 was nearly equal to the sum of the individual reactivity at 800°C and at 900°C but lower than it at 1000°C and 1100°C .
- The char gasification reactivity at 900°C in a mixture of 20% CO_2 + 20%H_2O can be expressed fairly by an additive law in a wide particle size range, from 0.2 mm to 13 mm. The char reactivity in mixed atmosphere was correctly modelled adopting a linear combination of the individual reactivities in H_2O and CO_2. The linear coefficients were optimized for a best fit to the experimental data. However, we could not draw conclusions on the mixed atmosphere reaction mechanisms as there was several possible combinations of the linear coefficients that ensure a good representation of the experimental data.
- The char reactivity at 900°C, for particle size range of 0.2 mm and 13 mm, does not depend on the historic of gasification. The char reactivity to H_2O or CO_2 at a defined conversion level is constant whatever the gas has the char anteriorly reacted with.

The main conclusions related to the unfolding of the H_2O, CO_2 and mixed atmosphere gasification of LHR-char are:

- H_2O and CO_2 gasification reactions have different pathways.
- The Raman spectra show different char structural evolution during the two reactions. H_2O reacts preferentially with D3 carbon form and probably induces ring condensation due to the presence of mobile H on the char surface, while CO_2 is likely reacting preferably with more ordered carbon forms (D1 and G).
- The emission profiles of the different gases during TPD experiments are also different. H_2O appears to react preferably with ethers, phenols and anhydrides in the first stages of the reaction as revealed by the TPD analysis. This observation can be correlated with the decrease of the $\frac{ID3}{ID1}$ ratio, as these functional groups belong to the D3 form in poorly organised carbonaceous materials. Moreover, the marked increase of surface H atoms due to steam gasification, as

revealed by TPD, is accompanied by the decrease of the $\frac{ID3}{ID1}$ ratio. The decrease of $\frac{ID3}{ID1}$ ratio is less marked beyond 20% of conversion and corroborated by the lower increase of H atoms on the char surface. The char surface chemistry is different for the two reactions as CO_2 chars contain more emitting CO surface functions, whileH_2O gasified chars are much more hydrogenated.

- The textural properties also differ.H_2O gasification leads to higher internal char porosity at the same conversion level (higher TSA), develops preferentially 10 Angstroms micropores and creates mesoporosity along the conversion. The CO_2 gasification develops mainly micropores, but with a larger pore size distribution, and a very low mesoporosity.

- SEM observations show different evolution of the global texture at the macropore scale under CO_2 and H_2O.

- AAEM species were seen to be the major constituents of the mineral phase of chars. K and Mg are present in a quite diffuse form while Ca and Si migrate to the char surface and form relatively big clusters

- The main difference between CO_2 and H_2O gasification regarding the minerals is perceived on the behaviour of Al and Si species which are removed in the presence of CO_2 and concentrated in the presence of steam.

- The mix char structural evolution tends to that of theH_2O char as revealed by Raman spectroscopy. This is reasonable as steam gasification would be more active than CO_2 gasification.

- The CO_2 TPD profile of mix chars denotes the contribution of the two reactions as it appears as a blend of the CO_2 TPD profiles obtained for single atmosphere chars.

- The micropore size distribution of mix chars tend toward those of CO_2 char. The microporosity in the range of 10 to 40 Angstroms is better developed in mixed atmosphere gasification. Micropores of 25 to 40 Angstroms are exclusively developed in the case of CO_2 gasification. H_2O may thus enhance the access of CO_2 to these kind of micropores to react on. The other case is also possible, as the developed micropores by CO_2 may become the preferential reactive sites for H_2O, explaining thus the enhanced development of these latter.

- There may be a competition between CO_2 and H_2O for the reaction on part of the active surface, and simultaneously a mutual synergy effect by an enhancement of the internal diffusivity or by acting on the retention or volatilization of inhibitor mineral species such as Al and Si. The two opposite effects would lead to the observed additivity.

- The char reactivity is proportional to the product of surface oxygen concentration (calculated from TPD experiments) and TSA. We believe that the first term is related to the chemical reactivity while the second is related to diffusional transfer inside the porous particle, as we found that for the 0.2 mm char particle there exist diffusional limitations during the reaction.

- At this stage and despite the numerous highlights concerning the gasification reactions unfolding, we are not able to state definitely on the mechanisms involved in mixed atmosphere gasification. Although, we are almost sure that there are numerous phenomena involving synergy and others involving competition. The whole leading to an observed additivity.

The drawn conclusions show well that we answered many questions related to the effects of CO_2 on biomass pyro-gasification in HHR and LHR conditions. From pyrolysis and char reactivity modelling to the chemistry of gasification we were able to shed light on many interrogations and provided many practical data that can be used for the design and modelling of biomass gasifiers. Nevertheless, as the reader has certainly understood, this issue is not totally clarified due to the reactions complexity and the numerous phenomena involved in. Despite we bring valuable information on the mixed atmosphere gasification mechanism, the question is still open. We believe that the adopted methodology based on analysing the three principal char characteristics: chemical, structural and textural, during the gasification reaction is well adapted to understand the reaction unfolding. This issue has to be further developed in future works. Concerning the benefits of CO_2 adding in a large scale biomass gasifier, we are not able to state on its feasibility in the scope of this thesis. It needs a global approach gathering gasification in pilot gasifier for gas analysis and reactor modelling as well as technical, economical and environmental studies of a CO_2 operating gasifier.

Conclusion générale et perspectives

Ce travail a été réalisé afin d'analyser les effets du CO_2 sur les réactions de pyrolyse de la biomasse et de gazéification du char, dans des conditions de vitesse de chauffe rapide et lente. L'étude a été réalisée à l'échelle des particules de biomasse et de char, et ce avec deux objectifs principaux appartenant à des sphères différentes :

- le premier était de fournir des données concrètes sur la pyrolyse et la gazéification du char en présence de CO_2. L'analyse des effets du CO_2 porte aussi bien sur la vitesse de la pyrolyse de la biomasse que sur celle de la réactivité du char. Cette partie du travail appartient au domaine du Génie chimique.
- Le second objectif était de comprendre le déroulement des réactions de gazéification du char par CO_2, H_2O et leur mélange. Pour ce faire, les caractéristiques chimiques, structurelles et texturales du char ont été suivies tout au long de la réaction de gazéification. Cette partie du travail relève du domaine de la physico-chimie du solide.

Nous avons étudié les effets du CO_2 sur les chars préparés par des pyrolyses lente et rapide. Il s'avère d'un point de vue général que pour les mêmes conditions de température et de pression partielle de gaz, la réactivité du char HHR est presque 4 fois supérieure à celle du char LHR. L'introduction du CO_2 comme co-réactif avec la vapeur améliore la vitesse de gazéification du char pour les deux vitesses de chauffe. La réactivité du char en atmosphères mixtes peut être correctement exprimée par une loi d'additivité réflétant une coopération passive "apparente" de la vapeur et du dioxide de carbone dans la réaction de gazéification. Des expériences spécifiques menées dans ce travail ont montré que la gazéification d'un char sous CO_2 à un niveau de conversion défini n'a pas d'incidence sur sa réactivité durant une conversion supplémentaire sous H_2O.

Nous allons développer les principales conclusions dans les paragraphes suivants :

Dans la première grande partie, nous nous sommes intéressés aux conditions de vitesse de chauffe rapide, telles que rencontrées dans les gazogènes à lits fluidisés. Nous avons effectué la réaction de pyrolyse de la biomasse sous CO_2 à 850°C et avons analysé les effets du CO_2 sur la vitesse de pyrolyse, sur le rendement en gaz et sur les propriétés réactives du char. Ensuite nous avons étudié la gazéification de chars obtenus par pyrolyse rapide sous CO_2, H_2O et leurs mélanges tout en variant la fraction molaire du gaz réactif entre 0,1 et 0,4 dans une gamme de températures de 800 à 950°C.

Puis, nous avons entrepris l'étude de la réaction globale de la pyro-gazéification dans du CO_2 pur à 850°C en vue d'analyser le déroulement de la transformation globale d'une particule de biomasse en gaz - y compris les étapes de la pyrolyse et de la gazéification du char - lorsqu'elle est introduite rapidement dans un réacteur chaud contenant du CO_2 pur. Le dispositif Macro-TG utilisé dans le présent travail permet de contrôler avec précision la perte de masse dans des conditions de chauffe rapide. Nous avons développé en parallèle un modèle numérique dans le but de mieux comprendre la réaction globale de pyro-gazéification dans du CO_2 pur.

Les principales conclusions concernant les effets du CO_2 sur la pyrolyse en chauffe rapide et la gazéification du char sont :

- Le CO_2 n'influence pas la vitesse de pyrolyse de la biomasse
- Le CO_2 réagirait avec les radicaux formés à la surface du char; il a une légère influence sur le rendement du char.
- La présence de CO_2 provoque une plus grande production de CO. Le CO_2 peut avoir réagi avec le char, ou en phase phase gazeuse, menant à plus de CO.
- Le char obtenu après pyrolyse sous CO_2 est différent de celui obtenu après pyrolyse sous azote. Ces derniers ont des TSA et des profils d'oxydation différents. Néanmoins, leurs réactivités envers CO_2, H_2O ou O_2 étaient à peu près les mêmes.
- L'introduction du CO_2 avec la vapeur provoque une augmentation de la vitesse de réaction du char.
- Des expériences de gazéification des chars HHR à 900°C en atmosphères mixtes pour différentes concentrations de CO_2 + H_2O, montrent que la réactivité du char peut être exprimée comme la somme des réactivités individuelles.
- Les résultats expérimentaux de pyro-gazéification des particules de biomasse de 1 mm d'épaisseur par du CO_2 pur à 850°C ont montré que l'étape de gazéification du char est l'étape limitante. La pyrolyse s'est terminée au bout de 25 s alors que presque 600 s. sont nécessaires pour achever la réaction de gazéification du char.

La deuxième grande partie de la thèse a été consacrée à l'étude de la réaction de gazéification du char préparé dans des conditions de vitesse de chauffe lente représentatives d'un lit fixe.

En premier lieu, nous nous sommes concentrés sur la question des conditions intrinsèques ainsi que sur l'influence de la taille des particules du char sur la réactivité. Cette question a été abordée en utilisant l'approche du module de Thiele. Nous avons effectué les expériences de gazéification du char par CO_2 et H_2O à 900°C sur une large gamme de particules de char allant de la poudre de 0.04 mm à celles relativement grandes de 13 mm de diamètre. Grâce à ceci, nous avons montré l'étendue des limitations diffusionnelles quand on augmente la taille des particules et avons déterminé les conditions dans lesquelles la réaction a lieu dans le régime chimique.

En second lieu, nous avons étudié l'influence de la température et de la dimension des particules de char sur la réactivité lors de la gazéification en atmosphère mixte de CO_2 et H_2O. Nous avons aussi abordé la question de la gazéification en atmosphère cyclique en analysant les effets de l'alternance de CO_2 et H_2O sur la réactivité du char. Cette partie de l'étude a fourni de précieuses informations sur la réactivité du char dans des conditions pratiques de gazéification couvrant une large gamme de tailles de particules.

Finalement, nous avons étudié l'évolution des propriétés chimiques, structurelles et texturales du char au cours de la gazéification sous 20% de CO_2, 20% de H_2O et leur mélange à 900°C dans le but de mieux comprendre le déroulement de la réaction de gazéification du char. Cette question n'est pas encore totalement clarifiée dans la littérature, car la réaction de gazéification est généralement abordée d'un point de vue macroscopique, et ce dans le but d'avoir des données sur la réactivité du char. La structure du char, sa chimie de surface, le contenu en minéraux, la texture et l'ASA ont été analysés sur des chars à des niveaux de conversion de 20%, 50% et 70%.

Cette partie du travail a fourni des informations notables sur le déroulement des réactions de gazéification.

Les conclusions principales relatives aux effets du CO_2 sur la vitesse de chauffe lente de la gazéification du char sont :

- La réactivité apparente du char dépend fortement de la taille des particules. En augmentant la taille des particules de 0.04 à 13 mm, on réduit de presque 20 fois la réactivité apparente du char au CO_2 comme à H_2O à 900°C.

- A 900°C, la gazéification du char par H_2O et CO_2 est réalisée dans le régime chimique pour des particules de 0.04 mm ou de taille inférieure.

- Dans les réactions de gazéification aussi bien par H_2O que par CO_2, nous avons trouvé la même évolution du facteur d'efficacité suivant la taille des particules. La compétition diffusion - réaction était à peu près la même pour les deux molécules. Néanmoins H_2O a révélé une réactivité et une diffusivité supérieures à celles du CO_2. L'équivalence de la concurrence diffusion-réaction est "fortuite" et spécifique à nos conditions opératoires.

- Pour des particules de char de 0.2 mm, la réactivité dans une atmosphère mixte de H_2O et CO_2 est à peu près égale à la somme des réactivités individuelles à 800 ou 900°C, mais elle lui est inférieure à des températures de 1000 et 1100°C.

- La réactivité du char à 900°C dans un mélange 20% CO_2 + 20% H_2O peut être correctement exprimée par une loi d'additivité, et ce pour une large gamme de taille de particules de 0.2 à 13 mm.

- La réactivité du char en atmosphère mixte peut être correctement décrite par une combinaison linéaire des réactivités individuelles à H_2O etau CO_2. Cependant, nous ne pouvons tirer de conclusions sur les mécanismes de la réaction dans une atmosphère mixte du fait de l'existence de plusieurs combinaisons possibles des coefficients linéaires qui permettent une bonne représentation des données expérimentales.

- La réactivité du char à 900°C pour des particules de 0.2 et 13 mm ne dépend pas de l'historique de la gazéification. La réactivité du char au CO_2 ou à H_2O à un niveau de conversion défini est constante quel que soit le gaz avec lequel le char a réagi antérieurement.

Les principales conclusions relatives au déroulement de la gazéification des chars-LHR par H_2O, CO_2 ou leur mélange sont :

- Les réactions de gazéification par H_2O ou CO_2 suivent des mécanismes différents.

- Les spectres Raman a montré différentes évolutions de la structure du char lors de la gazéification au CO_2 et à H_2O. H_2O réagit de préférence avec des structures appartenant à la bande D3 et provoque probablement une condensation des systèmes aromatiques à faible nombre de cycles en des systèmes aromatiques à grand nombre de cycles. Ceci est lié à la présence des radicaux H mobiles à la surface du char. Le CO_2 réagit préférentiellement avec des formes de carbone mieux ordonnées de type D1 et G.

- Les profils d'émission des différents gaz durant les expériences TPD sont aussi différents. H_2O semble réagir de préférence avec les éthers, les phénols et les anhydrides dans les premières étapes de la réaction. Cette observation peut être corrélée par la diminution du ratio $\frac{ID3}{ID1}$ car ces groupes fonctionnels appartiennent à la forme D3 dans les matériaux carbonés mal organisés. En outre, l'augmentation marquée des atomes H de surface due à la gazéification à la vapeur, comme révélé par TPD, est accompagnée d'une baisse du ratio $\frac{ID3}{ID1}$. La diminution du ratio $\frac{ID3}{ID1}$ est moins marquée au delà de 20% de conversion et est corroborée par une

augmentation plus faible des radicaux H à la surface du char. La chimie de surface du char est différente pour les deux réactions car les chars par CO_2 contiennent plus de fonctions de surface émettant du CO tandis que les chars gazéifiés par H_2O sont beaucoup plus hydrogénés.

- Les propriétés texturales différent également. La gazéification par H_2O provoque une plus grande porosité interne du char à un meme niveau de conversion (TSA plus élevée) , développe de préférence des micropores de 10 angstroms et crée de la mesoporosité tout au long de la conversion. La gazéification par le CO_2 développe principalement des micropores avec une distribution de taille plus grande et une mésoporosité plus basse.

- Les observations MEB montrent un changement de la texture globale à l'échelle macropore sous CO_2 et H_2O.

- Les minéraux alcalins et alcalino-terreux sont les principaux constituants de la phase minérale du char.

- En ce qui concerne les minéraux, la grande différence entre la gazéification par CO_2 et par H_2O est remarquée dans le comportement des espèces *Al* et *Si* qui se dévolatilisent en présence du CO_2 et sont concentrées en présence de la vapeur.

- L'évolution de la structure du char sous atmosphère mixte est semblable à celle du char gazéifié par H_2O. Ceci est logique car la gazéification par la vapeur est plus active que celle par le CO_2.

- Le profil TPD-CO_2 du char gazéifié sous une atmosphére mixte indique que la contribution des 2 réactions car il apparait comme une moyenne des profils TPD-CO_2 obtenus sous des atmosphères simples.

- La distribution de taille de pores de chars gazéifiés sous mélange CO_2 + H_2O tend vers celle du char CO_2. La microporosité dans la gamme de 10 à 40 Angstroms est mieux développée dans une atmosphère de gazéification mixte. Les micropores de 25 à 40 Angstroms sont exclusivement développés dans le cas de gazéification par le CO_2. H_2O peut donc améliorer l'accès du CO_2 à ce genre de micropores. L'autre cas est aussi possible car les micropores développés par le CO_2 pourraient devenir de meilleurs sites réactifs pour H_2O.

- Il peut y avoir une concurrence entre le CO_2 et le H_2O pour une réaction sur une partie de la surface active et simultanément un effet de synergie mutuel par un renforcement de la diffusivité interne ou en agissant sur la rétention ou la volatilisation d'espèces minérales inhibitrices comme *Al* ou *Si*. Les deux effets contraires pouvant mener à l'additivité observée.

- A ce stade, et malgré les nombreux faits saillants concernant le déroulement des réactions de gazéification, nous ne sommes pas capables de statuer définitivement sur les mécanismes de la gazéification en atmosphère mixte. Bien que nous soyons à peu près sûrs qu'il existe de nombreux phénomènes implicant la synergie et d'autres implicant la concurrence, l'ensemble conduit à une additivité observée.

- La réactivité du char est proportionnelle au produit de la concentration en oxygène de la surface - calculée à partir des expériences TPD - et de la TSA. Nous estimons que le premier terme est lié à la réactivité chimique tandis que le second est lié au transfert diffusionnel à l'intérieur des particules poreuses car nous avons trouvé qu'il existe des limitations diffusionnelles pour ces particules de char au cours de la réaction.

Ces diverses conclusions montrent bien que nous avons répondu à de nombreuses questions concernant les effets du CO_2 sur la pyro-gazéification de la biomasse dans des conditions de vitesse de chauffe rapide HHR et lente LHR.

De la pyrolyse et de la modélisation de la réactiivité du char jusqu'à la chimie de la gazéification, nous avons pu faire la lumière sur de nombreuses interrogations et fournir de nombreuses données pratiques pouvant être utilisées pour la conception et la modélisation des gazogènes de biomasse. Néanmoins, comme le lecteur l'a certainement compris, cette question n'est pas totalement clarifiée en raison de la complexité des réactions et des nombreux phénomènes qui y sont rattachés.

La méthodologie adoptée visant à analyser les trois caractéristiques principales du char : chimique, structurelle et texturale au cours de la réaction de gazéification est bien adaptée pour comprendre le déroulement de la réaction. Cette question doit encore être développée dans des travaux futurs.

En ce qui concerne la pertinence de l'injection de CO_2 dans les gazogènes de biomasse, nous ne sommes pas en mesure de statuer sur sa faisabilité dans le cadre de cette thèse. Ceci requiert une approche globale réunissant des essais de gazéification dans un pilote pour les analyses de gaz et une modélisation à l'échelle du réacteur ainsi qu'une étude technique, économique et environnementale d'un tel procédé.

Bibliography

[1] Mikael Höök and Xu Tang. Depletion of fossil fuels and anthropogenic climate change-A review. *Energy Policy*, 52:797–809, January 2013.

[2] Fraser Armstrong and Katherine Blundell. *Energy beyond oil*. OXFORD, OUP, 2007.

[3] James Hansen, Makiko Sato, Pushker Kharecha, David Beerling, Robert Berner, Valerie Masson-delmotte, Mark Pagani, Maureen Raymo, Dana L Royer, James C Zachos, Institut Pierre, Simon Laplace, and Cea-cnrs-universite De Versailles. Target Atmospheric CO2: Where Should Humanity Aim ? *The Open Atmospheric Science Journal*, pages 217–231, 2008.

[4] P.D M. Salmon Jones, D. H. Lister, and T. J. Osborn. Hemispheric and large-scale land surface air temperature variations : An extensive revision and an update to 2010. *J. Geophys. Res.,*, (January), 2012.

[5] R. Prinn Forster, P., V. Ramaswamy, P. Artaxo, T. Berntsen, R. Betts, D.W. Fahey, J. Haywood, J. Lean, D.C. Lowe, G. Myhre, J. Nganga, M. Schulz G. Raga, and R. Van Dorland. Changes in Atmospheric Constituents and in Radiative Forcing. In: Climate Change 2007: The Physical Science Basis. Contribution of Working Group I to the Fourth Assessment Report of the Intergovernmental Panel on Climate Change. Technical report, Cambridge University Press, Cambridge, United Kingdom and New York, NY, USA, 2007.

[6] R S Dhillon and George Von Wuehlisch. Mitigation of global warming through renewable biomass. *Biomass and Bioenergy*, 48:75–89, 2012.

[7] Prabir Basu. *Biomass Gasification and Pyrolysis :Practical Design and Theory*. Elsevier, 2010.

[8] Heidi C Butterman and Marco J Castaldi. Influence of CO2 Injection on Biomass Gasification. *Society*, pages 8875–8886, 2007.

[9] Y Schenkel and B Boufeldja. *Guide biomasse énergie*. 2005.

[10] Forest Products Laboratory. *Wood Handbook :Wood as an Engineering Material*. 2010.

[11] J.F. Siau. *Transport processes in wood.* New York., 1984.

[12] Energy research Centre of the Netherlands. Phyllis2, database for biomass and waste, 2014.

[13] Patrick Perre and Ian W Turner. A 3-D version of TransPore : a comprehensive heat and mass transfer computational model for simulating the drying of porous media. *International Journal of Heat and Mass Transfer*, 42:4501–4521, 1999.

[14] Colomba Di Blasi. Combustion and gasification rates of lignocellulosic chars. *Progress in Energy and Combustion Science*, 35(2):121–140, April 2009.

[15] Wei-Hsin Chen, Chih-Jung Chen, Chen-I Hung, Cheng-Hsien Shen, and Heng-Wen Hsu. A comparison of gasification phenomena among raw biomass, torrefied biomass and coal in an entrained-flow reactor. *Applied Energy*, 112:421–430, December 2013.

[16] Fredrik Weiland, Martin Nordwaeger, Ingemar Olofsson, Henrik Wiinikka, and Anders Nordin. Entrained flow gasification of torrefied wood residues. *Fuel Processing Technology*, 125:51–58, September 2014.

[17] L. Van de steene, J.P. Tagutchou, F. Mermoud, E. Martin, and S. Salvador. A new experimental Continuous Fixed Bed Reactor to characterise wood char gasification. *Fuel*, 89(11):3320–3329, November 2010.

[18] Paola Brachi, Riccardo Chirone, Francesco Miccio, Michele Miccio, Antonio Picarelli, and Giovanna Ruoppolo. Fluidized bed co-gasification of biomass and polymeric wastes for a flexible end-use of the syngas: Focus on bio-methanol. *Fuel*, 128:88–98, July 2014.

[19] Susanna Nilsson, Alberto Gómez-Barea, Diego Fuentes-Cano, and Pedro Ollero. Gasification of biomass and waste in a staged fluidized bed gasifier: Modeling and comparison with one-stage units. *Fuel*, 97:730–740, July 2012.

[20] Manuel Campoy, Alberto Gómez-Barea, Pedro Ollero, and Susanna Nilsson. Gasification of wastes in a pilot fluidized bed gasifier. *Fuel Processing Technology*, 121:63–69, May 2014.

[21] Reza Alipour Moghadam, Suzana Yusup, Yoshimitsu Uemura, Bridgid Lai Fui Chin, Hon Loong Lam, and Ahmed Al Shoaibi. Syngas production from palm kernel shell and polyethylene waste blend in fluidized bed catalytic steam co-gasification process. *Energy*, pages 2–6, May 2014.

[22] Kai-Cheng Yang, Keng-Tung Wu, Ming-Huan Hsieh, Hung-Te Hsu, Chih-Shen Chen, and Hsiao-Wei Chen. Co-gasification of woody biomass and microalgae in a fluidized bed. *Journal of the Taiwan Institute of Chemical Engineers*, 44(6):1027–1033, November 2013.

[23] a. Gómez-Barea and B. Leckner. Modeling of biomass gasification in fluidized bed. *Progress in Energy and Combustion Science*, 36(4):444–509, August 2010.

[24] Roger Gadiou. Les matériaux carbonés issus de la biomasse : structure et réactivité. Institut de Science des Matériaux de Mulhouse, 2009.

[25] M. Kumar and R. Gupta. Scanning electron microscopic study of acacia and eucalyptus wood chars. *Journal of Material Science*, 30:544–551, 1995.

[26] Satish M Manocha. Porous carbons. *Sadhana*, 28(April):335–348, 2003.

[27] Ru Yang, Guoqiang Liu, Min Li, Jianchun Zhang, and Xinmin Hao. Microporous and Mesoporous Materials Preparation and N2, CO2 and H2 adsorption of super activated carbon derived from biomass source hemp (Cannabis sativa L .) stem. *Microporous and Mesoporous Materials*, 158:108–116, 2012.

[28] Meriem Belhachemi, Mejdi Jeguirim, Lionel Limousy, and Fatima Addoun. Comparison of NO2 removal using date pits activated carbon and modified commercialized activated carbon via different preparation methods: Effect of porosity and surface chemistry. *Chemical Engineering Journal*, 253(2):121–129, October 2014.

[29] Naomi Klinghoffer. *Utilization of char from biomass gasification in catalytic applications*. PhD thesis, 2013.

[30] Peng Fu, Song Hu, Lushi Sun, Jun Xiang, Tao Yang, Anchao Zhang, and Junying Zhang. Structural evolution of maize stalk/char particles during pyrolysis. *Bioresource technology*, 100(20):4877–83, October 2009.

[31] Peng Fu, Song Hu, Jun Xiang, Weiming Yi, Xueyuan Bai, Lushi Sun, and Sheng Su. Evolution of char structure during steam gasification of the chars produced from rapid pyrolysis of rice husk. *Bioresource technology*, 114:691–7, June 2012.

[32] F. Salver-Disma, J.-M. Tarascon, C. Clinard, and J.-N. Rouzaud. Transmission electron microscopy studies on carbon materials prepared by mechanical milling. *Carbon*, 37(12):1941–1959, January 1999.

[33] Victor Fernandez-Alos, Justin K. Watson, Randy Vander Wal, and Jonathan P. Mathews. Soot and char molecular representations generated directly from HRTEM lattice fringe images using Fringe3D. *Combustion and Flame*, 158(9):1807–1813, September 2011.

[34] S. Septien, S. Valin, M. Peyrot, C. Dupont, and S. Salvador. Characterization of char and soot from millimetric wood particles pyrolysis in a drop tube reactor between 800°C and 1400°C. *Fuel*, 121:216–224, April 2014.

[35] Harry Marsh and Francisco Rodriguez-reinoso. *Activated Carbon*. 2005.

[36] Oskar Paris, Cordt Zollfrank, and Gerald Zickler. Decomposition and carbonisation of wood biopolymers: a microstructural study of softwood pyrolysis. *Carbon*, 43(1):53–66, January 2005.

[37] Alon Zaida, Ezra Bar-Ziv, Ljubisa R. Radovic, and Young-Jae Lee. Further development of Raman Microprobe spectroscopy for characterization of char reactivity. *Proceedings of the Combustion Institute*, 31(2):1881–1887, January 2007.

[38] T Jawhari, A Roid, and J Casado. Raman spectroscopic characterization of some commercially available carbon black materials. *Carbon*, 33(11):1561–1565, 1995.

[39] C Sheng. Char structure characterised by Raman spectroscopy and its correlations with combustion reactivity. *Fuel*, 86(15):2316–2324, October 2007.

[40] Mohammad Asadullah, Shu Zhang, Zhenhua Min, Piyachat Yimsiri, and Chun-Zhu Li. Effects of biomass char structure on its gasification reactivity. *Bioresource technology*, 101(20):7935–7943, June 2010.

[41] Hui-Ling Tay, Shiro Kajitani, Shu Zhang, and Chun-Zhu Li. Effects of gasifying agent on the evolution of char structure during the gasification of Victorian brown coal. *Fuel*, April 2011.

[42] Daniel M. Keown, Jun-Ichiro Hayashi, and Chun-Zhu Li. Drastic changes in biomass char structure and reactivity upon contact with steam. *Fuel*, 87(7):1127–1132, June 2008.

[43] a. Sadezky, H. Muckenhuber, H. Grothe, R. Niessner, and U. Pöschl. Raman microspectroscopy of soot and related carbonaceous materials: Spectral analysis and structural information. *Carbon*, 43(8):1731–1742, July 2005.

[44] Hui-Ling Tay, Shiro Kajitani, Shuai Wang, and Chun-Zhu Li. A preliminary Raman spectroscopic perspective for the roles of catalysts during char gasification. *Fuel*, 121:165–172, April 2014.

[45] Shiyong Wu, Sheng Huang, Liyuan Ji, Youqing Wu, and Jinsheng Gao. Structure characteristics and gasification activity of residual carbon from entrained-flow coal gasification slag. *Fuel*, 122:67–75, April 2014.

[46] Tingting Li, Lei Zhang, Li Dong, and Chun-Zhu Li. Effects of gasification atmosphere and temperature on char structural evolution during the gasification of Collie sub-bituminous coal. *Fuel*, 117:1190–1195, January 2014.

[47] Daniel M Keown, Xiaojiang Li, Jun-ichiro Hayashi, and Chun-zhu Li. Evolution of biomass char structure during oxidation in revealed with FT-Raman spectroscopy. *Fuel Processing Technology*, 89(12):1429–1435, 2008.

[48] Stanislav V. Vassilev, David Baxter, Lars K. Andersen, Christina G. Vassileva, and Trevor J. Morgan. An overview of the organic and inorganic phase composition of biomass. *Fuel*, (October), October 2011.

[49] Ange Nzihou and Brian Stanmore. *The fate of heavy metals during combustion and gasification of contaminated biomass-A brief review.*, volume 256-257C. Elsevier B.V., March 2013.

[50] Ange Nzihou, Brian Stanmore, and Patrick Sharrock. A review of catalysts for the gasification of biomass char, with some reference to coal. *Energy*, 58:305–317, September 2013.

[51] J L Figueiredo, M F R Pereira, M M A Freitas, and J J M Orfao. Modification of the surface chemistry of activated carbons. *Fuel*, 37:1379–1389, 1999.

[52] Patrice Brender, Roger Gadiou, Jean-Christophe Rietsch, Philippe Fioux, Joseph Dentzer, Arnaud Ponche, and Cathie Vix-Guterl. Characterization of carbon surface chemistry by combined temperature programmed desorption with in situ X-ray photoelectron spectrometry and temperature programmed desorption with mass spectrometry analysis. *Analytical chemistry*, 84(5):2147–53, March 2012.

[53] Camelia Matei Ghimbeu, Roger Gadiou, Joseph Dentzer, Loïc Vidal, and Cathie Vix-Guterl. A TPD-MS study of the adsorption of ethanol/cyclohexane mixture on activated carbons. *Adsorption*, 17(1):227–233, January 2011.

[54] Qianlin Zhuang, Takashi Kyotani, and Akira Tomita. Dynamics of Surface Oxygen Complexes during Carbon Gasification with Oxygen. *Energy & Fuels*, (14):630–634, 1995.

[55] W Klose and M Wolki. On the intrinsic reaction rate of biomass char gasification with carbon dioxide and steam. *Fuel*, 84(7-8):885–892, May 2005.

[56] Santiago Septien Stringel. *High temperature gasification of millimetric wood particles between 800°C and 1400°C*. Ph.d. thesis, Université de Toulouse, Institut National Polytechnique de Toulouse, 2011.

[57] a. Gómez-Barea, P. Ollero, and C. Fernández-Baco. Diffusional Effects in CO2 Gasification Experiments with Single Biomass Char Particles. 1. Experimental Investigation. *Energy & Fuels*, 20(5):2202–2210, September 2006.

[58] Alejandro Montoya and Fanor Mondrago. Formation of CO precursors during char gasification with O2 , CO2 and H2O. *Fuel Processing Technology*, 78:125–130, 2002.

[59] Ljubisa R. Radovic. The mechanism of CO2 chemisorption on zigzag carbon active sites: A computational chemistry study. *Carbon*, 43(5):907–915, January 2005.

[60] P.a. Gauden and M. Wiśniewski. CO2 sorption on substituted carbon materials. *Applied Surface Science*, 253(13):5726–5731, April 2007.

[61] Juan F. Espinal, Fanor Mondragón, and Thanh N. Truong. Thermodynamic evaluation of steam gasification mechanisms of carbonaceous materials. *Carbon*, 47(13):3010–3018, November 2009.

[62] A Lizzio, Hong Jiang, and Ljubisa R Radovic. On the kinetics of carbon (char) gasification: reconciling models with experiments. *Carbon*, 28(I):7–19, 1989.

[63] Ljubisa R Radovic and L Walker. Importance gasification of carbon active sites in the of coal chars. *Fuel*, 62:849–855, 1983.

[64] N.R Laine, F.J Vastola, and P.L Walker. The importance of active surface area in the carbon-oxygen reaction. *J. Phys. Chem*, 67:2030–2034, 1963.

[65] Peter Causton and McEnaney Brian. Determination of active surface areas of coal chars using a temperature-programmed desorption technique. *Fuel*, 64:1447–1451, 1985.

[66] Hui-Ling Tay, Shiro Kajitani, Shu Zhang, and Chun-Zhu Li. Effects of gasifying agent on the evolution of char structure during the gasification of Victorian brown coal. *Fuel*, 103:22–28, January 2013.

[67] K Raveendran, Anuradda Ganesh, and Kartic C Khilart. Influence of mineral matter on biomass pyrolysis characteristics. *Fuel*, 74(12):1812–1822, 1995.

[68] Â M Encinar, Juan F Gonza, and Juan J Rodrõ. Catalysed and uncatalysed steam gasification of eucalyptus char : influence of variables and kinetic study. *Fuel*, 80, 2001.

[69] Y Zhang, M Ashizawa, S Kajitani, and K Miura. Proposal of a semi-empirical kinetic model to reconcile with gasification reactivity profiles of biomass chars. *Fuel*, 87(4-5):475–481, April 2008.

[70] Keiichirou Mitsuoka, Shigeya Hayashi, Hiroshi Amano, Kenji Kayahara, Eiji Sasaoaka, and Md. Azhar Uddin. Gasification of woody biomass char with CO2: The catalytic effects of K and Ca species on char gasification reactivity. *Fuel Processing Technology*, 92(1):26–31, January 2011.

[71] Yanqin Huang, Xiuli Yin, Chuangzhi Wu, Congwei Wang, Jianjun Xie, Zhaoqiu Zhou, Longlong Ma, and Haibin Li. Effects of metal catalysts on CO2 gasification reactivity of biomass char., 2009.

[72] Capucine Dupont, Timothée Nocquet, José Augusto Da Costa, and Christèle Verne-Tournon. Kinetic modelling of steam gasification of various woody biomass chars: influence of inorganic elements. *Bioresource technology*, 102(20):9743–8, October 2011.

[73] Céline Hognon, Capucine Dupont, Maguelone Grateau, and Florian Delrue. Comparison of steam gasification reactivity of algal and lignocellulosic biomass: Influence of inorganic elements. *Bioresource Technology*, May 2014.

[74] F Mermoud, F Golfier, S Salvador, L Vandesteene, and J Dirion. Experimental and numerical study of steam gasification of a single charcoal particle. *Combustion and Flame*, 145(1-2):59–79, April 2006.

[75] Floriane Mermoud. *Gazéification de charbon de bois à la vapeur d ' eau : de la particule isolée au lit fixe continu*. PhD thesis, INPT Toulouse, 2006.

[76] V. Kirubakaran, V. Sivaramakrishnan, R. Nalini, T. Sekar, M. Premalatha, and P. Subramanian. A review on gasification of biomass. *Renewable and Sustainable Energy Reviews*, 13(1):179–186, January 2009.

[77] L. Van de steene, J.P. Tagutchou, F.J. Escudero Sanz, and S. Salvador. Gasification of woodchip particles: Experimental and numerical study of char-H2O, char-CO2, and char-O2 reactions. *Chemical Engineering Science*, 66(20):4499–4509, October 2011.

[78] Ulrik Henriksen, Claus Hindsgaul, Bjø rn Qvale, Jan Fjellerup, and Anker Degn Jensen. Investigation of the Anisotropic Behavior of Wood Char Particles during Gasification. *Energy & Fuels*, 20(5):2233–2238, September 2006.

[79] Claudio Avila, Cheng Heng Pang, Tao Wu, and Ed Lester. Morphology and reactivity characteristics of char biomass particles. *Bioresource technology*, 102(8):5237–43, April 2011.

[80] F Mermoud, S Salvador, L Vandesteene, and F Golfier. Influence of the pyrolysis heating rate on the steam gasification rate of large wood char particles. *Fuel*, 85(10-11):1473–1482, July 2006.

[81] E Cetin, B Moghtaderi, R Gupta, and T F Wall. Influence of pyrolysis conditions on the structure and gasification reactivity of biomass chars. *Fuel*, 83:2139–2150, 2004.

[82] E. Cetin, R. Gupta, and B. Moghtaderi. Effect of pyrolysis pressure and heating rate on radiata pine char structure and apparent gasification reactivity. *Fuel*, 84(10):1328–1334, July 2005.

[83] Teeranai Pattanotai, Hirotatsu Watanabe, and Ken Okazaki. Gasification characteristic of large wood chars with anisotropic structure. *Fuel*, 117:331–339, January 2014.

[84] Alfredo Zolin, Anker Degn Jensen, Peter Arendt Jensen, and Kim Dam-Johansen. Experimental study of char thermal deactivation. *Fuel*, 81(8):1065–1075, May 2002.

[85] Osvalda Senneca and Piero Salatino. A semi-detailed kinetic model of char combustion with consideration of thermal annealing. *Proceedings of the Combustion Institute*, 33(2):1763–1770, January 2011.

[86] Kongvui Yip, Minghou Xu, Chun-Zhu Li, San Ping Jiang, and Hongwei Wu. Biochar as a Fuel: 3. Mechanistic Understanding on Biochar Thermal Annealing at Mild Temperatures and Its Effect on Biochar Reactivity. *Energy & Fuels*, 25(1):406–414, January 2011.

[87] Mary J. Wornat, Robert H. Hurt, Nancy Y.C. Yang, and Thomas J. Headley. Structural and compositional transformations of biomass chars during combustion. *Combustion and Flame*, 100(1-2):131–143, January 1995.

[88] Peng Fu, Weiming Yi, Xueyuan Bai, Zhihe Li, Song Hu, and Jun Xiang. Effect of temperature on gas composition and char structural features of pyrolyzed agricultural residues. *Bioresource technology*, 102(17):8211–9, September 2011.

[89] P R Bonelli, P a Della Rocca, E G Cerrella, and a L Cukierman. Effect of pyrolysis temperature on composition, surface properties and thermal degradation rates of Brazil Nut shells., January 2001.

[90] M. Guerrero, M.P. Ruiz, M.U. Alzueta, R. Bilbao, and a. Millera. Pyrolysis of eucalyptus at different heating rates: studies of char characterization and oxidative reactivity. *Journal of Analytical and Applied Pyrolysis*, 74(1-2):307–314, August 2005.

[91] Mohammad Asadullah, Shu Zhang, Zhenhua Min, Piyachat Yimsiri, and Chun-Zhu Li. Importance of Biomass Particle Size in Structural Evolution and Reactivity of Char in Steam Gasification. *Industrial & Engineering Chemistry Research*, 48(22):9858–9863, November 2009.

[92] Teeranai Pattanotai, Hirotatsu Watanabe, and Ken Okazaki. Experimental investigation of intraparticle secondary reactions of tar during wood pyrolysis. *Fuel*, 104:468–475, February 2013.

[93] Roger Khalil, Susanne Ja, Morten G Grø nli, and Johan Hustad. CO2 Gasification of Biomass Chars : A Kinetic Study. *Energy & Fuels*, (11):94–100, 2009.

[94] Indraneel Sircar, Anup Sane, Weichao Wang, and Jay P. Gore. Experimental and modeling study of pinewood char gasification with CO2. *Fuel*, 119:38–46, March 2014.

[95] Gang Xue, Marzena Kwapinska, Witold Kwapinski, Krzysztof M. Czajka, James Kennedy, and James J. Leahy. Impact of torrefaction on properties of Miscanthus giganteus relevant to gasification. *Fuel*, 121:189–197, April 2014.

[96] Ashish Bhat, J V Ram Bheemarasetti, and T Rajeswara Rao. Kinetics of rice husk char gasification. *Energy Conversion and Management*, 42:2061–2069, 2001.

[97] Susanna Nilsson, Alberto Gómez-Barea, and Diego Fuentes Cano. Gasification reactivity of char from dried sewage sludge in a fluidized bed. *Fuel*, 92(1):346–353, February 2012.

[98] M.R. Díaz-Rey, M. Cortés-Reyes, C. Herrera, M.a. Larrubia, N. Amadeo, M. Laborde, and L.J. Alemany. Hydrogen-rich gas production from algae-biomass by low temperature catalytic gasification. *Catalysis Today*, July 2014.

[99] P. Ollero, a. Serrera, R. Arjona, and S. Alcantarilla. The CO2 gasification kinetics of olive residue. *Biomass and Bioenergy*, 24(2):151–161, February 2003.

[100] M Barrio, B Gø bel, H Risnes, U Henriksen, J E Hustad, Nils Koppel Allé, and Dk-Kongens Lyngby. Steam gasification of wood char and the effect of hydrogen inhibition on the chemical kinetics . *In: Bridgwater AV, editor. Progress in themochemical biomass conversion*, pages 32–46, 2001.

[101] Kentaro Umeki, Antero Moilanen, Alberto Gómez-Barea, and Jukka Konttinen. A model of biomass char gasification describing the change in catalytic activity of ash. *Chemical Engineering Journal*, 207-208:616–624, October 2012.

[102] Muhammad F. Irfan, Muhammad R. Usman, and K. Kusakabe. Coal gasification in CO2 atmosphere and its kinetics since 1948: A brief review. *Energy*, 36(1):12–40, January 2011.

[103] Tagutchu. J.P. *Gazéification du charbon de plaquettes forestières : particule isolée et lit fixe continu*. PhD thesis, Université de perpignan, 2008.

[104] Michiel J Groneveld and Van Swaaij W.P.M. Gasification of char particles with CO2 and H2O. *Chemical Engineering Science*, 35:307–313, 1980.

[105] Fuad Azmi Tanjung. Gasification of single wood particles in CO2. *Fuel*, 67:666–672, 1988.

[106] S Dasappa and P J Paul. The gasification of wood-char spheres in CO2-N2 mixtures: analysis and experiments. *Chemical Engineering Science*, 49(2):223–232, 1994.

[107] A Gomezbarea, P Ollero, and A Villanueva. Diffusional Effects in CO2 Gasification Experiments with Single Biomass Char Particles. 2. Theoretical Predictions. *Energy & Fuels*, (2):2211–2222, 2006.

[108] Thilakavathi Mani, Nader Mahinpey, and Pulikesi Murugan. Reaction kinetics and mass transfer studies of biomass char gasification with CO2. *Chemical Engineering Science*, 66(1):36–41, January 2011.

[109] F. Golfier, L. Van de steene, S. Salvador, F. Mermoud, C. Oltean, and M.a. Bues. Impact of peripheral fragmentation on the steam gasification of an isolated wood charcoal particle in a diffusion-controlled regime. *Fuel*, 88(8):1498–1503, August 2009.

[110] Kentaro Umeki, Seon-Ah Roh, Tai-Jin Min, Tomoaki Namioka, and Kunio Yoshikawa. A simple expression for the apparent reaction rate of large wood char gasification with steam. *Bioresource technology*, 101(11):4187–92, June 2010.

[111] J. P. Tagutchou, L. Van de steene, F. J. Escudero Sanz, and S. Salvador. Gasification of Wood Char in Single and Mixed Atmospheres of H2O and CO2. *Energy Sources, Part A: Recovery, Utilization, and Environmental Effects*, 35(13):1266–1276, July 2013.

[112] Alberto Gómez-Barea. *Modelling of diffusional effects during gasification of biomass char particles in fluidised-bed*. PhD thesis, University of Seville, 2006.

[113] Wei Huo, Zhijie Zhou, Fuchen Wang, Yifei Wang, and Guangsuo Yu. Experimental study of pore diffusion effect on char gasification with CO2 and steam. *Fuel*, 131:59–65, September 2014.

[114] E. W. Thiele. Relation between Catalytic Activity and Size of Particle. *Industrial & Engineering Chemistry*, 31((7)):916–920, 1939.

[115] a. Bliek, J.C. Lont, and W.P.M. van Swaaij. Gasification of coal-derived chars in synthesis gas mixtures under intraparticle mass-transfer-controlled conditions. *Chemical Engineering Science*, 41(7):1895–1909, January 1986.

[116] A Go, P Ollero, and C Ferna. Diffusional Effects in CO2 Gasification Experiments with Single Biomass Char Particles. 1. Experimental Investigation. *Energy & Fuels*, 20:2202–2210, 2006.

[117] T. Renganathan, M.V. Yadav, S. Pushpavanam, R.K. Voolapalli, and Y.S. Cho. CO2 utilization for gasification of carbonaceous feedstocks: A thermodynamic analysis. *Chemical Engineering Science*, 83:159–170, December 2012.

[118] Paphonwit Chaiwatanodom, Supawat Vivanpatarakij, and Suttichai Assabumrungrat. Thermodynamic analysis of biomass gasification with CO2 recycle for synthesis gas production. *Applied Energy*, 114:10–17, February 2014.

[119] Huiyan Zhang, Rui Xiao, Denghui Wang, Guangying He, Shanshan Shao, Jubing Zhang, and Zhaoping Zhong. Biomass fast pyrolysis in a fluidized bed reactor under N2, CO2, CO, CH4 and H2 atmospheres. *Bioresource technology*, 102(5):4258–64, March 2011.

[120] Eilhann E. Kwon, Young Jae Jeon, and Haakrho Yi. New candidate for biofuel feedstock beyond terrestrial biomass for thermo-chemical process (Pyrolysis/Gasification) enhanced by carbon dioxide (CO2). *Bioresource Technology*, July 2012.

[121] Eilhann E Kwon, Haakrho Yi, and Marco J Castaldi. Utilizing Carbon Dioxide as a Reaction Medium to Mitigate Production of Polycyclic Aromatic Hydrocarbons from the Thermal Decomposition of Styrene Butadiene Rubber. *Environmental science & technology*, 46:10752–10757, 2012.

[122] Eilhann E Kwon, Eui-Chan Jeon, Marco J Castaldi, and Young Jae Jeon. Effect of carbon dioxide on the thermal degradation of lignocellulosic biomass. *Environmental science & technology*, 47(18):10541–7, September 2013.

[123] Heidi C Butterman and Marco J Castaldi. CO2 as a carbon neutral fuel source via enhanced biomass gasification. *Environmental science & technology*, 43(23):9030–7, December 2009.

[124] Bayu Prabowo, Kentaro Umeki, Mi Yan, Masato R. Nakamura, Marco J. Castaldi, and Kunio Yoshikawa. CO2-steam mixture for direct and indirect gasification of rice straw in a downdraft gasifier: Laboratory-scale experiments and performance prediction. *Applied Energy*, 113:670–679, January 2014.

[125] M. Pohorelý, M. Jeremiáš, K. Svoboda, P. Kameníková, S. Skoblia, and Z. Beno. CO2 as moderator for biomass gasification. *Fuel*, 117:198–205, January 2014.

[126] Toshiaki Hanaoka, Shou Hiasa, and Yusuke Edashige. Syngas production by gasification of aquatic biomass with CO2/O2 and simultaneous removal of H2S and COS using char obtained in the gasification. *Biomass and Bioenergy*, 59:448–457, December 2013.

[127] Scott Hurley, Hanning Li, and Chunbao Charles Xu. Effects of impregnated metal ions on air/CO2-gasification of woody biomass. *Bioresource technology*, 101(23):9301–7, December 2010.

[128] Toshiaki Hanaoka, Kinya Sakanishi, and Yukihiko Okumura. The effect of N2/CO2/O2 content and pressure on characteristics and CO2 gasification behavior of biomass-derived char. *Fuel Processing Technology*, 104:287–294, December 2012.

[129] a.G. Borrego, L. Garavaglia, and W.D. Kalkreuth. Characteristics of high heating rate biomass chars prepared under N2 and CO2 atmospheres. *International Journal of Coal Geology*, 77(3-4):409–415, January 2009.

[130] Hirotatsu Watanabe, Kiyomi Shimomura, and Ken Okazaki. Effect of high CO2 concentration on char formation through mineral reaction during biomass pyrolysis. *Proceedings of the Combustion Institute*, (x), August 2012.

[131] G A O Song-ping, Zhao Jian-tao, Wang Zhi-qing, Wang Jian-fei, Fang Yi-tian, and Huang Jie-jie. Effect of CO2 on pyrolysis behaviors of lignite. *Journal of Fuel Chemistry and Technology*, 41(3):257–264, 2013.

[132] Kawser Jamil, Jun-ichiro Hayashi, and Chun-Zhu Li. Pyrolysis of a Victorian brown coal and gasification of nascent char in CO2 atmosphere in a wire-mesh reactor. *Fuel*, 83(7-8):833–843, May 2004.

[133] Yonghui Bai, Pei Wang, Lunjing Yan, Changlong Liu, Fan Li, and Kechang Xie. Effects of CO2 on gas evolution and char structure formation during lump coal pyrolysis at elevated pressures. *Journal of Analytical and Applied Pyrolysis*, 104:202–209, November 2013.

[134] Maria Barrio. *Experimental investigation of small scale gasification of biomass*. Phd thesis, The Norwegian University of Science and Technology, 2002.

[135] V Minkova, S P Marinov, R Zanzi, E Bjornbom, T Budinova, M Stefanova, and L Lakov. Thermochemical treatment of biomass in a flow of steam or in a mixture of steam and carbon dioxide. *Fuel Processing Technology*, 62:45–52, 2000.

[136] Susanna Nilsson, Alberto Gómez-Barea, and Pedro Ollero. Gasification of char from dried sewage sludge in fluidized bed: Reaction rate in mixtures of CO2 and H2O. *Fuel*, 105:764–768, March 2013.

[137] Susanna Nilsson, Alberto Gómez-Barea, Diego Fuentes-Cano, and Manuel Campoy. Gasification kinetics of char from olive tree pruning in fluidized bed. *Fuel*, 125(February):192–199, June 2014.

[138] Truls Liliedahl and Krister Sjöström. Modelling of char-gas reaction kinetics. *Fuel*, 76(1):29–37, 1997.

[139] D.G. Roberts and D.J. Harris. Char gasification in mixtures of CO2 and H2O: Competition and inhibition. *Fuel*, 86(17-18):2672–2678, December 2007.

[140] Raymond C. Everson, Hein W.J.P. Neomagus, Henry Kasaini, and Delani Njapha. Reaction kinetics of pulverized coal-chars derived from inertinite-rich coal discards: Gasification with carbon dioxide and steam. *Fuel*, 85(7-8):1076–1082, May 2006.

[141] Zhimin Huang, Jiansheng Zhang, Yong Zhao, Hai Zhang, Guanxi Yue, Toshiyuki Suda, and Masahiro Narukawa. Kinetic studies of char gasification by steam and CO2 in the presence of H2 and CO. *Fuel Processing Technology*, 91(8):843–847, August 2010.

[142] Chao Chen, Jing Wang, Wei Liu, Sen Zhang, Jingshu Yin, Guangqian Luo, and Hong Yao. Effect of pyrolysis conditions on the char gasification with mixtures of CO2 and H2O. *Proceedings of the Combustion Institute*, 34(2):2453–2460, January 2013.

[143] Satoshi Umemoto, Shiro Kajitani, and Saburo Hara. Modeling of coal char gasification in coexistence of CO2 and H2O considering sharing of active sites. *Fuel*, 103:14–21, January 2013.

[144] Yonghui Bai, Yulong Wang, Shenghua Zhu, Lunjing Yan, Fan Li, and Kechang Xie. Synergistic effect between CO2 and H2O on reactivity during coal chars gasification. *Fuel*, (February):1–7, February 2014.

[145] T Bergman, A Lavine, F Incropera, and D Dewitt. *Fundamentals of Heat and Mass Transfer*. 7th editio edition, 2011.

[146] Colomba Di Blasi. Modeling chemical and physical processes of wood and biomass pyrolysis. *Progress in Energy and Combustion Science*, 34(1):47–90, February 2008.

[147] Jacques Lédé. Biomass Pyrolysis: Comments on Some Sources of Confusions in the Definitions of Temperatures and Heating Rates. *Energies*, 3(4):886–898, April 2010.

[148] Josefien Swagten, Daniël Bossus, and Hanny Vanwersch. The calibration of XRF polyethylene reference materials with k0-NAA and ICP-AES. *Nuclear Instruments and Methods in Physics Research Section A: Accelerators, Spectrometers, Detectors and Associated Equipment*, 564(2):761–765, August 2006.

[149] Ezra Bar-Ziv, Alon Zaida, Piero Salatino, and Osvalda Senneca. Diagnostics of carbon gasification by raman microprobe spectroscopy. *Proceedings of the Combustion Institute*, 28(2):2369–2374, January 2000.

[150] V.P. Chabalala, N. Wagner, and S. Potgieter-Vermaak. Investigation into the evolution of char structure using Raman spectroscopy in conjunction with coal petrography; Part 1. *Fuel Processing Technology*, 92(4):750–756, April 2011.

[151] Li Chen. *Fast pyrolysis of millimetric wood particles between 800°C and 1000°C*. PhD thesis, Claude Bernard Lyon I, 2009.

[152] M.V. Gil, J. Riaza, L. Álvarez, C. Pevida, J.J. Pis, and F. Rubiera. Oxy-fuel combustion kinetics and morphology of coal chars obtained in N2 and CO2 atmospheres in an entrained flow reactor. *Applied Energy*, 91(1):67–74, March 2012.

[153] Renu Kumar Rathnam, Liza K. Elliott, Terry F. Wall, Yinghui Liu, and Behdad Moghtaderi. Differences in reactivity of pulverised coal in air (O2/N2) and oxy-fuel (O2/CO2) conditions. *Fuel Processing Technology*, 90(6):797–802, June 2009.

[154] C. Guizani, F.J. Escudero Sanz, and S. Salvador. The gasification reactivity of high-heating-rate chars in single and mixed atmospheres of H2O and CO2. *Fuel*, March 2013.

[155] Mejdi Jeguirim and Gwenaelle Trouvé. Pyrolysis characteristics and kinetics of Arundo donax using thermogravimetric analysis. *Bioresource technology*, 100(17):4026–31, September 2009.

[156] I.I. Ahmed and A.K. Gupta. Characteristics of cardboard and paper gasification with CO2. *Applied Energy*, 86:2626–2634, 2009.

[157] P Gilbert, C Ryu, V Sharifi, and J Swithenbank. Tar reduction in pyrolysis vapours from biomass over a hot char bed. *Bioresource technology*, 100(23):6045–51, December 2009.

[158] Shu Zhang, Zhenhua Min, Hui-Ling Tay, Yi Wang, Li Dong, and Chun-Zhu Li. Changes in Char Structure during the Gasification of Mallee Wood: Effects of Particle Size and Steam Supply. *Energy & Fuels*, 26(1):193–198, January 2012.

[159] D Sutton and S M Parle. The CO reforming of the hydrocarbons present in 2 a model gas stream over selected catalysts. *Fuel Processing Technology*, 75:45–53, 2002.

[160] Francisco Rodriguez-reinoso, M Molina-sabio, and M T Gonzalez. THE USE OF STEAM AND CO2 AS ACTIVATING AGENTS IN THE PREPARATION OF ACTIVATED CARBONS. *Carbon*, 33(1):15–23, 1995.

[161] Abdul Rahman Mohamed, Maedeh Mohammadi, and Ghasem Najafpour Darzi. Preparation of carbon molecular sieve from lignocellulosic biomass: A review. *Renewable and Sustainable Energy Reviews*, 14(6):1591–1599, August 2010.

[162] Ajay Kumar, David D. Jones, and Milford a. Hanna. Thermochemical Biomass Gasification: A Review of the Current Status of the Technology. *Energies*, 2(3):556–581, July 2009.

[163] Satoshi Umemoto, Shiro Kajitani, and Saburo Hara. Modeling of coal char gasification in coexistence of CO2 and H2O considering sharing of active sites. *Fuel*, November 2011.

[164] Chao Chen, Jing Wang, Wei Liu, Sen Zhang, Jingshu Yin, Guangqian Luo, and Hong Yao. Effect of pyrolysis conditions on the char gasification with mixtures of CO2 and H2O. *Proceedings of the Combustion Institute*, August 2012.

[165] T.G. Bridgeman, L.I. Darvell, J.M. Jones, P.T. Williams, R. Fahmi, A.V. Bridgwater, T. Barraclough, I. Shield, N. Yates, S.C. Thain, and I.S. Donnison. Influence of particle size on the analytical and chemical properties of two energy crops. *Fuel*, 86(1-2):60–72, January 2007.

[166] L. Van de steene, J.P. Tagutchou, F.J. Escudero Sanz, and S. Salvador. Gasification of woodchip particles: Experimental and numerical study of charâĂŞH2O, charâĂŞCO2, and charâĂŞO2 reactions. *Chemical Engineering Science*, 66(20):4499–4509, October 2011.

[167] Kongvui Yip, Fujun Tian, Jun-ichiro Hayashi, and Hongwei Wu. Effect of Alkali and Alkaline Earth Metallic Species on Biochar Reactivity and Syngas Compositions during Steam Gasification âĂă. *Energy & Fuels*, 24(1):173–181, January 2010.

[168] Rolando Zanzi, Krister Sjostrom, and Emilia Bjornbom. Rapid pyrolysis of agricultural residues at high temperature. *Biomass and Bioenergy*, 23:357–366, 2002.

[169] Susanna Nilsson, Alberto Gómez-Barea, and Pedro Ollero. Gasification of char from dried sewage sludge in fluidized bed: Reaction rate in mixtures of CO2 and H2O. *Fuel*, (September), September 2012.

[170] Georgios a Florides and Paul Christodoulides. Global warming and carbon dioxide through sciences., February 2009.

[171] Boxun Hu, Curtis Guild, and Steven L. Suib. Thermal, electrochemical, and photochemical conversion of CO2 to fuels and value-added products. *Journal of CO2 Utilization*, 1:18–27, June 2013.

[172] Heidi C Butterman and Marco J Castaldi. NAWTEC16-1949 CO 2 Enhanced Steam Gasification of Biomass Fuels. *Scanning Electron Microscopy*, (May):1–16, 2008.

[173] C. Guizani, J.E. Sanz, and S. Salvador. Effects of CO2 on biomass fast pyrolysis: Reaction rate, gas yields and char reactive properties. *Fuel*, (August), August 2013.

[174] Carmen Branca and Colomba Di Blasi. Kinetics of the isothermal degradation of wood in the temperature range 528-708 K. *Journal of Analytical and Applied Pyrolysis*, 67(2):207–219, May 2003.

[175] Y. Haseli, J.a. van Oijen, and L.P.H. de Goey. Modeling biomass particle pyrolysis with temperature-dependent heat of reactions. *Journal of Analytical and Applied Pyrolysis*, 90(2):140–154, March 2011.

[176] Dong Kyun Seo, Sun Ki Lee, Min Woong Kang, Jungho Hwang, and Tae-U. Yu. Gasification reactivity of biomass chars with CO2. *Biomass and Bioenergy*, 34(12):1946–1953, December 2010.

[177] Carole Couhert, Jean-Michel Commandré, and Sylvain Salvador. Failure of the component additivity rule to predict gas yields of biomass in flash pyrolysis at 950°C. *Biomass and Bioenergy*, 33(2):316–326, February 2009.

[178] W.C Chan. Modeling and Experimental Verification of Physical and Chemical Process during Pyrolysis of a Large Biomass Particle. *Fuel*, 64:1505–1513., 1985.

[179] Abhishek Sharma, Vishnu Pareek, Shaobin Wang, Zhezi Zhang, Hong Yang, and Dongke Zhang. A phenomenological model of the mechanisms of lignocellulosic biomass pyrolysis processes. *Computers & Chemical Engineering*, 60:231–241, January 2014.

[180] Guillaume Gauthier, Thierry Melkior, Maguelone Grateau, Sébastien Thiery, and Sylvain Salvador. Pyrolysis of centimetre-scale wood particles: New experimental developments and results. *Journal of Analytical and Applied Pyrolysis*, 104:521–530, November 2013.

[181] Hayat Bennadji, Krystle Smith, Shaka Shabangu, and Elizabeth M. Fisher. Low-Temperature Pyrolysis of Woody Biomass in the Thermally Thick Regime. *Energy & Fuels*, 27(3):1453–1459, March 2013.

[182] P Mousquès, J.L Dirion, and D Grouset. Modeling of solid particles pyrolysis. *Journal of Analytical and Applied Pyrolysis*, 58-59:733–745, April 2001.

[183] B Feng. Structural ordering of coal char during heat treatment and its impact on reactivity. *Carbon*, 40(4):481–496, April 2002.

[184] Alfredo Zolin, Anker Jensen, Peter Arendt Jensen, Flemming Frandsen, and Kim Dam-Johansen. The Influence of Inorganic Materials on the Thermal Deactivation of Fuel Chars. *Energy & Fuels*, 15(5):1110–1122, September 2001.

[185] Daniel M Keown, George Favas, Jun-ichiro Hayashi, and Chun-Zhu Li. Volatilisation of alkali and alkaline earth metallic species during the pyrolysis of biomass: differences between sugar cane bagasse and cane trash. *Bioresource technology*, 96(14):1570–7, September 2005.

[186] Catherine E Brewer, Klaus Schmidt-rohr, Justinus A Satrio, and Robert C Brown. Characterization of Biochar from Fast Pyrolysis and Gasification Systems. *Environmental Progress & Sustainable Energy*, 28(3), 2009.

[187] S Lowell and J.E Shields. *Powder surface area and porosity*. Chapman and Hall, third edit edition, 1991.

Effets du CO_2 sur la pyro-gazéification de de la biomasse dans des conditions de chauffe lente et de chauffe rapide

Résumé

La présente étude porte sur les effets de CO_2 sur la pyrolyse de la biomasse et la gazéification de chars dans des conditions de chauffe lente et de chauffe rapide.

Dans la première partie de ce travail, nous avons étudié les effets du CO_2 sur la réaction de pyrolyse rapide à haute température et évalué ses effets sur la vitesse de pyrolyse, sur le rendement de gaz ainsi que sur les propriétés du char. Nous avons aussi étudié la réaction de gazéification en atmosphère mixte en présence de CO_2 et de H_2O. Enfin, nous avons imaginé le cas hypothétique d'un gazogène au CO_2 pur. Le cas d'une pyro-gazéification sous CO_2 pur a été abordé au niveau de la particule de biomasse, expérimentalement et théoriquement par la modélisation numérique avec l'objectif de fournir des temps caractéristiques de pyrolyse et de gazéification, et de comprendre le déroulement de la pyro-gazéification sous CO_2.

Dans la deuxième partie, nous nous sommes intéressés à la question de la gazéification des chars obtenus par chauffe lente, en présence de CO_2 avec deux objectifs principaux : d'une part, de fournir des données de réactivité dans des conditions opératoires de réacteurs de gazéification et d'autre part, de comprendre les mécanismes de réaction de gazéification sous CO_2, H_2O et leurs mélanges. Nous avons examiné l'influence de la taille des particules sur la vitesse de gazéification sous des atmosphères simples de CO_2 et H_2O en utilisant une approche basée sur le module de Thiele. Nous avons également étudié les effets de la température et de la taille des particules sur la gazéification du char sous atmosphères mixtes contenant CO_2 et H_2O à 900 ° C. Nous avons également abordé la question des atmosphères cycliques en examinant l'effet de la gazéification du char sous CO_2 sur sa réactivité à H_2O et vice versa. Pour mieux comprendre les mécanismes de gazéification dans des atmosphères simples et mixtes de CO_2 et H_2O, nous avons suivi l'évolution de la texture, de la structure et de la chimie de surface du char le long de la gazéification sous CO_2, H_2O et leurs mélanges. Des caractérisations chimiques, texturales et structurales ont été ainsi effectuées sur des particules de char partiellement gazéifiés à 20 %, 50 % et 70 % de conversion sous CO_2, H_2O et leurs mélanges. Ces caractérisations conduisent à une meilleure compréhension du déroulement de la réaction de gazéification.

Mots-clés: Biomasse, pyrolyse, gazéification , CO_2, H_2O , atmosphéres mixte, Cinétique, propriétés réactives du char.

Effects of CO_2 on the biomass pyro-gasification in High Heating Rate and Low Heating Rate Conditions

Abstract

The present work deals about the effects of CO_2 enriched atmospheres on biomass pyrolysis and char gasification reactions in High Heating Rate (HHR) and Low Heating Rate (LHR) conditions, at the biomass particle level.

In the first part, we studied the effects of CO_2 on the high temperature fast pyrolysis reaction and evaluate its effects on the pyrolysis rate, on the gas yield as well as on the char properties including chemical composition, texture and reactivity at 850°C. We focused also on the effects of CO_2 on the HHR-char gasification reaction when injected as a co-reactant with steam. We studied the mixed atmosphere gasification reaction in CO_2 and H_2O for different atmosphere compositions. Finally, we imagined a hypothetical case of a pure CO_2 operating gasifier. The case of a pure CO_2 pyro-gasification process was tackled experimentally and theoretically by numerical modelling with aim to provide pyrolysis and gasification characteristic reaction times, and to understand the unfolding of the global CO_2 pyro-gasification reaction.

In the second part, we were interested on the issue of LHR-char gasification in the presence of CO_2 with two principal objectives: on one hand, providing reactivity data for practical gasification operations and on the other hand, understanding the gasification reaction mechanisms (in CO_2, H_2O and their mixtures) at the level of the char basic structural units (BSU). We examined the influence of particle size on the single atmosphere gasification in CO_2 and H_2O using the Thiele modulus approach. We also studied the effects of temperature and particle size on the char gasification in mixed atmosphere of CO_2 and steam at 900°C. We also had a focus on the issue of cyclic atmosphere gasification and studied the effects of a prior CO_2 gasification on the char reactivity towards H_2O and vice versa. To further understand the char gasification mechanisms in single and mixed atmospheres of CO_2 and H_2O, we opted to monitor the evolution of the chemical, structural and textural char properties along the gasification in CO_2, H_2O and their mixtures. Deep char characterization were performed on small LHR-char particles partially gasified at 20%, 50% and 70% of conversion in CO_2, H_2O and their mixtures. These characterisations are of high interest as they shed light on the unfolding of the gasification reaction in CO_2, H_2O and their mixtures.

Keywords: Biomass, Pyrolysis, Char gasification, CO_2, H_2O, Mixed atmospheres, Kinetics, Char reactive properties.